การเตรียม การพิสูจน์เอกลักษณ์ และการจำลองโมเลกุลของ พอลิ(แลคติค แอซิด)/พอลิ(เอธิลีน ไกลคอล) บล็อกโคพอลิเมอร์และบล็อกโคพอลิเมอร์ผสม

นายอดิศักดิ์ ทาขุลี

วิทยานิพนธ์นี้เป็นส่วนหนึ่งของการศึกษาตามหลักสูตรปริญญาวิทยาศาสตรดุษฎีบัณฑิต
สาขาวิชาเคมี
มหาวิทยาลัยเทคโนโลยีสุรนารี
ปีการศึกษา 2556

PREPARATION, CHARACTERIZATION AND MOLECULAR SIMULATION OF POLY(LACTIC ACID) /POLY(ETHYLENE GLYCOL) (PLA/PEG) BASED BLOCK COPOLYMER AND BLENDS

Adisak Takhulee

A Thesis Submitted in Partial Fulfillment of the Requirements for the Degree of Doctor of Philosophy in Chemistry

Suranaree University of Technology

Academic Year 2013

PREPARATION, CHARACTERIZATION AND MOLECULAR SIMULATION OF POLY(LACTIC ACID)/POLY(ETHYLENE GLYCOL) BASED BLOCK COPOLYMERS AND BLENDS

Suranaree University of Technology has approved this thesis submitted in partial fulfillment of the requirements for the Degree of Doctor of Philosophy.

Thesis Examining Committee

_____
(Assoc. Prof. Dr. Jatuporn Wittayakun)
Chairperson

_____
(Assoc. Prof. Dr. Visit Vao-soongnern)
Member (Thesis Advisor)

_____
(Assoc. Prof. Dr. Yoshiaki Takahashi)
Member

_____
(Asst. Prof. Dr. Chaiwat Ruksakulpiwat)
Member

_____
(Prof. Dr. Kritsana Sagarik)
Member

_____
(Prof. Dr. Vinich Promarak)
Member

_____
(Prof. Dr. Sukit Limpijumnong)
Vice Rector for Academic Affairs and Innovation

_____
(Prof. Dr. Santi Maensiri)
Dean of Institute of Science

อดิศักดิ์ ทาขุลี : การเตรียม การพิสูจน์เอกลักษณ์ และการจำลองโมเลกุลของพอลิ(แลคติค แอซิค)/พอลิ(เอธิลีน ไกลคอล) บล็อกโคพอลิเมอร์ และบล็อกโคพอลิเมอร์ผสม (PREPARATION, CHARACTERIZATION AND MOLECULAR SIMULATION OF POLY(LACTIC ACID)/POLY(ETHYLENE GLYCOL) (PLA/PEG) BASED BLOCK COPOLYMER AND BLENDS) อาจารย์ที่ปรึกษา : รองศาสตราจารย์ ดร.วิสิษฐ์ แววสูงเนิน, 254 หน้า.

พอลิ(แลคติค แอซิค) (PLA) เป็นวัสดุพอลิเมอร์ที่สามารถย่อยสลายเองได้ในธรรมชาติและไม่เป็นพิษต่อมนุษย์และสิ่งแวดล้อม ด้วยเหตุนี้ PLA จึงได้รับความสนใจเป็นอย่างมากในการนำไปใช้ประโยชน์ในช่วงทศวรรษที่ผ่านมา แต่อย่างไรก็ตามยังมีสมบัติทางกายภาพบางประการที่ยังเป็นข้อจำกัดในการนำ PLA ไปใช้งานตามต้องการ เช่น ความเปราะ ยืดหยุ่นได้น้อย จึงทำให้ต้องมีการแก้ไขคุณสมบัติด้อยของ PLA เช่น การผสมกับพอลิ(เอธิลีน ไกลคอล) (PEG) ซึ่งมีสมบัติเชิงวัสดุที่ยืดหยุ่นกว่า ซึ่งพบว่า PEG ช่วยลดข้อด้อยของ PLA ได้เป็นอย่างดี อย่างไรก็ตาม ระบบพอลิเมอร์ผสมของ PLA/PEG จะมีการแยกตัวของแต่ละองค์ประกอบออกจากกันเมื่อเวลาผ่านไป ซึ่งส่งผลให้พอลิเมอร์ผสมของ PLA/PEG มีสมบัติเชิงกลด้อยลง ดังนั้นการศึกษานี้จึงมีวัตถุประสงค์เพื่อลดการแยกตัวของแต่ละองค์ประกอบในพอลิเมอร์ผสมโดยใช้บล็อกโคพอลิเมอร์ PLA-PEG-PLA เป็นสารเติมแต่งสำหรับ PLA ได้นำข้อมูลจากการวิเคราะห์เชิงความร้อนและวิทยากระแสของพอลิเมอร์ผสม PLA/PEG และ PLA/PLA-PEG-PLA ในการพิจารณาคุณสมบัติการเข้ากันได้ของแต่ละองค์ประกอบในพอลิเมอร์ผสม การศึกษานี้ยังได้ใช้วิธีการจำลองโมเลกุลด้วยคอมพิวเตอร์ในระดับอะตอมและมีโซสเกลเพื่อสร้างความเข้าใจเชิงลึกในการอธิบายผลที่ได้จากการทดลอง นอกจากนี้เพื่อให้เกิดความเข้าใจลักษณะทางฟิสิกส์ของวัสดุพอลิเมอร์ที่มีหลายวัฏภาคจึงได้ศึกษาพอลิเมอร์ระบบผสมของพอลิเอธิลีนและพอลิโพรพิลีน (PE/PP) และ พอลิเอธิลีน นาโนคอมพอสิตด้วยวิธีการจำลองมอนติ คาร์โล โดยผลการศึกษาหลักที่ได้ในแต่ละส่วนสามารถสรุปได้ดังนี้

PLA-PEG-PLA มีประสิทธิภาพในการลดการแยกตัวของพอลิเมอร์ผสมกับ PLA ได้ดีกว่าการใช้ PEG ข้อมูลดังกล่าวนี้สอดคล้องเป็นอย่างดีกับผลการศึกษาแบบจำลองโมเลกุลทางคอมพิวเตอร์ทั้งเทคนิคพลวัตเชิงโมเลกุล (MD) และ พลวัตอนุภาคเชิงกระจาย (DPD)

สำหรับระบบ PE/PP ที่มีของสเตอริโอของ PP ต่างกัน พบว่า ขนาดของโมเลกุล ความแข็ง (C_n) และการแพร่ (D) ของสายโซ่ PE ในพอลิเมอร์ผสมจะเปลี่ยนแปลงตามโครงสร้างสเตอริโอเคมีของ PP นอกจากนี้ยังพบว่าระบบ PE/*a*PP และ PE/*i*PP PE นั้นจะเข้ากันได้บางส่วนในขณะที่ระบบ PE/*s*PP จะไม่เข้ากันที่สภาวะหลอมเหลว

สำหรับการศึกษานาโนคอมพอสิตของ PE ที่มีการกระจายน้ำหนักโมเลกุลสองค่า พบว่าผลของการเติม PE สายสั้นลงไป จะรบกวนการเกิดโครงสร้างแบบสะพานระหว่างสายโซ่ยาวของ PE และอนุภาคนาโน นอกจากนี้สมบัติเชิงพลวัตของพอลิเอธิลีนสายโซ่ยาวจะเคลื่อนที่ช้าลงเมื่อบริเวณระหว่างอนุภาคนาโนแคบมากๆ

สาขาวิชาเคมี ลายมือชื่อนักศึกษา _____

ปีการศึกษา 2556 ลายมือชื่ออาจารย์ที่ปรึกษา _____

ADISAK TAKHULEE : PREPARATION, CHARACTERIZATION AND MOLECULAR SIMULATION OF POLY(LACTIC ACID)/ POLY(ETHYLENE GLYCOL) (PLA/PEG) BASED BLOCK COPOLYMER AND BLENDS. THESIS ADVISOR: ASSOC. PROF. VISIT VAO-SOONGNERN, Ph.D. 254 PP.

POLY(LACTIC ACID)/POLY(ETHYLENE GLYCOL)/BLOCK COPOLYMER/ BLEND/COMPUTER SIMULATION

Poly(lactic acid) (PLA) is a bioplastics that is biodegradable in nature and non-toxic to human and environment. For this reason, there has been a great interest during the past decade to develop this material for various applications. According to its brittleness and low elongation at break, it is necessary to improve the properties of PLA for practical usage. Blending PLA with plasticizer such as polyethylene glycol (PEG) has been recognized as an effective method to toughen PLA. Unfortunately, PLA/PEG blends usually phase separate over time at room temperature. To solve the problem of phase separation of these blends, a triblock copolymer of PLA and PEG (PLA-PEG-PLA) was proposed as the plasticizer for PLA in this work. Thermal and rheological properties of PLA/PEG and PLA/PLA-PEG-PLA blends were used to determine the miscibility of these mixtures. Atomistic molecular dynamic and mesoscale simulations were also performed to validate experimental findings and gain more insight at an atomistic and nanoscale level of these materials. To extend an understanding of the physical characteristics of multiphase polymeric material, structure and dynamics of bidisperse polyethylene (PE) nanocomposites and

polyethylene/polypropylene (PE/PP) blends with different PP tacticity were investigated by Monte Carlo simulation of a coarse-grained polymer model. The key findings of this thesis can be summarized as followings.

PLA-PEG-PLA triblock copolymer is capable to reduce phase separation compared to blending PLA with bare PEG. This finding is in good agreement with the results obtained from molecular dynamics (MD) and dissipative particle dynamics (DPD) simulations.

For the PE/PP blend with different tacticity of PP chains, molecular dimensions, characteristic ratio (C_n) and self-diffusion coefficient (D) of PE chains in the blends are sensitive to the stereochemistry of PP component. In addition, the results suggest that PE/*a*PP and PE/*i*PP are partial miscible while PE/*s*PP is completely immiscible at the melt.

The presence of short PE chains in the polymer matrix of bidisperse PE nanocomposites leads to a reduction of the bridge conformation of long PE chains. Under the strong confinement, the mobility of the long chains in bidisperse nanocomposites was slower than those in monodisperse PE nanocomposite systems.

School of Chemistry Student's Signature _____

Academic Year 2013 Advisor's Signature _____

ACKNOWLEDGEMENTS

I am grateful to my thesis advisor, Assoc. Prof. Dr. Visit Vao-Soongnern, for his valuable advices, comments and suggestions for my thesis. I am also very thankful to the thesis examining committee members for their efforts throughout the entire process. I really thank all professors at School of Chemistry, Suranaree University of Technology (SUT) for their kind attitude and providing me valuable knowledge.

I would like to pay special thanks to Prof. Dr. Yoshiaki Takahashi at Department of Advanced Device Materials, Institute for Materials Chemistry and Engineering, Kyushu University, Japan for giving me valuable advices, kind suggestions and providing me with a good hospitality during my time in their group.

I would like to thank the Office of the Higher Education Commission, Thailand for supporting by grant fund under the program Strategic Scholarships for Frontier Research Network for the Join Ph.D. Program Thai Doctoral degree for this research. I would like to thank the National Nanotechnology Center (NANOTEC), National Science for the permission to use molecular simulation software through National Nanoscience Consortium (CNC).

Finally, I most gratefully acknowledge my parents and my friends for all their support throughout the period of this research.

Adisak Takhulee

CONTENTS

CONTENTS (Continued)

CONTENTS (Continued)

CONTENTS (Continued)

CONTENTS (Continued)

CONTENTS (Continued)

Page

LIST OF TABLES

LIST OF TABLES (Continued)

LIST OF FIGURES

LIST OF FIGURES (Continued)

LIST OF FIGURES (Continued)

LIST OF FIGURES (Continued)

LIST OF FIGURES (Continued)

LIST OF FIGURES (Continued)

LIST OF FIGURES (Continued)

LIST OF FIGURES (Continued)

LIST OF FIGURES (Continued)

LIST OF FIGURES (Continued)

LIST OF FIGURES (Continued)

LIST OF ABBREVIATIONS

T_g	Glass transition
°C	Degree Celsius
N	Overall degree of polymerization
SCFT	Self-consistent field theory
SAXS	Small angle X-ray scattering
DPD	Dissipative Particle Dynamics
MD	Molecular Dynamics
f_A	Block fraction
χ	Flory-Huggins interaction parameter
GPC	Gel Permeation Chromatography
ϕ_{bridge}	Bridge fraction
MC	Mote Carlo
D	Wall to wall distance
w	Polymer-filler interaction
wt%	Weight percent
wt/wt	Weight by weight
T_m	Melting temperature
ΔH_m	Enthalpy of melting
QM	Quantum Mechanics

LIST OF ABBREVIATIONS (Continued)

NPT	The Isothermal-Isobaric Ensemble
NVT	The Canonical Ensemble
2nnd	Second nearest neighbor diamond
G′	Storage modulus
G″	Loss modulus
LA	Lactide unit
EG	Ethylene glycol unit
ml	Milliliter
Å	Angstrom
$\overline{DP}$	Degree of polymerization
MPa	Mega Pascal
$\overline{M}_n$	Average molecular weight by number
$\overline{M}_W$	Average molecular weight by weight
kg•mol^{-1}	Kilogram per mole
ΔH_c	Enthalpy of crystallization
X_c	Degree of crystallinity
T_c	Crystallization temperature
g(r)	Radial distribution functions
N_{DPD}	Number of DPD bead
C_n	Characteristic ratio

LIST OF ABBREVIATIONS (Continued)

a_{ij}	Bead interaction parameter
V_m	Molar volume
R	Gas constant

CHAPTER I

INTRODUCTION

In recent years, there has been considerable interest in multiphase polymer materials which contain more than one minor phase. This interest is motivated by the commercial quest for new materials with improved properties (Sperling, 2001). Because of this unique properties, the multiphase polymeric materials have been used in various applications, such as electronic and memory devices, medical therapy systems, and high impact resistance components (Singla, 2004). Since it is well established that most of properties including mechanical, optical, rheological, and barrier properties of polymeric materials are strongly influenced by the type and the fineness of the phase structure, the study of the morphology of such materials to design a new material has emerged as an area of interest to polymer material science and technology. The realm of multiphase polymer systems can be broadly classified into two classes, one with covalently linked components and the other where no covalent bonds are present between the different components. Block copolymer, polymer blends and polymer nanocomposites are examples of that system (Singla, 2004).

Polymers from renewable resources known as biodegradable polymers have attracted increasing amount of attention over past two decades, predominantly due to two major reasons. Firstly, there are environmental concerns, and secondly, it has to be considered that the realization of our petroleum resources are finite (Siracusa,

Rocculi, Romani, and Rosa, 2008; Mecking, 2004; Okada, 2002; Wanamaker, 2009). Due to composability, non-toxic and environmental friendly characteristics, biodegradable polymers have been promoted to replace petrochemical-based polymers. Unfortunately, there are limitation of biodegradable polymer and only a few have the potential to replace petroleum-based products. Main disadvantages of biodegradable polymers are their dominant hydrophilic character, fast degradation rates and unsatisfactory mechanical properties, particularly under wet environments (Yu, Dean, and Li, 2006). For example, poly(3-hydroxybutyrate) (P3HB), polyglycolide (PGA), and poly(lactic acid) (PLA), all of which have high stiffness and tensile strength, but are inherently brittle and cannot replace the commodity plastics that are tough and flexible such as polyethylene (PE), polystyrene (PS) and polypropylene (PP). In order to overcome the disadvantages of biodegradable polymer such as poor mechanical properties or to offset the high price of synthetic biodegradable polymers, various blends, block copolymer and composites have been developed. Thermal stability, gas barrier properties, strength, low melt viscosity, and degradation rate are among the properties that could be achieved by "multiphase systems" (Harrats, Thomas, and Groeninckx, 2006).

A very promising biodegradable polymer is poly(lactic acid) (PLA) because it exhibits good properties, *i.e.*, high modulus and stiffness, biocompatibility and good transparency comparable to those petrochemical-based polymers such as PE, PP and PS. With its inherent and important renewable feature, PLA and their copolymer has been developed as a biomaterials which cover a wide range of application such as food packaging, medical and pharmaceutical area (Huang, 1985; Auras, Lim, Selke, and Tsuji, 2010; Cheng, Deng, Chen, and Ruan, 2009; Nair and Laurencin, 2007).

PLA can be produced by condensation polymerization directly from its basic building block (lactic acid), which is derived by fermentation of sugars from carbohydrate sources, *i.e.*, corn starch, sugarcane or tapioca. Most commercial routes, however, utilize the more efficient conversion of lactide monomer to PLA via ring-opening polymerization (ROP) catalyzed by a Sn(II)-based catalyst rather than polycondensation (Garlotta, 2001). PLA can be either amorphous or semicrystalline, depending on the stereochemistry and thermal history. Poly(L-lactic acid) (PLLA) and poly(D-lactide) (PDLA) are a semicrystalline polymer, exhibit high modulus, while poly(D, L-lactic acid) (PDLLA) is an amorphous polymer. Generally, PLA have glass transition (T_g) and melting temperature (T_m) of about 55-60 ºC and 175-180 ºC, respectively (Kaitian, Kozluca, Denkbaş, and Pişkin, 1996; Santis, Pantani, and Titomanlio, 2011). More recently, become of the high demand of bio-packaging products, PLA has been anticipated to be used as packaging materials for food and consumer goods (transparent bottles, meat trays, bags, films, etc.). These applications are benefitial from their ability to decompose relatively quickly in landfill or environments. However, PLA has not been used extensively in these areas due to its brittleness, low crystallization rate and lower impact resistance at room temperature. These drawbacks are especially a disadvantage in the film type application. To address this major disadvantage, various strategies including addition of low molecular weight plasticizers, copolymerization and melt blending with flexible polymers or rubbers, have been extensively studied in the literatures. (Ren, 2011; Cheng, Deng, Chen, and Ruan, 2009). Compared to other methods, plasticization appears more industrially practical due to cost-effectiveness and high efficiency. Various low molecular weight compounds have been investigated as potential

plasticizers for PLA. Triacetine (Ljungberg and Wesslen, 2002), citrate esters (Ljungberg and Wesslen, 2005), poly(ethylene glycol) (PEG) (Sheth, Kumar, Dave, Gross, and McCarthy, 1997; Hu, Hu, Topolkaraev, Hiltner, and Baer, 2003) and low molecular weight poly(propylene glycol) (PPG) (Kulinski, Piorkowska, Gadzinowska, and Stasiak, 2006) have been found to be the efficient plasticizers for PLA. The role of the plasticizer is to reduce the modulus of elasticity in PLA and it is of great importance that the plasticizer is compatible with PLA in order to be evenly distributed in its matrix. However, since most of plasticizers are low molecular weight compounds and they easily migrate from the bulk of polymer matrix to the surface, ultimately leading to the blend regaining an inherent brittle property. Therefore, plasticizers with high molecular weights and good compatibility are always desirable because of their higher stability. As it is non-toxic, biocompatible and well miscible with PLA, PEG has been intensively studied as the plasticizer for PLA. However, there is (Hu, Hu, Topolkaraev, Hiltner, and Baer, 2003) a report that the promising mechanical properties of PLA/PEG blends disappear with time because of the slow phase separation and crystallization of PEG from homogeneous blends. In addition, the cold crystallization of PLA was also found to reduce the elongation at break of plasticized PLA. To avoid these disadvantages, plasticizer have to be modified to enhance its compatibility. One of the most successful techniques is the use of graft and block copolymer as polymeric compatibilizer. Block copolymers which one block is chemically identical or is good miscible in polymer matrices has been proposed as the plasticizer for touhenig PLA (Jia, Tan, Han, Yang, and Dong, 2009; Rathi *et al*., 2011). A simple hypothesis is that an end block of copolymers acts as a polymeric surfactant by spanning the interface between the phases, while the soft block could be

served as the toughening agent. The end block of copolymer has several molecular effects. First, the interface tension between the phases is lowered, which reduces the driving force for the phase separation. Secondly, the presence of the end block of copolymer at the interface reduces the tendency of the domains to coalesce.

A number of experimental and theoretical studies have been reported on the homopolymer and block copolymer blends, considering the effect of block copolymer on the morphology and mechanical properties. For examples, Rathi *et al*. investigated the mechanical properties and morphology of plasticized PLLA by triblock copolymer of PDLA-PEG-PDLA (Rathi *et al*., 2011). The results showed that the brittleness of semicrystalline PLLA was improved via stereocomplex forming of PDLA block in copolymer with PLLA. In addition, they concluded that the increasing of dispersion of soft midblock PEG in the crystalline region of PLLA contributes to the improvement in the mechanical properties. In theoretical studies, coarse grained simulation is a powerful tool to study the morphology and molecular structure of polymer blends. Figueroa *et al*. (Figueroa, Vicente, Magada´n, and Hidalgo, 2007) performed a Dissipative Particle Dynamics (DPD) simulation technique to investigate the influence of the composition, packing density and solubilization of PS homopolymer chains into the compatible microdomains of the asymmetric copolymer of polystyrene-polyisoprene (PS-PI) on phase morphology. Their results agree well with available experimental results. As mentioned above, the role of block segments in the copolymer is well accepted for enhancing the miscibility in homopolymer/block copolymer blends.

One of the fascinating characteristics of block copolymers is the ability to self-assemble in the melt or in solution into a variety of ordered structures with

characteristic dimensions in nanometer length scale. These ordered structures are remarkable keys to many valuable properties which make block copolymers of great nanotechnological interest such as drug delivery (Subbu S. Venkatraman, Jie, Min, Freddy, and Leong-Huat, 2005), nano-lithography, digital storage ect. (Tseng and Darling, 2010). Ordered structures are formed via the thermodynamic process of microphase separation due to the repulsive interaction between the components and are driven by the enthalpy and entropy of demixing of the constituent components of the block copolymers (Hamley, 1998). The phase behavior of ordered structures of a bulk block copolymer is determined by three experimentally controllable factors; (i) the overall degree of polymerization (N), (ii) architectural constrains (diblock, triblock, star block etc.) and composition and (iii) the segment interaction parameter (χ). The ordered structures can be classified as classical body-centered-cubic (BCC), face-centered-cubic (FCC), hexagonally packed cylinders (HEX), and lamellar structures (LAM), and more complex structures, such as bicontinuous cubic (Gyroid), hexagonally perforated lamellar (HPL) phase. Figure 1.1 shows the equilibrium morphologies documented for diblock copolymers by self-consistent field theory (SCFT). The main strategy employed for ordered structures control is to modify these factors in the synthetic process (variation of architectures and chain topologies) and depends on polymerization techniques (Matyjaszewski and Shigemoto, 1996). Another important way for morphology modification is given by blending with homopolymer. In such blends, there is an interplay between macrophase separation of the homopolymers and microphase separation of the block copolymer (Mykhaylyk, Collins, and Hamley, 2004). Which effect predominates depends on the relative lengths of polymers, and on the composition of the blend.

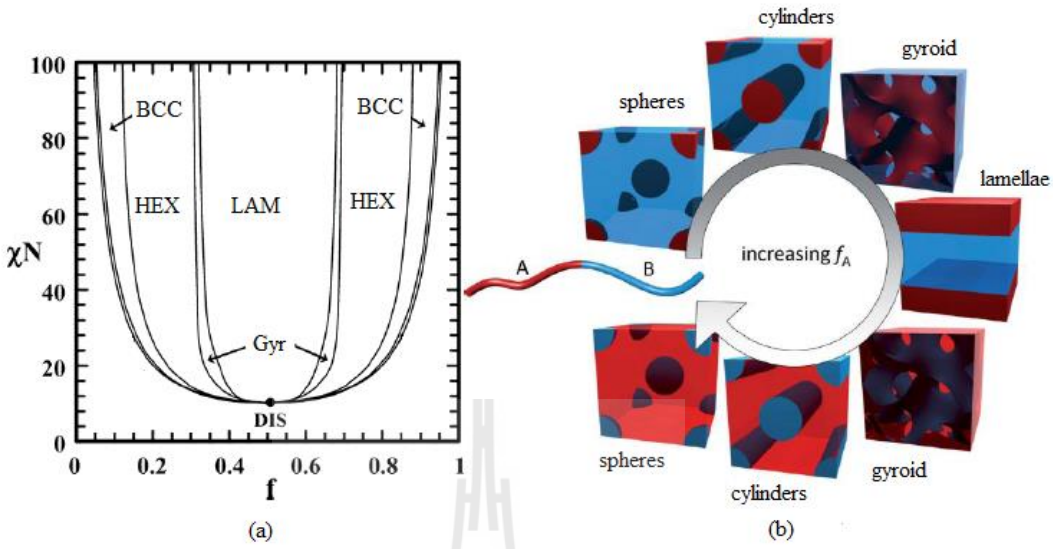

Figure 1.1 (a) Typical phase diagram of a coil-coil diblock copolymer (b) lamellae (LAM), hexagonally packed cylinders (HEX), gyroid phase (Gyr), body-centered spheres (BCC) and disordered (DIS) structures of the different phases as described in Figure 1.1 (a) (Tseng and Darling, 2010).

From a molecular point of view, the polymer chains in ordered structures are linked throughout the microphases to form bridges and loops structure. Despite the similarity of the domain structures and thermodynamic properties between AB and ABA, the chain conformations of ABA triblock copolymers are different from those of AB diblock copolymers when the B domain of ABA triblock copolymer forms continuous phase. Diblock copolymers have only end blocks which always adopt tail conformations, while middle block chains of triblock copolymers choose either a loop conformation whose two ends are anchored on the same domain interface or a bridge conformation whose two ends are pulled apart into the different interfaces as shown in Figure 1.2.

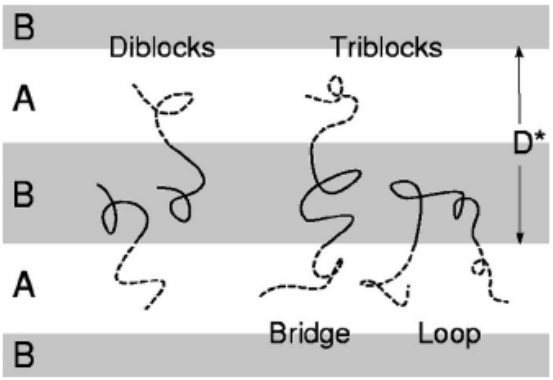

Figure 1.2 Typical configurations of AB diblock and ABA triblock copolymers in a lamellar morphology. Triblock molecules are shown in both bridge- and loop-type configurations (Banaszak, Wołoszczuk, Pakula, and Jurga, 2002).

The bridge is considered fundamental to the elastic behavior of the materials while the loops do not contribute to the mechanical strength of the materials and tend to decrease the elastic modulus (Lazzari, Liu, and Lecommandoux, 2006). Thus, the structure of the triblock copolymer can be specified with the loop/bridge ratio of middle block chains, or bridge fraction (ϕ_{bridge}). This fraction should significantly influence viscoelasticity, mechanical strength, and other physical properties of triblock copolymers that are often used as thermoplastic elastomers (Takano, Kamaya, Takahashi, and Matsushita, 2005).

Experimental and theoretical efforts have been undertaken to predict and explore the phase morphology, chain conformations and macroscopic properties of the block copolymer. The main experimental techniques for characterizing the microstructures of block copolymers are the transmission electron microscope (TEM), small angle X-ray scattering (SAXS) or small angle neutron scattering (SANS) and

oscillatory shear rheometry (Hamley, 1998; Harrats, Thomas, and Groeninckx, 2006). For example, Takano *et al*. (Takano, Kamaya, Takahashi, and Matsushita, 2005) employed the TEM technique and dynamic viscoelastic measurement to elucidate the phase morphology and ϕ_{bridge} values of polystyrene-polyisoprene-polystyrene (SIS) They found that ϕ_{bridge} values of such block copolymer was 0.93 while Watanabe *et al*. (Watanabe, Sato, and Osaki, 2000). reported that value was 0.6 for same block copolymer sample.

Computer simulation is also a powerful technique to elucidate the microstructure of block copolymers because it provides much useful information of polymer on atomistic levels, which are not easily obtained by experiment. The coarse-grained modeling including Dissipative Particle Dynamics (DPD), MesoDyn and Monte Carlo (MC) techniques is usually techniques to study the structure and morphology of block copolymer (Jo and Yang, 2002). For instance, Abu-Sharkh and AlSunaidi (Abu-Sharkh and Al Sunaidi, 2006) performed DPD simulation to predict the phase morphology and determine ϕ_{bridge} of ABA triblock copolymer at difference χN values (N =16) and different composition (f_A). The obtained results of ϕ_{bridge} were 0.44, 0.52, 0.58 and 0.75 for lamellar, perforated lamellar, hexagonal cylinders and spherical micelles, respectively.

In addition, to have better understanding the miscibility behavior of polymer blends, the effect of tacticity of polymer chains on mixing/demixing behavior of polymer blends was investigated in this study. Small changes in the covalent structure of polymeric hydrocarbon chains can easily produce immiscibility of their high polymers, even though miscibility may be retained with mixtures of small oligomers (Haliloglu and Mattice, 1999). Melts composed of two different polymeric

hydrocarbons provide numerous examples. This shows that hydrocarbon polymer is sensitive to structural changes which make the miscibility of polyolefins in the melt difficult to predict. Therefore, two-component systems composed of pairs of hydrocarbon homopolymers are the subject of intense experimental (Loos, Bonnet, and Petermann, 2000) and theoretical (Mattice, Helfer, Rane, Von meerwall, and Farmer, 2004; Wasekaran, Curro, and Honeycutt, 1995) investigation due to their academic interest and also the implications for the utilization of polymer blends in society.

Polyethylene (PE) and polypropylene (PP) are in the class of polyolefins which are used in a variety applications such as packaging, pipeline base material, etc.. In general, they have a good thermal and electrical insulation properties, low density and high resistance to chemicals (Mourad, 2010) but they are mechanically weaker and exhibit lower elastic modulus than metals In order to overcome these limitations, numerous studies have been carried out to improve the mechanical behaviour of these polymers. One of effective and convenient methods is blending.

PE and PP are of considerable industrial relevance, especially in the form of polymer blend. Over the years, their blends are among those binary systems that have attracted a lot of attention. PE and PP blends at the melt are compatible but thought to be only partially miscible. The polymer pairs tend to separate into two liquid phases. This observation is quite surprising. Since the two polymers are simple olefins, it might be expected that miscibility would be observed in melted mixtures. If the melt is truly isotropic, the fully entangled, highest entropy state would be one in which polymers are mixed on a molecular level. Molecular origin of the miscibility of PE/PP melts blends have been extensively investigated by experimentally and theoretically.

For examples, Varennes *et al*. (Varennes, Charlet, and Delmas, 1984) used the small angle neutron scattering to study the phase morphology of a 50/50 blend of high-density polyethylene (HDPE)/*i*-PP, using deuterium labeling to enhance contrast. A phase-segregated morphology was observed at temperatures as high as 200 ^{o}C, which is well above the melting temperatures of two polymers. The domain dimensions were found to be about the same as those observed in blends crystallized from the melt. Incompatibility between PE and PP was also indicated by observation of mutual solutions in a common solvent. In addition, many theoretical studies including molecular dynamics simulation (MD) (Choi, Blom, Kavassalis, and Rudin, 1995) and coarse-grained modeling simulation (Freischmidt, Shanks, Moad, and Uhlherr, 2001; Akten and Mattice, 2001) have been employed to explore the miscibility behavior of PE/PP systems. Their results showed that miscibility behavior depends on tacticity of PP chain.

To extend the understanding about the effect of molecular chain structures, *i.e.*, bridge, loop etc. on physical properties of multiphase polymeric materials, polymer filled with nano-spherical particles represented as a model of the spherical ordered structure would be investigated. As well as with other multiphase systems, polymer filled with nanoparticles of polymer nanocomposites (PNCs) have been the subject of interest in both scientific and industrial communities due to their extraordinary improved properties (Gupta, Kennel, and Kim, 2008). Because of dramatically improved properties compared with conventional polymer composites, several studies were attempted to elucidate the reinforcement mechanism behind these improved performance. Although the understanding of the reinforcement mechanism behind these improvements are still debated, it is well accepted that the well

dispersion of nanoparticle in polymer matrices and the filler spacing between neighboring particles in comparable to the unperturbed chain dimensions, both factors play an important role in property enhancement (Zhang and Archer, 2002; Anderson and Zukoski, 2010). Several theoretical and experimental studies (Zhang and Archer 2002; Dionne, Ozisik, and Picu, 2005) have proposed that the reinforcement is obtained once the neighboring fillers connected by adsorbed polymer chains forming a "secondary" network, which is also called a polymer-mediated transient network. This network can be formed when the wall-to-wall distance (D) between fillers is in the order of several times the radius of gyration (R_g) of polymer chain. The polymer-filler structure is formed as sequences (subsections) of the chain adsorbed onto the filler particles. Various types of subchain segments in transient network models are bridges, loops, trains and dangling ends (see details in Chapter V).

Most of experimental and theoretical studies of the structure and dynamics of PNCs have been focused on a monodisperse of polymer matrice. However, in reality, polymers are polydisperse. It is well known that the polydispersity of polymer matrix plays a critical role in defining the properties of polymer nanocomposites but a comprehensive understanding of the effect of polydispersity on polymer chain structure and dynamics in polymer nanocomposites is lacking. Therefore, the study of polydispersity via molecular computations is appealing.

As all mentioned above, there is a widespread interest in understanding both macroscopic and microscopic properties of multiphase polymer systems, both for practical purposes and as a basic research, and thus this research problem is of interest to study by means of both theory and experiment.

1.1 Research objectives

1.1.1 To investigate the effect of block composition of PLA-PEG-PLA triblock copolymer on the miscibility of PLA/PLA-PEG-PLA blends.

1.1.2 To predict the miscibility and morphology of PLA-PEG-PLA triblock copolymers and the mixtures of PLA/PEG and PLA/PLA-PEG-PLA by multiscale computer simulation.

1.1.3 To investigate the effect of tacticity of PP on the miscibility of PE/PP by Monte Carlo simulation of coarse-grainned polymer model.

1.1.4 To investigate the effect of polydispersity, confinement and polymer-filler interaction on the structure and dynamics of bidisperse PE nanocomposites.

1.2 Scope and limitation of the study

The work in this thesis can be separated into two parts; the first part is an experimental study of thermal and rheological properties of PLA-PEG-PLA triblock copolymers and polymer blends of PLA/PEG and PLA/PLA-PEG-PLA systems. The second part is the computer simulation study of (i) the multiscale simulation of PLA-PEG-PLA and polymer blends of PLA/PEG and PLA/PLA-PEG-PLA and (ii) coarse-graining model base on MC simulation of PE/PP melt blends and bidisperse PE nanocomposites systems.

1.2.1 Experimental study

In this section, a series of PLA-PEG-PLA triblock copolymers with different LA/EG ratios was synthesized via ring opening polymerization by using Tin(II)-2 ethylhexanoate as a catalyst. Two kinds of stereochemical lactide (LA)

monomer, namely L-LA and D, L-LA were used to synthesize PLLA-PEG-PLLA and PDLLA-PEG-PDLLA block copolymers, respectively. PEG with M_w of ~8,000 and ~10,000 g·mol^{-1} were used as initiator polymerization. The chemical structure and chemical composition of triblock copolymers and homopolymers were determined by using fourier transform infrared spectrometry (FTIR), proton and carbon-13 nuclear magnetic resonance (^{1}H, ^{13}C-NMR) spectrometry and gel permeation chromatography (GPC) techniques. Differential scanning calorimetry (DSC), X-ray diffractrometry (XRD), polarized optical microscopy (POM) and rheometry methods were proformed to characterize the thermal, morphological and rheological properties of the polymer samples. The miscibility of PLA/PEG and PLA/PLA-PEG-PLA blends with various composites was investigated by using DSC and rheometry techniques.

1.2.2 Computer simulation study

Atomistic and coarse graining model computer simulations were performed in this study. The scopes of the study in this section were as follows.

- The miscibility of the PLA/PEG and PLA/PLA-PEG-PLA blends were predicted using molecular dynamic (MD) simulation via the determination of Flory-Huggins interactions parameter (χ) of pair polymers. Morphology of triblock copolymers of PLA-PEG-PLA and PLA/PEG and PLA/PLA-PEG-PLA blends were simulated by dissipative particle dynamics (DPD) simulation technique. The bridge fraction (ϕ_{bridge}) was investigated in each system.

- The effect of tacticity of PP on the miscibility of 50 wt% PE/PP melt blends was investigated by mean of a coarse-graining model base on MC method. Isotactic PP (*i*PP), atactic PP (*a*PP) and syndiotactic PP (*s*PP) were used to mix with PE. The chain dimensions, characteristic ratio (C_n), self-diffusion coefficient

(*D*) and interchain pair correlation functions (PCFs) are used to assess the miscibility of the mixtures.

- The mixtures of 50:50 (by mole) of long and short chains of PE ($C_{160}H_{322}/C_{80}H_{162}$ and $C_{160}H_{322}/C_{40}H_{82}$) filled with spherical nanoparticles were constructed in simulation box. The coarse-graining model base on MC method was performed to evaluate the effect of wall-to-wall distance between fillers (*D*), polymer-filler interaction (*w*) and polydispersity (number of short chains in the mixture) on the structure and dynamic of the long PE chains.

1.3 References

Abu-Sharkh, B. and AlSunaidi, A. (2006). Morphology and conformation analysis of self-assembled triblock copolymer melts. **Macromolecular Theory and Simulations** 15: 507-515.

Akten, E. D. and Mattice, W. L. (2001). Monte Carlo simulation of head-to-head, tail-to-tail polypropylene and its mixing with polyethylene in the melt. **Macromolecules** 34: 3389-3395.

Anderson, B. J. and Zukoski, C. F. (2010). Rheology and microstructure of polymer nanocomposite melts: Variation of polymer segment-surface interaction. **Langmuir** 26: 8709-8720.

Auras, R., Lim, L. T., Selke, S. E. M. and Tsuji, H. (2010). **Poly(lactic acid); Synthesis, structures, properties, processing and applications.** Canada: John Wiley & Sons, Inc..

Banaszak, M., Wołoszczuk, S., Pakula, T. and Jurga, S. (2002). Computer simulation of structure and microphase separation in model A-B-A triblock copolymer. **Physical Review E** 66: 031804-1.

Cheng, Y., Deng, S., Chen, P. and Ruan, R. (2009). Polylactic acid (PLA) synthesis and modifications: a review. **Frontiers of Chemistry in China** 4(3): 259-264.

Choi, P., Blom, H. P., Kavassalis, T. A. and Rudin, A. (1995). Immiscibility of poly(ethylene) and poly(propylene): A molecular dynamics study. **Journal of Chemical Physics** 28: 8247-8250.

Dionne, P. J., Ozisik, R. and Picu, C. R. (2005). Structure and dynamics of polyethylene nanocomposites. **Macromolecules** 38: 9351-9358.

Figueroa, C. S., Vicente, L., Magada´n, J. M. M. and Hidalgo, M. R. (2007). Mesoscopic simulation of asymmetric-copolymer/homopolymer blends: Micro phase morphological modification by homopolymer chains solubilization. **Polymer** 48: 3902-3911.

Freischmidt, H. M., Shanks, R. A., Moad, G. and Uhlherr, A. (2001). Characterization of polyolefin melts using the polymer reference interaction site model integral equation theory with a single-site united atom model. **Journal of Polymer Science: Part B: Polymer Physics** 39: 1803-1814.

Garlotta, D. (2001). A literature review of poly(lactic acid). **Journal of Polymers and the Environment** 9(2): 63-84.

Gupta, R. K., Kennel, E. and Kim, K. J. (2008). **Polymer Nanocomposites Handbook**. New York: CRC Press.

Haliloglu, T. and Mattice, W. L. (1999). Detection of the onset of demixing in simulations of polypropylene melts in which the chains differ only in stereochemical composition. **The Journal of Chemical Physics** 111: 4327.

Hamley, I. W. (1998). **The Physics of Block Copolymer**. New York: Oxford University Press.

Harrats, C., Thomas, S. and Groeninckx, G. (2006). **Micro- and nanostructured multiphase polymer blend systems: Phase morphology and interface**. New York: CRC press.

Hu, Y., Hu, Y. S., Topolkaraev, V., Hiltner, A. and Baer, E. (2003). Crystallization and phase separation in blends of high stereoregular poly(lactide) with poly(ethylene glycol). **Polymer** 44: 5681-5689.

Huang, S. J. (1985). **Encycle polymer science and engineer 2: Biodegradable polymers**. New York: Wiley-Interscience.

Jia, Z., Tan, J., Han, C., Yang, Y. and Dong, L. (2009). Poly(ethylene glycol-co-propylene glycol) as a macromolecular plasticizing agent for polylactide: Thermomechanical properties and aging. **Journal of Applied and Polymer Science** 114: 1105-1117.

Jo, W. H. and Yang, J. S. (2002). Advances in polymer science: Molecular simulation fracture gel theory. New York: Springer-Verlag Berlin Heidelberge.

Kaitian, X., Kozluca, A., Denkbaş, E. B. and Pişkin, E. (1996). Poly(D, L-lactic acid) homopolymers: synthesis and characterization. **Trukis Journal of Chemistry** 20: 43-53.

Kulinski, Z., Piorkowska, E., Gadzinowska, K. and Stasiak, M. (2006). Plasticization of poly(L-lactide) with poly(propylene glycol). **Biomacromolecules** 7: 2128-2135.

Lazzari, M., Liu, G. and Lecommandoux, S. (2006). **Block copolymer in nanoscience**. Berlin: John Wiley & Sons, Inc..

Ljungberg, N. and Wesslen, B. J. (2002). The effects of plasticizers on the dynamic mechanical and thermal properties of poly(lactic acid). **Journal of Applied and Polymer Science** 86: 1227-1234.

Ljungberg, N. and Wesslen, B. (2005). Preparation and properties of plasticizer poly(lactic acid) films. **Biomacromolecules** 6: 1789.

Loos, J., Bonnet, M. and Petermann, J. (2000). Morphologies and mechanical properties of syndiotactic polypropylene (sPP)/polyethylene (PE) blends. **Polymer** 41: 351-356.

Mattice, W. L., Helfer, C. A., Rane, S. S. Von meerwall, E. D. and Farmer, B. L. (2005). Some mechanisms for subtle influences of stereochemical composition on the physical properties of macromolecules. **Journal of Polymer Science: Part B: Polymer Physics** 43: 1271-1282.

Matyjaszewski, K., Shigemoto, T., Frechet, J. M. and Leduc, M. (1996). Controlled/“living” radical polymerization with dendrimers containing stable radicals. **Macromolecules** 29: 4167-4171.

Mecking, S. (2004). Nature or petrochemistry?- Biologically degradable materials. **Angewandte Chemie International Edition** 43: 1078-1085.

Mourad, A. I. (2010). Thermo-mechanical characteristics of thermally aged polyethylene/polypropylene blends. **Materials and Design** 31: 918-929.

Mykhaylyk, T. A., Collins, S. and Hamley, I. W. (2004). Ordered structures and phase transitions in thin films of polystyrene/polyisoprene block copolymer and blends with the corresponding homopolymers. **Journal of Materials Science** 39: 2249-2252.

Nair, L. S. and Laurencin, C. T. (2007). Biodegradable polymers as biomaterials. **Progress in Polymer Science** 32: 762-798.

Okada, M. (2002). Chemical syntheses of biodegradable polymers. **Progress in Polymer Science** 27: 87-133.

Rathi, S., Chen, X., Coughlin, E. B., Hsu, S. L., Golub, C. S. and Tzivanis, M. J. (2011). Toughening semicrystalline poly(lactic acid) by morphology alteration. **Polymer** 52: 4181-4188.

Ren, J. (2011). **Biodegradable poly(lactic acid): synthesis, modification, processing and applications**. Beijing: Tsinghua University press.

Santis, F. D., Pantani, R. and Titomanlio, G. (2011). Nucleation and crystallization kinetics of poly(lactic acid). **Thermochemica Acta** 522: 128-134.

Sheth, M., Ananda, K. R., Dave, V., Gross, R. A. and Mcchathy, S. P. (2006). Biodegradable polymer blends of poly(lactic acid) and poly(ethylene glycol). **Journal of Applied Polymer Science** 66: 1495-1505.

Singla, S. (2004). **Topological effects on properties of multicomponents polymer systems**. Ph. D. dissertation, Georgia Institute of Technology. Unnited State.

Siracusa, V., Rocculi, P., Romani, S. and Rosab, M. D. (2008). Biodegradable polymers for food packaging: a review. **Trend in Food Science and Technology** 19: 634-643.

Sperling, L. H. (2001). **Introduction to physical polymer science**. 3rd edition, New Jersy: John Wiley & Sons, Inc..

Takano, A., Kamaya, I., Takahashi, Y. and Matsushita, Y. (2005). Effect of loop/bridge conformation ratio on elastic properties of the sphere-forming ABA triblock copolymers: preparation of samples and determination of loop/bridge ratio. **Macromolecules** 38: 9718-9723.

Tseng, Y. C. and Darling, S. B. (2010). Block copolymer nanostructures for Technology. **Polymers** 2: 470-489.

Varennes, S., Charlet, G. and Delmas, G. (1984). Use of the lower critical solution temperature for the characterization of polymer mixtures and the study of their compatibility: Application to polyethylenes, polypropylene, and their copolymers. **Polymer Engineering & Science** 24: 98.

Venkatraman, S. S., Jie, P., Min, F., Freddy, B. Y. C. and Leong-Huat, G. (2005). Micelle-like nanoparticles of PLA–PEG–PLA triblock copolymer as chemotherapeutic carrier. **International Journal of Pharmaceutics** 298: 219-232.

Wanamaker, C. L. (2009). **Fully-renewable and degradable thermoplastic elastomers**. Ph. D. dissertation, University of Minnesota, United State.

Wasekaran, J. J., Curro, J. G. and Honeycutt, J. D. (1995). Theory for the phase behavior of polyolefin blends: Application to the polyethylene/isotactic polypropylene blend. **Macromolecules** 28: 6843-6853.

Watanabe, H., Sato, T. and Osaki, K. (2000). Concentration dependence of loop fraction in styrene-isoprene-styrene triblock copolymer solutions and

corresponding changes in equilibrium elasticity. **Macromolecules** 33: 2545-2550.

Yang, J., Zhao, T., Liu, L., Zhou, Y., Li G., Zhou, E. and Chen, X. (2006). Isothermal crystallization behavior of the poly(l-lactide) block in poly(l-lactide)-poly(ethylene glycol) diblock copolymers: Influence of the the PEG block as diluted solvent. **Polymer Journal** 38: 1251-1257.

Yu, L., Dean, K. and Li, L. (2006). Polymer blends and composites from renewable resources. **Progress in Polymer Science** 31: 576-602.

Zhang, Q. and Archer, L. (2002). Poly(ethylene oxide)/silica nanocomposites: Structure and rheology. **Langmuir** 18: 10435-10442.

CHAPTER II

LITERATURE REVIEW

2.1 Biodegradable polymers

Littering and waste disposal with regard to environmental pollution has created urgency and need to develop biodegradable materials that have comparable properties with current petrochemical polymeric materials at equivalent or lower cost. Biodegradable polymers have been proposed to replace conventional polymer to address environmental pollution in the past two decades (Gatenholm, Kubát, and Mathiasson, 1992; Gross and Kalra, 2002). Biodegradable materials (neat polymer, blended product, or composite) are obtained completely from renewable resources called “green polymeric material”. Renewable sources of polymeric materials offer an answer to maintaining sustainable development of economically and ecologically attractive technology. The innovations in the development of materials from biopolymers, the preservation of fossil-based raw materials, complete biological degradability, the reduction in the volume of garbage and compostability in the natural cycle, protection of the climate through the reduction of carbon dioxide released, as well as the application possibilities of agricultural resources for the production of biogreen materials are some of the reasons why such materials have attracted the public interest (Lörcks, 1998). The life cycle of compostable biodegradable polymers is represented in Figure 2.1.

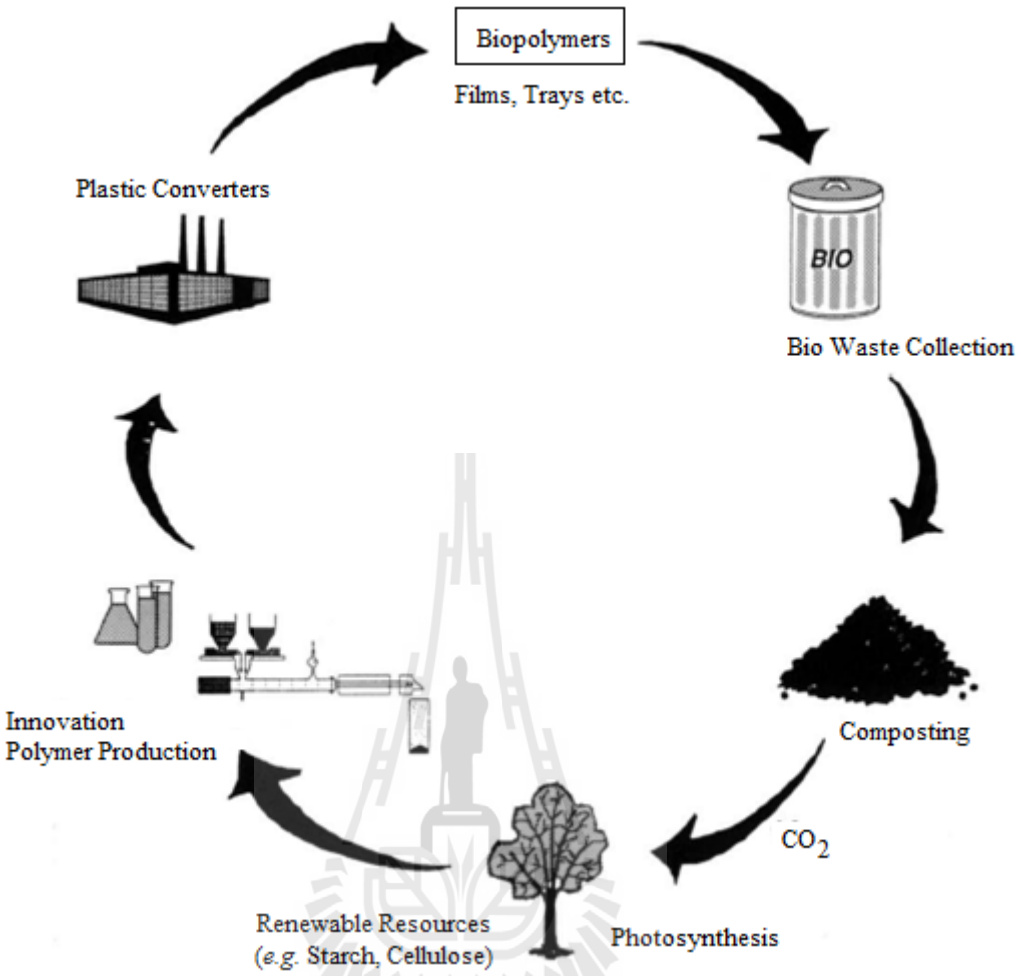

Figure 2.1 Life cycle of compostable, biodegradable polymers (Lörcks, 1998).

There are many types of biodegradable polymers which fall into two main categories. There are the biodegradable polymers which are naturally produced or based primarily on renewable sources (commonly starch) (Nampoothiri, Nair, and John, 2010). These include polysaccharides (starch, cellulose, etc.), proteins (gelatine, wool, silk, *etc*.), lipid fats (fats and oil), polyesters produced by plants or microorganisms (polyhydroxyalkanoates PHAs), polyesters derived from bioderived monomers (polylactic acid), and several miscellaneous polymers like natural rubbers and composites. The other type is non-renewable, synthetic, biodegradable plastics

which are petroleum based *i.e.*, polybutylene succinate (PBS) and polycaprolactone (PCL). Other polymers which are biodegradable but do not fit neatly into either category are polyanhydrides and polyvinyl alcohol.

2.2 Polylactic acid (PLA): Synthesis, properties and applications

PLA is the one of the first commodity polymers produced from annually renewable resources with excellent properties comparable to many petroleum-based plastics (Martin and Averous, 2001). Some of the environmental benefits of PLA and opportunities for the future are presented by many studies. These include PLA requiring less energy to produce as well as reduced greenhouse gas production. PLA resin has high mechanical properties, thermal plasticity, processing properties, and biocompatibility and has been proposed as a renewable and degradable plastic for uses in service ware, grocery, waste-composting bags mulch films, controlled release matrices for fertilizers, pesticides, and herbicides (Fang and Hanna, 1999). Furthermore, the many advantages of PLA can also be summarized from two review articles (Dorgan *et al*., 2000, Auras, 2004). These include:

- Production of the lactide monomer by fermentation of a renewable agricultural source (corn).
- Production consumes significantly carbon dioxide.
- Significant energy savings.
- The ability to recycle back to lactic acid by hydrolysis or alcoholysis.
- The capability of producing hybrid paper-plastic consumer packaging that is compostable.
- Reduction of landfill volumes.

- Improvement of farm economy.
- The physical and mechanical properties can be manipulated through the polymer architecture.

The synthesis of PLA is a multistep process which starts with the production of lactic acid and ends with its polymerization as shown in Figure 2.2. Lactic acid can be obtained either by carbohydrate fermentation or by common chemical synthesis. Also known as “milk acid”, it is the simplest hydroxyl acid with an asymmetric carbon atom and two optically active configurations, namely the L- and D- isomers (S-, R-) (Figure 2.3), which can be produced in bacterial systems (Gupta and Kumar, 2007), whereas mammalian organisms only produce the L isomer, which is easily assimilated during metabolism.

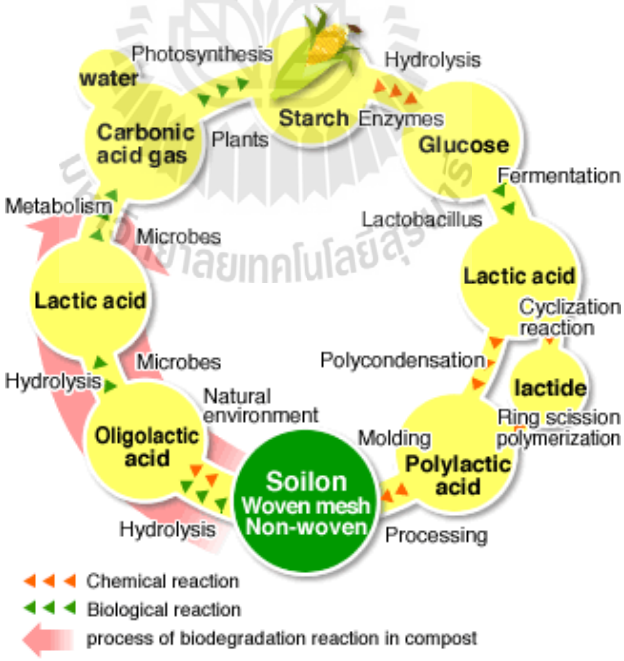

Figure 2.2 The cycle of PLA production (Sanguinisch, 2011).

PLA can be synthesized by several methods. The preferred route for the preparation of high molecular weight PLA is by ring opening bulk polymerization (ROP) of lactide as shown in Figure 2.3 (Södergård and Stolt, 2002). The reaction has been performed as melt or bulk polymerization, in solution or emulsion. A catalyst is always necessary to start the polymerization. Stannous (II) 2-ethylhexanoate ($SnOct_2$) is mostly used as catalysts. PLA can be either amorphous or semicrystalline, depending on the stereochemistry and thermal history. Poly(L-lactic acid) (PLLA) is semicrystalline polymer, exhibit high modulus, while poly(D-lactic acid) (PDLA) is an amorphous polymer. Generally, PLA have a T_g and melting temperature of about 55-60 ºC and 175-180 ºC, respectively. Commercial PLA are copolymers of PLLA and poly(D, L-lactic acid) (PDLLA), which are produced from L-lactides and D, L-lactides, respectively. The ratio of L- to D, L-enantiomer is known to affect the properties of the polymer obtained, such as melting temperature and degree of crystallinity. PLA polymers with L-content greater than 90% tend to be crystalline while those with lower optical purity are amorphous. This polymer complies with the rising worldwide concept of sustainable development and is classified as an environmentally friendly material. It has been recognized as the polymer with the greatest performance in application *i.e.*, biodegradable packaging, medical and pharmaceutical application (Södergård and Stolt, 2002; Gupta and Kumar, 2007).

Lactide, the cyclic dimer of lactic acid, is formed by the condensation of two lactic acid molecules as follows: L-lactide (two L-lactic acid molecules), D-lactide (two D-lactic acid molecules) and meso-lactide (an L-lactic acid and D-lactic acid molecule). Figure 2.4 shows the chemical structure of lactide monomer. (Södergård and Stolt, 2002).

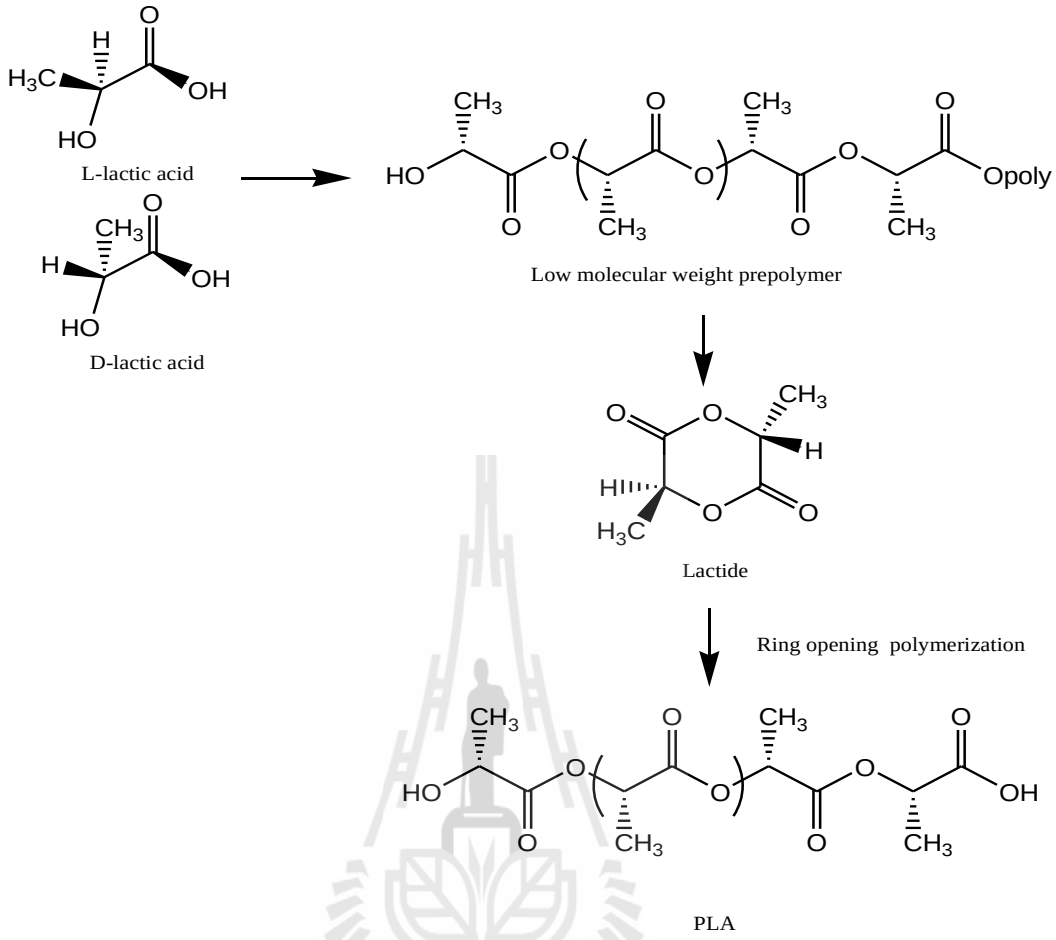

Figure 2.3 Ring opening polymerization for PLA synthesis (Södergård and Stolt, 2002).

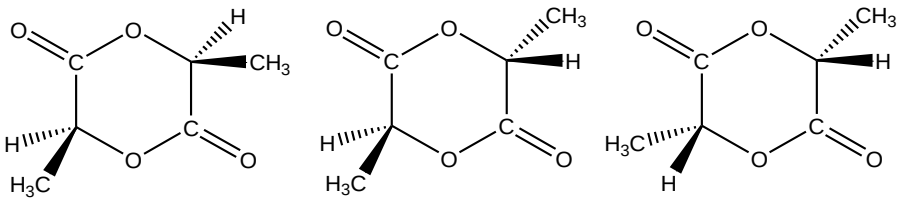

Figure 2.4 Chemical structures of LL-, Meso-, and D- lactides (m.p. is melting point) (Södergård and Stolt, 2002).

PLA has a balance of mechanical properties, thermal plasticity, biodegradeability, and is readily fabricated. It is thus a favored polymer for various end-uses. The physical properties of PLA are summarized in Table 2.1. When PLA is burned, it produces no nitrogen oxide gases and only one-third of the combustion heat generated by polyolefin.

Table 2.1 Physical properties of PLA (Doi and Steinbuchel, 2002)

Property	**Typical Value**
Molecular weight ($kg \cdot mol^{-1}$)	100-300
Glass transition temperature, T_g (°C)	55-70
Melting temperature, T_m (°C)	130-215
Heat of melting, ΔH_m ($J \cdot g^{-1}$)	8.1-93.1
Degree of crystallinity, X (%)	10-40
Surface energy (dynes)	38
Solubility parameter, δ $(J/ml)^{1/2}$	19.0-20.5
Density, ρ (kg/m^3)	1.25
Permeability of O_2 and CO_2 ($mol \cdot m^{-1} \cdot s^{-1} \cdot Pa^{-1}$)	4.25 and 23.2
Tensile modulus, E (GPa)	1.9-4.1
Yield strength (MPa)	70/53
Strength at break (MPa)	66/44
Flexural strength	119/88
Elongation at break (%)	100/180
Notched Izod impact strength ($J \cdot m^{-1}$)	66/18

The markets of PLA-based material are divided into three main groups, the biomedical (initial market), the textile (mainly in Japan) and the packaging (mainly food, *i.e.*, short-term applications) market. For instance, reported types of manufactured products are blow molding bottles, the injection molding cups, spoons and the forks, thermoformed cups and trays, fibers textile industry or sutures, films and various molded products (Doi and Steinbuchel, 2002).

2.3 Advantages and limitations of poly(lactic acid)

2.3.1 Advantages

- Biocompatibility. Most interesting feature of PLA, especially with the consideration focused on biomedical applications where biocompatibility with the human body is a requisite. A biocompatible material should not have toxic or carcinogenic effects in local tissues. In addition, the degradation products should not interfere with tissue healing. PLA hydrolyzes to its monomer α-hydroxy acid when degrading in living organisms, including the human body. It is then incorporated into the tricarboxylic acid cycle and digested. Moreover, PLA degradation products are non-toxic making it an ideal natural choice for biomedical applications (Kimura, Shirotani, Yamane, and Kitao, 1988).

- Ecological friendly. PLA is biodegradable. Derived from renewable resources, it is recyclable, and compostable. Its production also consumes carbon dioxide which is good in the light of the greenhouse effect. (Dorgan, Lehermeier, Palade, and Cicero, 2001). These special eco-friendly characteristics make PLA an attractive biopolymer.

- Energy concern. PLA need 25-55% less energy to be produced compared to petroleum-based polymers and estimations mean that these can be further reduced to less than 10% in the future (Vink, Rabago, Glassner, and Gruber, 2003). Lower energy use makes PLA production potentially advantageous with respect to cost as well.

2.3.2 Disadvantages

- Poor toughness. PLA is a very brittle material with less than 10% elongation at break (Hiljanen-Vainio, Varpomaa, Seppala, and Tormala, 1996; Rasal, and Hirt, 2008). With tensile strength and elastic modulus are comparable to polyethylene (PE) (Auras, Harte, and Selke, 2004), the poor toughness limits its use in applications that need plastic deformation at higher stress levels.

- Hydrophobicity. PLA is classified in relatively hydrophobic material, with a static water contact angle of approximately about 80º (Burg *et al*., 1999). This results in slow degradation, because PLA degrades through the hydrolysis of backbone ester groups. The slow degradation rate leads to a long life time, which could be up to years in some cases.

- Poor processibility. PLA has a poor processibility by itself because of its high crystallinity and limitation of mechanical properties by high brittleness. This is a limit for instance for processing steps such as film extrusion blow, blow mold extrusion etc.

2.4 PLA-based blends

As mentioned above, PLA needs to be modified for the specific end uses. Blending is the most widely used methodology to improve properties of polymers.

PLA is a brittle polymer that has poor elongation at break (<10%). Polymer blending has been used to dropping the glass transition temperature, increase ductility, and improve processibility. Hillmyer *et al*. (Wang and Hillmyer, 2001; Anderson, Lim, and Hillmyer, 2003) blended PLA with low density poly(ethylene) (LDPE) to improve the toughness. PLA crystallinity was found to significantly impact the blend toughness. Amorphous PLA blends with LDPE used PLA-LDPE diblock copolymer compatibilization, therefore semi-crystalline PLA blends with LDPE showed toughening even without the block copolymer. Gajria *et al.* (Gajria, Dave, Gross, and McCarthy, 1996) studied PLA-poly(vinyl acetate) (PVAc) blends, they were found to be miscible, that results showed improved tensile strength between 5 and 30 wt% PVAc, and improved elongation at break with 5 wt% PVAc. Martin and Averous (Martin and Averous, 2001) used glycerol, citrate ester, PEG, PEG monolaurate, and oligomeric lactic acid to plasticize PLA and found that oligomeric lactic acid and low molecular weight PEG (Mw~400 Da) gave the best results while glycerol was found to be the least efficient plasticizer. Citrate esters (molecular weight 276-402 Da) derived from naturally occurring citric acid were found to be miscible with PLA at all compositions. For these blends with citrate esters, elongation at break was significantly improved accompanied with considerable loss of tensile yield strength (Labrecque, Kumar, Dave, Gross, and McCarthy, 1997).

In 2003, Hu *et al.* (Hu, Rogunova, Topolkaraev, Hiltner, and Baer, 2003) to improve mechanical properties of PLA was blended with low molecular weight polyethylene glycol (PEG). The blending with up to 30 wt% of PEG was miscible at ambient temperature. However with PEG significantly decreased the T_g, decreased the modulus of PLA. Thermograms of PLA/PEG blend showed a single glass transition,

confirming that the blends were miscible. Increasing PEG content of the blend caused the T_g to decrease from 58 ºC for quenched PLA through ambient temperature to 9 ºC for PLA/PEG 70/30 blend. In case mechanical properties, the yield stress dropped to about 24 MPa and the elongation increased to nearly 200%. Blending with PEG significantly improved the softness of PLA and the elongation at break by decreasing the T_g. In the modifications of PLA that offer durable toughness and processibility improvements without significantly affecting biodegradability are critical.

2.5 PLA-based block copolymers

One of powerful for toughening PLA is block copolymerization. The synthesis of block copolymers is an effective strategy towards altering PLA's tensile properties. The most common copolymer architectures utilized for this purpose include statistical copolymers, ABA triblock copolymers, and AB multiblock copolymers, where the A block is PLA and the B block is a soft, low T_g polymer. The tensile properties of these copolymers generally have higher elongations than PLA and lower stiffness and strength. The many biodegradable polyesters that have been polymerized with PLA include those derived from renewable and non-renewable resources. Studies have been reported in which the properties of completely biodegradable copolymers containing a renewable resource polymer and a non-renewable resource polymer are presented, as described in the following subsections.

2.5.1 Polylactide/poly(ε-caprolactone) copolymers

Poly(ε-caprolactone) is the most common biodegradable polymer to copolymerize with polylactide. Relative to PLA, PCL is stable towards hydrolytic degradation; for example, PCL has been reported to lose only 30% of its initial

molecular weight after 45 weeks with no indication of mass loss after 60 weeks (Huang, Li, and Vert, 2004). A variety of PCL/PLA copolymers including AB diblock copolymers, AB multiblock copolymers, and random copolymers can be found in literature.

A series of PLLA–PCL–PLLA triblock copolymers was synthesized by polymerizing differing amounts of L-lactide off of a difunctional PCL of 2000 $g \bullet mol^{-1}$ molecular weight (Cohn and Hotovely Salomon, 2005). These triblock copolymers were then coupled to give PLLA-PCL multiblock copolymers. The tensile behavior of these thermoplastic elastomers was highly dependent on the morphology and composition of the copolymers. For all compositions, the tensile strength remained around 32 MPa, while the modulus ranged from 30 MPa to 800 MPa, and the elongation ranged from ~1600% to ~200% with increasing PLLA content. The influence of hydrolytic degradation on the properties of the multiblock copolymers was investigated. In vitro degradation (pH = 7.4 at 37 ºC) of the multiblock copolymers revealed significant loss of mechanical strength and elongation at break after about 8-9 weeks for all samples.

Statistical PCL/PLA and PCL/PLLA copolymers with varied compositions were synthesized by Hiljanen-Vainio *et al.* (Hiljanen-Vainio, Varpomaa, Seppala, and Tormala, 1996; Rasal and Hirt, 2008). The polymerization of PCL is much slower than that of PLA, and as a result the statistical copolymers were more “blocky” with minor amounts of random structure (3-20% random structure). Higher average sequence lengths and higher crystallinity resulted in higher tensile modulus and tensile strength. The copolymers ranged from weak elastomers (Young’s

modulus = 2.8 MPa, elongation >100%) to tougher thermoplastics (Young's modulus = 52 MPa, elongation = 30%).

2.5.2 Polylactide/poly(3-hydroxybutyrate) copolymers

Poly(3-hydroxybutyrate) are produced by bacterial fermentation and by transgenic microorganisms and plants. For the purpose of copolymerization with LLA, Hiki et al. have utilized synthetic P3HB. Synthetic P3HB has been synthesized from the ring-opening polymerization of a four-membered b-butyrolactone, a monomer derived from a non-renewable resource. Syndiotactic-rich (R, S)-P3HB, an elastomeric polymer due to low crystallinity, was utilized as the soft (B) segment in a PLLA-containing triblock copolymer. Copolymers of around 50% P3HB displayed tensile moduli ranging from 30 to 130 MPa, tensile strengths around 12 MPa, and elongations of 200% or lower (Hiki, Miyamoto, and Kimura, 2000).

2.5.3 Polylactide/poly(ethylene glycol) copolymers

Despite the fact that polyethylene glycol (PEG) is not a renewable resource polymer and does not degrade hydrolytically, it is included in this summary because of its use in biomedical hydrogels. PEG is a hydrophilic polymer and speeds up the degradation of PLA/PEG copolymers because it is able to bring water into the polymer (Sawhney, Pathak, and Hubbell, 1993). PLA/PEG copolymers have been utilized as drug-delivery carriers and medical devices. More recently, PLA–PEG–PLA triblock copolymer stereocomplexes have been investigated as drug-delivery devices because of their improved thermal and hydrolytic stability (Venkatraman, Jie, Min, Freddy, and Gan Leong-Huat, 2005).

Cohn and Hotovely-Salomon have synthesized multiblock PEG/PLLA thermoplastic elastomers and have investigated the changes in the mechanical

properties when the polymers are wetted. They found that these copolymers absorbed between 70% and 120% water, and even though the strength of the hydrated polymers were typically about one third that of their respective dry counterparts, these multiblock copolymers were still stronger than other biodegradable elastomers (Cohn and Hotovely-Salomon, 2005).

2.6 Computer simulation study

Since the development of the first computers in the early 1950's, scientists have tried to explore how these machines might be used in Chemistry. From the very beginning, the field of Computational Chemistry focused either on solving complex mathematical problems, typically quantum mechanical, or has tried to model the dynamical behavior of atomic and molecular systems. The boundaries between these two areas have never been well defined and, today, we see a convergence between quantum chemistry and simulation in studying chemical reactions (Curtiss *et al.*, 2004).

With advances in computer technology leading to ever faster computers, Computational Chemistry has become an increasingly reliable tool for investigating systems where experimental techniques still provide too little information. Ultra-fast spectroscopy can be used to follow fast reactions but only at a molecular level. A variety of diffraction techniques can also give detailed information about crystalline structure, but have difficulties monitoring changes at a molecular level. This is why the exponential growth in computer power has led to a corresponding growth in the number of computational chemists and in the variety of different computational techniques available for solving chemical problems: *ab initio* Quantum Mechanics

(QM), semi-empirical methods, Density Functional Theory (DFT), Monte Carlo (MC), Molecular Mechanics (MM), Molecular Dynamics (MD), QM/MM, Car-Parrinello, *etc*.

2.6.1 Molecular dynamics (MD) simulation

- **Theory of MD simulation**

In reality, atoms and molecules in solid materials are far from static unless the temperature is low; but even at 0 K, vibrational motion remains. MD allows us to simulate the dynamics of the particles in a well defined system to gain greater insights into local structure and local dynamics, such as drug and ion transport in polymeric materials (Accelrys, 2007).

In an MD simulation, atomic motion in a chemical system is described in classical mechanics terms by solving Newton's equations of motion:

$$\vec{F}_i = m_i \vec{a}_i \qquad (2.1)$$

For each atom *i* in a system of *N* atoms: m_i is their respective atomic mass; $\vec{a}_i = \frac{d^2\vec{r}_i}{dt^2}$ is their acceleration; and $\vec{F}_i$ is the force acting upon atom *i* due to interactions with all other particles in the system. The forces are generated from a universal energy potential *E*:

$$-\frac{dE}{d\vec{r}_i} = \vec{F}_i = m_i \frac{d^2\vec{r}_i}{dt^2} \qquad (2.2)$$

The basic idea of MD goes back to classical idea in Physics that if one knows the location of the particles in the Universe, and the forces acting between them, one is able to predict the entire future. In a normal MD simulation, this Universe comprises only a few thousand atoms; in extreme cases, up to a million.

With Newton's equations, it is possible to calculate sequentially the locations and velocities of all particles in the system. This generates a sequence of snapshots which constitutes a "movie" of the simulated system on the atomic scale. Due to the massive computer time necessary to solve these equations for a large number of particles, the movies are generally fairly short (in this work is in the pico- or nanosecond regime). All that is needed to solve the equations of motion are the masses of the particles and a description of the potentials, *E*.

In order to solve Equation (2.2), various kinds of numerical integration methods such as Gear, Verlet, and leapfrog have been developed. The Verlet algorithm is one of the simplest algorithms and at the same time one of the best for most cases. It gives good long time accuracy at the cost of a quite poor short time accuracy which leads to shorter allowed time steps. The memory usage of this integrator is as small as possible and it is also fast. This algorithm is based on particle position at time *t*, $r_i(t)$, acceleration at time *t*, $a(t)$, and the position from previous time $r_i(t-\Delta t)$, the new position of a particle after time Δt is given by:

$$r_i(t+\Delta t) = 2r_i t - r_i(t-\Delta t) + \Delta t^2 a(t) \qquad (2.3)$$

Then, the velocity at time *t* can be calculated by:

$$v(t) = \frac{r_i(t + \Delta t) - r_i(t - \Delta t)}{2\Delta t} \tag{2.4}$$

The Verlet algorithm uses no explicit velocities. The advantage of the Verlet algorithm is straightforward and the storage requirements are modest comprising two sets of positions ($r_i(t)$ and $r_i(t\text{-}\Delta t)$) and $a(t)$. The disadvantage is that the algorithm is of moderate precision. The leapfrog algorithm works stepwise by: Calculating the acceleration at time t according to Equation (2.2). Updating the velocity at time $t + \Delta t/2$ using

$$v(t + \frac{\Delta t}{2}) = v(t - \frac{\Delta t}{2}) + a(t)\Delta t \tag{2.5}$$

Calculating the atom position in the snapshot using

$$r_i(t + \Delta t) = r_i(t) + v(t + \frac{\Delta t}{2})\Delta t \tag{2.6}$$

In this way, the velocities *leap* over the positions, and then the positions *leap* over the velocities. The advantage of this algorithm is that the velocities are explicitly calculated, however, the disadvantage is that they are not calculated at the same time as the positions.

The MD simulation method is very straightforward, but one must bear in mind that it is based on some severe approximations. At the highest level, the Born-Oppenheimer approximation is made, separating the wave function for the electrons from those of the nuclei. The Schrödinger equation can then be solved for every fixed nuclear arrangement, given the electronic energy contribution. Together

with the nuclear-nuclear repulsion, this energy determines the potential energy surface, *E*. At the next level of approximation, all nuclei are treated as classical particles moving on the potential energy surface, and the Schrödinger equation is replaced by Newton's equations of motion. At the lowest level of approximation, the potential energy surface is approximated to an analytical potential energy function which gives the potential energy and interatomic forces as a function of atomic coordinates.

- **Force fields for MD simulations**

In the context of molecular modeling, a force field implies to the energy functions and parameter sets used to calculate the potential energy of a system of particles (*i.e.*, molecules and atoms). The energy functions and parameter sets are either derived from quantum chemistry calculations or empirically from experimental data. In MD simulation, the interaction of atoms, which might be connected through chemical bonds are calculated. Each atom is represented by a sphere with position vector ($\vec{r}$). The COMPASS (Condensed phase Optimized Molecular Potentials for Atomistic Simulation Studies) based on PCFF (Polymer Consistent Force-Field), and is the first ab initio force-field used for modeling interatomic interactions were used in this work. The potential energy of a system can be expressed as a sum of valence (or bond), crossterm, and non-bond interactions (Arenaza, Meaurio, Coto, and Sarasua, 2010; Accelrys, 2007):

$$E_{total} = E_{valence} + E_{crossterm} + E_{non\text{-}bond} \quad (2.7)$$

The energy of valence interactions ($E_{valence}$) comprises the bond stretching energy (E_{bond}), valence angle bending energy (E_{angle}), dihedral angle torsion energy ($E_{torsion}$),

and inversion energy (also called out of plane interactions and denoted as $E_{inversion}$ or E_{oop}) terms which are expressed as:

$$E_{valence} = E_{bond} + E_{angle} + E_{torsion} + E_{oop} \quad (2.8)$$

The energy of crossterm ($E_{crossterm}$) was used to account for such factors as bond or angle distortions caused by nearby atoms. These terms are required to accurately reproduce experimental vibrational frequencies and, therefore, the dynamic properties of molecules. In some cases, research has also shown them to be important in accounting for structural deformations. Cross terms can include the following: stretch-stretch, stretch-bend-stretch, bend-bend, torsion-stretch, torsion-bend-bend, bend-torsion-bend and stretch-torsion-stretch (Accelrys, 2007). Finally, the non-bond interaction term ($E_{non\text{-}bond}$) accounts for the interaction between non-bonded atoms (also called secondary interactions) and includes the van der Waals energy (E_{vdW}), the Coulomb electrostatic energy ($E_{coulomb}$) and the hydrogen bond energy ($E_{H\text{-}bond}$) as:

$$E_{non\text{-}bond} = E_{vdW} + E_{Coulomb} + E_{H\text{-}bond} \quad (2.9)$$

The first term in Equation (2.9) is van der Waals interaction which is usually computed by Lennard-Jones potential function. The Lennard-Jones potential is the most commonly used form:

$$V_{LJ}(r) = 4\varepsilon\left[\left(\frac{\sigma}{r}\right)^{12} - \left(\frac{\sigma}{r}\right)^{6}\right] \quad (2.10)$$

where ε is the depth of the potential well, σ is the finite distance at which the inter-particle potential is zero, r is the distance between the particles. Coulomb electrostatic energy ($E_{Coulomb}$) term calculates the electrostatic charges of the atoms pair which represented as:

$$V_{Coulomp}(r) = \frac{Q_1 Q_2}{4\pi\varepsilon_0 r} \tag{2.11}$$

where Q_1, Q_2 are the charges and ε_0 is the permittivity of free space. The H-bonding term is used to calculate the interaction of polar molecules in which hydrogen (H) is bound to a highly electronegative atom *i.e.*, nitrogen (N), oxygen (O) or fluorine (F). The detailing expression used to represent the energy surface of each is shown in the Appendix A.

- **Periodic boundary conditions and other requirements**

Since the computation time required for calculating the trajectories of all N particles in a simulation box increases with N^2, the simulated system cannot be made large enough to accurately represent the bulk properties of an actual crystal or amorphous material: surface effects will always be present. This problem is solved by implementing periodic boundary conditions, in which the simulation box is replicated through space in all directions; see Figure 2.5. The set of atoms present in the box is thus surrounded by exact replicas of itself, *i.e.* periodic images. If an atom moves through a boundary on one side of the simulation box, so will its replica on the other side. This keeps the number of atoms in one box constant, and if the box has constant volume the simulation then preserves the density of the system, which can affect the properties of the simulation, but much less than the surface effect would

have done without the periodicity. An MD simulation should also follow the laws of thermodynamics. At equilibrium, it should have a specific temperature, volume, energy, density, pressure, heat capacity, *etc.*

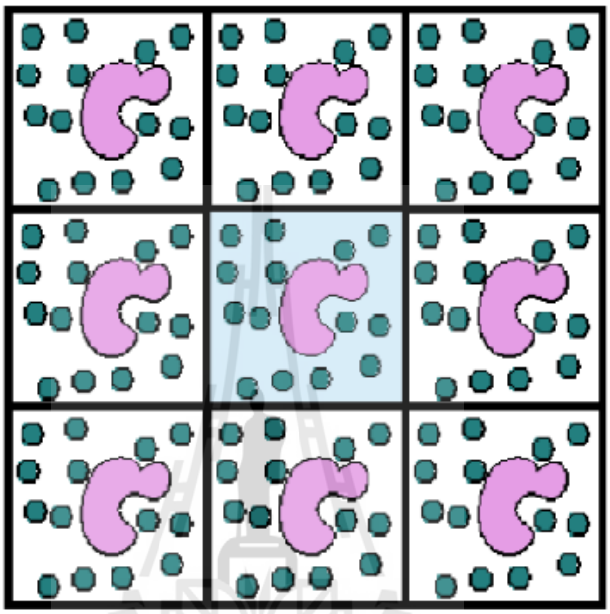

Figure 2.5 Periodic boundary conditions in Molecular Dynamics (CCL.NET, 1996).

In statistical thermodynamics, this constitutes the state of the system; its *ensemble*. Since MD is a statistical mechanics method, an evaluation of these physical quantities can be made from the velocities and masses of the particles in the system, and MD can serve as a link between these atomic-level quantities and macroscopic properties. When performing an MD simulation model is retained. This ensemble then scales the velocities of the particles. Three different ensembles have been used here:

- **The Microcanonical Ensemble (NVE)**; NVE maintains the system under constant energy (E) and with constant number of particles (N) in a well-

defined box with volume (V). This is appropriate during the initial equilibration phase of a simulation.

• **The Isothermal-Isobaric Ensemble (NPT)**; With NPT number of particles (N), temperature (T), and pressure (P) are kept constant. This is normally the best model of the experimental conditions.

• **The Canonical Ensemble (NVT)**; With NVT number of particles (N), volume (V), and temperature (T) are kept constant. This ensemble has been used for most simulations, so that comparisons can be made with experimental data from structures with fixed dimensions.

2.6.2 Monte Carlo (MC) simulation

MC method is a stochastic strategy that is relied on probabilities which gathers simplest in a random method. The simulation uses random numbers for making decision for enhance step during a run. In terms of molecular mechanics, MC simulation provides another way to explore a conformational space. This simulation can find a conformational state in a stochastic way by generating random numbers. For example, a given potential like Equation (2.12), the simulation involves a successive energy evaluation to make a decision for acceptance of a move attempt which is chosen randomly. The decision is accomplished by Metropolis algorithm (Metropolis *et al.*, 1953) in the most cases, which has the criteria as express in Equation (2.13).

$$V_{total} = \underbrace{V(r)_{bond} + V(\theta)_{angle} + V(\phi)_{torsion} + V(\chi)_{out-of-plane}}_{V_{bonded}} + \underbrace{V(r)_{vdw} + V(r)_{elec}}_{Vnon-bonded} \quad (2.12)$$

$$\Delta E = V(r)_{new} - V(r)_{old} \leq 0 \text{ (accepted)}$$

$$\Delta E = V(r)_{new} - V(r)_{old} > 0 \, AND \, \exp(-\Delta E / kT) \geq rand(0,1) \text{ (accepted)}$$

$$\Delta E = V(r)_{new} - V(r)_{old} > 0 \, AND \, \exp(-\Delta E / kT) < rand(0,1) \text{ (rejected)} \quad (2.13)$$

To consider the new state, if it is in a lower energy state, then, it will replace the previous state. If it is in a higher energy state, the energy difference between two states will be used to make a decision. MC simulation allows a system to move to higher energy state. The probability to overcome the higher energy barrier depends on the energy difference between the new and the current conformation. By such method, the ensemble averaged properties are calculated. One of the efforts to increasing the computational efficiency of MC simulation is to run the simulation on a suitable lattice, which reduces the floating number calculation. Another way to gain speed in the MC simulation is to use an efficient move algorithm that allows the faster relaxation. With such that way, many polymer beads can move at a single move attempt. The computational time of the lattice simulation based on MC method is proportional to the power of 1 to 2 depending on the quality of the potential energy function.

- **MC simulation of polymer chains on a high coordination lattice**

There is considerable interest in an application of Monte Carlo algorithm to determine the properties of large molecules. The approach was used for small flexible molecules and could be extended to large molecular weight materials such as polymers. However, the practice of changing randomly the torsional angle

leads to a high rejection rate. Even a relatively small change in the torsional angle in the middle of large flexible molecule results in a large translational displacement of the terminal atoms. Therefore, there is a high probability of molecular overlap resulting in the rejection of the move. The limitation of the small flexible molecule approach is determining Euler angles or using quaternion ions for each atom of a large molecule requires considerable computational effort.

- **Coarse graining of polymer model**

Often the energy state of a molecule can be described by a sum of energetic contributions of internal coordinates and non-bonded interactions. The bond stretching and angle bending are very strong effect due to the large force constants. They just slightly change with time and stay at the most probable bond length and bond angle. Since computational efficiency is indispensable for a polymer simulation, those terms are neglected in most cases. Accordingly, a property of a polymer chain is not dependent on the remaining energy terms, torsional energy and non-bonded energy. Furthermore, if a polymer chain is not perturbed by the existence of others, the importance of the long-range interaction is diminished. In that case, the partition function of a single chain can be expressed by only torsional partition function or conformational partition function, then the average of a property, <A>, can be written as Equation (2.14) - (2.16). The continuous torsional states can be grouped to have several discrete states. This assumption is reasonable because the discrete torsional states are separated by an activation barrier. These torsional states are called Rotational Isomeric State (RIS), the conformational partition function can be rewritten as the summation over the discrete conformational space as express in Equation (2.16).

$$Z = \int_{\phi_1} \ldots \int_{\phi_n} \exp\left(\frac{-E_{\phi_1 \ldots \phi_n}}{kT}\right) d\phi_1 \ldots d\phi_n \tag{2.14}$$

$$< A >= Z^{-1} \int_{\phi_1} \ldots \int_{\phi_n} \exp\left(\frac{-E_{\phi_1 \ldots \phi_n}}{kT}\right) A(\phi_1 \ldots \phi_n) d\phi_1 \ldots d\phi_n \tag{2.15}$$

$$Z = \sum_{\phi_1} \ldots \sum_{\phi_n} \exp\left(\frac{-E_{\phi_1 \ldots \phi_n}}{kT}\right) \tag{2.16}$$

The RIS model (Mattice and Suter, 1994) is a coarse grained polymer model, which only considers the discrete rotational isomeric states with other internal coordinates frozen. Schematically, the mapping from a realistic polymer chain to a RIS chain is illustrated in Figure 2.6. Figure 2.7 shows the structure of the high coordination lattice and the twelve coordination sites around a central bead. This coarse-grained lattice provides a better computational efficiency due to the reduction in the number of particles and in the number of conformational states, which facilitates its application to the fairly large polymeric systems. A further coarse-grained lattice from the RIS model can be obtained by discarding every second site from the tetrahedral lattice. The coarse graining generates a slanted cubic cell whose length is 2.5 Å in a, b, and c directions, and the angles between any two unit vectors are 60º.

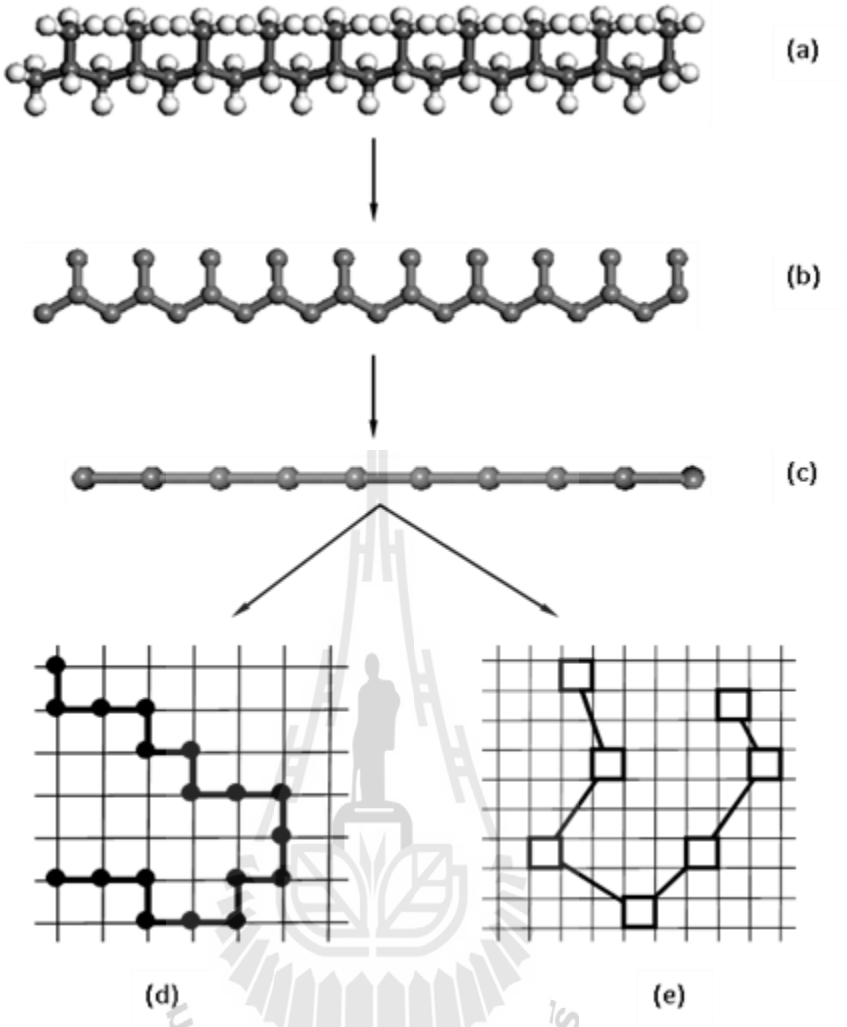

Figure 2.6 Schematic representations of different models of PP chains. (a) Fully atomistic model, (b) united atom model, (c) high coordination lattice model, (d) simple cubic lattice model, (e) bond fluctuation model, (d) and (e) are the representations in two dimensions (Mattice and Suter, 1994).

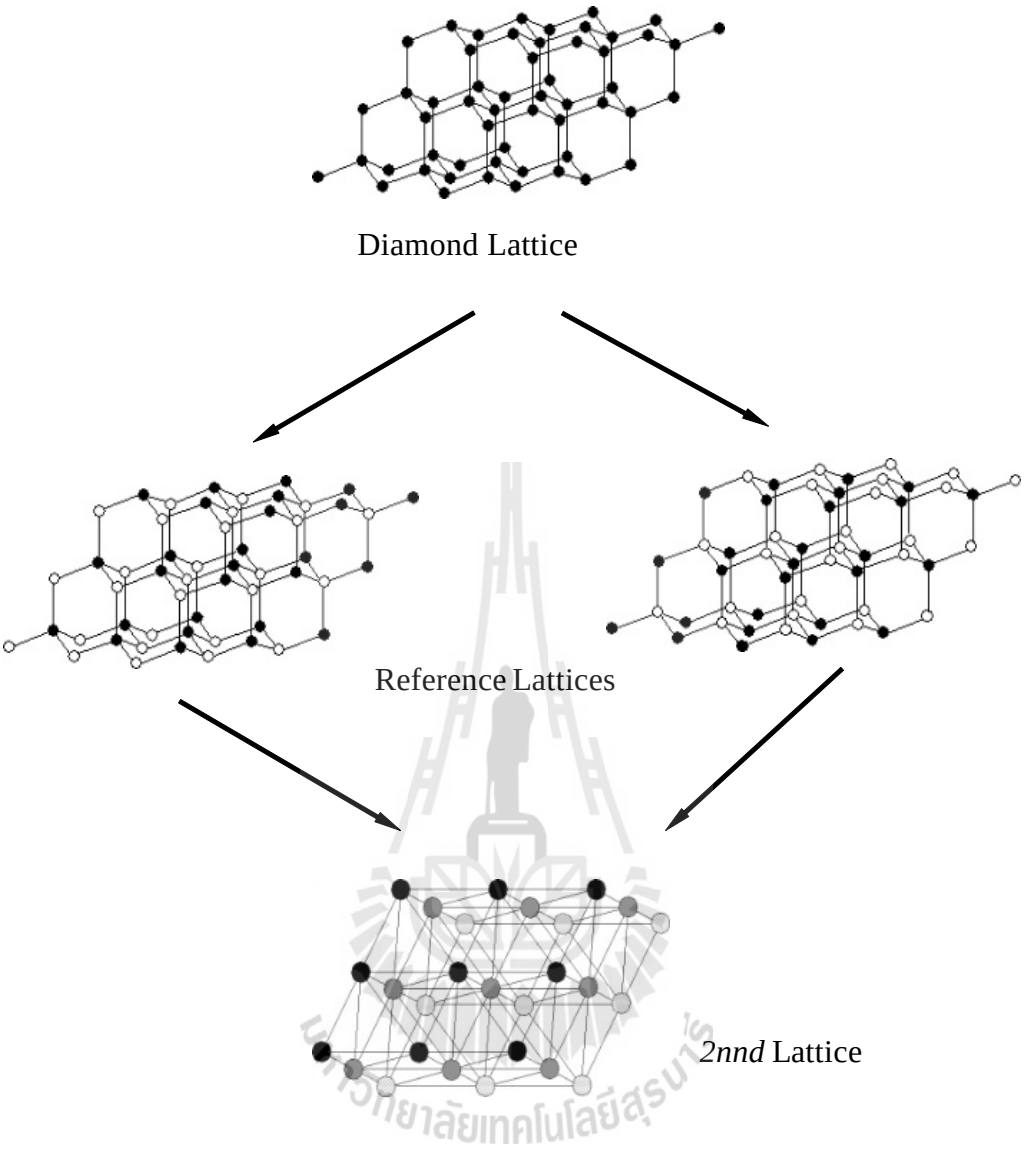

Figure 2.7 Construction of *2nnd* lattice from a diamond lattice (Mattice and Suter, 1994).

The modification produces a coordination number of 12 (or $10i^2 + 2$ sites in shell i), which is higher than that of the tetrahedral lattice. The high coordination number provides a flexibility to define a rotational state in the lattice. The new lattice is identical to the closest packing of uniform hard spheres and is named as the “second

nearest neighbor diamond (*2nnd*) lattice". Each occupied site in this model represents an ether ethylene (-CH_2-CH_2-) or propylene (-CH_2-CH-CH_3-) group.

- **Short-range intramolecular interaction of PE and PP chain**

A Hamiltonian consisting of two parts (short- and long-range interactions) is introduced into the simulation on the 2nnd lattice. The short-range interactions come from the local intramolecular contribution of the chain conformation, which is based on the RIS models to describe the nature of bead polymer chains. A RIS model for PE is defined by the following statistical weight matrix.

$$\mathbf{U} = \begin{bmatrix} 1 & \sigma & \sigma \\ 1 & \sigma & \sigma\omega \\ 1 & \sigma\omega & \sigma \end{bmatrix} \tag{2.17}$$

The unperturbed PE has the values E_σ, E_ω of 2.1, 8.4 kJ/mol, respectively.

$$\sigma = \exp(-E_\sigma / RT) \tag{2.18}$$

$$\omega = \exp(-E_\omega / RT) \tag{2.19}$$

The rows and columns of the matrix are the conformation state of $(i\text{-}1)^{th}$ bond and i^{th} bond, respectively. The orders of indexing are *t*, g^+ and g^-. The detailed description of the statistical weight matrix for coarse-grained PE bonds was discussed and summarized in a textbook written by Mattice and Suter.

In the case of PP, the specific RIS model is described the values for the short-range energies of E_η, E_τ and E_ω with 0.29, 3.9 and 8.0 kJ·mol^{-1}, respectively

(Suter *et al.*, 1975). Due to PP have different stereochemical sequences, *isotactic*, *syndiotactic* and *atactic*, it could be represented by the statistical weight matrix of diad, such as *m* and *r* diad. Different situations have the following statistical weight matrixes as expressed in Equation (2.20) and (2.21). During the simulations, the statistical weight matrixes are applied to calculate the partition function in the discretized form which express in Equation (2.22). Then the bond probability of a specific state, η, at bond *i* could be expressed by Equation (2.23).

$$U_d = \begin{bmatrix} \eta & 1 & \tau \\ \eta & 1 & \tau\omega \\ \eta & \omega & \tau \end{bmatrix}, U_l = \begin{bmatrix} \eta & \tau & 1 \\ \eta & \tau & \omega \\ \eta & \tau\omega & 1 \end{bmatrix}, U_{dd} = \begin{bmatrix} \eta\omega & \tau\omega & 1 \\ \eta & \tau\omega & \omega \\ \eta\omega & \tau\omega^2 & \omega \end{bmatrix},$$

$$U_{dl} = \begin{bmatrix} \eta & \omega & \tau\omega \\ \eta\omega & 1 & \tau\omega \\ \eta\omega & \omega & \tau\omega^2 \end{bmatrix}, U_{ld} = \begin{bmatrix} \eta & \tau\omega & \omega \\ \eta\omega & \tau\omega^2 & \omega \\ \eta\omega & \tau\omega & 1 \end{bmatrix} \quad (2.20)$$

$$U_{ll} = \begin{bmatrix} \eta\omega & 1 & \tau\omega \\ \eta\omega & \omega & \tau\omega^2 \\ \eta & \omega & \tau\omega \end{bmatrix} \quad (2.21)$$

$$Z = \prod_i U_i \quad (2.22)$$

$$p_{\eta;i} = \frac{Z_{\eta;i}}{Z} = \frac{U_1 U_2 \cdots U_{i-1} U'_{\eta;i} U_{i+1} \cdots U_n}{Z} \quad (2.23)$$

$$p_{\xi\eta;i} = \frac{Z_{\xi\eta;i}}{Z} = \frac{U_1 U_2 \cdots U_{i-1} U'_{\xi\eta;i} U_{i+1} \cdots U_n}{Z} \quad (2.24)$$

$$q_{\xi\eta;i} = \frac{p_{\xi\eta;i}}{p_{\xi;i-1}} \quad (2.25)$$

$$p_{\text{short}} = \frac{p_{\text{new}}}{p_{\text{old}}} = \frac{q^{-}_{\alpha\beta^*;i-1} q^{+}_{\beta^*\gamma^*;i-1} q^{-}_{\gamma^*\delta^*;i} q^{+}_{\delta^*\varepsilon^*;i} q^{-}_{\varepsilon^*\eta^*;i+1} q^{+}_{\eta^*\xi^*;i+1} q^{-}_{\xi^*\lambda;i+2}}{q^{-}_{\alpha\beta;i-1} q^{+}_{\beta\gamma;i-1} q^{-}_{\gamma\delta;i} q^{+}_{\delta\varepsilon;i} q^{-}_{\varepsilon\eta;i+1} q^{+}_{\eta\xi;i+1} q^{-}_{\xi\lambda;i+2}} \tag{2.26}$$

$$\Delta E_{\text{short}} = -RT \ln p_{\text{short}} \tag{2.27}$$

Similarly, the probability of two neighbor bonds, which have different states, for example, bond *i*-1 in ξ state and bond *i* in η state, can be written as Equation (2.24). The conditional probability $q_{\xi\eta;i}$, which is defined that bond *i* is in η state given the bond *i*-1 is in ξ state, has the following expression by Equation (2.25). During the simulation, the bond states change before and after moves. The probability of the move can be calculated by the conditional probability of C–C bonds by the Equation (2.26). Here, the asterisk denotes the new state. The difference of short-range interactions before and after move can be obtained by a logarithm expression.

- **Long-range intermolecular interaction**

The long-range interaction includes the intermolecular interaction and long-range intramolecular interaction, which can be obtained by modification of the classic technique for description of the second virial coefficient, B_2, of a non-ideal ethane (for PE) or propane (for PP) gas using the Mayer function, *f*, and the Lennard-Jones (LJ) potential energy function.

The long-range interaction is non-bonded interaction. On the *2nnd* lattice, the parameters for this interaction may be equal to parameters representing the interaction between one monomer at the origin and the other in the specified *2nnd* lattice site. A spherically symmetric potential is acting between two monomers.

According to the imperfect gas theory, the B_2 can be written as Equation (2.28) where $\beta = 1/kT$ and k is the Boltzmann constant. The f replaces the integral in Equation (2.28). On the *2nnd* lattice, B_2 is written in a descretized form by separating the integral into the sub-integrals for each lattice cell and regrouping them for each neighbor which are expressed in Equation (2.29). The volume element $\int_{\text{cell}} d\mathbf{r}$ is the volume V_c of one lattice cell of the *2nnd* lattice. The cell averaged Mayer function, $\langle f \rangle$, is introduced in Equation (2.30). In the calculation of $\langle f \rangle$, the center of the one monomer is allowed to be anywhere in the given lattice cell if the other one is fixed in the origin. Therefore Equation (2.29) could be rewritten as Equation (2.31). Here, z_i is the coordination number of the i^{th} shell with the form of $10\,i^2 + 2$. The overall average Mayer function is the arithmetic mean of $\langle f \rangle$.

$$B_2 = \frac{1}{2}\int \{\exp[-\beta u(r)] - 1\} d\mathbf{r} = \frac{1}{2}\int f d\mathbf{r} \tag{2.28}$$

$$\begin{aligned} B_2 &= -\frac{1}{2}[-\int d\mathbf{r} + \sum_{1\text{st}}\int_{\text{cell}} f d\mathbf{r} + \sum_{2\text{nd}}\int_{\text{cell}} f d\mathbf{r} + \sum_{3\text{rd}}\int_{\text{cell}} f d\mathbf{r} + \cdots] \\ &= \frac{V_c}{2}[1 - \sum_{1\text{st}} \langle f \rangle_{1\text{st}} - \sum_{2\text{nd}} \langle f \rangle_{2\text{nd}} - \sum_{3\text{rd}} \langle f \rangle_{3\text{rd}} - \cdots] \end{aligned} , \tag{2.29}$$

$$\langle f \rangle = \int_{\text{cell}} f d\mathbf{r} \Big/ \int_{\text{cell}} d\mathbf{r} \tag{2.30}$$

$$B_2 = \frac{V_c}{2}[1 - z_1 \bar{f}_{1\text{st}} - z_2 \bar{f}_{2\text{nd}} - z_3 \bar{f}_{3\text{rd}} - \cdots] \tag{2.31}$$

$$\exp(-\beta u_i) - 1 = \bar{f}_{i\text{th}} \tag{2.32}$$

$$u = \begin{cases} \infty & r < 2.5\text{Å} \\ u_{\text{LJ}} = 4\varepsilon\left[(\frac{\sigma}{r})^{12} - (\frac{\sigma}{r})^{6}\right] & r \geq 2.5\text{Å} \end{cases} \tag{2.33}$$

Finally, the effective interaction parameter, u_i, representing the i^{th} neighbor is defined as Equation (2.32) in which only one interaction parameter is applied to a given shell. In this simulation, the LJ potential energy function with hard core is used to ensure the volume exclusion as shown in Equation (2.33).

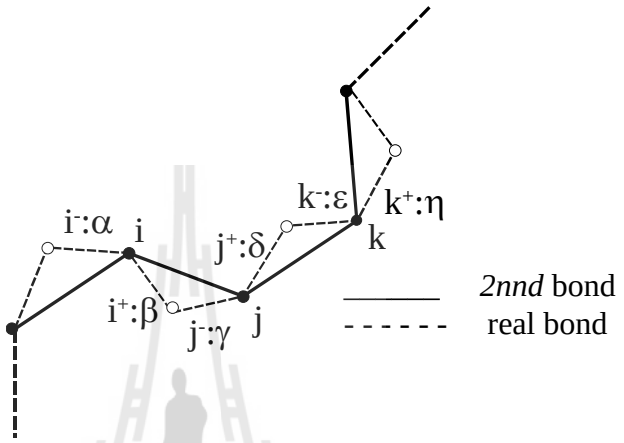

Figure 2.8 Schematic of representation a subchain on the *2nnd* lattice and the corresponding detailed backbone chain on the underlying diamond lattice.

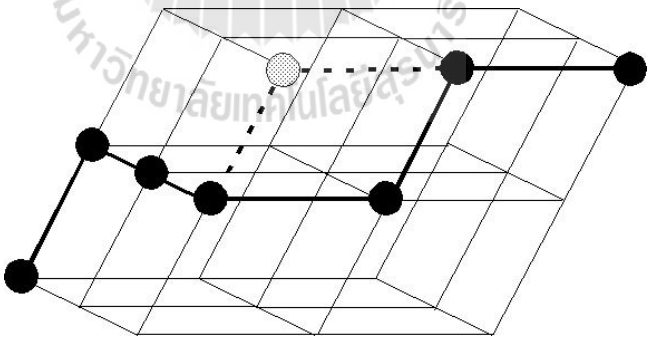

Figure 2.9 Schematic of representation for single bead move on *2nnd* lattice.

The parameters used in the simulations were the values from the experiments. For PE, the LJ parameters employed ε = 185 K, σ = 0.55 nm and interaction

energies between first (u_1), second (u_2) and third (u_3) neighboring shells were 16.214, 0.731 and -0.623 kJ/mol at 473 K, respectively. In case of PP, the input LJ potential used σ = 0.512 nm and ε/k_B = 237 K, which reproduced the experimental density of the melt at 473 K.

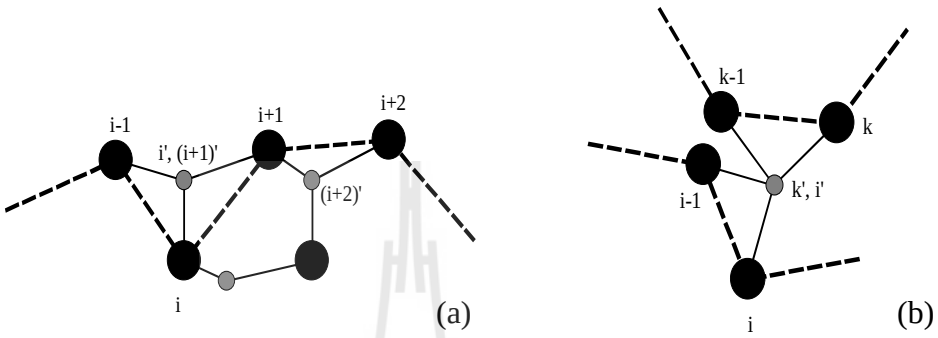

Figure 2.10 Schematic of representation for two kinds of unphysical collapses; (a) intramolecular collapse, and intermolecular collapse. i´ and i+1´ in (a), k´ and i´ in (b) occupy the same lattice site after reverse-mapping.

2.6.3 Moves

For every Monte Carlo Step (MCS), a single bead and pivot moves are performed. Every bead is tried once, on average, both in single bead moves and pivot moves, respectively. Therefore every bead is attempted twice, on average, within one MCS. Moves to cause double occupy and collapses are prohibited and the Metropolis rule with the following formalism is applied to determine whether the move is made or not.

$$P = \begin{cases} \exp(-\Delta E / RT) & \Delta E > 0 \\ 1 & \Delta E \le 0 \end{cases} \qquad (2.34)$$

ΔE is the energy difference between the new and old conformation, which includes the short- and long-range interactions. R is the universal gas constant and T is the absolute temperature. In case of $\Delta E \leq 0$, the move is accessed. Otherwise, a random number is generated to determine whether the move is successful or not

2.7 References

Accelrys. (2007). **Materials Studio** 4.2. San Diego.

Anderson, K. S., Lim, S. H. and Hillmyer, M. A. (2003). Toughening of polylactide by melt blending with linear low-density polyethylene. **Journal of Applied Polymer Science** 89: 3757-3768.

Arenaza, I., Meaurio, E., Coto, B. and Sarasua, J. R. (2010). Molecular dynamics modeling for the analysis and prediction of miscibility in polylactide/ polyvinilphenol blends. **Polymer** 51: 4431-4438.

Auras R., Harte B. and Selke S. (2004). An overview of polylactide as packaging material. **Macromolecular Bioscience** 4: 835-864.

Auras, R. A. (2004). Investigation polylactide as packaging material. Doctor of Philosophy, Michigan State University.

Burg, K. J. L. (1999). Parameters affecting cellular adhesion to polylactide films. **Journal of Biomaterials Science: Polymer Edition** 10: 147-161.

CCL.NET. (1996). **Molecular Dynamics and Monte Carlo**. [On-line]. Available: http://www.ccl.net/cca/documents/molecular-modeling/node9.html.

Cohn, D. and Hotovely-Salomon, A. (2005). Biodegradable multiblock PEO/PLA thermoplastic elastomers: molecular design and properties. **Polymer** 46: 2068-2075.

Cohn, D. and Hotovely Salomon, A. (2005). Designing biodegradable multiblock PCL/PLA thermoplastic elastomers. **Biomaterials** 26: 2297–2305.

Curtiss, L. A. and Gordon, M. S. (2004). **Computational Materials Chemistry: Methods and Applications**. London, Springer.

Doi, Y. and Steinbuchel, A. (2002). **Biopolymers, Application and Commercial Product-Polester**. Weinheim: Wiley-VCH.

Dorgan, J. R., Lehermeier, H. and Mang, M. (2001). Thermal and rheological properties of commercial-grade poly(lactic acid)s. **Journal of Polymers and the Environment** 8: 1-9.

Dorgan, J. R. and Williams, J. S. (1999). Melt rheology of poly(lactic acid): Entanglement and chain architecture effects. **Journal of Rheology** 43: 1141-1155.

Fang, Q. and Hanna, M. A. (1999). Rheological properties of amorphous and semicrystalline polylactic acid polymers. **Industrial Crops and Products** 10: 47-53.

Gajria, A. M., Dave, V., Gross, R. A. and McCarthy, S. P. (1996). Miscibility and biodegradability of blends of poly(lactic acid) and poly(vinyl acetate). **Polymer** 37: 437-444.

Gatenholm, P., Kubát, J. and Mathiasson, A. (1992). Biodegradable natural composites. I. Processing and properties. **Journal of Applied Polymer Science** 45: 1667-1677.

Gross, R. A. and Kalra, B. (2002). Biodegradable polymers for the environment. **Science** 297: 803-807.

Gupta A. P. and Kumar V. (2007). New emerging trends in synthetic biodegradable polymers (polylactide): A Critique**. European Polymer Journal** 43: 4053-4074.

Hiki, S., Miyamoto, M. and Kimura, Y. (2000). Synthesis and characterization of hydroxy-terminated [RS]-poly(3-hydroxybutyrate) and its utilization to block copolymerization with L-lactide to obtain a biodegradable thermoplastic elastomers. **Polymer** 41: 7369-7379.

Hiljanen-Vainio, M., Varpomaa, P., Seppala, J. and Tormala, P. (1996). Modification of poly(L-lactides) by blending: mechanical and hydrolytic behavior. **Macromolecular Chemistry and Physics** 197: 1503-1523.

Hu, Y., Rogunova, M., Topolkaraev, V., Hiltner, A. and Baer, E. (2003). Aging of poly(lactide)/poly(ethylene glycol) blends. Part 1. Poly(lactide) with low stereoregularity. **Polymer** 44: 5701-5710.

Huang, M. H., Li, S. and Vert, M. (2004). Synthesis and degradation of PLA-PCL-PLA triblock copolymer prepared by successive polymerization of ε-caprolactone and DL-lactide. **Polymer** 45: 8675-8681.

Kimura, Y., Shirotani, K., Yamane, H. and Kitao, T. (1988). Ring-opening polymerization of 3(S)-[(Benzyloxycarbonyl)methyl]-1,4-dioxane- 2,5-dione: a new route to a poly(a-hydroxy acid) with pendant carboxyl groups. **Macromolecules** 21: 3338-3340.

Labrecque, L. V., Kumar, R. A., Dave, V., Gross, R. A. and McCarthy, S. P. (1997).

Citrate esters as plasticizers for poly(lactic acid). **Journal of Applied Polymer Science** 66: 1507-1513.

Lörcks, J. (1998). Properties and applications of compostable starch-based plastic material. **Polymer Degradation and Stability** 59: 245-249.

Martin, O. and Averous, L. (2001). Poly(lactic acid) : plasticization and properties of biodegradable multiphase systems. **Polymer** 42: 6209-6219.

Mattice, W. L. and Suter, U. W. (1994). **Conformational theory of large molecules: The rotational isomeric state model in macromolecular systems**. New York: Wiley,

Metropolis, N., Rosenbluth, A. W., Rosenbluth, M. N., Teller, A. H. and Teller, E. (1953). Equation of State Calculations by Fast Computing Machines. **The Journal of Chemical Physics** 21: 1087-1092.

Nampoothiri, K. M., Nair, N. R. and John, R. P. (2010). An overview of the recent developments in polylactide (PLA) research. **Bioresource Technology** 101: 8493-8501.

Rasal, R. M. and Hirt, D. E. (2008). Toughness decrease of PLA-PHBHHx blend films upon surface-confined photopolymerization. **Journal of Biomedical Materials Research Part A** 88: 1079-1086.

Sanguinisch, O. (2011). **Bioplastics**. [On-line]. Avilable: http://oak-arc.blogspot.com.

Sawhney, A. S., Pathak, C. P. and Hubbell, J. A. (1993). Bioerodible hydrogels based on photopolymerized poly(ethylene glycol)-co-poly(.alpha.-hydroxy acid) diacrylate macromers. **Macromolecules** 26: 581-587.

Södergård, A. and Stolt, M. (2002). Properties of lactic acid based polymers an their correlation with composition. **Progress in Polymer Science** 27(6): 1123-1163.

Suter, U. W., Pucci, S. and Pino, P. (1975). Epimerization of 2, 4, 6, 8-tetramethylnonane and 2, 4, 6, 8, 10-pentamethylundecane, low molecular weight model compounds of polypropylene. **Journal of the American Chemical Society** 97: 1018-1023.

Venkatraman, S. S., Jie, P., Min, F., Freddy, B. Y. C. and Gan Leong-Huat. (2005). Micelle-like nanoparticles of PLA–PEG–PLA triblock copolymer as chemotherapeutic carrier. **Pharmaceutical Nanotechnology** 298: 219-232.

Vink, E. T. H. Rabago, K. R., Glassner, D. A. and Gruber, P. R. (2003). Application of lifecycle assessment to Nature Works ™ polylactide (PLA) production. **Polymer Degradation and Stability** 80: 403-419.

Wang, Y., and Hillmyer, M. A. (2001). Polyethylene-poly(L-lactide) diblock copolymers: synthesis and compatibilization of poly(Llactide)/polyethylene blends. **Journal of Polymer Science Part A: Polymer Chemistry** 39: 2755-2766.

CHAPTER III

PREPARATION AND CHARACTERIZATION OF POLY(LACTIC ACID) AND POLY(ETHYLENE GLYCOL) BASED BLOCK COPOLYMER AND BLENDS

3.1 Abstract

Triblock copolymers and polymer blends based on poly(lactic acid) (PLA) and poly(ethylene glycol) (PEG) were prepared to study their thermal and rheological properties. The series of PLA-PEG-PLA triblock copolymers with different LA/EG ratios were prepared by ring opening polymerization. Two kinds of stereochemical lactide (LA) monomer, L-LA and D, L-LA were used to prepare PLLA-PEG-PLLA and PDLLA-PEG-PDLLA block copolymers, respectively. PEG with $\overline{M}_w$ of 8,000 and 10,000 g·mol^{-1} was used as initiator polymerization. The chemical structure and composition of block copolymers were characterized by FT-IR, ^{1}H-, ^{13}C-NMR and GPC techniques. DSC thermograms revealed the microphase separation of PLLA-PEG-PLLA block copolymers at ϕ_{PLLA} of 0.37 and 0.47, observing two distinct melting peaks for the PLLA and PEG. This observation agrees well with XRD and POM data. The glass transition temperature (T_g) of PLA-PEG-PLA copolymers decreased as the LA/EG ratio decreased. Isothermal crystallization kinetic of PLLA-PEG-PLLA block copolymers was studied and the resulting data were analyzed with Avrami equation. The obtained Avrami exponent is equal to 2.53 in the crystallization

temperature range from 100 to 125 ^{o}C. This reflects that the crystallization process of PLLA segments in the block copolymer occurs in two-dimensional aggregates. For polymer blend study, the miscibility of PLLA/PEG and PLLA/PDLLA-PEG-PDLLA blends with varying PEG concentrations was investigated using DSC and rheological measurements. From DSC results, blending with PEG and PDLLA-PEG-PDLLA accelerated the crystallization of PLLA. When PLLA/PEG 70/30 (wt/wt) blend was slowly cooled from the melt, phase separation was observed due to the crystallization of PEG. However, this phenomenon was not observed in PLLA/PDLLA-PEG-PDLLA blend. In addition, the melting temperature (T_m) depression of PLLA/PDLLA-PEG-PDLLA blends was pronounced comparing with PLLA/PEG blends. These results indicate that PDLLA-PEG-PDLLA is more miscible with PLLA than PEG. Moreover, it was found that PDLLA-PEG-PDLLA at ϕ_{PDLLA} of 0.44 gave the most composition effective to plasticize PLLA. Rheological technique is also a powerful tool to study the miscibility of binary blend. PDLLA-PEG-PDLLA with ϕ_{PDLLA} of 0.44 was selected to blend with PLLA for rheological study. The rheological properties of these samples were studied at the melts. PLLA/PEG and PLLA/PDLLA-PEG-PDLLA samples at all composition exhibited the shear thinning behavior. Zero shear viscosity (η_0) decreased with increasing the plasticizer content and the decreased η_0 was pronounced in PLLA/PEG systems. To study the miscibility in polymer blends, storage modulus (G′) and loss modulus (G″) curves in terminal region were determined. The deviation of slope of G′ curve from 2 indicates that the binary mixture is immiscible. The slope of G′ curves for PLLA/PEG 75/25 and 70/30 (wt/wt) was less than 2 while this deviation was found at 70/30 (wt/wt) for

PLLA/PDLLA-PEG-PDLLA. This indicates that the PDLLA block in PDLLA-PEG-PDLLA copolymer was contributed to the PEG miscible in PLLA.

3.2 Introduction

Poly(lactic acid) (PLA) is a biodegradable polymer produced from annually renewable resources. Due to the excellent properties such as non-toxicity, biocompatibility, good mechanical properties and hydrolyzability, PLA has been using in a wide array of applications *i.e.*, biomedical and pharmaceutical fields, food packaging, textile (Auras, Lim, Selke, and Tsuji, 2010). PLA is most commonly synthesized by ring opening polymerization (ROP) of lactide with various metal catalysts (Leenslag and Pennings, 1987; Auras, Lim, Selke, and Tsuji, 2010; Mehta, Kumar, Bhunia, and Upadyay, 2005). Lactide (LA) is the cyclic dimer of lactic acid produced by fermentation from biomass such as corn and sugar beets. Due to the chirality of the lactic acid molecule, lactide has three enantiomers: L-lactide with two *S*-stereocenters, D-lactide with two *R*-stereocenters, and meso-lactide with one *S*-stereocenter and one *R*-stereocenter (Dechy-Cabaret, Martin-Vaca, and Bourissou, 2004; Auras, Lim, Selke, and Tsuji, 2010). The stereochemistry of lactide monomers significantly affects on thermal and mechanical properties of PLA. Polymerization of D- and L- lactide (D, L-lactide) mixture typically results in atactic, amorphous poly(D, L-lactic acid) (PDLLA) whereas polymerization of L-lactide or D-lactide results in isotactic, semicrystalline poly(L-lactide) (PLLA) or poly(D-lactide) (PDLA), respectively (Garlotta, 2001; Van de Velde and Kiekens, 2002).

PLA generally has a high modulus (~3 GPa), high strength (50-70 MPa) and good transparency comparing to other commodity thermoplastics like polyethylene

terephthalate (PET), polystyrene (PS) (Gupta and Kumar, 2007) making it is marketable material for packaging. While the stiffness of PLA is considered as an asset in some applications, a property issue that limits PLA's use on a broader scale is its low impact strength or brittleness. This drawback makes it unsuitable for using in the applications where elasticity and ductility are essential. Therefore, the studies have attempted to improve the elasticity and ductility of PLA. Strategies have been developed to improve the properties of PLA including block copolymerization (Lui and Zhang, 2011), blending (Eguiburu, Iruin, Fernandez-Berridi, and Roman, 1998) and plasticization (Kulinski, Piorkowska, Gadzinowska, and Stasiak, 2006). By the copolymerization of PLA with other monomers, a wide range of mechanical properties can be achieved. However, none of the copolymerization approaches is economically practical for many applications. Blending PLA with other polymers such as poly(hydroxybutyrate) (Koyama and Doi, 1995), poly(ethylene oxide) (Sheth, Kumar, Dave, Gross, and McCarthy, 1997) has been investigated, however only moderate improvement in mechanical properties was achieved because the polymer blends generally exhibit phase separation in the whole or part of the composition range. Other efforts have focused on finding a plasticizer for toughening PLA. It is evident that plasticization is most efficient and practical method to improve the processability, flexibility and ductility compared with other approaches. An efficient plasticizer has to reduce the glass transition temperature (T_g) and also to depress the melting point and the crystallinity. Numerous plasticizers for toughening PLA were intensively studied such as diethyl bishydroxymethyl malonate, glucose monoesters, citrate esters, oligomeric lactic acid and glycerol (Lemmouchi *et al*., 2009; Ljungberg and Wesslen, 2002, 2005; Jacobsen and Fritz, 1999). However, it was found that the

low molecular weight plasticizers tend to migrate from the bulk material to the film surface, ultimately leading to the blend regaining the inherent brittle properties of neat PLA. To address the migration, plasticizers with high molecular weight such as poly(ethylene glycol) (PEG), poly(propylene glycol) (PPG), poly(diethylene adipate) and oligoesteramide have been investigated (Hu, Hu, Topolkaraev, Hiltner, Baer, 2003; Kulinski, Piorkowska, Gadzinowska, and Stasiak, 2006; Ljungberg and Wesslen, 2002; Park, Hwang, Yoon, Yoo, and Im, 2012). However, these plasticizers, which commonly needs more than 20 wt% to get a satisfied result, lead to a drastic phase separation and degrade their mechanical properties.

PEG is well known as an efficient plasticizer for PLA because it is biocompatible polymer, good miscibility with PLA, low cost and more efficient to improve the ductility and flexibility of PLA (Kulinski, Piorkowska, Gadzinowska, and Stasiak, 2006; Sungsanit, Kao, and Bhattacharya, 2011; Pillin, Montrelay, and Grohens, 2006). Many studies have extensively investigated thermal and mechanical properties of PLA/PEG blends. The results demonstrated that the crystallization of PLA was accelerated by PEG depending on the composition of PEG in the blends (Hu, Hu, Topolkaraev, Hiltner, and Baer, 2003). Jacobsen and Fritz investigated the mechanical properties of the mixtures between PLA and 2.5–10 wt% of PEG (MW. $1.5x10^3$ g•mol^{-1}). They reported that the addition of PEG to PLA led to a decrease of both tensile strength and elasticity modulus but increased elongation at break (Jacobsen and Fritz, 1999). Although, PEG appeared to be an effective plasticizer for PLA, however there was evidence that the mixture was not stable with time because of the slow phase separation causing crystallization of PEG from homogeneous blends. This leads to a loss of the mechanical properties of the material (Hu, Hu,

Topolkaraev, Hiltner, and Baer, 2003; Hu, Rogunova, Topolkaraev, Hiltner, and Baer, 2003).

As previously mentioned, to minimize the migration and phase separation of plasticizers in the blend, plasticizer with high molecular weight and good miscible with polymer matrix are most desirable. Block copolymers, for which one part of block segment is identical or miscible within polymer matrix and another part is a chemical acting as plasticizer, have been proposed for use as plasticizer or compatibilizer (Hamley, 1998; Nakafuku and Takehisa, 2004). The identical block segment can be seen as a surfactant. Its function is to reduce the interfacial tension between plasticizer and polymer matrix and inhibits coalescence leading to reduction of the minor phase and they are dispersed as fine particles in the blend. There have been studies regarding the use of block copolymers as plasticizer (Anderson, Lim, and Hillmyer, 2002; Jia, Tan, Han, Yang, and Dong, 2009; Rathi *et al*., 2011; Hansen, Neilson, Hvilsted, 2004). For example, Hansen *et al*. investigated the miscibility of polystyrene and block copolymer mixture *i.e.* polystyrene-*b*-alkyl etc. DSC data showed that polystyrene was plasticized, as seen by a reduction in T_g, by block copolymers consisting of a polystyrene block with molecular weight of approximately 1 kg/mol and an alkyl block with a molecular weight of approximately of 0.3 kg/mol. Rathi *et al*. demonstrated that the improved mechanical properties of PLLA was achieved by incorporation of PDLA-PEG-PDLA block copolymer via stereocomplex mechanism of PLLA chain and PDLA block segments in the crystalline region.

Biodegradable block copolymer of PLA and PEG are being used in an increasingly large number of biomedical applications such as drug delivery matrices, flexible implants, substrates for cell culture and scaffolds for tissue engineering

(Kissel, Li, and Unger, 2001). PLA and PEG triblock copolymers could be synthesized as designed properties by varying chemical composition, molecular weight and block ratio which allows modification of physical and chemical properties. Therefore, block copolymers made from PLA and PEG have evoked considerable interest as plasticizer to toughen PLA.

Preparation and characterization of PLA homopolymer, PLA-PEG-PLA block copolymer and PLA/PEG and PLA/PLA-PEG-PLA blends are reported in this chapter. The characteristics of PLA and PLA-PEG-PLA triblock copolymer were evaluated by ^{1}H-, ^{13}C-NMR spectroscopy, Fourier transform infrared spectroscopy (FTIR) and gel permeation chromatography (GPC). Thermal properties of polymer samples were investigated by differential scanning calorimetry (DSC). The crystal structure of PLA and PLA-PEG-PLA copolymers were characterized by polarized optical microscope (POM) and X-ray diffraction (XRD) techniques. Rheological properties of PLA, PLA-PEG-PLA copolymers and PLA/PEG and PLA/PLA-PEG-PLA blends were investigated. In the case of polymer blends, data from DSC and rheological measurement were analyzed to evaluate the miscibility of the blends.

3.3 Materials and methods

3.3.1 Materials

- 3, 6-Dimethyl-1, 4-dioxane-2, 5-dione (D, L-lactide), 98%, Aldrich
- (3*S*)-*cis*-3, 6-Dimethyl-1, 4-dioxane-2, 5-dione (L-lactide), 98%, Aldrich
- Polyethylene glycol ($\overline{M}_w$ = ~8000 and ~10000 g.mol^{-1}), Aldrich.
- Tin(II)-2 ethylhexanoate ($Sn(Oct)_2$), 95%, Aldrich.

- Poly(L-lactic acid) (PLLA2002D, $\overline{M}_w$ = ~118,785 g.mol^{-1}), Nature Work.
- Toluene, Analytical grade, Merck.
- Dichloromethane, Analytical grade, Merck.
- Hexane, Analytical grade, Merck.
- Petroleum ether, Analytical grade, Acros.
- Diethyl ether, Analytical grade, Acros.
- Acetone, Analytical grade, Acros.

3.3.2 Analysis Instruments

- Proton and Carbon-13 Nuclear Magnetic Resonance (^{1}H and ^{13}C-NMR), JEOL NMR spectrometer. (Kyushu University, Japan)
- Fourier Transform Infrared spectrometer (FTIR), Spectrum One, Perkin Elmer. (Suranaree University of Technology, Thailand)
- Gel Permeation Chromatography (GPC), LC 20A, Shimadzu. (Khon Kaen University, Thailand)
- Differential Scanning Calorimeter (DSC), Pyris diamond, Perkin Elmer. (Suranaree University of Technology, Thailand)
- Polarized Optical Microscope (POM), ECLIPSE E600 POL, Nikon (Suranaree University of Technology, Thailand)
- X-Ray Diffractometer (XRD), D5005, Bruker. (Suranaree University of Technology, Thailand)
- Rheometer, MCR300, Anton Parr rheometer. (Kyushu University, Japan)

3.3.3 Methodology

- **Purification of the starting chemicals**

The high purity of lactide monomer and initiator, and the reduction of moisture in the reaction system are the keys to successfully obtaining high molecular weight polymer. Thus, the starting materials for the polymerization have to be purified.

Lactide was placed into a 250 ml of an Erlenmeyer flask. The minimum amount of ethyl acetate was added into the flask to dissolve lactide. The mixture was heated up to 70 ^{o}C until lactide was completely dissolved. The flask was then removed from heat and allowed to cool down at an ambient temperature and then lactide solution was placed in the refrigerator (0 ^{o}C) for 1 hour. Subsequently, it was taken out and the resulting crystals in the flask were scrapped with a spatula into Buchner funnel. Lactide crystals was washed with a hot diethyl ether and filtered. The recrystallization of lactide was repeated three times. Lactide crystals were then dried in vacuum oven for 48 hours and kept in desiccator.

Polyethylene glycol was place into a 250 ml of beaker. Acetone was slowly added until PEG was fully dissolved. The purpose of this step was to dissolve PEG in a minimum amount of solvent. Subsequently, PEG solution was slowly poured into an excess amount of petroleum ether. The precipitated PEG was transferred to Buchner funnel and then filtered. The obtained PEG was dried in vacuum oven for 48 hours.

Toluene used for polymerizations was purified by passing through the molecular sieve (3 Å) columns followed by azeotropic distillation.

- **Synthesis of PLA homopolymer**

Poly(L-lactic acid) (PLLA) and poly(D, L-lactic acid) (PDLLA) were synthesized by ring opening polymerization using $Sn(Oct)_2$ as the catalyst. Under nitrogen atmosphere, the predetermined amount of dried lactide was transferred into a 50 ml two-neck round-bottomed flask equipped with a stirrer. The flask was connected to a vacuum system and heated up to 50 ^{o}C for 12 hours in oil bath to eliminate residual water. After that, the system was evacuated and back filled with nitrogen gas more than three times and heated up to 130 ^{o}C. After the mixture was fully melted, a few amount of $Sn(Oct)_2$ (0.05 % w/w) in dried toluene was injected into the flask and maintained at 130 ^{o}C for 24 hours. This product was then dissolved in dichloromethane and precipitated in *n*-hexane. The dissolution and precipitation were performed at least three times. The isolated product was dried at 50 ^{o}C in vacuum oven for 48 hours.

- **Synthesis of PLA-PEG-PLA triblock copolymer**

Triblock copolymers of lactide (LA) and PEG were synthesized via ring opening polymerization using $Sn(Oct)_2$ as a catalyst. PEG with molecular weight ($\overline{M}_w$) of 8,000 and 10,000 g•mol^{-1}, represented as PEG8k and PEG10k, respectively, were used for polymerization. Two stereochemicals of lactide, L-lactide (LLA) and D, L-lactide (DLLA) were used to prepare the PLLA-PEG-PLLA and PDLLA-PEG-PDLLA, respectively. The molecular weight of these block copolymers was controlled by varying the ratio of LA monomer to PEG (LA/EG).

The predetermined amount of dried LA and PEG were introduced to the 50 ml two-neck round-bottomed flask equipped with a stirrer under nitrogen atmosphere. The mixture of LA and PEG was then dried at 50 ^{o}C by vacuum system

for 12 hours. The polymerizing flask was evacuated and back filled with nitrogen gas more than three times and heated up to 130 ^{o}C with stirring. After the mixture was fully melted, a few amount of $Sn(Oct)_2$ (0.05 % w/w) in dried toluene was injected into the flask. After a given amount of time, the reaction was removed from heating and placed under room temperature. The reaction equipments were set as Figure 3.1 (left). The polymer product was dissolved and precipitated in dichloromethane and diethyl ether. The polymer was filtered and dried under vacuum oven for 48 hours. The synthesis information of these copolymers is shown in Table 3.1. The notation of copolymer such as LLA_{71}-EG_{187}-LLA_{71} is represented by the PEG block with degree of polymerization (DP) of 187 connected to PLLA block with DP of 71.

Figure 3.1 (Left) the polymerization equipment set for synthesizing PLA-PEG-PLA and (right) the obtained PLA-PEG-PLA copolymer.

- **Preparation of PLA/PLA-PEG-PLA blends**

To study PLA/PLA-PEG-PLA blend, the commercial grade of PLA (PLLA2002D, Nature Work) was used as polymer matrix. Prior to blending, PLA and PLA-PEG-PLA were dried at 50 ^{o}C in vacuum oven for 24 hours. The mixture compositions of PLA/PLA-PEG-PLA with 90/10, 80/20, 70/30 and 50/50 were prepared by solution casting. The solutions of PLA and PLA-PEG-PLA (5 % w/v) were prepared by dissolution each polymer with dichloromethane. Each solution was then mixed together. The solution was cast on glass Petri dishes, and the solvent was allowed to evaporate at room temperature. All obtained films were further dried overnight under vacuum at room temperature to eliminate residual solvent. PLA/PEG blends were used as the control system.

- **Specimen Preparation**

The sample specimens for rheogical and mechanical measurement were prepared by compression molding. Prior to compression molding, the polymer was again dried in vacuum oven at 50 ^{o}C overnight. This was especially important to be completed before compression molding, as residual water in the blend may enhance the appearance of air bubbles in the samples. The layout of the compression molding is shown in Figure 3.2. Polymer was placed into the mold at room temperature. The compression molder was then heated up to 180 ^{o}C for neat PLA and polymer blends and 45 ^{o}C for PLA and PEG triblock copolymer. The temperature was maintained for 5 minute. The polymer was first pressed at low pressure for 1 min, followed by a high-pressure cycle at 40 MPa for 2-3 minute, and were then cooled under pressure (20 MPa) for 5-7 minute.

Figure 3.2 Compression molding machine.

3.3.4 Characterization

- **Fourier Transform Infrared Spectroscopy (FT-IR)**

Vibrational spectra of the polymer film were recorded on a Perkin Elmer (Spectrum One) FT-IR spectrometer. Polymer films were prepared by dissolving in toluene and coating on KBr disk. Samples were then dried in vacuum oven at 50 ^{o}C for 24 hours before measurement. The measurement was performed at a resolution of 4 cm^{-1} in the range of 4000-400 cm^{-1} for a total of 4 scans.

- **Nuclear Magnetic Resonance (NMR) Spectroscopy**

^{13}C and ^{1}H-NMR experiments were performed to investigate the chemical structure and block composition of the polymers. ^{13}C and ^{1}H-NMR spectra were collected at 395.75 and 99.45 MHz, respectively, on JEOL NMR spectrometer at

room temperature. 50 mg of polymer was dissolved by 600 μL of deuterated chloroform ($CDCl_3$) with 1% v/v of trimethylsilane (TMS).

- **Gel Permeation Chromatography (GPC)**

Molecular weight ($\overline{M}_w$ and $\overline{M}_n$) and molecular weight distribution (MWD) of the polymers were determined using Shimadzu LC 20A gel permeation chromatograph (Figure 3.3) equipped with the reflective index detector (RID-10A). A PLgel 5 mm MIXED-D column, with a guard column was used. The measurement was operated at 40 ^oC using tetrahydrofuran (THF) as a mobile phase with flow rate of 0.5 ml/min. Molecular weights of the polymers were obtained relative to polystyrene (PS) standards. A 40 μl of 15 mg/ml of polymer in THF was injected for each analysis.

Figure 3.3 Shimadzu LC 20A gel permeation chromatograph.

- **Different Scanning Calorimetry (DSC)**

DSC thermograms of polymers were recorded on a Perkin-Elmer (Pyris Diamond) instrument with nitrogen as the purge gas. An indium standard was used for calibration. Samples of 5.0-8.0 mg were loaded into aluminum pans and the pans were sealed prior to measurement. The sample was first heated from -50 ^{o}C to 180 ^{o}C with a heating rate of 10 ^{o}C/min and held there for 5 minutes to delete thermal history. After that, the sample was cooled down to -50 ^{o}C and then reheated to 180°C with a rate of 10 ^{o}C/min to record the second scan data. The glass transition temperature (T_g), the crystallization temperature (T_c), the degree of crystallinity (X_c) and the melting temperature (T_m) were determined in the second heating scan. In the case of PDLLA and their block copolymers, the range of testing temperature of 0 ^{o}C to 100 ^{o}C was carried out to investigate T_g, T_c, X_c and T_m.

Isothermal crystallization kinetics of PLLA and their copolymers at 120, 115, 110, 105 and 100 ^{o}C were investigated by DSC. The sample was heated to 200 ^{o}C with a heating rate of 10 ^{o}C/min, held there for 5 minutes and then cooled down with 100 ^{o}C/min to crystallization temperature. The samples were held at the crystallization temperature until no change in the heat flow.

- **Polarized Optical Microscopy (POM)**

A polarized optical microscope (Nikon ECLIPSE E600 POL) equipped with a hot stage was used to investigate the spherulitic morphology and growth of the crystal in neat PLLA and their blends. The samples were first placed between glass slides and melt on a hot stage at 200 ^{o}C for 3 min and then rapidly cooled at given crystallization temperature (T_c). The annealing lasted for given time periods. The polarized optical microscope is shown in Figure 3.4.

Figure 3.4 Polarized optical microscope model ECLIPSE E600 POL, Nikon.

- **Powder X-ray Diffraction (XRD)**

X-ray diffraction patterns of the polymers were recorded on a Bruker D5005. An X-ray generator was used to give Cu K_α radiation (λ=1.54 Å). The diffraction patterns were recorded at the room temperature between 2θ values of 2^o to 30^o.

- **Rheometer**

Rheological measurements were carried out on a rheometer (Anton Parr MCR300) equipped with a parallel plate geometry with a diameter of 8 mm. All measurements were performed under nitrogen atmosphere. The samples were dried in vacuum oven for 24 hours before measurement. The sample disks were melted at predetermined temperature for 5 min to eliminate the residual thermal history, and

then carry out experiments immediately. Dynamic strain sweep tests were carried out to confirm the linearity of the viscoelastic region up to 100% strain at 10 rad/s frequency. Frequency sweeps were carried out to determine the dynamic moduli and complex viscosity over a frequency range of 0.1-100 rad/s at 10% strain.

3.4 Results and discussion

3.4.1 Structure characterization

The molecular structure, number average molecular weight ($\overline{M}_n$) and molecular weight distribution (MWD) of PLA and PLA-PEG-PLA block copolymers was characterized by FT-IR, NMR and GPC techniques.

- **FT-IR Spectroscopy**

The molecular structures of synthesized polymers were confirmed by FT-IR spectroscopy. Here, only FT-IR spectra of L-lactide, PEG8k, PLLA and LLA_{71}-EG_{187}-LLA_{71} which shown in Figure 3.5 and 3.6 are reported. For synthesized PLLA (Figure 3.5), FT-IR spectra exhibit characteristic peaks of both PLLA and L-lactide at 3006-2885 cm^{-1} for -CH stretching, 1764-1759 cm^{-1} for -C=O stretching, ~1453 cm^{-1} for $-CH_3$ bending, and 1182-1095 cm^{-1} for -C-O-C- vibration of aliphatic chain. However, as expect, absorption peak at 936 cm^{-1} for -CO-O- ring of L-lactide could not appear in FT-IR spectrum of PLLA. This peak is the characteristics for lactide monomer and has been used to differentiate between PLA and lactide (Boua-in, Chaiyut, and Ksapabutr, 2010).

For block copolymer of LLA_{71}-EG_{187}-LLA_{71} (Figure 3.6), most of the FT-IR bands associated with PLA and PEG partially overlap with other bands in the spectra. For example, the sharp CH stretching bands of PEG block appear at 2952-

2743 cm^{-1}. The broad absorption bands about 3476 cm^{-1} is the -OH stretching which is correspond to the terminal hydroxyl groups of PEG. The characteristic of an ester group, -C=O stretching and -C-O stretching of lactide units appear at 1769 cm^{-1} and 1100 cm^{-1}, respectively. The bands at 1472-1054 cm^{-1} are referred as CH bending. The bands at 962-863 cm^{-1} are known to be the characteristics of the PEG crystalline phase, while the bands at 796-746 cm^{-1} are assigned to the amorphous phase of lactide blocks. One can expect from FT-IR spectra of block copolymer is the shift of the band frequency of ~1760 cm^{-1} (-C=O stretching) to lower frequency compared to lactide monomer. It is evident that the vibrational frequency of -C=O stretching of LLA_{71}-EG_{187}-LLA_{71} shift to lower frequency (1760 to 1750 cm^{-1}). This result suggests that the PLA and PEG blocks are connected together.

- **^{1}H and ^{13}C-NMR NMR Spectroscopy**

^{1}H and ^{13}C-NMR were employed to verify the molecular structure and determine the $\overline{M}_n$ of synthesized polymers. NMR spectra of starting chemicals including PEG and lactide were used as a reference. The ^{1}H-NMR spectra of lactide, PEG, PLA and PLA-PEG-PLA were illustrated in Figure 3.7-3.10.

^{1}H-NMR spectrum of PEG8k is shown in Figure 3.7. The single peak at a chemical shift (δ) = 3.65 ppm represents a methylene protons (-CH_2) from the ethylene glycol (EG) units however the resonance of α-methine protons (-OH) of the hydroxyl chain end at $\delta \approx 4.87$ ppm is not observed.

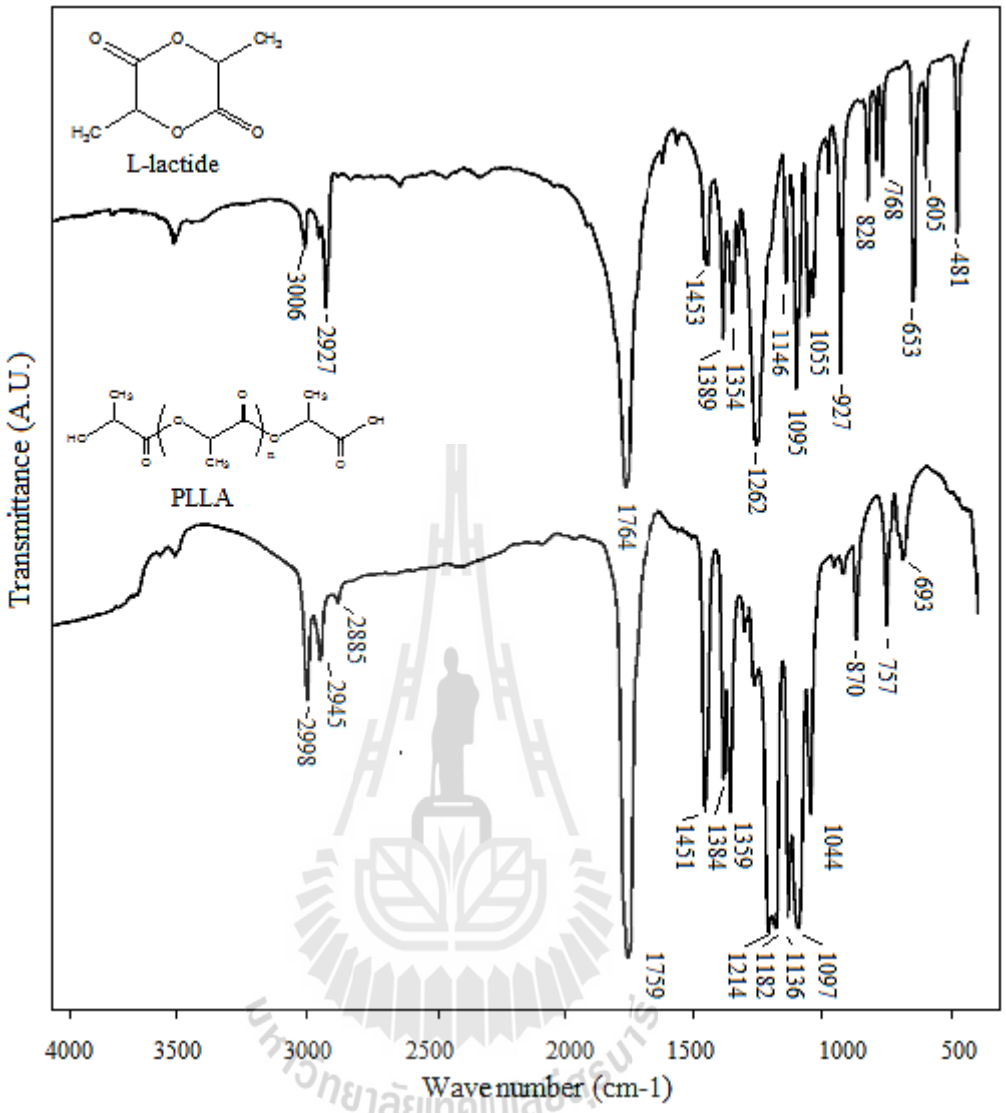

Figure 3.5 FT-IR spectra of L-lactide monomer and neat PLLA.

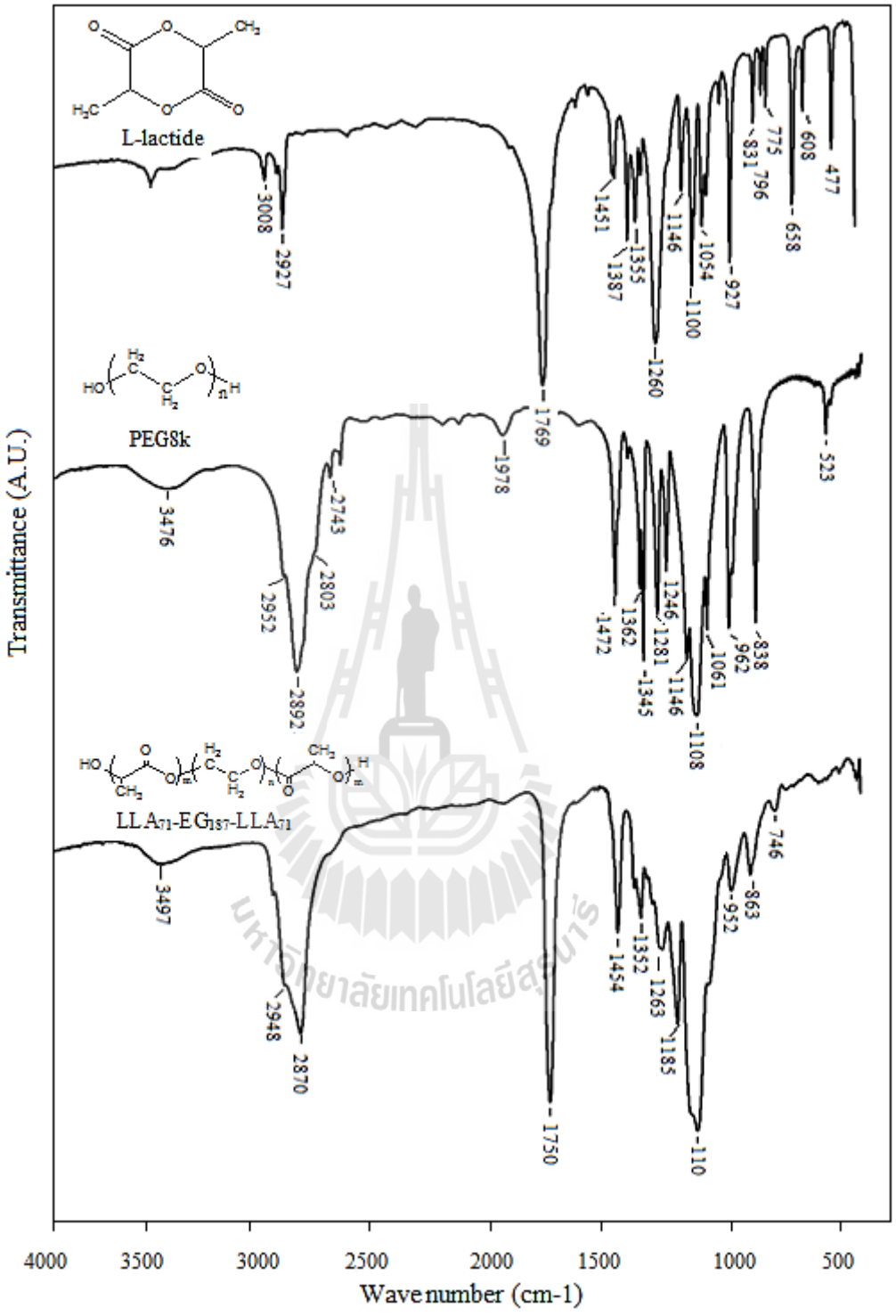

Figure 3.6 FT-IR spectra of L- lactide monomer, PEG8k and LLA_{71}-EG_{187}-LLA_{71} block copolymer.

- **^{1}H and ^{13}C-NMR NMR Spectroscopy**

^{1}H and ^{13}C-NMR were employed to verify the molecular structure and determine the $\overline{M}_n$ of synthesized polymers. NMR spectra of starting chemicals including PEG and lactide were used as a reference. The ^{1}H-NMR spectra of lactide, PEG, PLA and PLA-PEG-PLA were illustrated in Figure 3.7-3.10.

^{1}H-NMR spectrum of PEG8k is shown in Figure 3.7. The single peak at a chemical shift (δ) = 3.65 ppm represents a methylene protons (-CH_2) from the ethylene glycol (EG) units however the resonance of α-methine protons (-OH) of the hydroxyl chain end at δ ≈ 4.87 ppm is not observed.

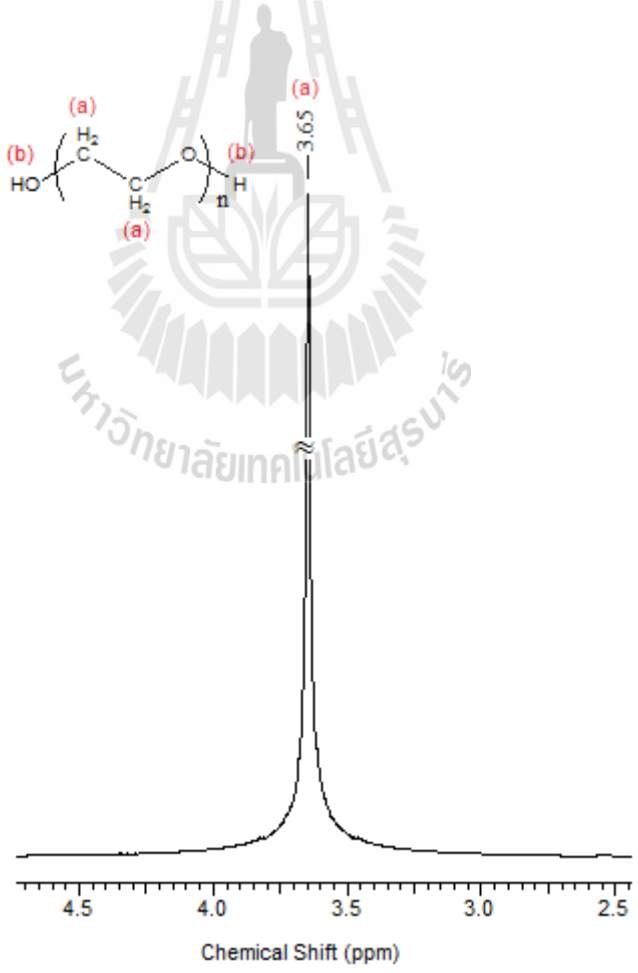

Figure 3.7 Typical ^{1}H-NMR spectrum of PEG8k in $CDCl_3$ at 25 ^{o}C.

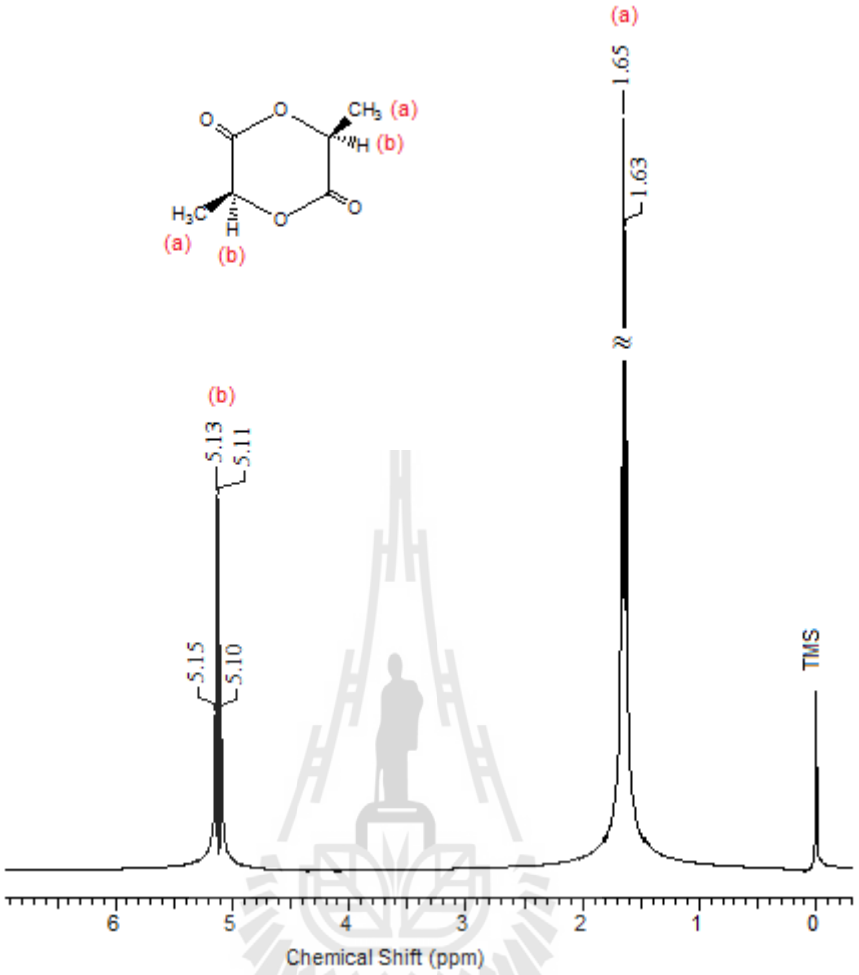

Figure 3.8 Typical ^{1}H-NMR spectrum of L-lactide in $CDCl_3$ at 25 ^{o}C.

^{1}H-NMR spectrum of L-lactide is shown in Figure 3.8. The doublet signals at δ = 1.65-1.65 ppm and quartet signals at δ = 5.15-5.10 ppm are assigned to methyl protons (-CH_3) and methine protons (-CH), respectively. These observation are quite similar to ^{1}H-NMR spectrum of PLLA with $\overline{M}_n$ = 13,773 g.mol^{-1} shown in Figure 3.9. ^{1}H-NMR spectrum of PLLA shows the doublet peak at δ = 1.59 and 1.58 ppm and quartet peak at δ ≈ 5.19 ppm correspond to the proton resonance of -CH_3 and

-CH groups, respectively. However, the terminal protons of -CH_3, -CH and -OH groups were not observed because the amount of these protons were small.

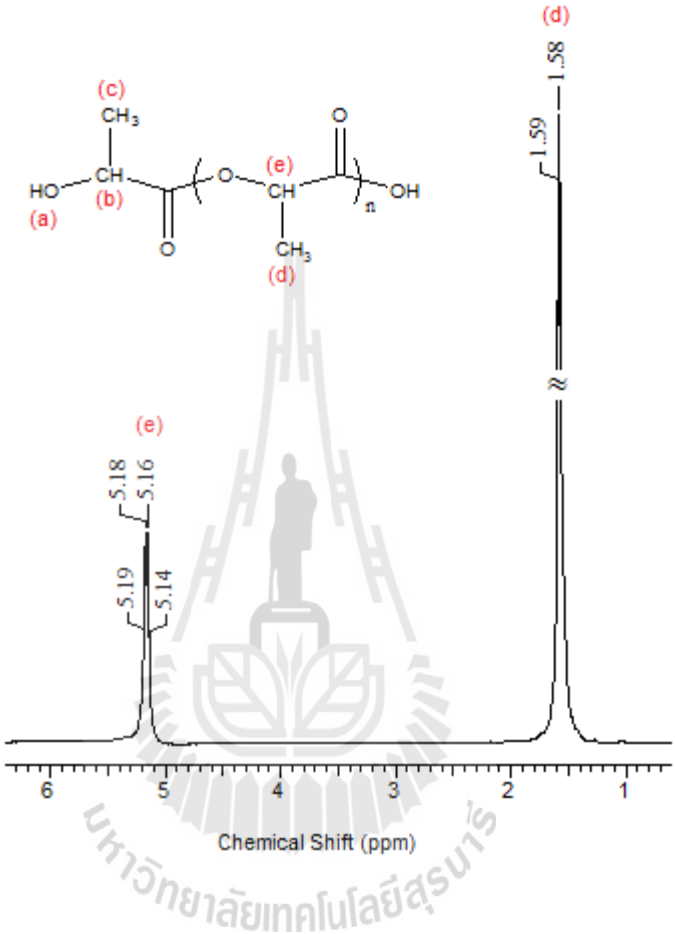

Figure 3.9 Typical ^{1}H-NMR spectrum of synthesized PLLA in $CDCl_3$ at 25 ^{o}C.

NMR spectra of PLLA-PEG-PLLA triblock copolymers with different LA/EG ratios of 0.34, 0.42 and 0.78 are illustrated in Figure 3.10 (a), (b) and (c), respectively. The peak at $\delta \approx 4.37$ ppm is denoted to the α-methylene protons of PLA connecting EG units (PLA-COO-CH_2-), together with CH protons of the hydroxylated lactyl end units. Resonances in the range of 5.20 - 5.14 ppm range (-CH) and 1.5-1.4 ppm (-CH_3) are belonged to PLA blocks, including both PEG

connecting and main chain units. Signal at δ ≈ 3.6 ppm is the characteristics of main chain methylene units within PEG blocks. The signals of carboxylated lactyl end units and free lactide of which methine protons should appear in the 5.0-4.9 ppm range and at 4.03 ppm were not observed. This indicates that homopolymerization of L-lactide did not occur under the selected polymerization conditions (Du, Lemstra, Nijenhuis, Aert, and Bastiaansen, 1995; Rashkov, Manolova, Li, Espartero, and Vert, 1996).

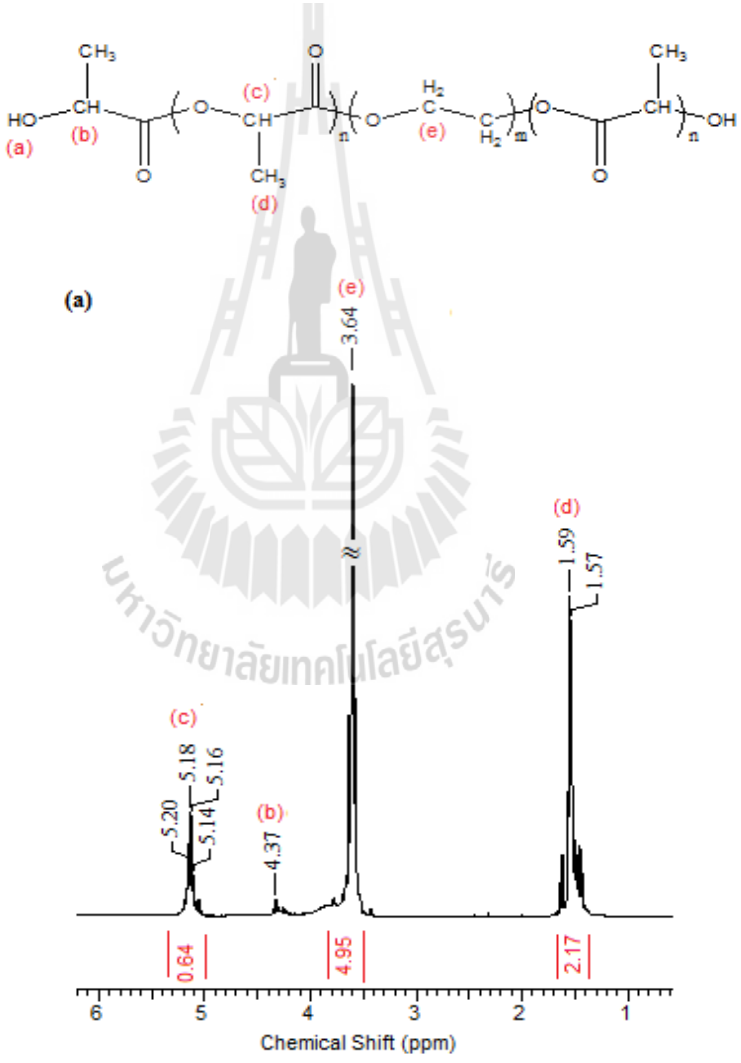

Figure 3.10 Typical ^{1}H-NMR spectra of (a) LLA_{49}-EG_{187}-LLA_{49}, (b) LLA_{71}-EG_{187}-LLA_{71} and (c) LLA_{347}-EG_{187}-LLA_{347} in $CDCl_3$ at 25 ^{o}C.

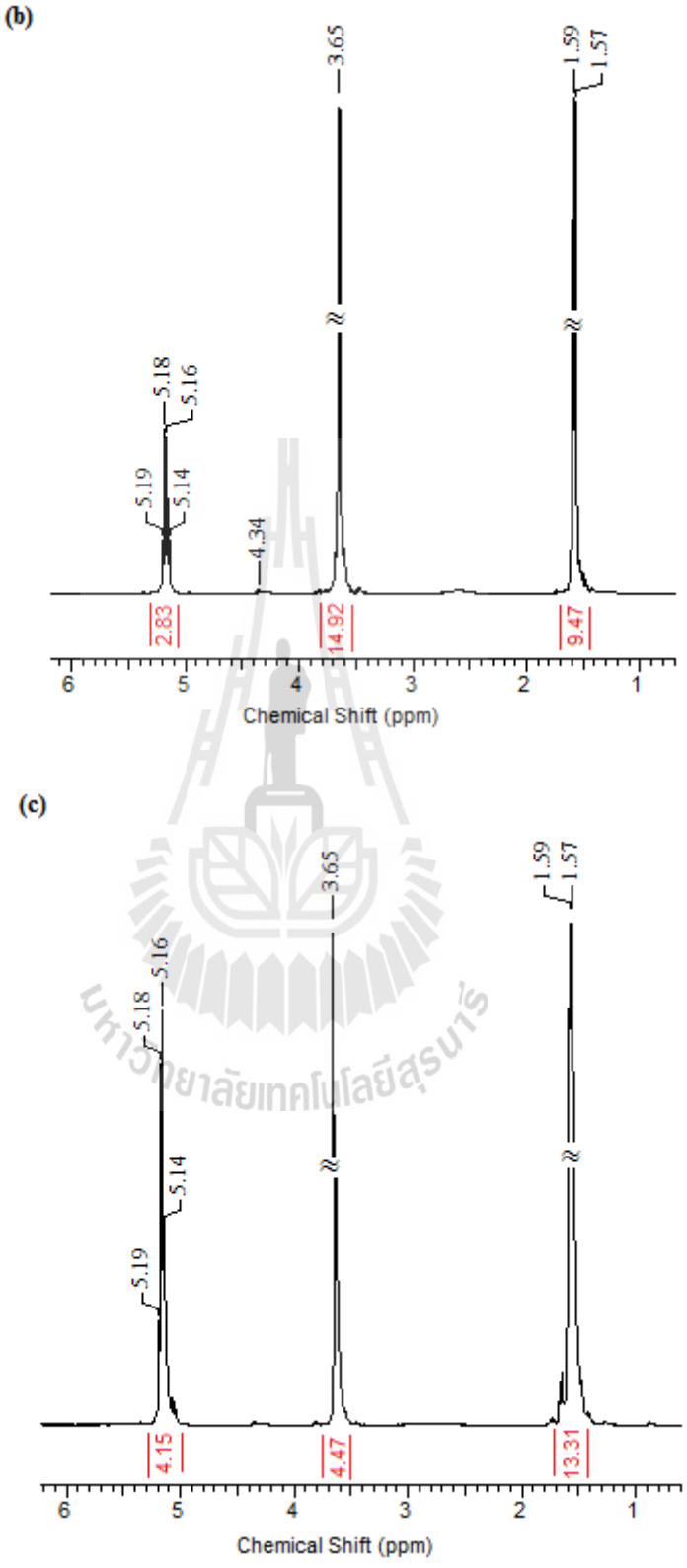

Figure 3.10 (Continued).

^{13}C-NMR technique was also performed to confirm the molecular structure of these copolymers. A typical ^{13}C-NMR spectrum of LLA_{71}-EG_{187}-LLA_{71} (LA/EG = 0.76) shown in Figure 3.11 reveals the presence of different carbon atoms belonging to various type units (a-i). In comparison with the spectra of PEG and PLA (not shown here), it is clear that peaks at 16.46, 68.89, and 169.54 ppm are corresponded to -CH_3, -CH, and -C=O in PLA segments, respectively, and the peak at 70.45 ppm corresponds to -CH, in PEG segments of the copolymer.

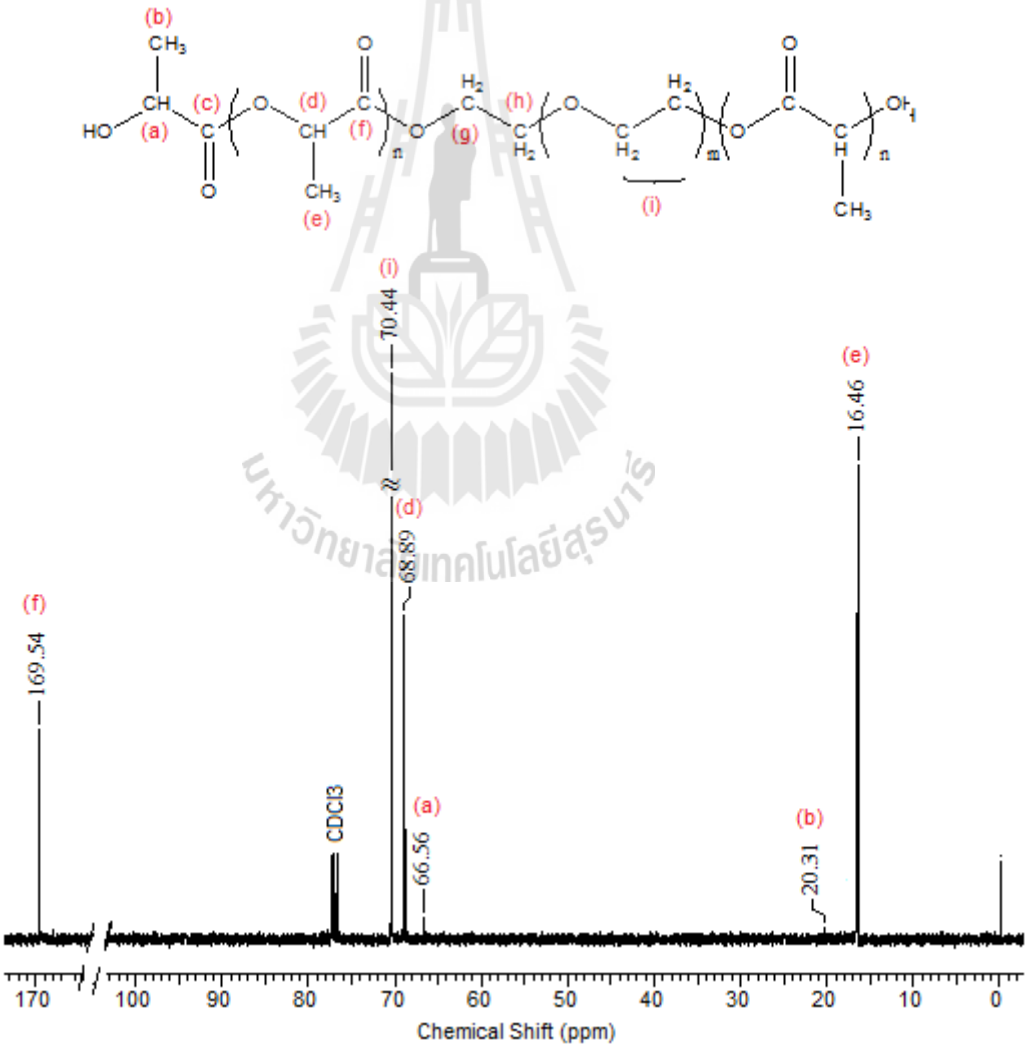

Figure 3.11 Typical ^{13}C-NMR spectrum of LLA_{71}-EG_{187}-LLA_{71} in $CDCl_3$ at 25 ^{o}C.

The peaks at 20.31 and 66.56 ppm are assigned to -CH_3 and -CH of the chains end. As the results from ^{1}H and ^{13}C-NMR, it can be conclude that the block copolymer was successfully synthesized as expected.

In addition, ^{1}H-NMR technique was utilized to evaluate molecular weight ($\overline{M}_n$) of block copolymer using the following relationship.

$$\overline{M}_{n(PLA\text{-}PEG\text{-}PLA)} = \overline{M}_{n(PEG)} + 2\overline{M}_{n(PLA)} + 18 \quad (3.1)$$

Where $\overline{M}_{n\,(PEG)}$ was estimated for starting PEG polymers and $\overline{M}n_{\,(PLA)}$ was calculated as:

$$\overline{M}_{n(PLA)} = \overline{DP}_{(PLA)} \times 72 \quad (3.2)$$

Where $\overline{DP}_{(PLA)}$ is the degree of polymerization of PLA blocks calculated by:

$$\overline{DP}_{(PLA)} = \frac{\overline{DP}_{(PEG)} \times (LA/EG)}{2} \quad (3.3)$$

Where $\overline{DP}_{(PEG)}$ is degree of polymerization of PEG which can be calculated from the molecular weight of PEG divided by molecular weight of PEG monomer. The mole ratio of LA and EG in block copolymer was deduced from the integration of NMR resonances belonging to PLA blocks at $\delta \approx 5.20$ ppm and to PEG blocks at $\delta \approx 3.65$ ppm (Rashkov, Manolova, Li, Espartero, and Vert, 1996). The characteristics of synthesized copolymer were summarized in Table 3.1.

Table 3.1 Characteristics of PEG, PLA, and PLA-PEG-PLA with different block compositions and PLA stereochemistries.

Sample	^{1}H-NMR			GPC		ϕ_{PLA}
	LA/EG	$\overline{DP}_{(PLA)}$	$\overline{M}_n$	$\overline{M}_n$	$\overline{M}_w/\overline{M}_n$	
PEG8k	-	-	-	8.23	1.24	-
PEG10k	-	-		9.87	1.27	-
PLLA	-	-	-	13.77	1.90	1
PDLLA	-	-	-	7.04	1.66	1
PLA2002D	-	-	-	58.32	3.32	1
LLA_{49}-EG_{187}-LLA_{49}	0.52	49	15.31	15.28	2.00	0.34
LLA_{71}-EG_{187}-LLA_{71}	0.76	71	18.48	22.60	2.30	0.43
LLA_{347}-EG_{187}-LLA_{347}	3.71	347	58.22	38.02	1.20	0.79
LLA_{101}-EG_{224}-LLA_{101}	0.91	101	24.43	-	-	0.47
DLA_{36}-EG_{187}-DLA_{36}	0.38	36	13.42	11.38	1.35	0.28
DLA_{72}-EG_{187}-DLA_{72}	0.78	72	18.62	17.13	1.45	0.44
DLA_{87}-EG_{187}-DLA_{87}	0.93	87	20.78	21.81	2.36	0.48

* LLA_x-EG_y-LLA_x and DLA_x-EG_y-DLA_x are represented as PLLA-PEG-PLLA and PDLLA-PEG-PDLLA, respectively.

$\overline{DP}$ of PEG8k = 187.

$\overline{DP}$ of PEG10k = 224.

ϕ_{PLA} was calculated from ^{1}H-NMR

$\overline{M}n$ is represented in kg• mol^{-1}.

- **Gel permeation chromatography (GPC)**

Number average molecular weight ($\bar{M}n$) and molecular weight distribution (MWD) of polymers were evaluated by GPC. Calibration was accomplished by polystyrene standards with molecular weight of 451,000, 186,000, 42,900 and 6,390 g•mol^{-1}. Figure 3.12 and 3.13 show the GPC curves of PEG8k and PLA-PEG-PLA copolymer with various compositions for each PLA stereochemistry.

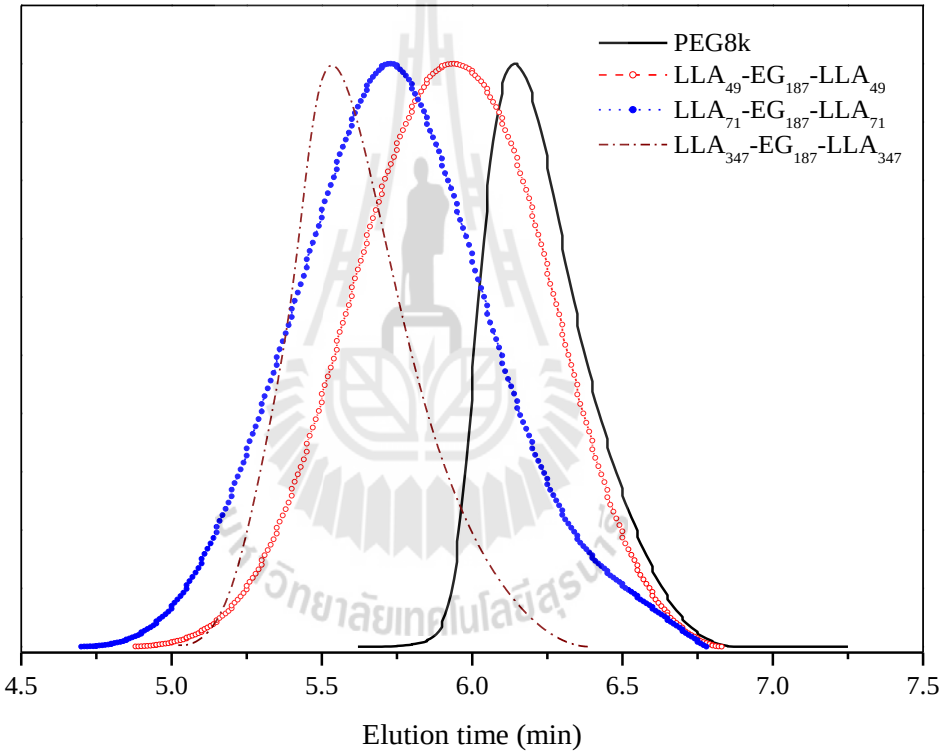

Figure 3.12 GPC curves of PEG8k, LLA_{49}-EG_{187}-LLA_{49}, LLA_{71}-EG_{187}-LLA_{71} and LLA_{347}-EG_{187}-LLA_{347}.

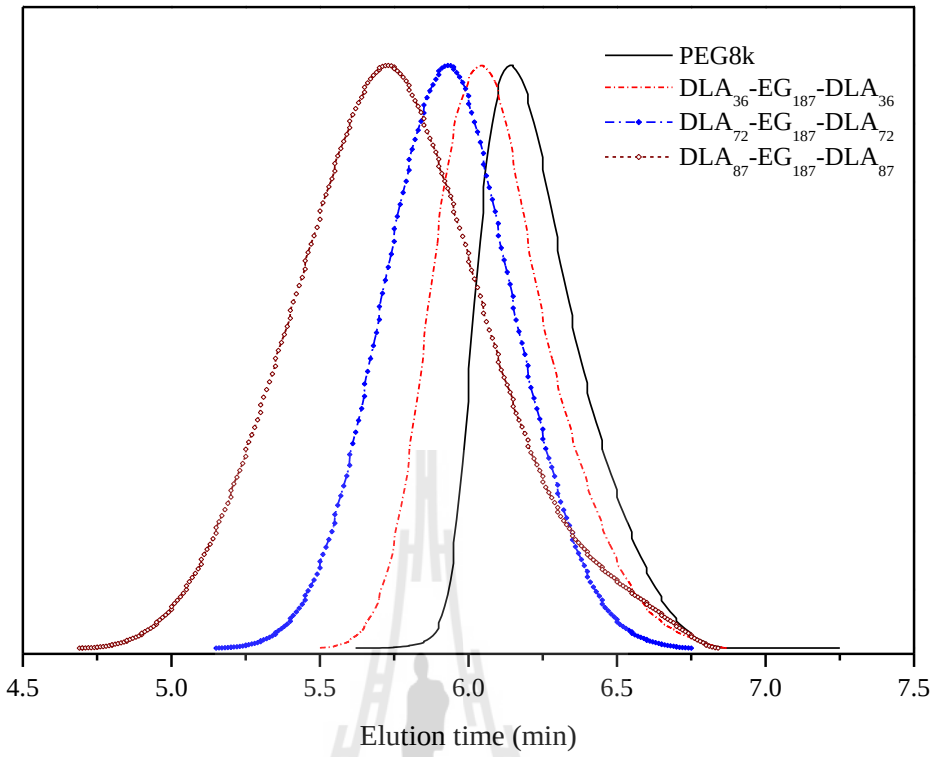

Figure 3.13 GPC curves of PEG8k, DLA_{36}-EG_{187}-DLA_{36}, DLA_{72}-EG_{187}-DLA_{72} and DLA_{87}-EG_{187}-DLA_{87}.

From GPC chromatograms, the single peak of each copolymer was observed indicating that copolymers were effectively obtained with no residual PEG or PLA homopolymer. Molecular weight distributions of these copolymers were quite board especially the block copolymers obtained from L-lactide monomer. Furthermore, we found that in the case of broader molar mass copolymers, higher polydispersity indices were obtained.

3.4.2 Thermal characterization

Thermal properties including glass transition temperature (T_g), crystallization temperature (T_c), melting temperature (T_m), degree of crystallinity (X_c) enthalpy of meting (ΔH_m) and enthalpy of crystallization (ΔH_c) of neat PLA, PEG and their copolymers were investigated by DSC technique. Considering the same thermal history of the prepared samples, the results of the second heating run are discussed. Thermal characteristics of PLA and PEG homopolymers were used to compare with block copolymers and polymer blends. As shown in Figure 3.14, PEG8k and PEG10k exhibit two endothermic melting peaks at 66.7 and 64.5 ^{o}C respectively. For PLLA thermograms, there are two pronounced melting peak; a smaller peak at ~171 ^{o}C and larger one at ~175 ^{o}C. This is attributed to the melting of two lamellae, the lower temperature peak is contributed to the melting of the small lamellae produced by the secondary crystallization, and the peak at higher temperature is originated from the melting of these major crystals formed in the primary crystallization process (Su, Li, Liu, Hu and Wu, 2009). For PDLLA, the endothermic melting peak was not detected because it is amorphous. Glass transition temperature (T_g) of PDLLA and PLLA are 50.5 and 43.7 ^{o}C, respectively, while T_g of PEG8k and PEG10k were not observed in this temperature range.

Compared with the parent semicrystalline neat PEG and PLLA and amorphous PDLLA homopolymers, the studied block copolymers show the modified thermal properties. Figure 3.15 and 3.16 showed block copolymers of PLLA-PEG-PLLA and PDLLA-PEG-PDLLA with different compositions.

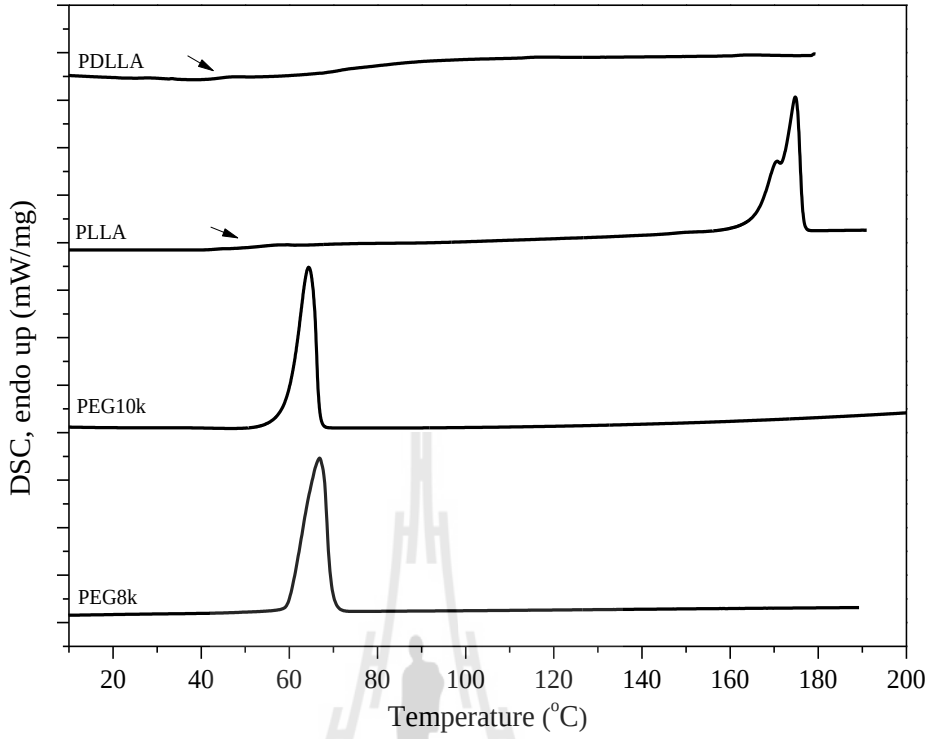

Figure 3.14 DSC curves of the second scan of PDLLA, PLLA, PEG8k and PEG10k (The arrow labels the T_g).

Since PLA-PEG-PLA copolymers contain at least one crystallizable block and the overlapping signals for melting and simultaneous crystallization as well as the appearance of relaxation phenomena, thermal properties of these materials are difficult to interpret. The LLA_{49}-EG_{187}-LLA_{49} copolymer exhibits a sharp melting peak at 48.7 ^{o}C and the weak broad peak at 126 ^{o}C which could be assigned to the melting of crystalline domain of PEG and PLLA, respectively. From this observation, the crystallizability of PLLA blocks is interfered by long PEG blocks.

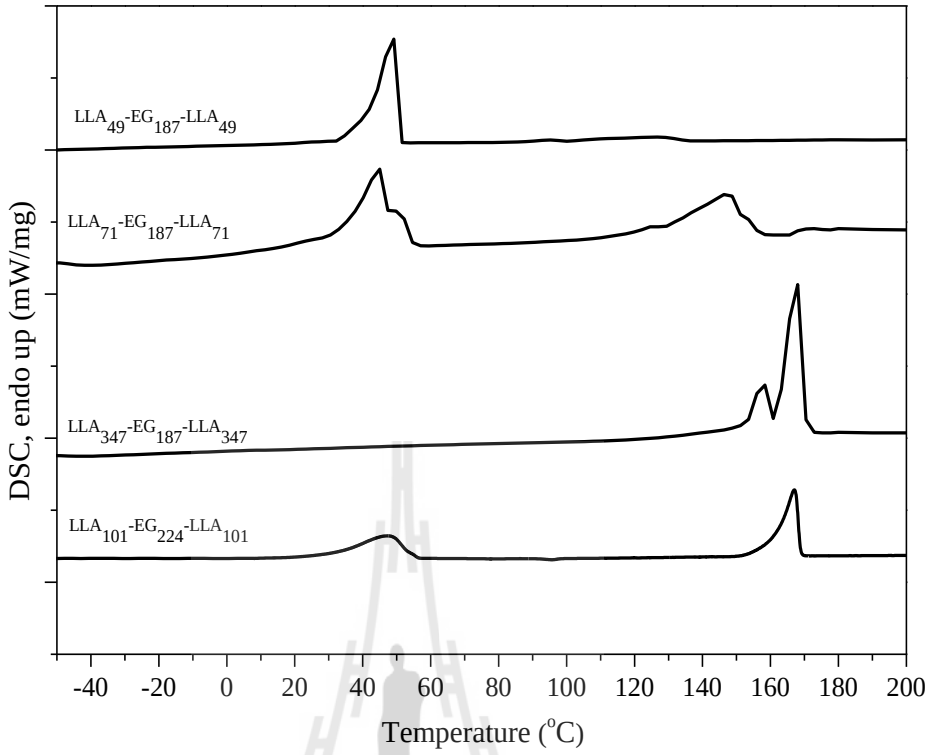

Figure 3.15 DSC curves of the second scan of LLA_{49}-EG_{187}-LLA_{49}, LLA_{71}-EG_{187}-LLA_{71}, LLA_{347}-EG_{187}-LLA_{347} and LLA_{101}-EG_{224}-LLA_{101}.

In the case of LLA_{71}-EG_{187}-LLA_{71}, a broad endothermal peak was detected at 44.5 ^{o}C followed by a small melting peak at 147.4 ^{o}C, indicating microphase separation. The endotherm at 44.5 ^{o}C corresponds to the melting of crystalline regions of PEG segments only, thus indicating the presence of a separated PEG phase with a certain degree of crystallinity. In the copolymer with longer PLLA blocks compared with PEG blocks (LLA_{347}-EG_{187}-LLA_{347}), the double meltings of PLLA segment at 157.5 and 167.4 ^{o}C are only observed. This might be due to an increased phase compatibility of a short PEO block within dominant PLA blocks and insufficient phase separation or because of the amorphous structure of PEG phase. To study the

effect of PEG block length on thermal properties of the copolymer, block copolymer of LLA_{101}-EG_{224}-LLA_{101} was investigated and compared. Thermal behavior of LLA_{101}-EG_{224}-LLA_{101} was quite similar to LLA_{71}-EG_{187}-LLA_{71} (same PLLA/PEG composition). There were two distinct melting peaks for PEG and PLLA at 47.3 and 167 ^{o}C, respectively. Small exothermic cold crystallization peak at 95.5 ^{o}C was also detected.

A decrease in melting temperature compared with the parent PEG and PLLA homopolymer is due to their incorporation within each phase and indicates partial phase compatibility. In addition, in the presence of relatively long PLA chain, short PEG segments (LLA_{347}-PEG_{187}-PLA_{347}) do not crystallize, which agrees well to the results of Li *et al*. (1996) (Rashkov, Manolova, Li, Espartero, and Vert, 1996). Similarly, for copolymers with longer PEG segments (LLA_{49}-PEG_{187}-PLA_{49}), crystallinity of PLA is less when the LA segment is short. X-ray diffraction patterns also support these results (Figure 3.17).

Block copolymers derived from DLLA (Figure 3.16) are monophasic and do not shows a first-order phase transition because more or less random segments of D- and L-lactic acid units do not crystallize. An overview of thermal behavior of these copolymers is quite similar with those mentioned above except the tendency of change in T_g change is quite contrast from the literature (Kubies, Rypáček, Kovárová, and Lednicky′, 2000). In this thesis, T_g of copolymer was slightly decreased with increasing of PLA block length. The summarized data are shown in Table 3.2.

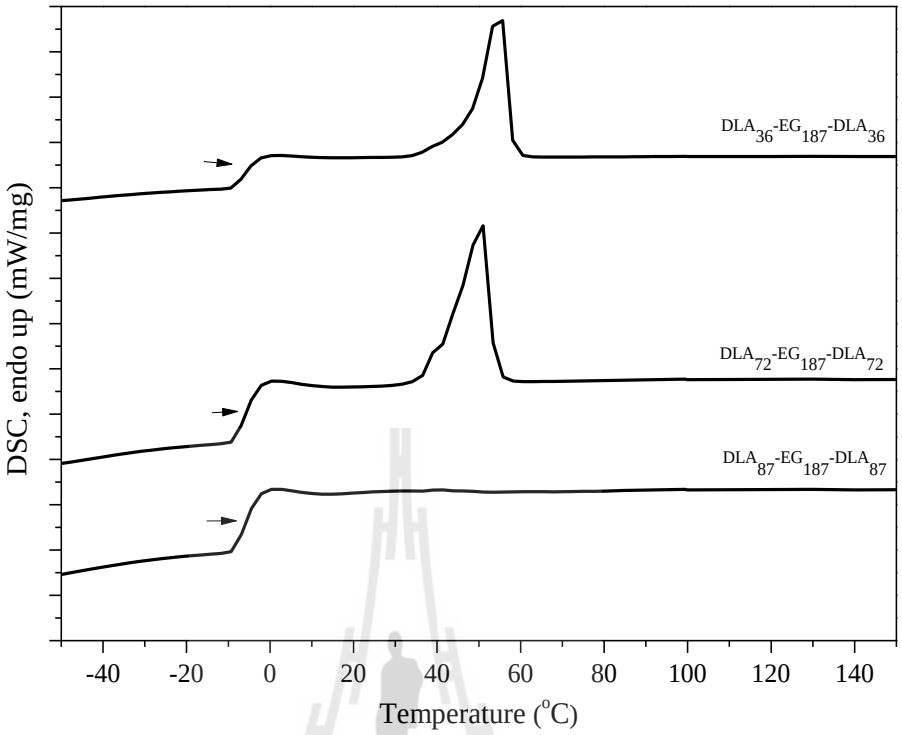

Figure 3.16 DSC curves of the second scan of DLA_{36}-EG_{187}-DLA_{36}, DLA_{72}-EG_{187}-DLA_{72} and DLA_{87}-EG_{187}-DLA_{87}.

Table 3.2 Thermal properties of PLA, PEG and their triblock copolymers.

Sample	T_m(°C)		ΔH_m	$T_{c(PLA)}$	ΔH_c	X_c	T_g
	PEG	PLA	(J/g)	(°C)	(J/g)	(%)	(°C)
PEG8k	66.7	-	-	-	-	-	-
PEG10k	64.5	-	-	-	-	-	-
PLLA	-	170.7(174.8)	48.57	-	-	51.9	50.5
PDLLA	-	-	-	-	-	-	43.7
PLA2002D	-	149.8	0.47	-	-	0.50	51.8
LLA_{49}-EG_{187}-LLA_{49}	48.7	126	-	-	-	0.6	-3.0
LLA_{71}-EG_{187}-LLA_{71}	44.5	147.4	22.6	-	-	24.2	-0.4
LLA_{347}-EG_{187}-LLA_{347}	-	157.3(167.7)	33.9	-	-	36.2	3.2
LLA_{101}-EG_{224}-LLA_{101}	47.3	167.0	2.93	95.5	0.03	31.9	-
DLA_{36}-EG_{187}-DLA_{36}	54.5	-	-	-	-	-	-5.4
DLA_{72}-EG_{187}-DLA_{72}	50.4	-	-	-	-	-	-5.7
DLA_{87}-EG_{187}-DLA_{87}	-	-	-	-	-	-	-5.9

* The value in parentheses is the second melting peak of PLLA segments

3.4.3 Morphological characterization

To confirm DSC results, X-ray diffraction (XRD) and polarized optical microscope (POM) techniques were employed to investigate the crystallization behavior of PLLA-PEG-PLLA copolymers. Figure 3.17 exhibits X-ray diffraction patterns of PLLA-PEG-PLLA copolymers and PLLA/PEG blend. The polymer blend was used as a reference system. The characteristic diffraction peaks of PEG appear at $2\theta = 19.3^{o}$ and 23.5^{o} while neat PLLA exhibited a broad peak at 16.0^{o}, indicating most of PLLA are amorphous or they are fine crystal structure. This is due to low crystallization of PLLA.

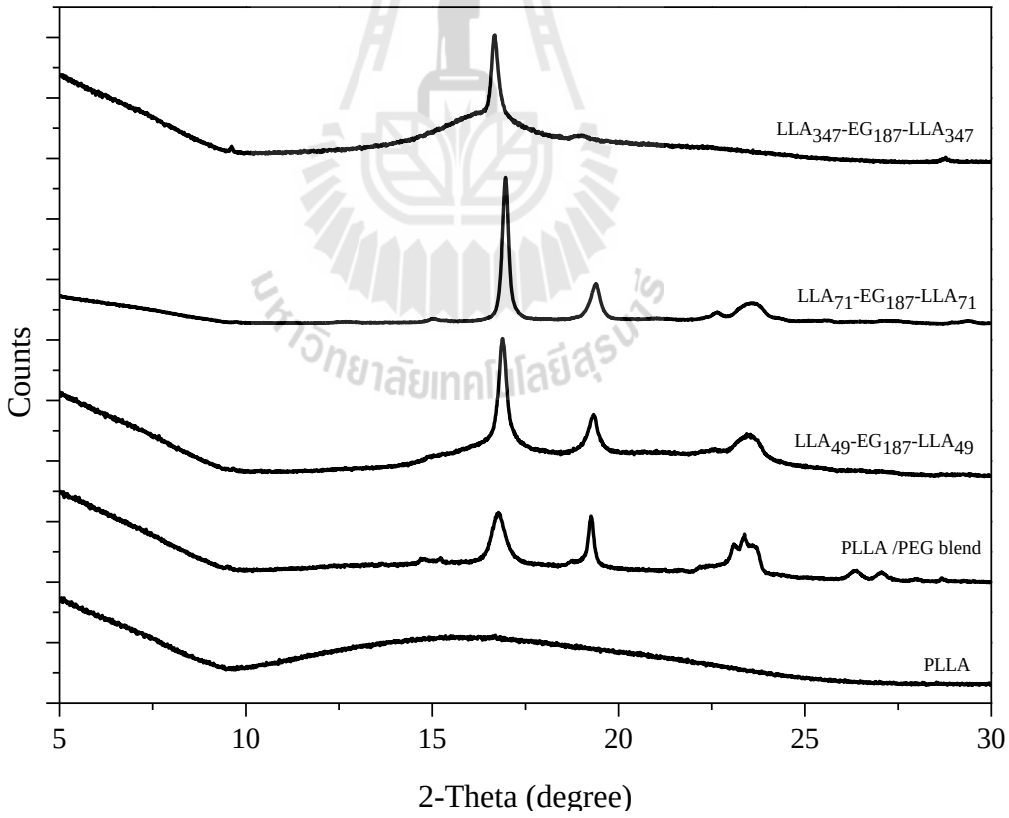

Figure 3.17 X-ray diffraction patterns of PLLA, 50% w/w PLLA/PEG blend, LLA_{49}-PEG_{187}-LLA_{49}, LLA_{71}-PEG_{187}-LLA_{71}, LLA_{347}-PEG_{187}-LLA_{347}.

However, the sharp diffraction peak of PLLA blocks was observed in polymer blend and block copolymers, indicating that PLLA blocks were able to crystallize although the presence of PEG blocks. The two peak characteristics of crystalline PEG can be detected for the systems in which the PEG blocks length is longer than the PLA block length (LLA_{49}-PEG_{187}-LLA_{49}, LLA_{71}-PEG_{187}-LLA_{71}) but not for the systems with longer length of PLA blocks (LLA_{347}-PEG_{187}-LLA_{347}). The absence of PEG peaks suggested that crystallizability of PEG blocks was very much decreased when they were covalently bound to rather long PLA blocks at both ends.

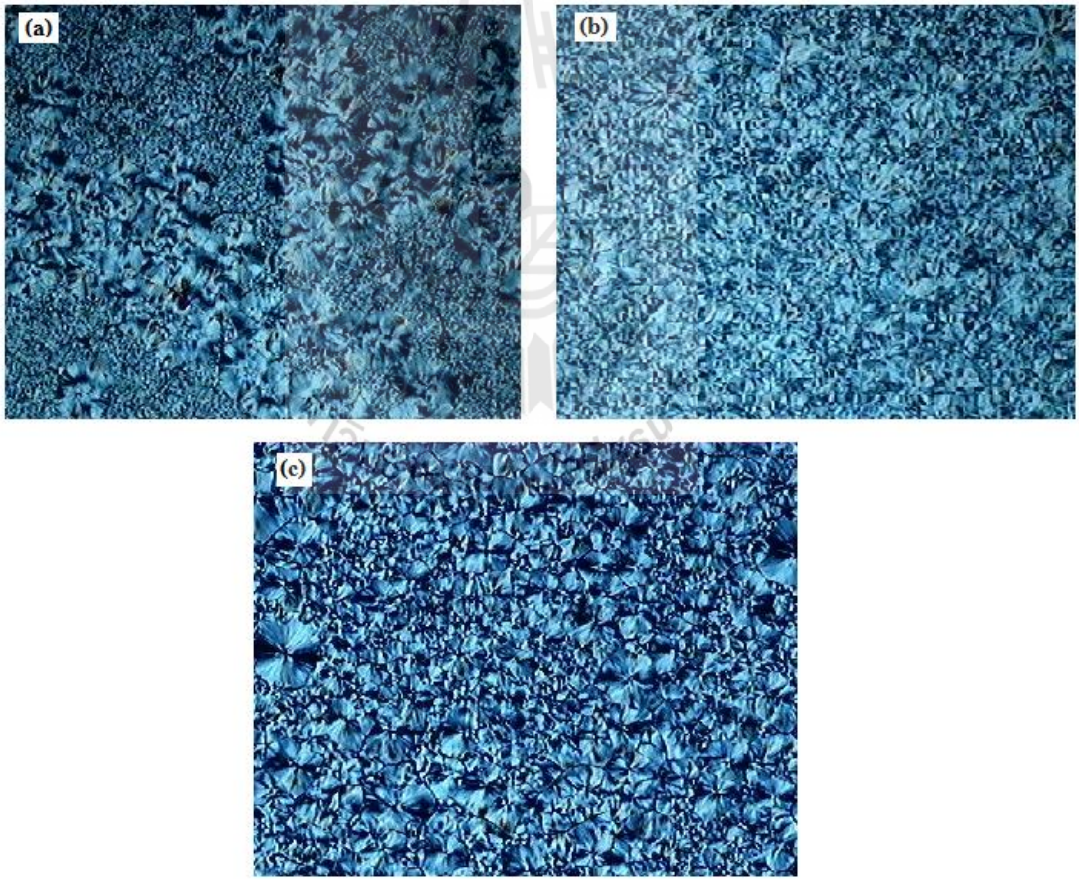

Figure 3.18 Polarize optical micrographs of neat (a) PLLA, (b) LLA_{71}-PEG_{187}-LLA_{71} and (c) LLA_{347}-PEG_{187}-LLA_{347}.

In addition, crystal morphology of PLLA and their block copolymers with different block compositions was investigated using POM technique. Figure 3.18 shows the crystalline morphology of the samples at room temperature after the melt (Some POM images not shown). It is evident that the crystalline morphology of copolymers depends on the block length of each component. In the cases of neat PLLA and LLA_{347}-PEG_{187}-LLA_{347}, they show only the Maltese cross crystalline structure of PLLA segments because the PEG part in these block copolymers cannot crystallize. While LLA_{71}-PEG_{187}-LLA_{71} shows the dendritic morphology due to co-crystallization of PLLA and PEG. Compared with neat PLLA, the crystal formation of LLA_{71}-PEG_{187}-LLA_{71} and LLA_{347}-PEG_{187}-LLA_{347} copolymer is over, implying that the crystallization of PLLA is accelerated by PEG blocks.

3.4.4 Isothermal crystallization kinetics

The subject of crystallization in block copolymers has attracted much attention in the past few decades as reviewed by several researchers (Kim, Chung, Chin, Kim, and Yoon, 1999; Yang *et al*., 2006). Mechanical and thermal properties of semicrystalline polymer are greatly depended on the crystallization and morphology. Moreover, their biodegradability is also influenced by the crystallization. So, it is quite important to understand the crystallization behavior to optimize polymer processing.

Isothermal crystallization behavior of neat PLLA and their triblock copolymers was studied by DSC technique. Avrami model was used to interpret isothermal crystallization process. With the recorded DSC exothermic curves in terms of the heat flow per gram of the sample dH(t)/dt as a function of time t for systems

undergoing the isothermal crystallization process at various T_c values. First, the relative crystallinity of PLLA, *X(t)*, can be calculated by the following equation.

$$X(t) = \frac{\int_0^t \frac{dH(t)}{dt} dt}{\int_0^\infty \frac{dH(t)}{dt} dt} \quad (3.4)$$

Once the values of *X(t)* versus t are obtained, the isothermal crystallization kinetics are interpreted by mean of the Avrami equation

$$X(t) = 1 - \exp(-kt^n) \quad (3.5)$$

Where *n* is known as the Avrami index, *t* is a annealing time and *k* is the overall crystallization rate constant including contributions from nucleation and crystal growth. Figure 3.19 presents the DSC exothermic curves as a function of time (*t*) for neat PLLA and their block copolymer undergoing an isothermal crystallization of PLLA at 120 ^{o}C, from which the values of *X(t)* calculated by Equation (3.4) versus *t* are obtained, and shown in Figure 3.20. From Figure 3.19, it is clear that the complete crystallization of PLLA-PEG-PLLA block copolymers takes a short time compared to neat PLLA. For the same PLLA block composition (LLA_{71}-PEG_{187}-LLA_{71} and LLA_{101}-EG_{224}-LLA_{101} systems), the crystallization rate of PLLA in copolymer containing high molecular weight PEG is slower than the copolymer with lower molecular weight PEG.

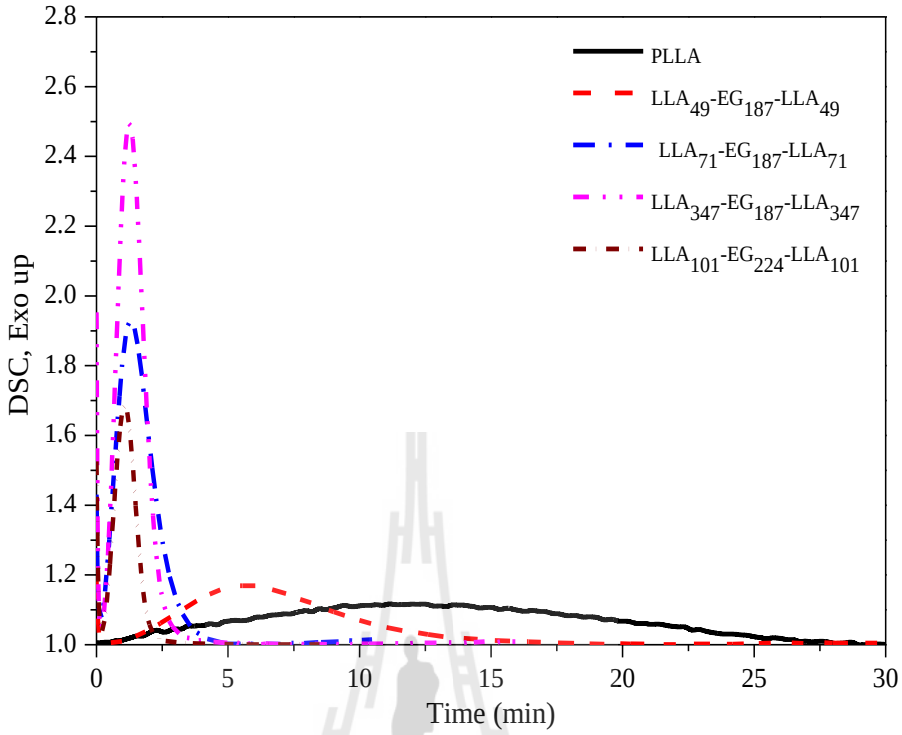

Figure 3.19 The DSC exothermic curves as a function of time (t) for neat PLLA and their block copolymer undergoing the isothermal crystallization of PLLA at 120 ^{o}C.

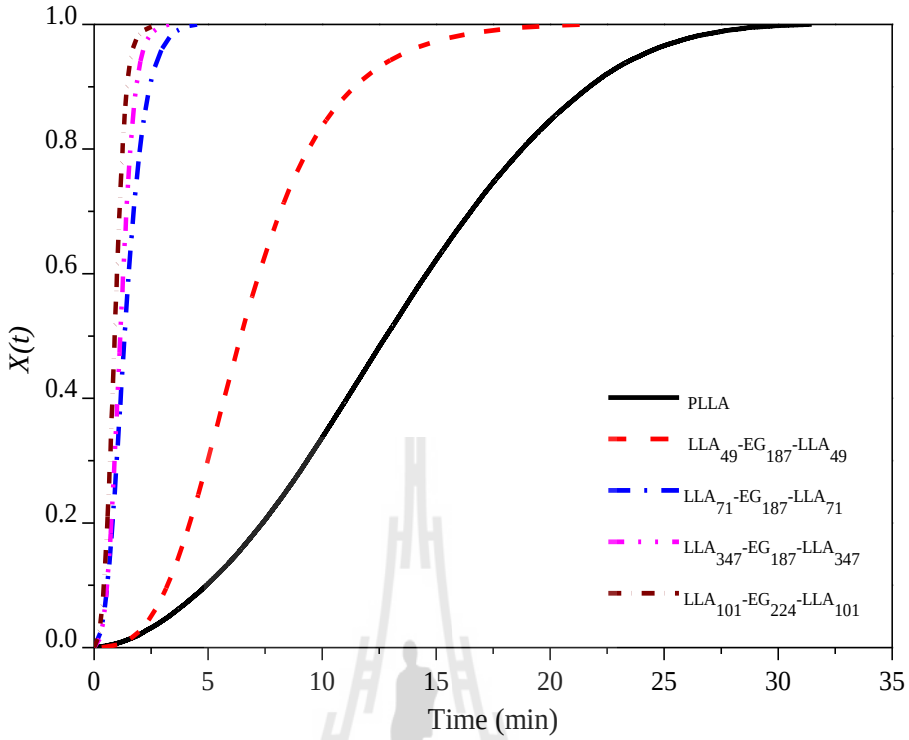

Figure 3.20 The crystallinity, *X(t)* of PLLA versus crystallization time for various systems undergoing an isothermal crystallization at T_c =120 ^{o}C.

Using Avrami equation in double-logarithmic form, and plotting log[-ln(1-*X(t)*)] against log *t* for each isothermal crystallization process, a straight line is obtained, from which two adjustable parameters, *k* and *n* can be obtained. The Avrami plots (log[-ln(1-*X(t)*)] against log *t*) of the PLLA homopolymer and PLLA block in triblock copolymers are shown in Figure 3.21, and kinetics parameters are summarized in Table 3.3.

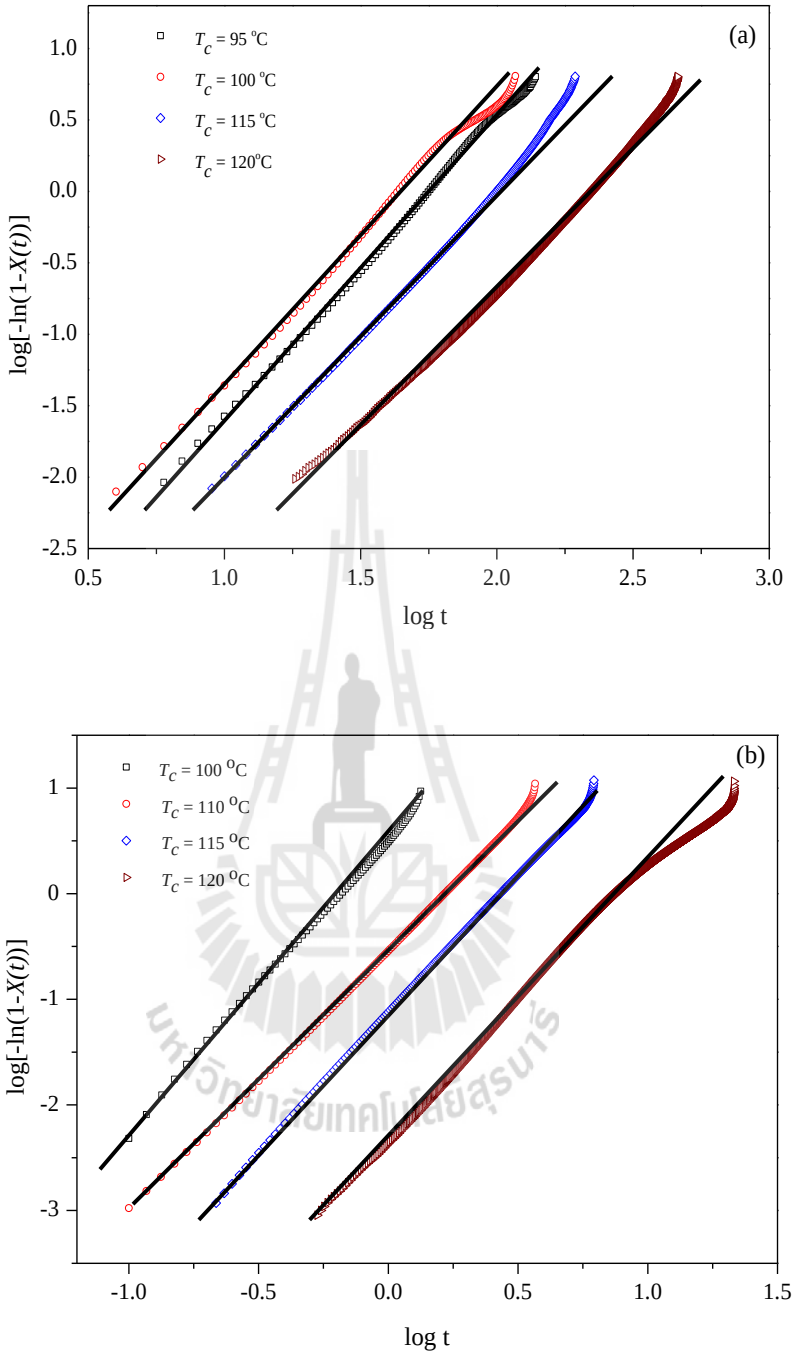

Figure 3.21 Avrami plots of log[-ln(1-*X(t)*)] versus log t of the PLLA block of block copolymers and PLLA homopolymer at different temperature: (a) neat PLLA, (b) LLA_{49}-EG_{187}-LLA_{49}, (c) LLA_{71}-EG_{187}-LLA_{71}, (d) LLA_{347}-EG_{187}-LLA_{347} and (e) LLA_{101}-EG_{224}-LLA_{101}.

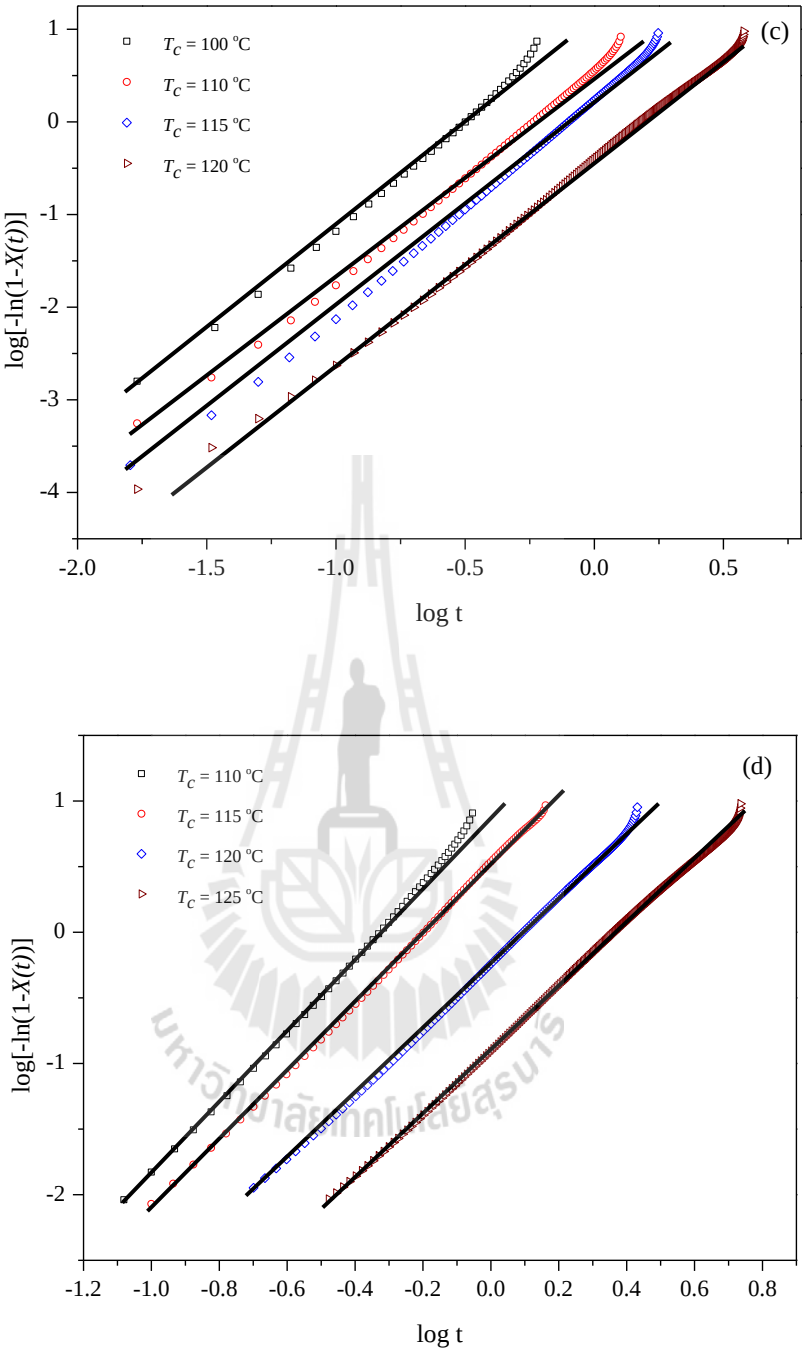

Figure 3.21 (Continued).

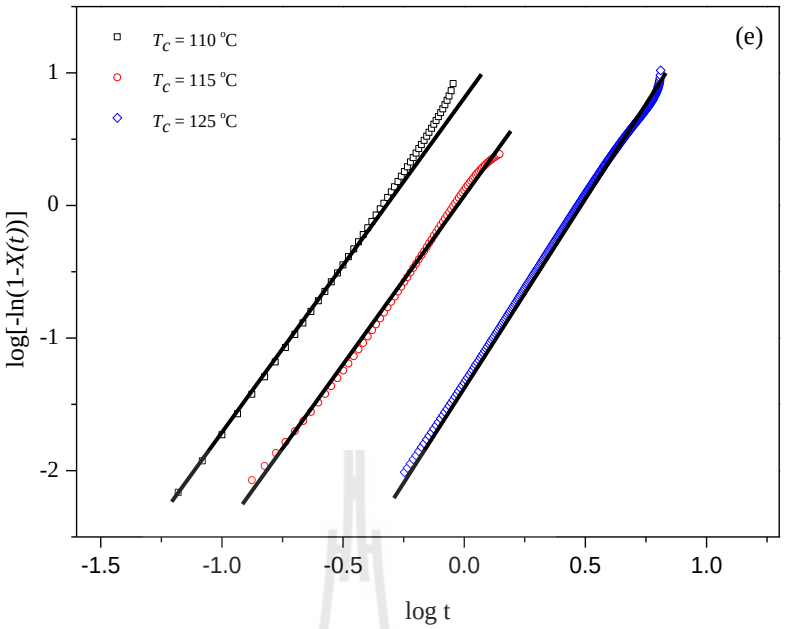

Figure 3.21 (Continued).

Polymer crystallization is generally made up of two processes: primary crystallization and secondary crystallization (Yang *et al*., 2006). One of the simplified assumptions in Avrami model is that there is no secondary crystallization process. As shown in Figure 3.21 (a) to (e), show good linear relation which indicates that the Avrami equation can be used to describe the isothermal crystallization process of these samples. An important parameter, which can easily be obtained from the plot similar to Figure 3.22, is the crystallization half-time ($t_{1/2}$) which is defined as the time spent from the onset of the crystallization to the point where the crystallization is 50% complete. Using the reciprocal of $t_{1/2}$ (G) reflects the radius growth rate of spherulites. These values are shown in Table 3.3.

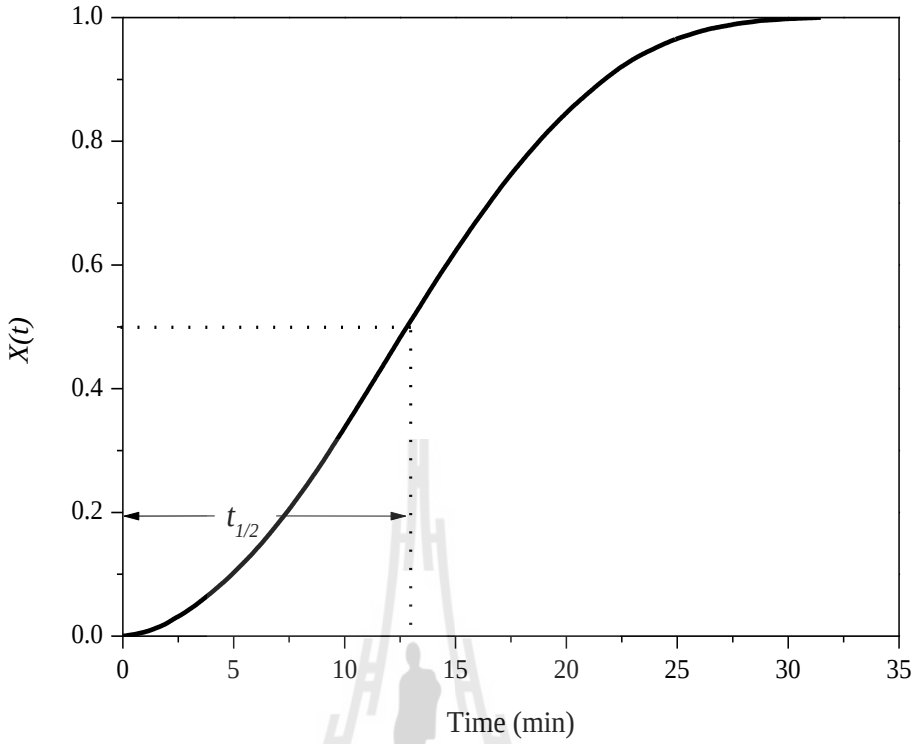

Figure 3.22 Typical plot of *X(t)* versus *t* of PLLA homopolymer at T_c = 120 °C for calculating the crystallization half-time ($t_{1/2}$).

Table 3.3 Characteristic parameters of PLLA block of triblock copolymers and PLLA homopolymer during isothermal crystallization process.

Sample	T_c (°C)	n	k	$t_{1/2}$ (min)	G (min^{-1})
PLLA	95	2.16	6.31×10^{-4}	2.81	0.36
	100	2.28	6.31×10^{-5}	2.16	0.46
	115	2.10	2.19×10^{-4}	5.17	0.19
	120	2.09	1.20×10^{-5}	12.71	0.08
LLA_{49}-EG_{187}-LLA_{49}	100	2.88	1.74×10^{-4}	0.57	1.75
	110	2.49	3.55×10^{-6}	1.43	0.70
	115	2.60	6.31×10^{-5}	2.37	0.42
	120	2.34	6.31×10^{-4}	6.53	0.15
LLA_{71}-EG_{187}-LLA_{71}	100	2.37	5.37×10^{-4}	0.27	3.70
	110	2.28	8.71×10^{-5}	0.50	2.00
	115	2.35	3.89×10^{-5}	0.68	1.47
	120	2.18	1.58×10^{-5}	1.28	0.78
LLA_{347}-EG_{187}-LLA_{347}	110	2.77	2.75×10^{-5}	0.42	2.38
	115	2.55	2.69×10^{-5}	0.56	1.79
	120	2.37	1.15×10^{-5}	1.08	0.93
	125	2.28	4.90×10^{-6}	2.00	0.50
LLA_{101}-EG_{224}-LLA_{101}	110	2.61	5.62×10^{-5}	0.40	2.50
	115	2.38	2.04×10^{-5}	0.82	1.22
	120	2.37	1.86×10^{-5}	0.88	1.14
	125	2.58	3.98×10^{-7}	2.65	0.38

From Table 3.3, the average values of the Avrami exponents (n) for primary crystallization are 2.16, 2.58, 2.30, 2.49 and 2.49 for PLLA, LLA_{49}-EG_{187}-LLA_{49}, LLA_{71}-EG_{187}-LLA_{71}, LLA_{347}-EG_{187}-LLA_{347} and LLA_{101}-EG_{224}-LLA_{101}, respectively. The exponent n is depended on the type of nucleation and growth dimension. Typical n values for polymer spherulitic crystallization are 3 or 4. The n = 3 indicates three-dimensional spherulitic growth from instantaneous nuclei (athermal nucleation), and n = 4 is interpreted as three-dimensional spherulites growing from sporadic nuclei (thermal nucleation). If crystallization occurs in two-dimensional aggregates (like axialites or lamellar aggregates), then n = 2 or n = 3 are expected depending on whether the nucleation is instantaneous or sporadic (Sperling, 2001). In this study, n values are below 3 could be related to the complex crystallization behaviors of the copolymer, including heterogeneous nucleation. Similar results have been reported for the crystallization of PLLA-PCL copolymers (Hamley, *et al.*, 2005) and PLLA-PEG diblock copolymer (Wu, He, Fan, Wei, and Li, 2008).

With an increase of isothermal temperature (T_c), the half crystallization time ($t_{1/2}$) was increased, while the constant of crystallization rate (k) trend was decreased and it was pronounced in block copolymers. To describe the crystallization growth rate, the parameter (G) is plotted as a function of T_c (Figure 3.23). The results show that the crystallization growth rate (G) decrease with increased T_c. Because at high temperature the chain mobility increases, it is overcome by a great decrease of the formed nucleation density, and the crystallization growth rate decreases. In addition, the crystallization growth rate was shifted to lower value with decreased PLLA block length. Compared to neat PLLA, the crystallization growth rate of block copolymer is higher, implying that the presence of PEG block that is chemically

connected to PLLA causes a significant increase of the PLLA crystallization growth rate. It is evident that the molecular weight of PEG significantly affect on the crystallization growth rate of PLLA in copolymer as seen in LLA_{101}-EG_{224}-LLA_{101} system.

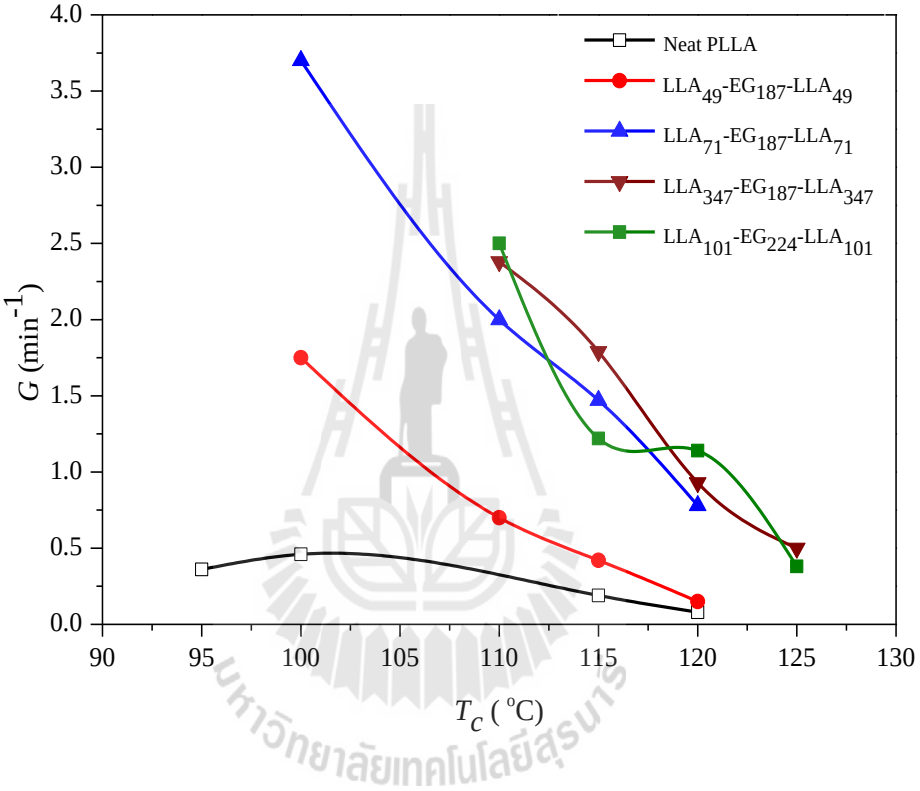

Figure 3.23 Plot of the PLLA crystallization growth rate (G) in pure PLLA and their block copolymers, as a function of crystallization temperature T_c.

3.4.5 PLLA/ PLA-PEG-PLA blends

Most serious problem about polymer blends, especially for toughening the rigid polymer, is the miscibility of polymer mixture. Several studies have been attempted to address this issue. As mentioned above, block copolymer was used as plasticizer to reduce phase separation in polymer mixture. The case studies in this work are PLLA/PEG and PLLA/PLA-PEG-PLA blends. PLLA/PEG systems were used as the controlled system. The commercial grade of PLLA (PLA2002D, Nature Work) was used as the polymer matrix and PEG with molecular weight of ~8,000 g•mol^{-1} was used as plasticizer. The equivalent molar of PEG in PLA-PEG-PLA block copolymer was synthesized to use in this study and compare with PEG homopolymer. To verify this hypothesis, DSC technique was used in this study.

Thermograms of quenched PLLA and PLLA/PEG blends are shown in Figure 3.24. Quenched PLLA was amorphous and did not cold-crystallize upon heating rate at 10 ^{o}C min^{-1}. The result showed that the glass transition (T_g) of PLLA/PEG blends shifted to lower temperature as the PEG content increased. The T_g decreased from 51.8 ^{o}C for quenched PLLA through to about 9.3 ^{o}C for the PLA/PEG 70:30 blend. It can be seen that PLLA/PEG with PEG content of 10-30 wt % displays a single T_g, intermediate between those two pure components reflecting that these samples are miscible. While the T_g of PLLA/PEG 50:50 sample cannot be observed but it shows two endothermic melting peaks at 57.0 ^{o}C and at 149.2 ^{o}C corresponding to melting peaks of PEG and PLLA, respectively. This observation is implied that the blend is phase separation by crystallization of PEG. When the blends were heated at 10 ^{o}C min^{-1}, PLA cold-crystallization in the range of 112-76 ^{o}C was observed. The cold-crystallization temperature (T_c) of PLA decreased slightly as the PEG content

increased in parallel with the shift in T_g. The subsequent melting temperature (T_m) and amount of crystallinity (X_c) relative to PLLA in the blend were slight decrease for PEG content of 10-30 wt % but a big change in the PLLA/PEG 50:50 system was detected. The thermogram of PLLA exhibited a single melting peak centered at about 150 ^{o}C, whereas that of PLLA/PEG with PEG content of 10 and 20 wt% were featured by a melting endotherm with two peaks, smaller at ~142-145 ^{o}C and bigger at ~150-151 ^{o}C. The thermal properties of the samples are shown in Table 3.3.

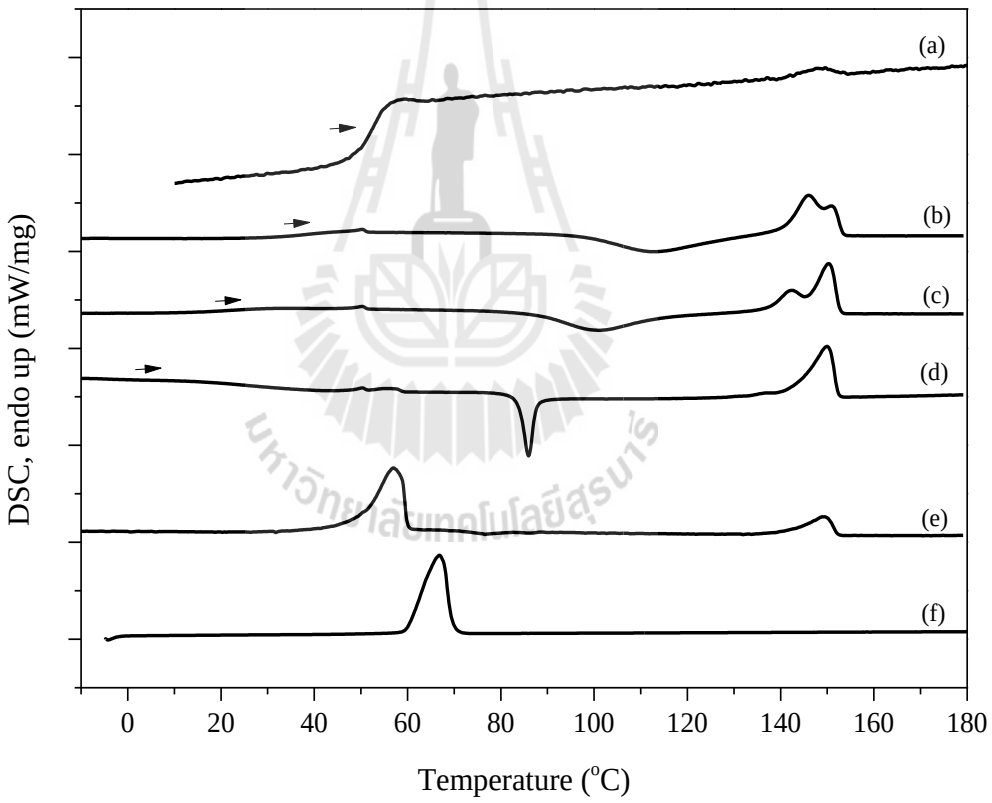

Figure 3.24 DSC thermograms of quenched samples of (a) PLLA, (b) PLLA/PEG 90:10, (c) PLLA/PEG 80:20, (d) PLLA/PEG 70:30, (e) PLLA/PEG 50:50 blends and (f) PEG8k obtained with a heating rate of 10 ^{o}C•min^{-1}.

As seen in Figure 3.24, we could say that PLA/PEG blends are miscible in the PEG content of 10-30 wt% under quench condition. Although the data showed that polymer blend was miscible in the melt, there has reported the phase separation of PLLA/PEG at room temperature due to slow crystallization of PEG (Hu, Hu, Topolkaraev, Hiltner, and Baer, 2003; Kulinsky and Piorkowska, 2005). Therefore, the slow cooling rate from the melt of the samples was performed to investigate the crystallization behavior of PEG. The subsequent heating DSC thermograms of PLLA/PEG samples obtained from cooling rate at 10 ^{o}C min^{-1} from the melt were exhibited in Figure 3.25.

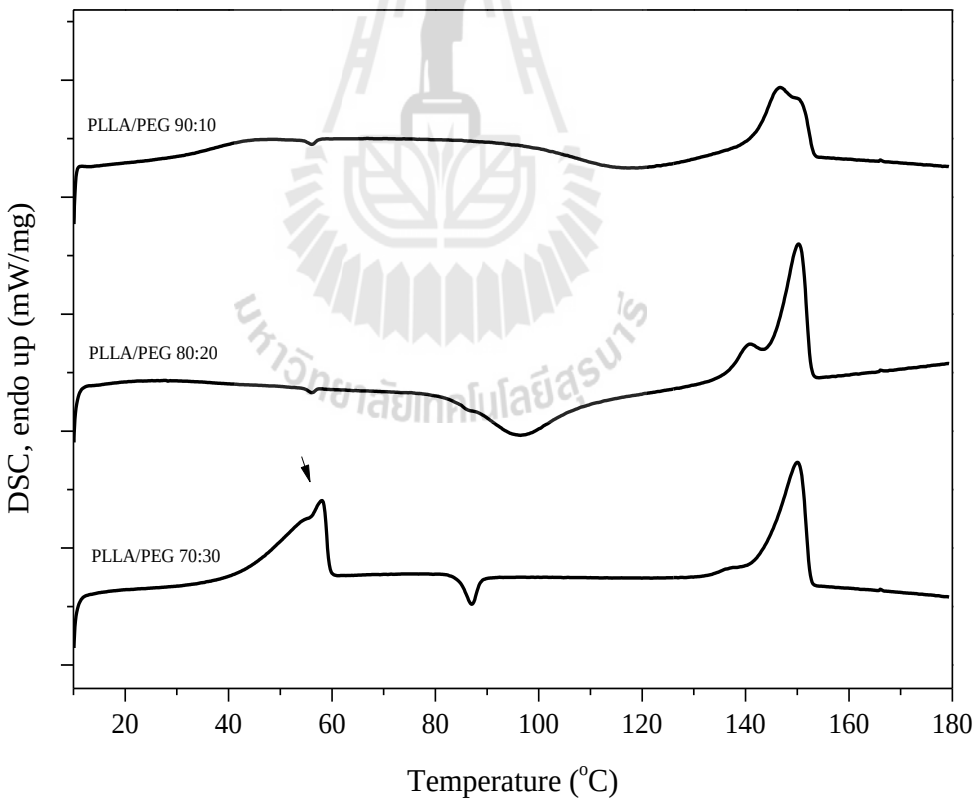

Figure 3.25 Subsequent heating DSC thermograms of aging samples of PLLA/PEG 90:10, PLLA/PEG 80:20 and PLLA/PEG 70:30 obtained with a heating rate of 10 ^{o}C• min^{-1}.

At this condition, the main characteristics of PLLA/PEG blends with 10-20 wt% of PEG are quite similar to those in quench samples, refer to the cooling rate from the melt does not have any effect to crystallization of PEG in these systems. Because PEG chains are well dispersed in amorphous region of PLLA, the polymer chain of PEG are difficult to crystallize in this region. Contrast with PLLA/PEG 70:30 sample, it showed two endothermic peaks at 57.9 and at 150.1 ^{o}C corresponding to melting of PEG and PLLA, respectively. This observation reflects that PEG can crystallize from the melt if the cooling rate is slow enough leading to the phase separation.

In this work, triblock copolymers PLA and PEG were used as the plasticizer to reduce the phase separation in this stage. To reduce the interference of crystallization from the crystallizable blocks in PLLA-PEG-PLLA, the amorphous PDLLA end block of PDLLA-PEG-PDLLA was selected to study in this work. The different molecular weight of block copolymer by varying the PDLLA block length was prepared for these blends. The blend systems are PLLA/DLA_{36}-EG_{187}-DLA_{36}, PLLA/DLA_{72}-EG_{187}-DLA_{72} and PLLA/DLA_{87}-EG_{187}-DLA_{87}. To simplify, we used the notation of B01, B02 and B03 to represent as DLA_{36}-EG_{187}-DLA_{36}, DLA_{72}-EG_{187}-DLA_{72} and DLA_{87}-EG_{187}-DLA_{87}, respectively. The PEG content in all blends is 30 wt% with equivalent to those PLLA/PEG systems. The temperature program for this system is same in above PLLA/PEG 70:30 systems. The subsequent heating DSC thermograms of these blends are displayed in Figure 3.26. It is clear that no endothermic melting peak of PEG in all blends. This result indicates the PEG segments cannot crystallize even though some copolymers *i.e.*, DLA_{36}-EG_{187}-DLA_{36} and DLA_{72}-EG_{187}-DLA_{72} can crystallize in quench condition (Figure 3.16).

Another interesting result is that the increasing of the T_g value in PLLA/B03 blend compared with other systems. As seen in Figure 3.26, the T_g values of PLLA/B01 and PLLA/B02 systems shifted to lower temperature as the PDLLA block length increased while PLLA/B03 blend exhibited higher T_g. When compared to PDLLA block length, we expect that PLLA/B03 blend have lower T_g. Several studies (Kuo, Xu, Huang, and Chang, 2002) have explained that the significant T_g increase caused from the retarding of polymer chain mobility by other component via intermolecular interactions *i.e.*, hydrogen bonding However, it does not clear for this case.

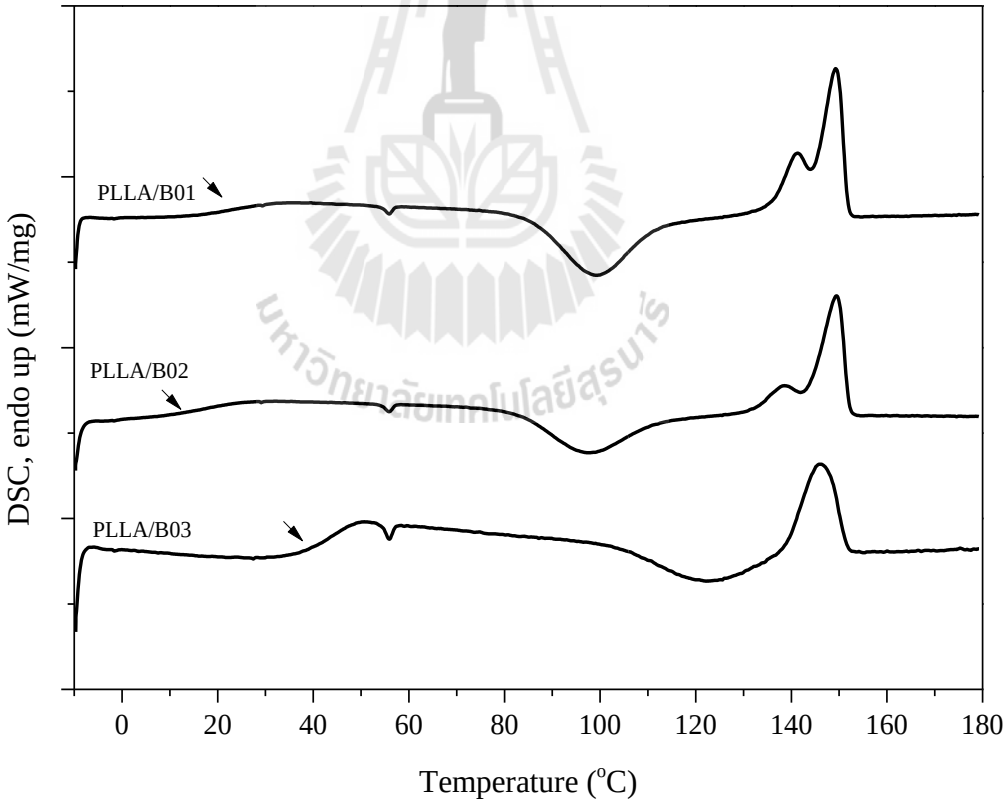

Figure 3.26 Subsequent heating DSC thermograms of PLLA/B01, PLLA/B02 and PLLA/B03 obtained with a heating rate of 10 $^{o}C \cdot min^{-1}$. The PEG content in the blends is 30 wt%.

Table 3.4 Thermal properties of PLLA/PEG and PLLA/PLA-PEG-PLA blends at a heating rate of 10 $^{o}C \cdot min^{-1}$.

Sample	T_g	Cold crystallization			Melting			
	(^{o}C)	T_c	ΔH_c	X_{cc}	T_m (^{o}C)		ΔH	X_c
		(^{o}C)	(J/g)	(%)	PEG	PLLA	(J/g)	(%)
PLLA	51.8	-	-	-	-	149.8	0.47	0.50
PEG8k	-	-	-	-	66.7	-	-	-
PLLA/PEG 90:10	37.4	112.5	-36.6	39.1	-	145.9(151.2)	38.3	40.9
PLLA/PEG 80:20	20.5	100.9	-39.3	42.0	-	142.2(150.4)	40.9	43.7
PLLA/PEG 70:30	9.3	85.9	-17.4	18.6	-	150.0	37.2	39.7
PLLA/PEG 50:50	-	76.4	-4.4	4.7	57.0	149.2	27.7	29.1
PLLA/PEG 90:10*	38.2	116.3	-17.8	19.0	-	146.7	26.2	28.0
PLLA/PEG 80:20*	15.9	96.5	-26.0	27.8	-	150.0	41.2	44.0
PLLA/PEG 70:30*	-	87.1	-3.5	3.7	58.0	150.0	39.6	42.3
PLLA/B01 70:30*	22.8	99.0	-30.0	32.1	-	141.4(149.2)	35.8	38.2
PLLA/B02 70:30*	15.3	97.5	-23.1	24.7	-	138.4(149.7)	27.2	29.1
PLLA/B03 70:30*	43.6	122.1	-10.9	11.6	-	146.3	10.3	11.0
PLLA/B02 90:10	41.6	116.5	-18.7	20.0	-	146.4	19.5	20.8
PLLA/B02 80:20	26.8	105.3	-33.2	35.5	-	142.2(149.4)	33.0	35.3
PLLA/B02 70:30	16.7	97.5	-24.2	25.9	-	138.4(149.4)	26.6	28.4
PLLA/B0250:50	-0.29	99.2	-32.0	34.2	-	136.0(147.6)	40.1	42.8

* PLLA/PEG 90:10* indicates this system obtained from slow cool down from the melt. 138.4(149.7) refer to the first and second T_m peaks of PLLA.

To investigate the influence of block copolymer content on thermal properties of the blends, block copolymer of DLA_{72}-EG_{187}-DLA_{72} (B02) was choosed to study. The PEG contents in the blends were varied as 10, 20, 30 and 50 wt %. The DSC thermograms of quench PLLA/B02 with different composition are shown in Figure 3.27. The correspondence of the enthalpies of cold crystallization and subsequent melting confirmed that the quenched PLLA/B02 were amorphous. This observation is similar to those in PLLA/PEG blends. Cold crystallization shifted to a lower temperature as the PEG content in the blends increased in parallel with the shift in T_g. Also, the crystallinity of PLLA also increased with the increase in the plasticizer content, as shown in Table 3.3.

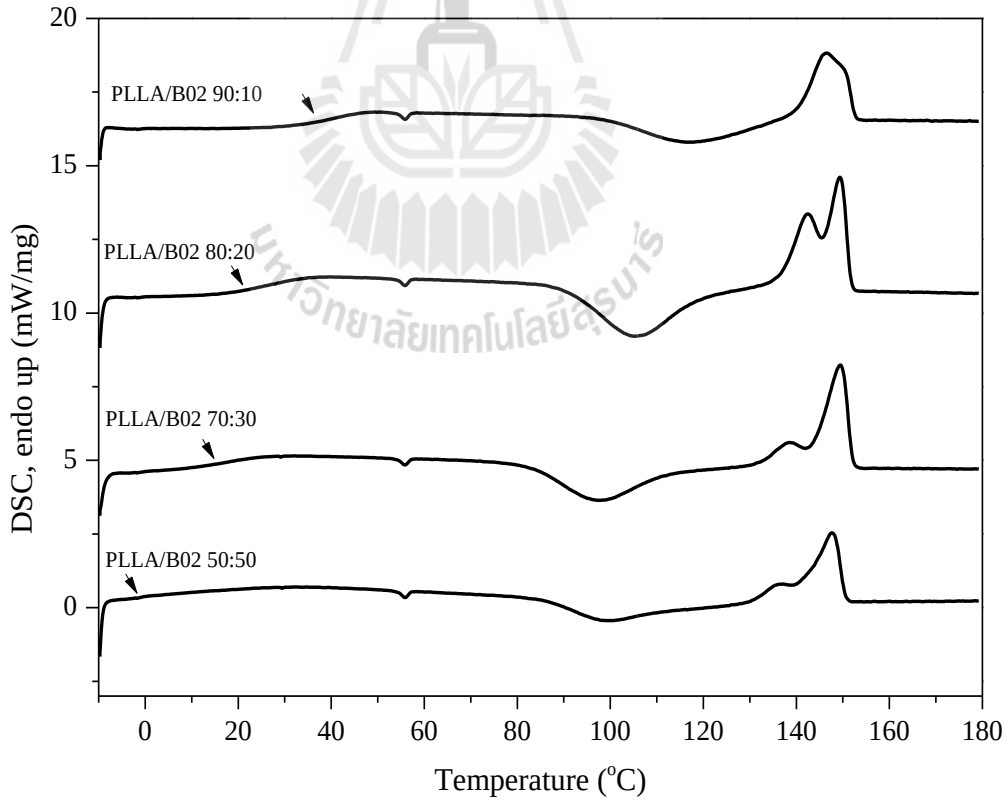

Figure 3.27 Subsequent heating DSC thermograms of quenched PLLA/B02 with different compositions obtained with a heating rate of 10 $^{o}C \cdot min^{-1}$.

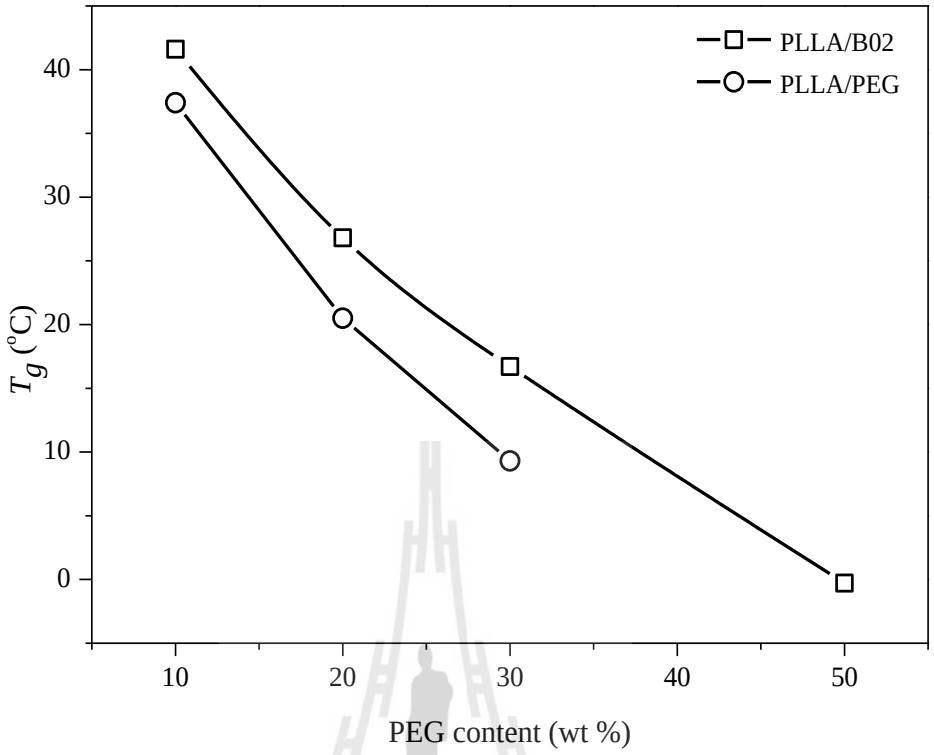

Figure 3.28 Plot of glass transition temperature (T_g) of PLLA/B02 and PLLA/PEG blends as a function of PEG content.

It is clear that all the quenched samples of PLLA/B02 exhibited only a single T_g, which might suggest that B02 is miscible with PLLA in the studied compositions. Figure 3.28 compare the T_g values between PLLA/PEG and PLLA/B02 samples, the result showed that T_g values of the PLLA/B02 are slightly higher than PLLA/PEG blends at same PEG content. This seems that PEG is better than B02 (DLA_{72}-EG_{187}-DLA_{72}) for plasticizing PLLA. However, in quench PLLA/PEG sample with a composition of 50:50 wt % exhibited phase separation (Figure 3.24) while PLLA/B02 was not. In addition the determination T_g for verifying the miscibility. For the blends containing a crystalline polymer, the melting point depression is also an indication of a miscible system. Figure 3.29 illustrated melting

temperature (T_m) of main peak of PLLA in the blends as a function of PEG content. The T_m values of PLLA in PLLA/B02 sample are apparently decreases than PLLA/PEG sample, implying that B02 is more efficiency to hider crystallization of PLLA in the blends than PEG. This is a typical characteristic of a miscible blend composed of an amorphous polymer and crystallizable polymer.

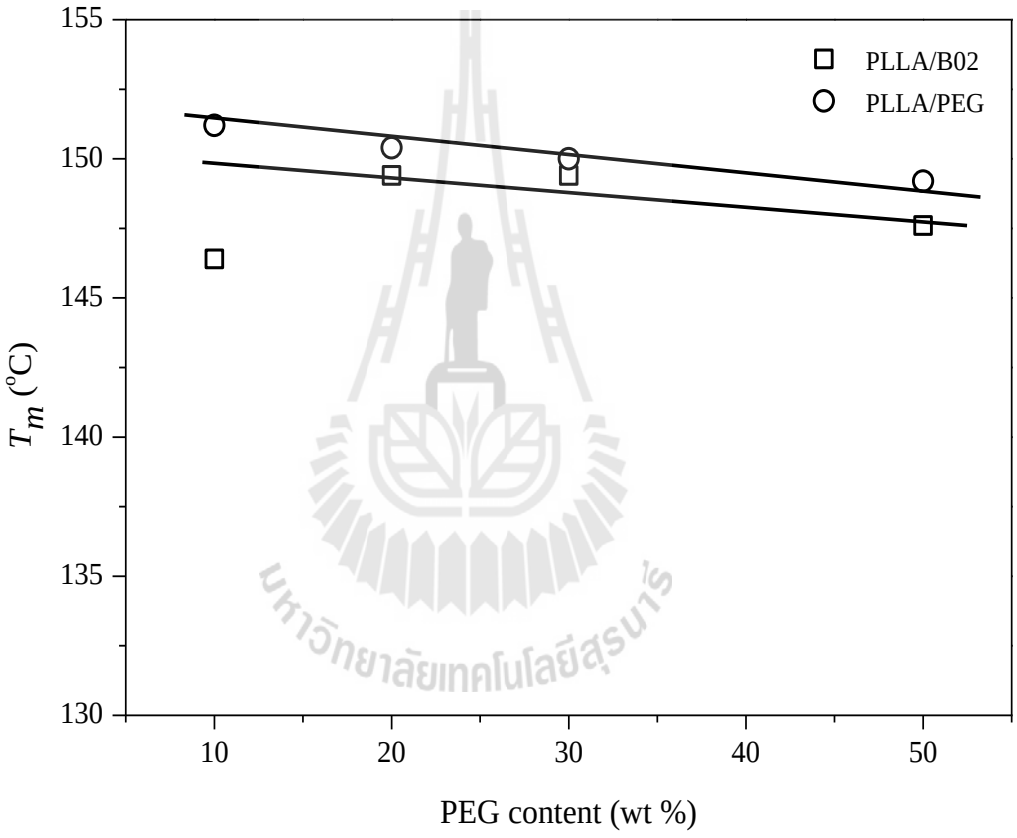

Figure 3.29 Plot of melting temperature (T_m) of PLLA/B02 and PLLA/PEG blends as a function of PEG content.

3.4.6 Rheological characterization

The viscoelastic properties of selected polymers were measured using rheometer, equipped with parallel plate geometry. Linear viscoelastic region (LVER) measurement has been carried out for all samples prior carring out detailed dynamic measurements to probe the sample's microstructure. This was determined by performing an amplitude sweep. The moduli initially are independent of stress, giving a plateau known as the linear viscoelastic region. The limit of linear viscoelasticity is taken as the point at which the storage modulus (G′) decreased by 5% from its low strain plateau value.

A dynamic oscillatory shear measurement is the technique most often used to determine the linear viscoelastic characteristics of a molten polymer. In an oscillatory shear experiment, the sample is subjected to a homogeneous deformation at a sinusoidally varying shear strain or shear stress. In a controlled strain experiment, one generates a strain that is as close as possible to a sine wave as shown in Equation (3.6).

$$\gamma(t) = \gamma_0 \sin(\omega t) \qquad (3.6)$$

Generally, the rheology of polymer melts depends strongly on the temperature at which the measurement is carried out. In the case of polymer samples, it is expected that at the temperatures and frequencies at which the rheological measurements were carried out. They should exhibit characteristic homopolymer-like terminal flow behavior, expressed by the power-laws $G' \propto \omega^2$ and $G'' \propto \omega$, where G′ and G″ are the

storage and loss moduli, respectively. In the linear region the relation between shear stress $\sigma(t)$ and shear $\gamma_0 \sin \omega(t)$ is (Wales and Den Otter, 1970) :

$$\sigma(t) = \gamma_0 [G' \sin \omega(t) + G'' \cos \omega(t)] \quad (3.7)$$

It is sometimes useful in deriving equations to consider the storage and loss moduli to be the real and imaginary components of the *complex modulus*, $G^*(\omega)$, which is defined as follows:

$$G^* (\omega) = G' (\omega) + i\, G''(\omega) \quad (3.8)$$

An alternative representation of dynamic data is in terms of the complex viscosity, η^*, defined as follows:

$$\eta^* = \eta' - i\, \eta'' \quad (3.9)$$

where the real and imaginary components, which are functions of frequency, are related to the storage and loss moduli as follows:

$$\eta' = G''/\omega \quad (3.10)$$

$$\eta'' = G'/\omega \quad (3.11)$$

Furthermore, the *tangent* of the *phase angle* ($\tan \delta$) describes the balance between the viscous and elastic behaviors in a polymer melt:

$$\tan \delta = G'/G'' \quad (3.12)$$

In this investigation, dynamic frequency sweep tests were performed for all sample and these all tests were performed over wide range of frequencies and hence for a long period of time. Some time it is very difficult to avoid thermal degradation of the sample at very high temperatures although nitrogen atmosphere was provided to avoid thermal degradation of the sample. Thermal degradation of the samples subjected to elevated temperatures for long time can have adverse effect on their microstructure. Changes in microstructure can lead to chain scission and cross-linking and/or other physico-chemical process that can adversely affects the material properties.

- **PDLLA-PEG-PDLLA block copolymers**

Viscoelastic properties of triblock copolymers of PDLLA-PEG-PDLLA with different block ratio were investigated at the melt. As discussed above, the stability of block copolymers were investigated at studied measurement. Figure 3.30 shows thermal degradation of DLA_{87}-EG_{187}-DLA_{87} at 60 ^{o}C. It is clear that the G′ and G′′ are constant at 60 ^{o}C indicating this copolymer is stable over time period of the temperature measurement.

To determine the linear viscoelastic limits of block copolymer, the dynamic strain sweep measurements were performed at 50 ^{o}C and a frequency of 10 rad/s. As shown in Figure 3.31. The sample exhibited a constant G′ in the 0.1-10 % range of applied strain. The end of the linear viscoelastic region is indicated by a decrease of G′ value. So, all further experiments should be carried out using a strain value inside the limits of linear viscoelasticity at less than 15 %

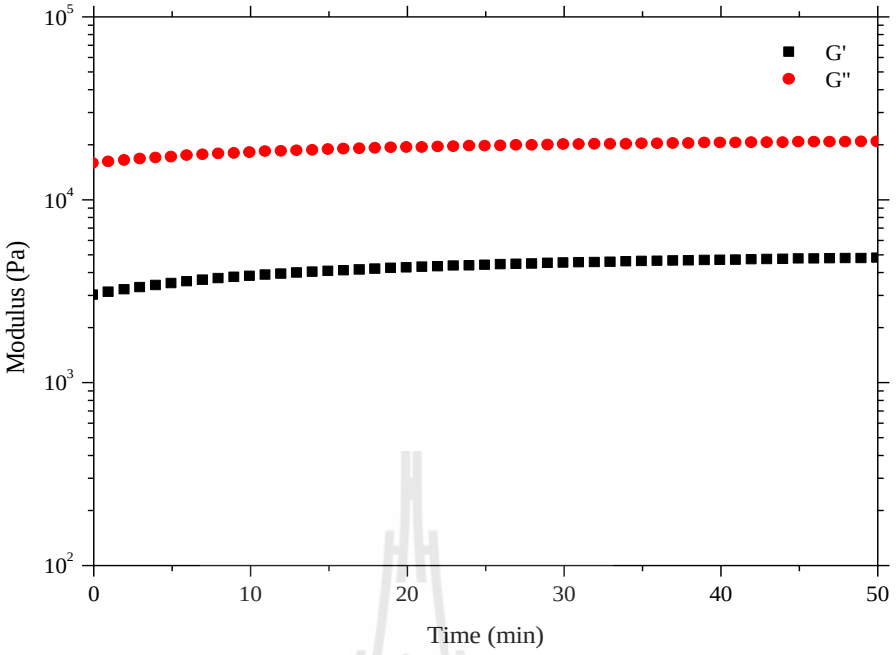

Figure 3.30 Time sweep of DLA_{87}-EG_{187}-DLA_{87} at 60 ^{o}C.

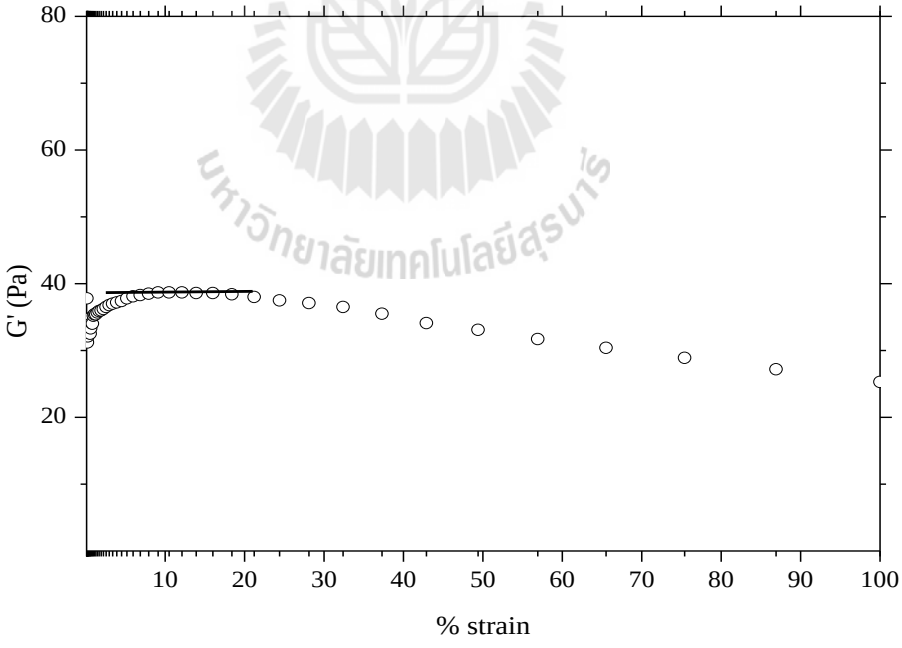

Figure 3.31 Typical dynamic strain sweep of DLA_{36}-EG_{187}-DLA_{36} at 60 ^{o}C and 10 rad/s.

Therefore, all dynamic rheological measurements were performed within the linear viscoelastic region (15% strain) as viscoelastic properties are dominated by chain structure within linear viscoelastic region. The viscoelastic shear properties of the polymers were studied by measuring the storage modulus (G′), loss modulus (G″) and the dynamic viscosity (η^*) within the linear viscoelastic region of the polymers. The storage modulus measures the elastic response of a polymer while the loss modulus measures the viscous energy dissipated during flow deformation. All these tests were performed at temperature ranging from 40 and 50 ^oC.

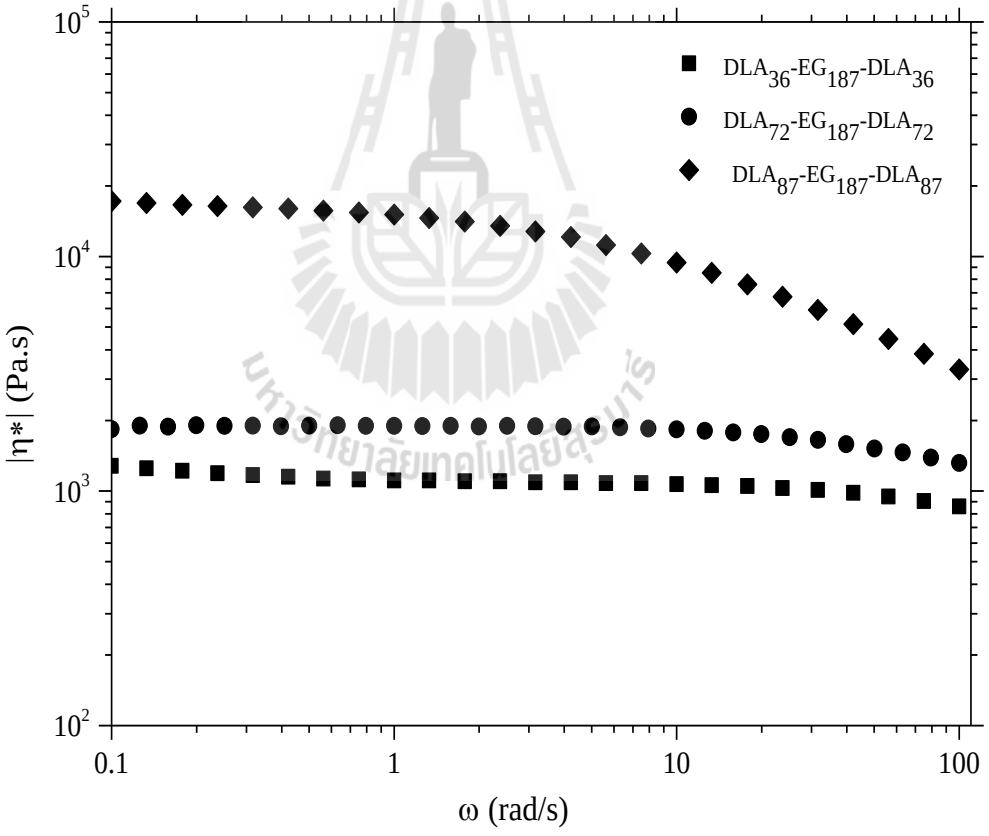

Figure 3.32 Representative complex shear viscosity of various PDLLA-PEG-PDLLA samples at T = 50 ^oC as a function of oscillatory shear frequency.

The flow behavior of these block copolymer at 50 ^{o}C were investigate by the dynamic oscillatory frequency sweep measurements. Complex viscosities were recorded over a range of different shear frequencies (0.1-100 rad/s). Figure 3.32 shows a representative set of complex viscosity curves as a function of frequency. Within a studied frequency range, all PDLLA-PEG-PDLLA samples exhibited shear thinning behavior typical for non-Newtonian fluids, such as polymer melts. As the block length of PDLLA increased, the shear thinning region shifted to lower shear rate.

The measured dynamic modulus data could be used to obtain more information on PDLLA-PEG-PDLLA melt characteristics. The master curves of block copolymer samples are shown in Figure 3.33(a)-(c). It is evident that parameters of interest are only truly observable when the measurements reach the low frequency terminal regime, which is confirmed by slopes of 2 for G′ and 1 for G″ as Maxwell model.

$$G^{'}(\omega) = \sum_{i=1}^{N} \frac{G_i(\omega\lambda_i)^2}{[1+(\omega\lambda_i)^2]} \tag{3.13}$$

$$G^{''}(\omega) = \sum_{i=1}^{N} \frac{G_i(\omega\lambda_i)}{[1+(\omega\lambda_i)^2]} \tag{3.14}$$

where G_i and λ_i are the initial modulus and relaxation time corresponding to the *i* th Maxwell element in Maxwell model.

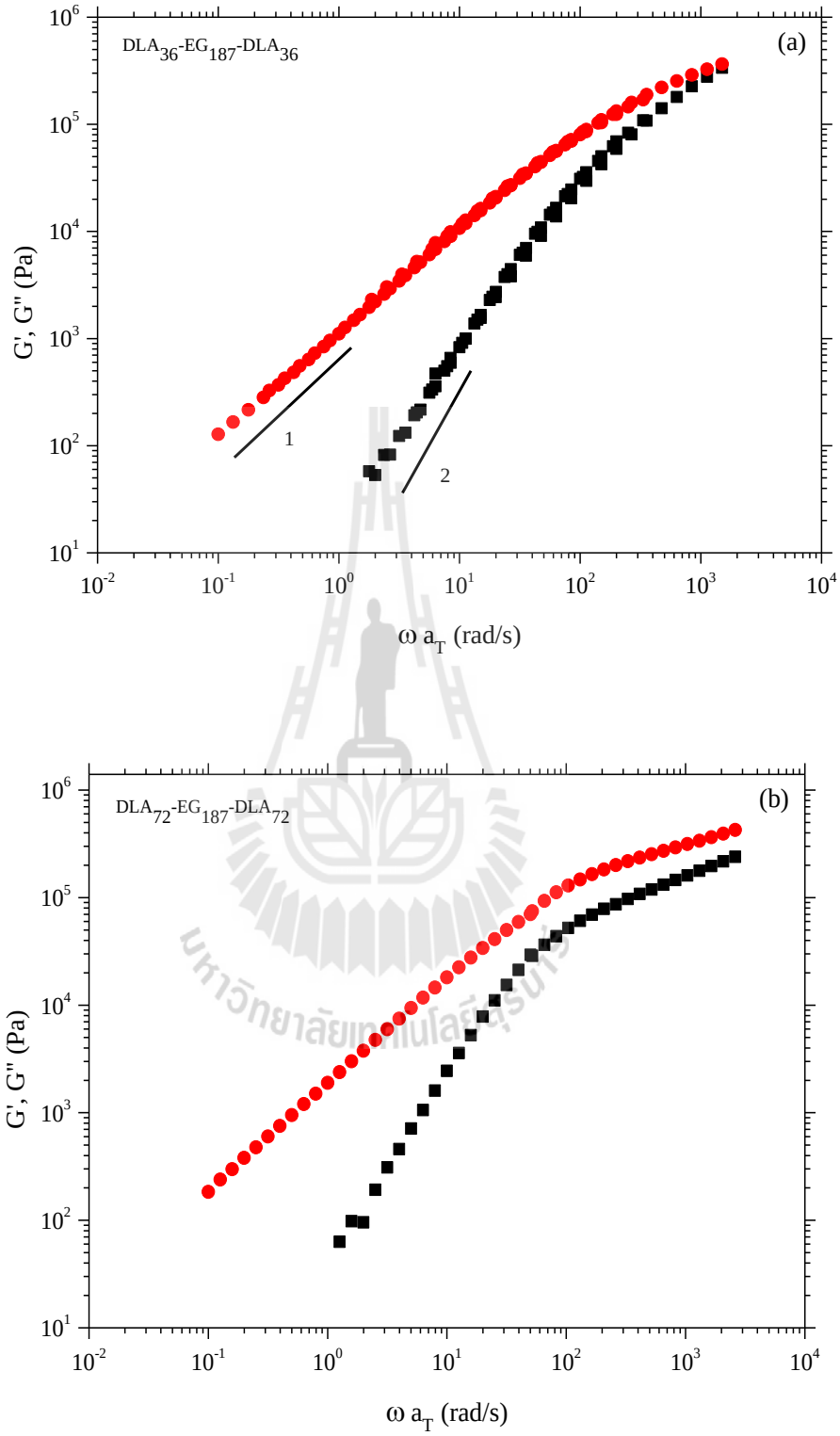

Figure 3.33 Master curves of storage and loss modulus for (a) DLA_{36}-EG_{187}-DLA_{36}, (b) DLA_{72}-EG_{187}-DLA_{72} and (c) DLA_{87}-EG_{187}-DLA_{87}.

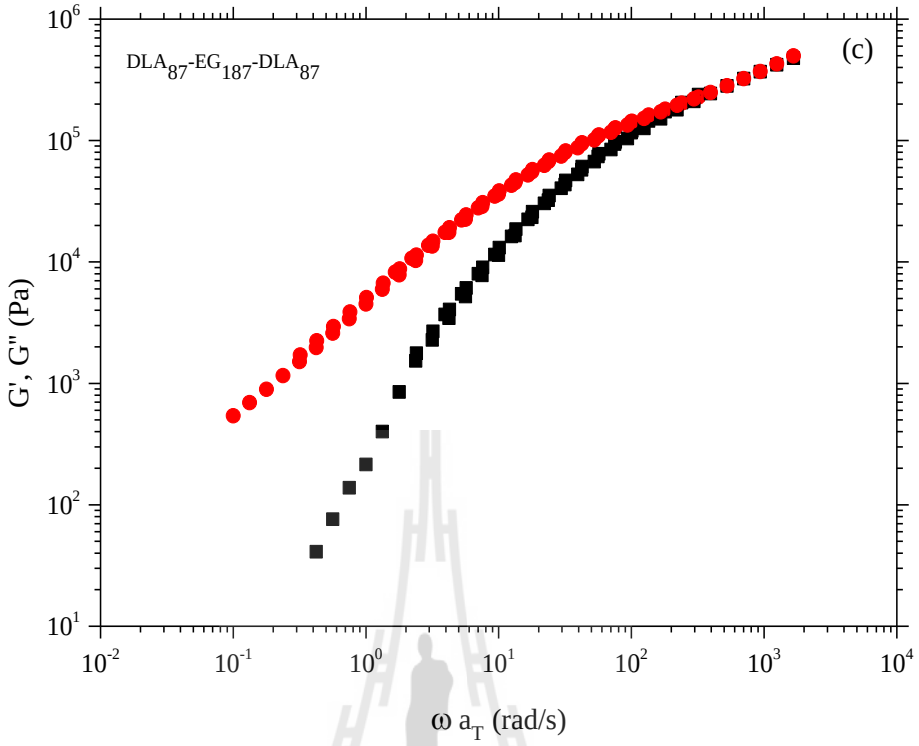

Figure 3.33 (Continued).

The lack of an apparent rubber plateau in the melt phase, especially with decreasing molecular weight, is in fact observed for many semicrystalline polymers, for example, polycaprolactam, PLLA etc, and is thought to be due to the lower molecular weight materials crystallizing below their melting point (at low temperatures extend the high frequency testing range and the crystallization of PEG affects the rheological measurement). The crossover point (ω_c) of G′ and G″ (G′=G″) was observed in DLA_{36}-EG_{187}-DLA_{36} and DLA_{87}-EG_{187}-DLA_{87} samples while DLA_{72}-EG_{187}-DLA_{72} sample was not observed. The $1/\omega_c$ would provide the characteristic relaxation time (λ). It is clear that the λ values of DLA_{87}-EG_{187}-DLA_{87} larger than DLA_{36}-EG_{187}-DLA_{36} as the molecular weight increasing. There is one interesting feature of

viscoelastic properties of DLA_{72}-EG_{187}-DLA_{72}, it exhibited G″ value larger than G′ in high frequency.

Figure 3.34(a) and (b) show the storage and loss modulus of the block copolymers at 50 ^{o}C. The tendency of both G′ and G″ values in terminal region is same, G′ and G″ increased as molecular weight of block copolymer increase. From the results in Figure 3.33 and 3.34, it is clear that these block copolymers are disorder morphology in the melt, the slope of G′ and G″ values are 2 and 1, respectively. This suggestion related to the data from temperature sweep of block copolymer in the range of 0-100 ^{o}C as shown in Figure 3.35(a)-(c).

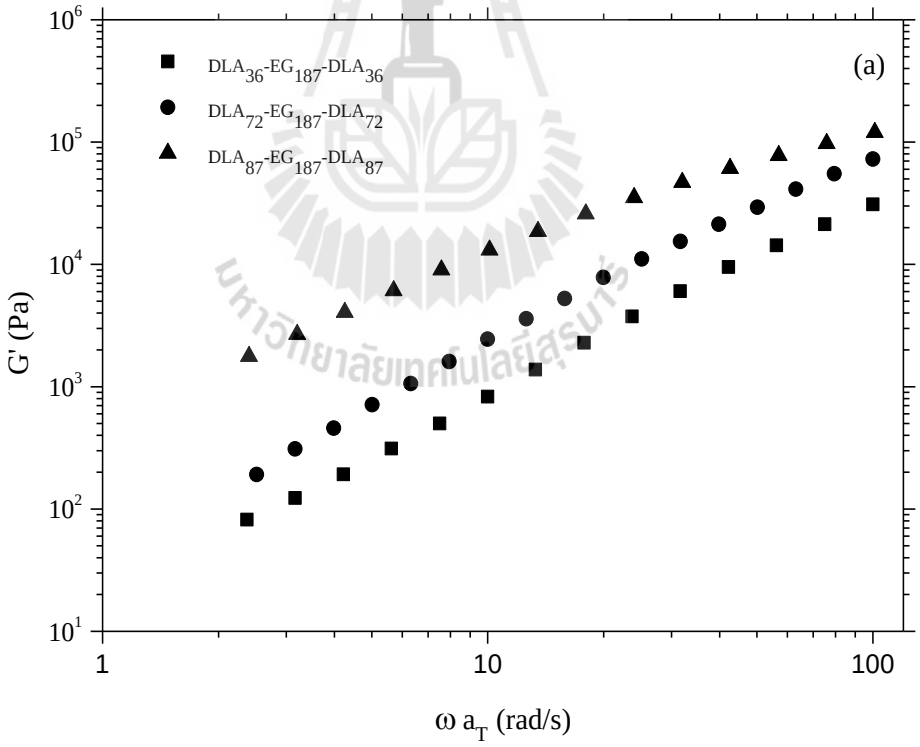

Figure 3.34 (a) The storage modulus (G′) and (b) loss modulus (G″) at 50 ^{o}C of DLA_{36}-EG_{187}-DLA_{36}, (b) DLA_{72}-EG_{187}-DLA_{72} and (c) DLA_{87}-EG_{187}-DLA_{87}.

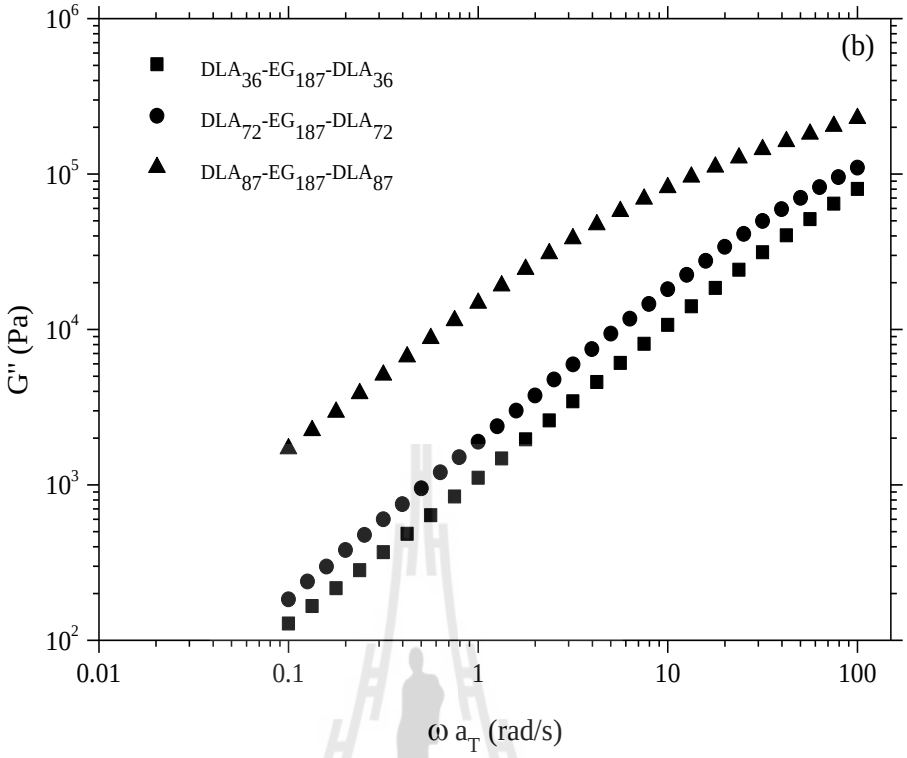

Figure 3.34 (Continued).

Temperature sweep of block copolymers were investigated within the temperature range of 0-100 ^{o}C to verify the phase transition as shown in Figure 3.34. In temperature sweep, both G′ and G″ were measured at a frequency of 1 rad/s and a heating rate of 1 ^{o}C/min. The phase transitions were associated with the significant changes of the dynamic moduli. As shown in Figure 3.34(a) and (b), the transition of crystal melting at about 45-50 ^{o}C which are mesophase/isotropic transition resulted in a drastic decrease of the dynamic moduli. This agrees with DSC results. The two stage change in G′ and G″ was observed in sample DLA_{87}-EG_{187}-DLA_{87}, first is at about 40 ^{o}C and other is at 60 ^{o}C.

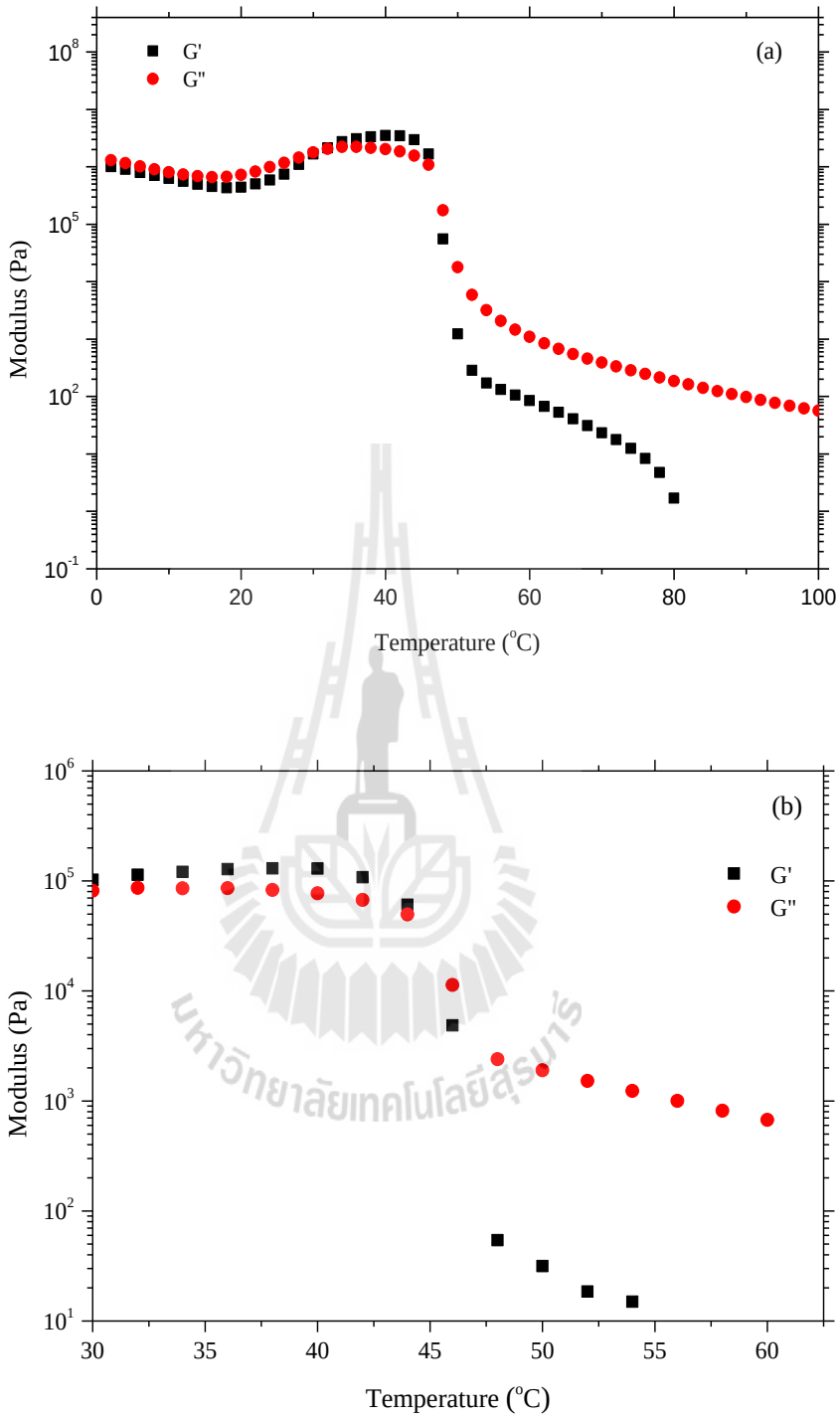

Figure 3.35 Temperature sweep test of (a) DLA_{36}-EG_{187}-DLA_{36}, (b) DLA_{72}-EG_{187}-DLA_{72} and (c) DLA_{87}-EG_{187}-DLA_{87}.

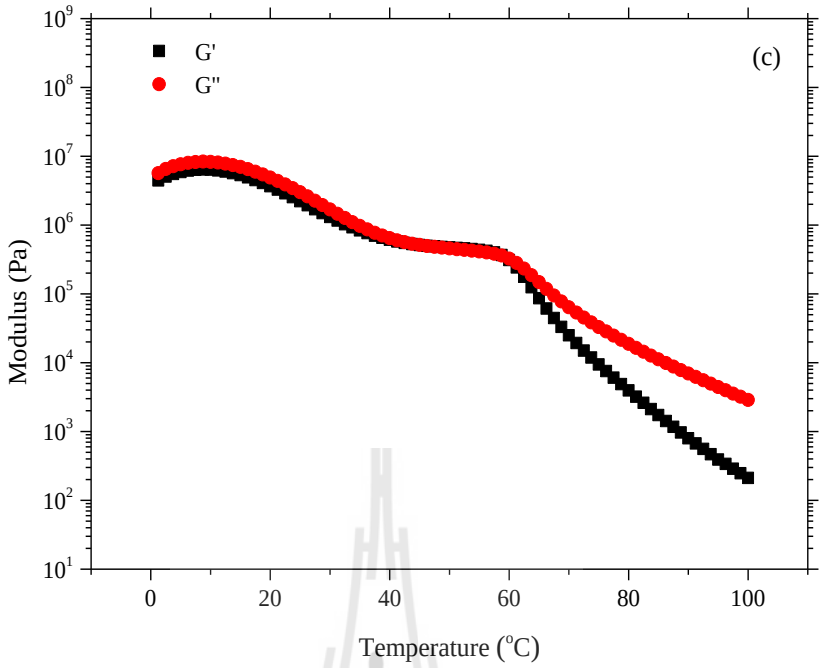

Figure 3.35 (Continued).

- **PLLA/PDLLA-PEG-PDLLA blends**

This section is the study of viscoelastic properties of PLLA/block copolymer blends. Homopolymer and block copolymer which used in this study are PLLA2002D (Nature Work) and block copolymer of DLA_{72}-EG_{187}-DLA_{72} (B02), respectively. The mixtures of PLLA/PEG (M_w of PEG = 8,000 $g.mol^{-1}$) were used for comparing to above systems. The weight fraction of PLLA and PEG in both of PLLA/DLA_{72}-EG_{187}-DLA_{72} and PLLA/PEG blends is equivalent. To simplify for presentation, 10 wt% B02 was represented as the PLLA/DLA_{72}-EG_{187}-DLA_{72} blends compose of 10 wt% of PEG. In addition, the miscibility of polymer blends was investigated by analysis the rheological data.

Since PLLA is biodegradable polymer, thermal stability of such material is important key for study for rheology testing. Figure 3.36 shows thermal

degradation (stability of modulus) of PLLA as a function of time at 180 ^{o}C. Temperature of 180 °C was selected which is same temperature used for dynamic frequency sweeps. Time sweep test was done at constant frequency at constant temperature (180 ºC) for 30 minute. The G″ value is constant over range of studied time while G″ gradually decreases within first 15 minute and constant after that time. This observation reflects that PLLA is stable during measurements because.

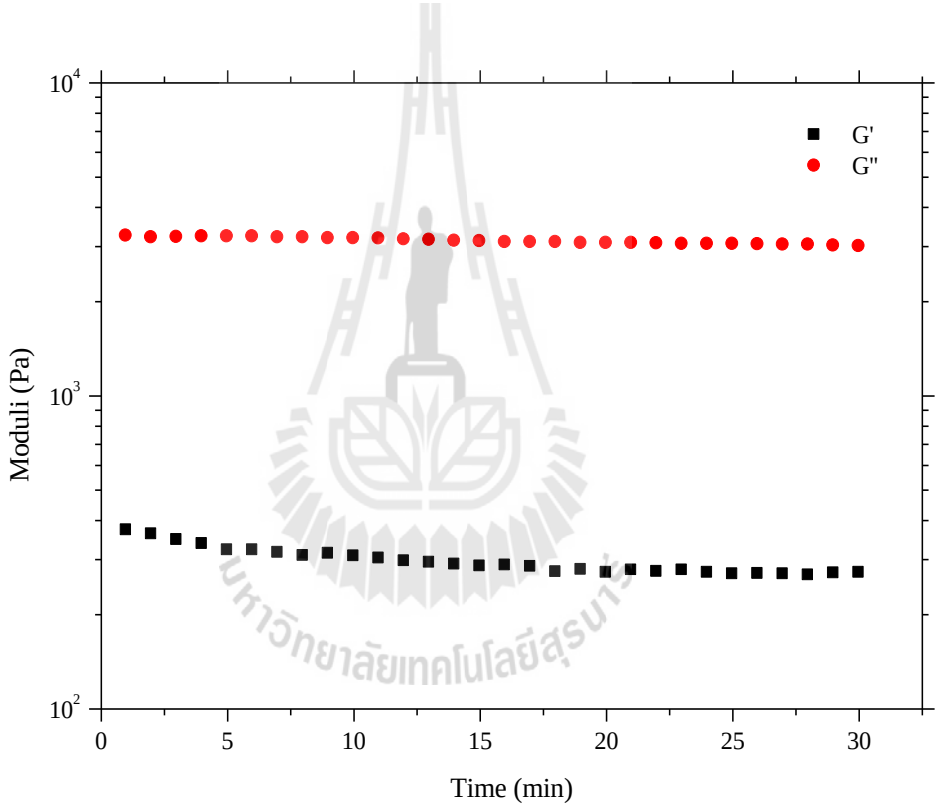

Figure 3.36 Time sweep test of PLLA at 180 ^{o}C with 1% strain and 1 rad/s.

The viscoelastic properties of the samples were obtained from the frequency sweep measurement. The linear viscoelastic region was determined and the value of 5% strain was used for all measurements. All these tests were performed at temperature ranging of 130-180 ^{o}C.

In order to establish the validity of the Cox-Merz Rule, steady state data was obtained over a range of shear rates for the PLLA at 180 ^{o}C to compare to the frequency sweep data. According to the Cox-Merz rule (Sperling, 2001), which applied to many polymer melts, the steady shear viscosity, $\eta(\dot{\gamma})$ is identical to the absolute value of complex shear viscosity $|\eta^*(\omega)|$:

$$\eta(\dot{\gamma}) = |\eta^*(\omega)| \quad \text{if } \dot{\gamma} = \omega \tag{3.15}$$

The comparison of the steady state and dynamic viscosities is shown in Figure 3.37. At the lower rates, there is a good agreement between the viscosities, the steady shear viscosity exhibited the higher values than dynamic viscosity. However, at the higher rates tested the steady shear plot of PLLA showed significantly shear thinning behavior at ~4 s^{-1}, while dynamic plot exhibited the slight shear thinning behavior at a frequency of ~15 rad/s.

The master curve of PLLA was created by the time temperature superposition (TTS) method with use a referenced temperature of 180 ^{o}C and is constructed from isothermal curves obtained at five different temperatures (130, 140, 150, 160, 170 and 180 ^{o}C). This curve is shown in Figure 3.38. The terminal region was observed corresponding to $G' \propto \omega^2$ and $G'' \propto \omega$. In addition, the crossover frequency which is referred to the relaxation time, could also be observed at a

frequency of 439 rad/s indicating relaxation time at 0.002 s. PLLA did not show the rubber plateau in the melt phase (high frequency region). This observation is caused from the crystallization below its melting point (Justin and Michael, 1999).

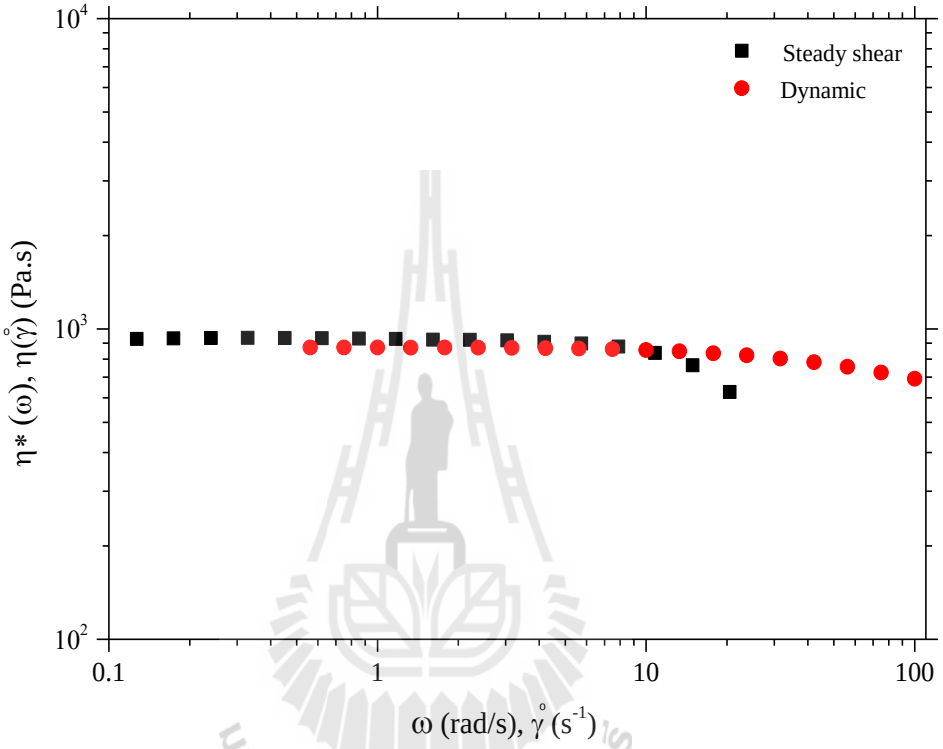

Figure 3.37 PLLA frequency sweep and steady state results at 180 ^{o}C to show validity of Cox-Merz rule.

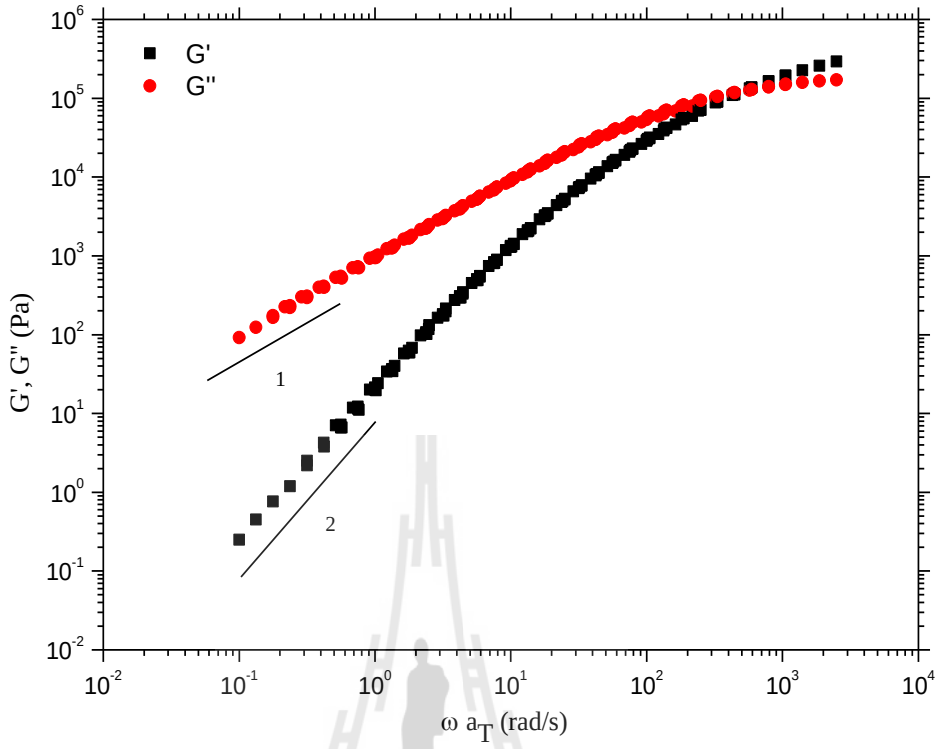

Figure 3.38 Time-Temperature superposition (TTS) plot of PLLA. The master curve is referenced to 180 ^{o}C and is constructed from isothermal curves obtained at 130, 140, 150, 160, 170 and 180 ^{o}C.

The linear viscoelastic properties of the PLLA/B02 and PLLA/PEG blends with different weight fraction were determined at 170 ^{o}C. Figure 3.39 shows the complex viscosity of PLLA/PEG blends with different PEG content. The PLLA exhibited a clear Newtonian Plateau at low oscillation frequency with a zero-shear rate viscosity (η_0) from 1294 Pa.s and to be shear thinning behavior at high oscillation frequency. All PLLA/PEG blends of varying PEG concentrations exhibited a more pronounced Newtonian response with an extended Newtonian plateau compared with

neat PLLA and also showed the decreasing η_0 values as the PEG concentration increased. This tendency is similar to those PLLA/B02 systems.

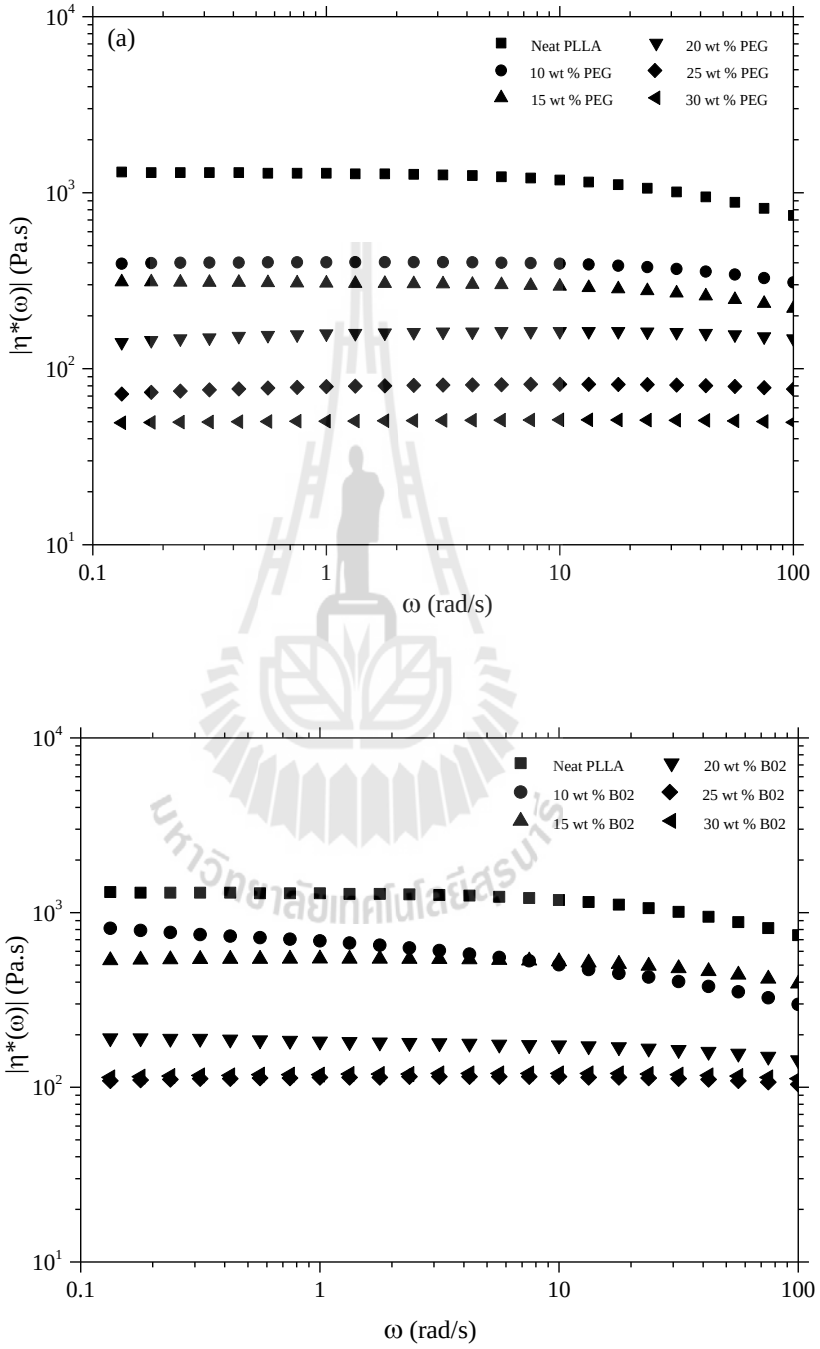

Figure 3.39 Complex viscosity $|\eta^*(\omega)|$ of (a) PLLA/PEG blends and (b) PLLA/B02 with different weight fraction of plasticizer at 170 ^{o}C.

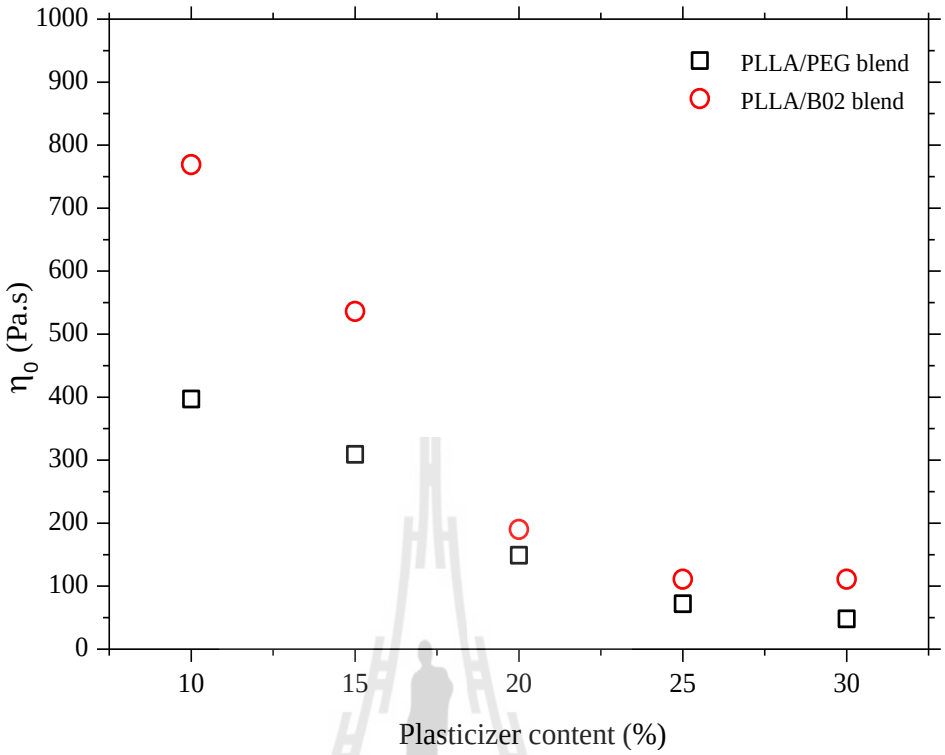

Figure 3.40 Zero shear viscosity (η_0) as a function of plasticizer content (wt %) of PLLA/PEG blends PLLA/B02 at 170 ^{o}C.

The effect of plasticizer on zero shear viscosity (η_0) of PLLA/PEG and PLLA/B02 blends was shown in Figure 3.40. Comparing with same PEG content in both systems, the η_0 values of PLLA/PEG blends are lower than PLLA/B02 blends, indicating that PEG more effective to enhance the segmental mobility of PLLA chains than in B02. These resultants agree well with the decreasing of T_g of both blends as mentioned in the section 3.4.4.

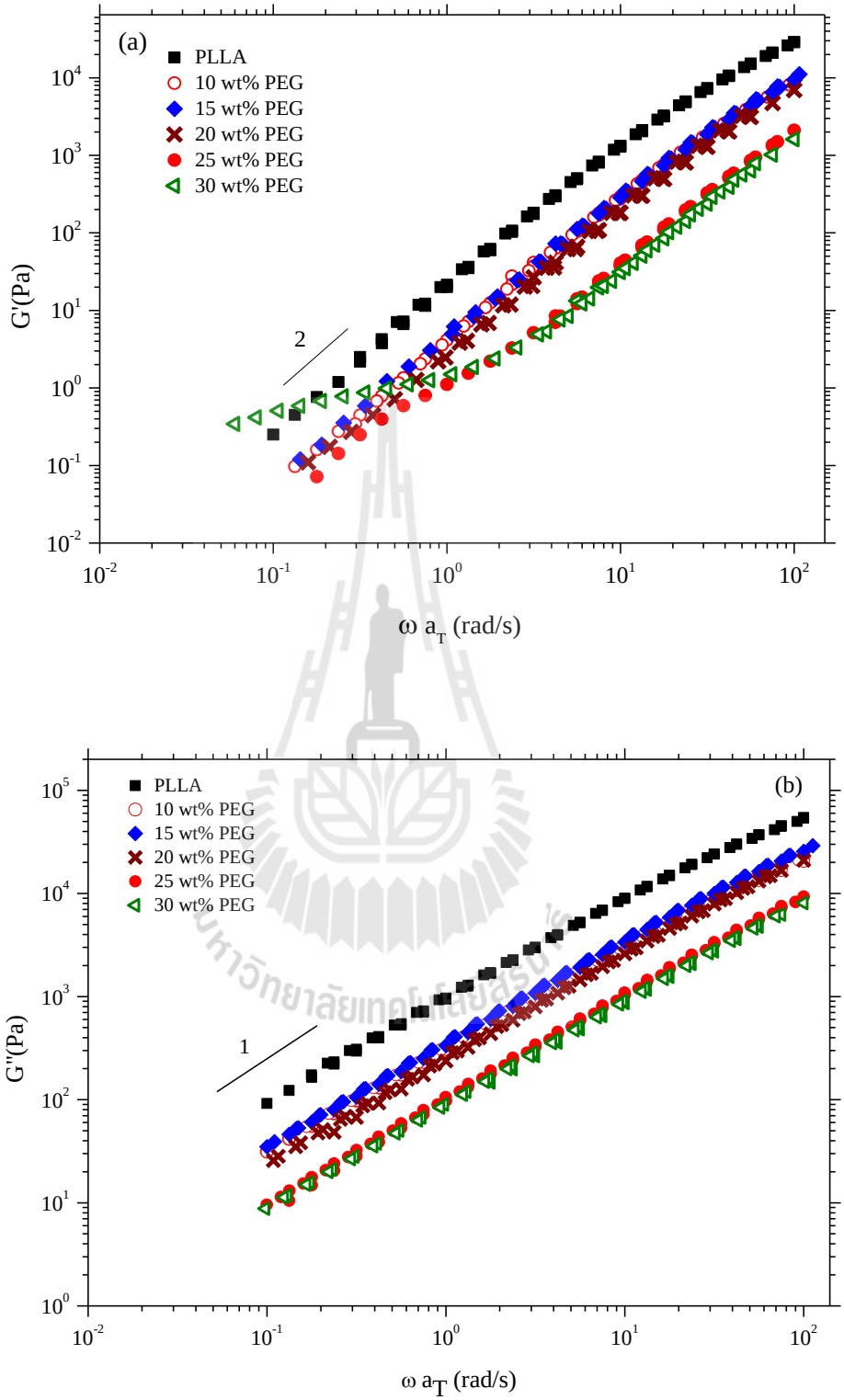

Figure 3.41 Master curves of (a) storage modulus (G′) (b) loss modulus (G″) of PLLA/PEG with different PEG contents.

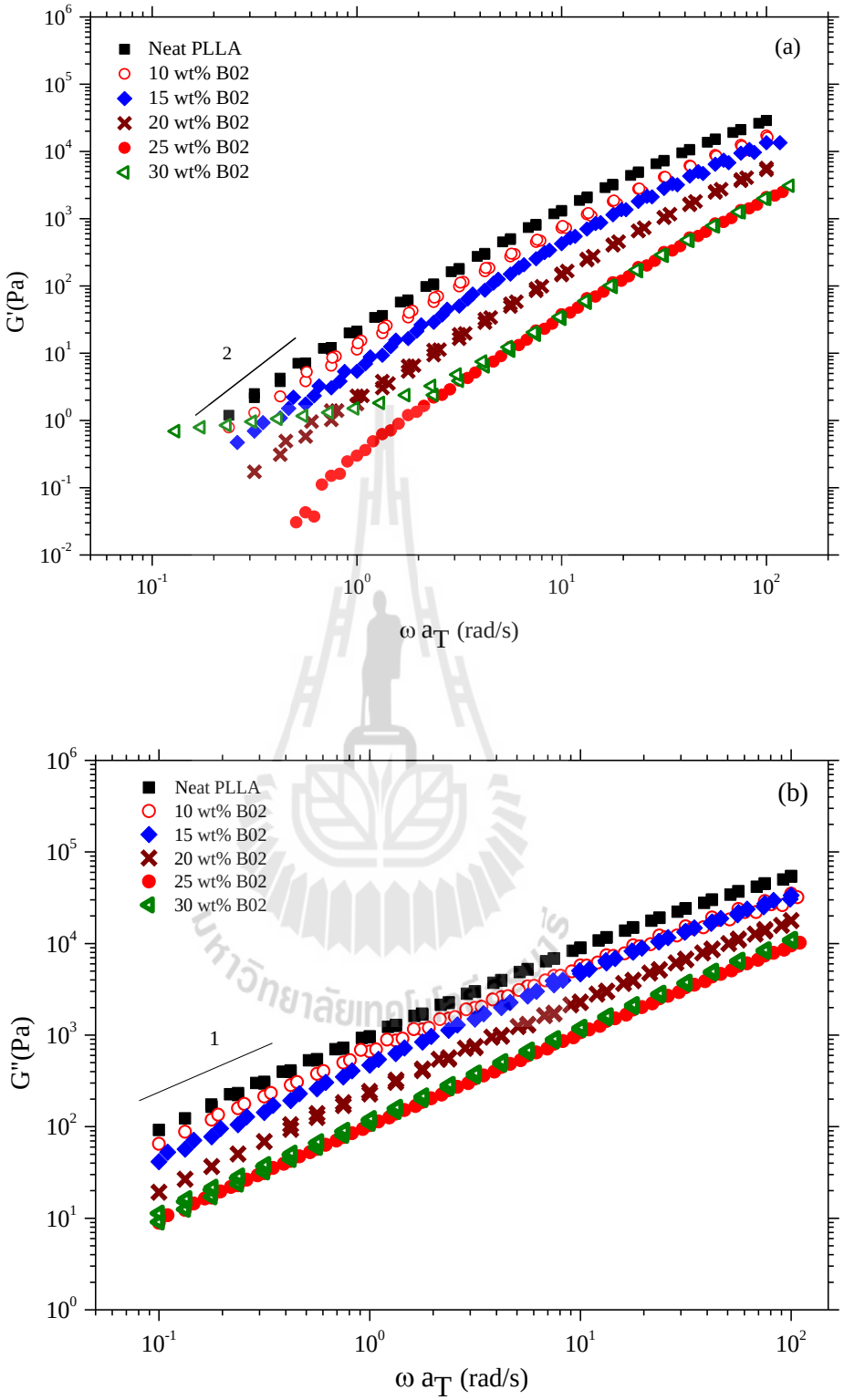

Figure 3.42 Master curves of (a) storage modulus (G′) (b) loss modulus (G″) of PLLA/PEG with different PEG contents.

The corresponding G′ and G″ for these blends are shown in Figure 3.41 and 3.42. As expected, the moduli of PLLA decreased with increasing plasticizer loading at all frequencies. All polymer samples exhibited the rheological behavior of a typical polymer melt as characterized by a G′ smaller than the G″. Both the G′ and G″ decreased with increasing plasticizer concentration. At high frequencies, all samples approximately showed a common storage modulus. In contrast, at the low frequency ($\omega < 1$) the elastic modulus of the blends significantly deviates from the characteristic slope of 2, which would have indicated terminal relaxation zone. The enhancement in elastic modulus has been reported in many studies for immiscible binary polymer blends (Noroozi, Schafer, and Hatzikiriakos, 2012; Gu, Zhang, Ren, and Zhan, 2008). This is accepted to be attributed to the change of the shape of the discrete phase in the polymer matrix during the oscillatory shear deformation, namely shape relaxation (Ferry, 1980). While the loss moduli of all blends are less dependent on the incorporation of plasticizers.

In the cases of PLLA/PEG blends, at the frequency less than 1 rad/s, the frequency dependent transition of the blend with PEG concentration less than 25 wt% could be observed. On the other hand, the frequency dependent transition of PLLA/PEG blends at PEG concentration higher than 25 wt% showed a medium frequency dependent region between 1-10 rad/s. It could be concluded that at higher PEG concentration the G′ curves exhibited a plateau distinctly at the low frequencies as the blends seemed to be a solid like behavior. While PLLA/B02 blends at PEG content of 30 wt% only showed the plateau distinctly at the low frequencies. As seen in Figure 3.40 and 3.41, the slope of G′ for neat PLLA was 2, similar to the thermo-rheologically simple polymer in the terminal regime. In contrast, the slopes of

the G′, at low frequency (0.1-1 rad/s) for PLLA/PEG with the PEG content of 25 and 30 wt% and PLLA/B02 with PEG content of 30 wt% deviated from 2. Noroozi *et al*., (2012) reported that the experimental values of the slope for G′ obtained from other phase separated or degraded polymer blends varied between 0.5 and 1. Therefore, the small values of these values suggested that the high concentration of PEG may have contributed to the phase separation in these blends as verified in the thermal and mechanical characterization. Compare with same PEG content, B02 is less contributes to the phase separation than PEG plasticizer, indicating that B02 is more miscible in PLLA than PEG.

3.5 Conclusions

The series of PLA-PEG-PLA block copolymers with different LA/EG ratio were synthesized via ring opening polymerization using stannous (II) octoate as a catalyst at 130 ^{o}C. Two kinds of stereochemical lactide (LA) monomer, L-LA and D, L-LA were used to prepare for PLLA-PEG-PLLA and PDLLA-PEG-PDLLA block copolymers, respectively. PEG with M_w of 8,000 and 10,000 g.mol^{-1} were used as initiator polymerization. The chemical structure and chemical composition of the synthesized PLA-PEG-PLA block copolymers were investigated by FT-IR, ^{1}H-, ^{13}C-NMR and GPC techniques. The results exhibited the characteristics of these block copolymers and agree well with literature data.

Thermal properties of PLLA-PEG-PLLA and PDLLA-PEG-PDLLA block copolymers were investigated by DSC technique. PLLA-PEG-PLLA is a double crystallizable block copolymer while the PDLLA-PEG-PDLLA copolymer is a single crystallizable copolymer (PDLLA is amorphous polymer). However, crystallization of

each block depends on block composition. PLLA-PEG-PLLA copolymers with PLLA block ratio, ϕ_{PLLA} = 0.37-0.47 showed two distinct melting peaks for the PLLA and PEG, indicating good microphase separation. This result agrees well with XRD and POM results. The presence of the PLLA sequences attached to PEG blocks decreased the melting temperature (T_m) of both the PEG block and PLA block. It can be found that at high PLLA block content (LLA_{347}-EG_{187}-LLA_{347}), the PEG segments do not crystallize. Similarly, for copolymer with high PEG block content (LLA_{49}-EG_{187}-LLA_{49}), the small crystallinity of PLA block is observed. This behavior is same in PDLLA-PEG-PDLLA system. For crystallization kinetic study, PLLA-PEG-PLLA block copolymers were selected to study. The result showed that the presences of PEG blocks in block copolymers accelerate the crystallization rate of PLLA block segments comparing to the crystallization rate of neat PLLA. From data analysis with Avrami model, the result showed the Avrami exponent (n) below 3 (2.1-2.6), indicating that the crystallization process of PLLA segments in block copolymer occurs in two-dimensional aggregates. The crystallization process with a nucleation and growth was described by isothermal crystallization growth rate (G) of PLLA. The G values decreased with a further increase in isothermal temperature.

Miscibility of PLLA/PDLLA-PEG-PDLLA blends was investigated by using DSC and rheological techniques. The polymer blends of PLLA and PEG with $\overline{M}_w$ of 8,000 $g.mol^{-1}$ (PLLA/PEG) were used as controller systems. The quench samples of PLLA/PEG blends with PEG content of 10-30 wt% showed a single T_g and showed only melting peak of PLLA. These results indicate PLLA/PEG is miscible over those compositions. While the PLLA/PEG 50/50 (wt/wt) blends showed phase separation. However, when the PLLA/PEG 70/30 (wt/wt) was slowly cooled down from the melt

(cooling rate 10 ^{o}C min^{-1}) the subsequent DSC thermogram of this sample showed the phase separation. In the same condition, PLLA/PDLLA-PEG-PDLLA systems did not show the phase separation. As the result indicated that the PDLLA end block of PDLLA-PEG-PDLLA block copolymer contributed to reduce the phase separation in the blends. When comparison the efficiency for plasticizing PLLA between PEG and PDLLA-PEG-PDLLA, it was found that the glass transition temperature (T_g) of PLLA/PEG blends are lower than PLLA/PDLLA-PEG-PDLLA.

To support the DSC results, rheological measurement of PLLA/PEG and PLLA/PDLLA-PEG-PDLLA blends were performed at the melt state. Rheological technique is a sensitive technique for detecting the change of microstructure of polymer chains. The rheological properties of PDLLA-PEG-PDLLA copolymers and PLLA/PEG and PLLA/PDLLA-PEG-PDLLA blends were studied. It is clear that the flow behavior of selected systems is shear thinning behavior. The microphase separation in the melt of PDLLA-PEG-PDLLA was not observed. Storage modulus (G′) and loss modulus (G′′) increased with increasing molecular weight of PDLLA-PEG-PDLLA. For polymer blends, zero shear viscosity (η_0) decreased with increasing the plasticizer content and the decreasing of η_0 is pronounced in PLLA/PEG systems. To study the miscibility in polymer blends, G′ and G′′ curves in low frequency region (0.1-1.0 rad/s) were determined. The deviation of slope of G′ curve from 2 indicates that the binary mixture is immiscible. The results showed that slope of G′ curves for PLLA/PEG at 75/25 and 70/30 (wt/wt) are less than 2 while this deviation was found in PLLA/PDLLA-PEG-PDLLA with equivalent PEG content of 70/30 (wt/wt). This indicates the PDLLA end block in PDLLA-PEG-PDLLA copolymer contribute to enhance miscibility of PEG in PLLA matrix.

3.6 References

Anderson, K. S., Lim, S. H. and Hillmyer, M. A. (2002). Toughening of polylactide by melt blending with linear low-density polyethylene. **Journal of Applied Polymer Science** 89: 3757-3768.

Auras, R., Lim, L. T., Selke, S. E. M. and Tsuji, H. (2010). **Poly(lactic acid): Synthesis, structures, properties, processing and applications.** Canada: John Wiley & Sons, Inc..

Boua-in, K., Chaiyut, N. and Ksapabutr, B. (2010). Preparation of polylactide by ring-opening polymerization of lactide. **Optoelectronics and Advance Materials-Rapid Communications** 9: 1404-1407.

Dechy-Cabaret, O., Martin-Vaca, B. and Bourissou, D. (2004). Controlled ring opening polymerization of lactide and glycolide. **Chemical Reviews** 104: 6147-6176.

Du, Y. J., Lemstra, P. j., Nijenhuis, A. J., Aert, H. A. M. V. and Bastiaansen, C. (1995). ABA type copolymers of lactide with poly(ethylene glycol): Kinetic, mechanistic, and model studies. **Macromolecules** 28: 2124-2132.

Eguiburu J. L., Iruin J. J., Fernandez-Berridi M. J., Roman J. S. (1998). Blends of amorphous and crystalline polylactides with poly(methyl methacrylate) and poly(methyl acrylate): a miscibility study. **Polymer** 39: 6891.

Garlotta, D. (2001). A literature review of poly(lactic acid). **Journal of Polymers and the Environment** 2(9): 63-84.

Gu, S. Y., Zhang, K., Ren, J. and Zhan, H. (2008). Melt rheology of polylactide/ poly(butylene adipate-*co*-terephthalate) blends. **Carbohydrate Polymers** 74: 79-85.

Gupta, A. P. and Kumar, V. (2007). New emerging trends in synthetic biodegradable polymers, Polylactide: A critique. **European Polymer Journal** 43: 4053-4074.

Hamley, I. W. (1998). **The physics of block copolymer**. New York: Oxford University Press.

Hamley, I. W., Castelletto, V., Castillo, R. V., Muller, A. J., Martin, C. M., Pollet, E. and Dubois, Ph. (2005). Crystallization in poly(L-lactide)-*b*-poly(*ε*-caprolactone) double crystalline diblock copolymers: A study using X-ray scattering, differential scanning calorimetry, and polarized optical microscopy. **Macromolecules** 38: 463-472.

Hansen, K. K., Neilson, C. J. and Hvilsted, S. (2004). Low molecular weights block copolymers as plasticizers for polystyrene. **Journal of Applied Polymer Science** 95: 981-991.

Hu, Y., Hu, Y. S., Topolkaraev, V., Hiltner, A. and Baer, E. (2003). Crystallization and phase separation in blends of high stereoregular poly(lactide) with poly(ethylene glycol). **Polymer** 44: 5681-5689.

Hu, Y., Rogunova, M., Topolkaraev, V., Hiltner, A. and Baer, E. (2003). Aging of poly(lactide)/poly(ethylene glycol) blends: Part 1. Poly(lactide) with low stereoregularity. **Polymer** 44: 5701-5710.

Jacobsen, S. and Fritz, H. G. (1999). Plasticizing polylactide-the effect of different plasticizers on the mechanical properties. **Polymer Engineering & Science** 39: 1303-1310.

Jia, Z., Tan, J., Han, C., Yang, Y. and Dong, L. (2009). Poly(ethylene glycol-co-propylene glycol) as a macromolecular plasticizing agent for polylactide: Thermomechanical properties and aging. **Journal of Applied Polymer Science** 114: 1105-1117.

Justin, J. C. and Michael, E. M. (1999). Rheological properties of poly(lactides). Effect of molecular weight and temperature on the viscoelasticity of poly(L-lactic acid). **Journal of polymer science: Part B: Polymer physics** 37: 1803-1814.

Kim, K. S., Chung, S., Chin, I. j., Kim, M. N. and Yoon, J. S. (1999). Crystallization behavior of biodegradable amphiphilic poly(ethylene glycol)-poly(L-lactide) block copolymers. **Journal of Applied Polymer Science** 72: 341-348.

Kissel, T., Li, Y. and Unger, F. (2001). ABA-triblock copolymers from biodegradable polyester A-blocks and hydrophilic poly(ethylene oxide) B-blocks as a candidate for in situ forming hydrogel delivery systems for proteins. **Advanced Drug Delivery Reviews** 54: 99-134.

Koyama, N. and Doi, Y. (1995). Morphology and biodegradability of a binary blend of poly((*R*)-3-hydroxybutyric acid) and poly((*R*,*S*)-lactic acid). **Canadian Journal of Microbiology** 166: 155.

Kubies, D., Rypáček, F., Kovárová, J. and Lednicky′, F. (2000). Microdomain structure in polylactide-*b*-poly(ethylene oxide) copolymer films. Biomaterials 21: 529-536.

Kulinsky, Z. and Piorkowska, E. (2005). Crystallization, structure and properties of plasticized poly(L-lactide). **Polymer** 46: 10290-10300.

Kulinski, Z., Piorkowska, E., Gadzinowska, K., and Stasiak, M. (2006). Plasticization of poly(L-lactide) with poly(propylene glycol). **Biomacromolecules** 7: 2128-2135.

Kuo, S., Xu, H., Huang, C. and Chang, F. (2002). Significant glass transition temperature increase through hydrogen-bonded copolymers. **Journal of Polymer Science: Part B: Polymer Physics** 40: 2313-2323.

Lai, W. C., Liau, W. B. and Lin, T. T. (2004). The effect of end groups of PEG on the crystallization behaviors of binary crystalline polymer blends PEG/PLLA. **Polymer** 45: 3037-3080.

Leenslag, J. W. and Pennings, A. J. (1987). Synthesis of high molecular weight poly(lactide) initiated with tin 2-ethylhexanoate. **Macromolecular Chemistry and Physics** 188: 1809-1814.

Lemmouchi, Y., Murariu, M., Margarida Dos Santos, A., Amass, A. J., Schacht, E. and Dubois, P. (2009). Plasticization of poly(lactide) with blends of tributyl citrate and low molecular weight poly(D,L-lactide)-b-poly(ethylene glycol) copolymers. **European Polymer Journal** 45: 2839-2848.

Ljungberg, N. and Wesslen, B. (2002). The effects of plasticizers on the dynamic mechanical and thermal properties of poly(lactic acid). **Journal of Applied Polymer Science** 86: 1227-1234.

Ljungberg, N. and Wesslen, B. (2002). Tributyl oligomers as plasticizers for poly (lactic acid): thermo-mechanical film properties and aging. **Polymer** 44: 7679-7688.

Ljungberg, N. and Wesslen, B. (2005). Preparation and properties of plasticized poly(lactic acid) films. **Biomacromolecules** 6: 1789-1796.

Lui, H. and Zhang, J. (2011). Research progress in toughening modification of poly(lactic acid). **Journal of Polymer Science Part B: Polymer Physics** 15(49): 1051-1083.

Mehta, R., Kumar, V., Bhunia, H. and Upadyay, S. N. (2005). Synthesis of poly(lactic acid): A review. **Journal of Macromolecule Science, Part C: Polymer Reviews** 45: 325-349.

Nakafuku, C. and Takehisa, S. Y. (2004). Glass transition and mechanical properties of PLLA and PDLLA-PGA copolymer blends. **Journal of Applied Polymer Science** 93: 2164-2173.

Noroozi, N., Schafer L. L. and Hatzikiriakos, S. G. (2012). Thermorheological properties of poly(ε-caprolactone)/polylactide blends. **Polymer Engineering and Science** 52: 2348-2359.

Park, J. Y., Hwang, S. Y., Yoon, W. J., Yoo, E. S. and Im, S. S. (2012). Compatibility and physical properties of poly(lactic acid)/poly(ethylene terephthalate glycol) blends. **Macromol Res** 20: 1300-1306.

Pillin, I., Montrelay, N. and Grohens, Y. (2006). Thermo-mechanical characterization of plasticized PLA: Is the miscibility the only significant factor? **Polymer** 47: 4676-4682.

Rashkov, I., Manolova, N., Li, S. M., Espartero, J. L. and Vert, M. (1996). Synthesis, characterization, and hydrolytic degradation of PLA/PEO/PLA triblock copolymer with short poly(L-lactic acid) chains. **Macromolecules** 20: 50-56.

Rathi, S., Chen, X., Coughlin, E. B., Hsu, S. L., Golub, C. S. and Tzivanis, M. J. (2011). Toughening semicrystalline poly(lactic acid) by morphology alteration. **Polymer** 52: 4181-4188.

Sheth, M., Kumar, R. A., Dave, V., Gross, R. A. and McCarthy, S. P. (1997). Biodegradable polymer blends of poly(lactic acid) and poly(ethylene glycol) **Journal of Applied and Polymer Science** 66: 1495-1505.

Sheth, M., Ananda, K. R., Dave, V., Gross, R. A. and Mcchathy, S. P. (2006). Biodegradable polymer blends of poly(lactic acid) and poly(ethylene glycol). **Journal of Applied Polymer Science** 66: 1495-1505.

Sperling, L. H. (2001). **Introduction to physical polymer science**. 3rd edition, Canada: John Wiley & Sons, Inc..

Su, Z., Li, Q., Liu, Y., Hu, G. and Wu, C. (2009). Multiple melting behavior of poly(lactic acid) filled with modified carbon black. **Journal of Applied Polymer Science** 47: 1971-1980.

Sungsanit, K., Kao, N. and Bhattacharya, S. N. (2011). Properties of linear poly (Lactic Acid)/Polyethylene glycol blends. **Journal of Applied and Polymer Science** 52(1): 108-116.

Van de Velde, K. and Kiekens, P. (2002). Biopolymers: overview of several properties and consequences on their applications. **Polymer Testing** 21: 433-442.

Wales, J. L. S. and Den Otter, J. L. (1970). Relations between steady flow and oscillatory shear measurements. **Rheologica Acta** 9: 115-119.

Wu, T., He, Y., Fan, Z., Wei, J. and Li, S. (2008). Investigations on the morphology and melt crystallization of poly(L-lactide)-*b*-poly(ethylene glycol) diblock copolymers. **Polymer Engineering and Science** 48: 425-433.

Yang, J., Zhao, T., Cui, J., Liu, L., Zhou, Y., Li, G. and Zhou, E. (2006). Nonisothermal crystallization behavior of the poly(ethylene glycol) block in poly(L-lactide)-poly(ethylene glycol) diblock copolymers: Effect of the poly (L-lactide) block length. **Journal of Applied Polymer Science** 44: 3215-3226.

Yang, J., Zhou T., Liu, L. Zhou, Y., LI, G., Zhou, E. and Chen, X. (2006). Isothermal crystallization behavior of the poly(L-lactide) block in poly(L-lactide)-poly(ethylene glycol) diblock copolymers: Influence of the PEG block as a diluted solvent. **Journal of Applied Polymer Science** 38: 1251-1257.

CHAPTER IV

MULTISCALE SIMULATION FOR PREDICTION OF MISCIBILITY AND MORPHOLOGY OF POLY(LACTIC ACID) AND POLY(ETHYLENE GLYCOL) BASED BLOCK COPOLYMERS AND BLENDS

4.1 Abstract

The miscibility and morphology of PLA and PEG based on block copolymers and blends were predicted by MD and DPD simulations. To determine the miscibility of polymer blends, Flory-Huggins interaction parameters (χ_{ij}-parameters) of PLA and PEG were calculated using MD simulation technique. The PLA/PEG compositions of 90/10, 80/20, 70/30, 50/50, 30/70, 20/80 and 10/90 (wt/wt) were simulated. The χ_{ij}-parameters of PLA/PEG blends exhibit that PLA and PEG is miscible at low PEG concentration (10-30 wt%) but is immiscible at PEG concentration of 50-90 wt%. The radial distribution functions *g(r)* of the inter-molecular carbon atomic pairs of PLA-PEG, PLA-PLA and PEG-PEG also indicate that 90/10, 80/20 and 70/30 (wt/wt) PLA/PEG is miscible. The PLA block fractions in PLA-PEG-PLA were varied from 0.1-0.5 in the study for PLA/PLA-PEG-PLA blends. It was found that the χ_{ij}-parameter values of all PLA/PLA-PEG-PLA blends show lower than the χ_{ij}-

parameter of PLA/PEG blend at the same PEG concentration. The χ_{ij}-parameter values of such systems increase with increasing of PLA block fractions. DPD simulation was used to investigate the morphologies of PLA/PEG, PLA-PEG-PLA and PLA/PLA-PEG-PLA systems. As the composition of the blends and block copolymers was varied, mesoscale simulation predicted the phase structures with defined morphologies of disorder, bicontinuous, perforated lamellas and spheres. Morphologies of 90/10, 80/20 and 70/30 (wt/wt) PLA/PEG blends show disorder structures indicating that PLA and PEG is miscible at these compositions. The phase separation was observed in the high PEG concentration (>50 wt%). The spherical like micelle was found at 10/90 (wt/wt) PLA/PEG composition. For PLA-PEG-PLA block copolymers, various morphologies were observed with different block compositions. The bridge/loop fractions (f_{bridge}) values of PLA-PEG-PLA were calculated and were found to be 0.49-0.73 with varying of PLA block compositions. The morphologies of PLA/PLA-PEG-PLA blends exhibited the reduction of PEG domain size comparing to the PLA/PEG blend. This implies that the PLA end blocks in PLA-PEG-PLA contribute to enhance the miscibility of PLA and PEG segments in the blends.

4.2 Introduction

Recently, much attention has been paid to the environment friendly materials, such as polyesters. They fit perfectly well in the ecosystem due to their natural origin and biodegradability. Poly(lactic acid) (PLA) is the biodegradable polymer which have attracted considerable research effort in the variety applications *i.e.*, medical field, packaging *etc*. However, because of its inherent brittle nature and low thermal stability, PLA needs to be modified to be suitable for use in various applications

where mechanical properties are important. There have been a considerable number of studies to toughen PLA with the goal of balancing and increasing tensile strength, impact strength and modulus while retaining the biocompatible and biodegradable nature (Sheth, Kumar, Dave, Gross, and McCarthy, 1997; Lemmouchi *et al*., 2009; Rathi *et al*., 2011).

One of the most efficient methods for toughening PLA is plasticization with low molecular weight polymers such as polyethylene glycol (PEG), polypropylene glycol (PPG) *etc*. PEG has been intensively studied for using as the plasticizer for PLA because of low cost, biocompatible polymer, non-toxicity. However, there were some reports that the promising mechanical properties of PLA/PEG blends disappear with time because of the slow phase separation and crystallization of PEG from homogeneous blends (Hu, Hu, Topolkaraev, Hiltner, and Baer, 2003). To address these disadvantages, PEG has to modify its compatibility with PLA. One of most successful techniques is the use of graft and block copolymer as polymeric compatibilizer. Block copolymer which one block is chemically identical or is good miscible with PLA matrices has been proposed as the plasticizer for toughening PLA (Jia, Tan, Han, Yang, and Dong, 2009; Rathi *et al*., 2011). A simplest hypothesis is that an end blocks of copolymers act as polymeric surfactant by spanning the interface between the phases, while the soft block could be served as the toughening agent. The end block of copolymer has several molecular effects. First, the interface tension between the phases is lowered, which reduces the driving force for the phase separation. Secondly, the presence of the end block of copolymer at the interface reduces the tendency of the domains to coalesce. For example, Ran and coworkers (Ran, Jia, Han, Yang, and Dong, 2010) used poly(ethylene glycol-*block*-

polypropylene glycol) (PEPG) as the plasticizer to improve PLA properties. They found that flexibility and mechanical properties of PLA/PEPG blends are better than PLA/PEG blend at the same composition. Poly(lactic acid-*block*-ethylene glycol-*block*-lactic acid) (PLA-PEG-PLA) should be one of promising materials used to reduce the immiscibility between PLA and plasticizer.

Polymer blending is a well-used technique whenever modification of polymer properties is required because this technique uses conventional technology at low cost. The usual objective for preparing a novel blend of two or more polymers is not to change the properties of the components drastically but to capitalize on the maximum possible performance of the blend. Unfortunately, the experimental study of polymer blends are cumbersome *i.e.,* time-consuming and expensive. In addition the contradictory results can be found in the literature for certain systems (Arenaza, Meaurio, Coto, and Sarasua, 2010).

In recent years, with advance in computer technology, molecular simulation is gaining acceptance as a reliable technique to analyze the microscopic and mesoscopic insights into the phase morphology and interfacial behaviors of polymer mixtures, which significantly influence on rheological and mechanical properties of materials (Fu *et al*, 2012; Spyriouni and Vergelati, 2001; Chen, Nhan Phan-Thien, Fan and Khoo, 2004).

Molecular modeling methods *i.e.*, molecular mechanics (MM), molecular dynamics (MD), and Monte Carlo (MC) simulation have been applied to study multiphase polymer systems (Rapaport, 2004; Fu *et al.*, 2012; Tükan and Mattice, 1999). Molecular simulation provides a bridge between models and experiments, as a method using mathematical models to perform an analysis by computers. For

examples, several MD simulation techniques applied to calculate the polymer-polymer interaction to predict the miscibility of polymer blends (Yang *et al*., 2004; Spyriouni and Vergelati, 2001). However, the broad range of time scales and underlying structure prohibits the fully atomistic simulation method that captures all of these processes.

Some alternatives methods have been developed to overcome these problems. The coarse-graining model or mesoscale method has been successful in extending of this scope. In this model about four to five of carbon atoms in a polymer chain are grouped into a single bead, and thus many states can be easily generated and equilibrated. One example is the dissipative particle dynamics (DPD), a mesoscale simulation technique developed to model Newtonian and non-Newtonian fluids (Glotzer and Paul, 2002). It is capable to investigate the phase morphology and interface properties of multiphase systems.

As mentioned above, MD and DPD simulations would be employed to predict the miscibility and morphology of PLA/PEG, PLA-PEG-PLA and PLA/PLA-PEG-PLA systems. For PLA/PEG and PLA/PLA-PEG-PLA blends, the miscibility of these blends would be estimated using MD simulation at room temperature. Flory-Huggins interaction parameter (χ_{ij}-parameter) of blends would be calculated to determine their miscibility. The calculated χ_{ij}-parameters are used as the input parameter for DPD simulation. The morphologies of PLA/PEG, PLA-PEG-PLA and PLA/PLA-PEG-PLA systems would be analyzed to grain in more understanding about the behavior of polymer chains at the interface.

4.3 Simulation setup

Multiscale simulations, including molecular dynamics (MD) and dissipative particle dynamics (DPD) simulations were performed to study the miscibility and phase morphology of PLA/PEG and PLA/PLA-PEG-PLA blends and PLA-PEG-PLA block copolymers. MD simulation was used to calculate the Flory-Huggins interaction parameter (χ-parameter) for predicting the miscibility of the polymer blends. The χ-parameter was used as an input parameter for DPD simulation. The phase morphology of PLA/PEG and PLA/PLA-PEG-PLA blends and PLA-PEG-PLA block copolymer was investigated using DPD simulation.

4.3.1 Molecular Dynamics Simulation

The miscibility of PLA/PEG blend PLA/PLA-PEG-PLA blends was investigated using MD simulation performed at room temperature (298 K). The Discover molecular dynamic simulation module of Materials Studio (v. 4.0) software package obtained from Accelrys was used for this task. This software was supported by National Nanotechnology Center (NANOTEC), Thailand.

Polymer chains for PLA and PEG were first built from LA and EG repeating units, respectively, using the rotational isomeric state (RIS) model (Flory, 1989) which describes the conformations of the unperturbed chains. The cubic simulation boxes were then constructed with the Amorphous Cell module based on the packing technique of Theodorou and Suter (Theodorou and Suter, 1986) and Meirovitch scanning method (Meirovitch, 1983). The polymer density in a simulation box corresponds to the bulk density of each polymer, *i.e.*, PLA is 1.206 g•cm^{-3}, PEG is 1.127 g•cm^{-3}. To avoid the long simulation time, the appropriate chain lengths for PLA and PEG were determined by investigating the solubility parameter (δ) of each

polymer as a function of the number repeating units. The optimized chain length for PLA and PEG used in this simulation were 30 and 50 repeating units, respectively. These values were obtained from the literatures (Mu, Huang, Lu, and Sun, 2008; Jawalkar and Aminabhavi, 2006).

In addition, triblock copolymers of PLA_3-PEG_{50}-PLA_3, PLA_{11}-PEG_{50}-PLA_{11} and PLA_{25}-PEG_{50}-PLA_{25} corresponding to the PLA block fraction (f_{PLA}) of 0.1, 0.3 and 0.5 were built for blending with PLA. The miscibility of PLA/PLA-PEG-PLA blends was investigated and compared with those of PLA/PEG blends. To simplify for the presentation, triblock copolymers of PLA_3-PEG_{50}-PLA_3, PLA_{11}-PEG_{50}-PLA_{11} and PLA_{25}-PEG_{50}-PLA_{25} were represented as B01, B03 and B05, respectively. The details of PLA/PEG and PLA/PLA-PEG-PLA blends were shown in Table 4.1.

After the polymer chains were constructed in the simulation box, 10,000 step minimization was subsequently carried out to eliminate the local non-equilibrium structures with the convergence threshold of 0.001 $kcal{\cdot}mol^{-1}{\cdot}Å^{-1}$. MD simulation was then performed at 500 K and 1 bar for 2 ns in NPT ensemble. Here, 500 K was chosen to ensure that polymers are in the molten (amorphous) state (the melting temperature of PLA is 433-453 K, PEG is about 333 K and PLA-PEG-PLA block copolymers is 333-453K). In order to further relax local hot-spots and to allow the system to achieve equilibrium, the polymer structures were subjected to a 10-circle thermal annealing from 300 to 1000 K and then back to 300 K with 50 K intervals. At each temperature, 100 ps NPT MD simulation was performed at the constant pressure (1 bar) with a time step of 1 fs. After the 10-circle annealing, the 2 ns for NVT MD simulation was carried out at constant volume. At the last stage, 100

ps NVT MD simulation was performed to collect data for later analysis. Trajectories were saved every 1 ps and the final 50 ps configurations were used for analysis.

Table 4.1 Simulated data for PLA/PEG and PLA/PLA-PEG-PLA blends with different compositions considered in MD simulations.

System	LA units	EG units	Block units*	Number of chains	Composition (wt% PLA)	Density ($g.cm^{-3}$)
PLA	30	-	-	1 PLA	100	1.206
PEG	-	50	-	1 PEG	-	1.127
PLA/PEG 90/10	30	50	-	9PLA/1PEG	90	1.198
PLA/PEG 80/20	30	50	-	4PLA/1PEG	80	1.190
PLA/PEG 70/30	30	50	-	7PLA/3PEG	70	1.180
PLA/PEG 50/50	30	50	-	1PLA/1PEG	50	1.167
PLA/PEG 30/70	30	50	-	3PLA/7PEG	30	1.151
PLA/PEG 20/80	30	50	-	1PLA/4PEG	20	1.143
PLA/PEG 10:90	30	50	-	1PLA/9PEG	10	1.135
PLA/B01 50/50	30	-	56	5PLA/5B01	50	1.190
PLA/B03 50/50	30	-	72	5PLA/5B03	50	1.198
PLA/B05 50/50	30	-	100	5PLA/5B05	50	1.206

* Calculated by summation of PLA and PEG blocks.

The COMPASS (Condensed phase Optimized Molecular Potentials for Atomistic Simulation Studies) force field was used for computing the intermolecular interactions. It has been specially optimized to provide accurate condensed phase equation of state and cohesive properties for molecules containing a wide range of functional groups (Sun, 1998). COMPASS is based on PCFF (Polymer Consistent Force-Field), and is the first ab initio force field used for modeling interatomic interactions. The detail of COMPASS force field was explained in Chapter II.

4.3.2 Dissipative particle dynamics

Dissipative particle dynamics (DPD) simulation technique, introduced by Hoogerbrugge and Koelman (Hoogerbrugge and Koelman, 1992), is a mesoscale method for simulating of coarse-grained systems over a long length and time scales. In DPD simulation, several atoms or repeating units are grouped together into a single bead. The polymer chains in DPD simulation can be considered to consist of number of beads (N_{DPD}) which are calculated by the following equation.

$$N_{DPD} = \frac{M_P}{M_m C_n} = \frac{N}{C_n} \tag{4.1}$$

where N_{DPD} is number of beads, M_p is polymer molar mass, M_m is molar mass of repeating units, C_n is the characteristic ratio and N is number of repeating units. From the literature (Chen, Nhan Phan-Thien, Fan, and Khoo, 2004), C_n of the polymer can be calculated using the Synthia module in Materials Studios software. The C_n values for PLA and PEG are 3.40 and 4.98, respectively.

The force acting on a bead is a sum of three pairwise contributions, a conservative force (f^C), a dissipative force (f^D) and a random force (f^R) which is shown in equation (4.2).

$$f_i = \sum_{j \neq i} (f_{ij}^C + f_{ij}^D + f_{ij}^R) \tag{4.2}$$

where the sum runs over all other particles within a certain cutoff radius (r_c). As this is the only length-scale in the system, we use the cutoff radius as our unit of length, r_c = 1. The different parts of the forces are given by equation (4.3) to (4.5).

$$f_{ij}^C = \begin{cases} a_{ij}(1 - r_{ij})e_{ij} & (r_{ij} < 1) \\ 0 & (r_{ij} \geq 1) \end{cases} \tag{4.3}$$

$$f_{ij}^D = -\gamma \omega^D(r_{ij})(v_{ij}e_{ij})e_{ij} \tag{4.4}$$

$$f_{ij}^R = \sigma \omega^R(r_{ij})\zeta_{ij}\Delta t^{-\frac{1}{2e_{ij}}} \tag{4.5}$$

where $\boldsymbol{r_{ij}} = \boldsymbol{r_i} - \boldsymbol{r_j}$, $r_{ij} = |\boldsymbol{r_{ij}}|$, $\boldsymbol{e_{ij}} = \mathbf{r_{ij}}/r_{ij}$, and $\boldsymbol{v_{ij}} = v_i - v_j$. ξ_{ij} is a random number with zero mean and unit variance. a_{ij} is a constant which describes the maximum repulsion between interacting beads. ω^D and ω^R represent r-dependent weight functions for the dissipative and random forces, respectively, and vanish for $r > r_c = 1$.

The bead interactions (a_{ij}) of DPD can be mapped onto Flory-Huggins theory through the χ-parameter (Groot and Warren, 1997) as shown in following equations.

$$a_{ij} = a_{ii} + 3.27\chi_{ij} \tag{4.6}$$

$$\chi_{ij} = \frac{V_{ij}(\delta_i - \delta_j)^2}{RT} \quad (4.7)$$

where V_{ij} is the arithmetic average of molar volumes of beads *i* and *j*. δ_i and δ_j are the solubility parameters of beads *i* and *j*, respectively, which were depend on the chemical nature of each species. The interaction parameter between the same type beads a_{ii} equals 25.

χ_{ij} parameter at 298 K for DPD simulation was obtained from MD simulation. The procedure for calculating χ_{ij} parameter was described in MD simulation section. The χ_{ij} parameter is put into the Equation (4.7), and the interaction in the DPD simulation is obtained.

DPD simulation of PLA/PEG, PLA/PLA-PEG-PLA blends and PLA-PEG-PLA triblock copolymers were performed in a simulation cell with the bead density (ρ) of 3. The influence of simulation box sizes (ranging from 20 x 20 x 20 to 50 x 50 x 50) on the simulation results was investigated and it was found that no apparent finite size effects when the box size is 30 x 30 x 30 or bigger. Our DPD system is therefore performed in a cubic box of size $30r_c$ x $30r_c$ x $30r_c$ with periodic boundary conditions in three directions. The simulations were performed at reduced temperature (k_BT) = 1, this allows a reasonable and efficient relaxation for each binary blend. A total of 10^5 time steps with step size Δt = 0.05 in DPD reduced units are performed for equilibration.

The molecular weight of 100,000 and 8,000 g·mol^{-1} for PLA and PEG homopolymers, respectively, were employed to study the PLA/PEG blends. While the molecular weight for PLA-PEG-PLA triblock copolymers were varied from 9,440-

125,936 g·mol^{-1}. The molar masses of these polymers correspond to those in our experimental studies.

To map the real polymer chain to Gaussian chain model, the number of DPD beads (N_{DPD}) for PLA, PEG and PLA-PEG-PLA is considered from the molar mass of the polymers, molar mass of a repeat unit, degree of polymerization and characteristic ratio of each system as described in Equation (4.1). The approximate 3 and 5 repeating units of PLA and PEG were grouped together into a single DPD bead. For DPD simulation of PLA/PEG blends, the number of bead per chain for PLA and PEG are 408 and 37 beads, respectively. The weight percent (wt%) of PLA in the PLA/PEG blends were varied from 90-10. The bead-bead pairs interaction parameters ($a_{PLA\text{-}PEG}$) for PLA/PEG blends are given in Table 4.2.

In the cases of PLA/PLA-PEG-PLA blends, PLA-PEG-PLA block copolymers with different PLA block lengths (f_{PLA} = 0.1, 0.3 and 0.5) were selected to blend with PLA homopolymer. The composition of PLA in PLA/PLA-PEG-PLA blend was set at 50wt% with respect to PEG content. The DPD chain length of PLA was fixed at 408 beads all systems. Gaussian chain model of PLA-PEG-PLA triblock copolymers at f_{PLA} of 0.1, 0.3 and 0.5 were shown in Table 4.4. The interaction between PLA and PEG beads in PLA/PLA-PEG-PLA blends can be divided into two kinds in this study. First is the PLA-PEG beads interaction within block copolymer. Second is the interaction of PLA homopolymer and PEG of block copolymer. Each interaction value depends on the PLA and PEG composition. The bead-bead pairs interaction parameters ($a_{PLA\text{-}PEG}$) for PLA/PLA-PEG-PLA systems were illustrated in Table 4.3.

Table 4.2 Parameters of the DPD simulations for PLA/PEG blends.

System	Chain length (N_{DPD})		Composition (wt% PLA)	$\chi_{PLA\text{-}PEG}$	$a_{PLA\text{-}PEG}$
	PLA	PEG			
PLA/PEG 90/10	408	37	90	-0.59	23.09
PLA/PEG 80/20	408	37	80	-1.01	21.70
PLA/PEG 70/30	408	37	70	-0.21	24.32
PLA/PEG 50/50	408	37	50	0.97	28.17
PLA/PEG 30/70	408	37	30	1.51	29.94
PLA/PEG 20/80	408	37	20	1.32	29.32
PLA/PEG 10/90	408	37	10	1.77	30.79

Table 4.3 The interaction parameters ($a_{PLA\text{-}PEG}$) of PLA-PEG beads for 50/50 wt% PLA/PLA-PEG-PLA blends. Two types of PLA were denoted as PLA_H: PLA homopolymer, PLA_B: PLA block copolymer.

PLA/PLA$_3$-PEG$_{37}$-PLA$_3$			
	PLA_B	**PEG**	**PLA_H**
PLA_B	25.00	30.79	25.00
PEG	30.79	25.00	28.17
PLA_H	25.00	28.17	25.00
PLA/PLA$_{12}$-PEG$_{37}$-PLA$_{12}$			
	PLA_B	**PEG**	**PLA_H**
PLA_B	25.00	29.94	25.00
PEG	29.94	25.00	28.17
PLA_H	25.00	28.17	25.00
PLA/PLA$_{27}$-PEG$_{37}$-PLA$_{27}$			
	PLA_B	**PEG**	**PLA_H**
PLA_B	25.00	28.17	25.00
PEG	28.17	25.00	28.17
PLA_H	25.00	28.17	25.00

The morphology of PLA-PEG-PLA triblock copolymers with different block compositions was also investigated in this work. The PLA block compositions (f_{PLA}) were varied from 0.1 to 0.9 with increment of 0.1. The molecular weight of PEG was held constant at 8,000 g·mol^{-1}, corresponding to degree of polymerization of 182. The real block copolymer chains of PLA-PEG-PLA were mapped to Gaussian

chain model by means as describe above. The DPD interaction parameters ($a_{PLA\text{-}PEG}$) for PLA and PEG beads in PLA-PEG-PLA block copolymers were obtained from χ-parameter of PLA/PEG blends at the same composition. The real block copolymer, Gaussian chain model and $a_{PLA\text{-}PEG}$ parameters of PLA-PEG-PLA block copolymers with different composition were depicted in Table 4.4.

Table 4.4 The Gaussian chain model and DPD bead interaction ($a_{PLA\text{-}PEG}$) parameter of block copolymer of PLA-PEG-PLA at different block compositions.

Real copolymer chain	**Gaussian chain model**	f_{PLA}	$a_{PLA\text{-}PEG}$
PLA_{10}-PEG_{182}-PLA_{10}	PLA_{3}-PEG_{37}-PLA_{3}	0.1	30.79
PLA_{23}-PEG_{182}-PLA_{23}	PLA_{7}-PEG_{37}-PLA_{7}	0.2	29.32
PLA_{39}-PEG_{182}-PLA_{39}	PLA_{12}-PEG_{37}-PLA_{12}	0.3	29.94
PLA_{61}-PEG_{182}-PLA_{61}	PLA_{18}-PEG_{37}-PLA_{18}	0.4	27.10
PLA_{91}-PEG_{182}-PLA_{91}	PLA_{27}-PEG_{37}-PLA_{27}	0.5	28.17
PLA_{137}-PEG_{182}-PLA_{137}	PLA_{40}-PEG_{37}-PLA_{40}	0.6	25.55
PLA_{212}-PEG_{182}-PLA_{212}	PLA_{62}-PEG_{37}-PLA_{62}	0.7	24.32
PLA_{364}-PEG_{182}-PLA_{364}	PLA_{107}-PEG_{37}-PLA_{107}	0.8	21.70
PLA_{819}-PEG_{182}-PLA_{819}	PLA_{241}-PEG_{37}-PLA_{241}	0.9	23.09

4.4 Results and discussion

4.4.1 MD simulation

- **Flory-Huggins parameters**

The miscibility of polymer blends was predicted by examining the Flory-Huggins parameter (χ_{AB}) calculated according to Equation (4.8).

$$\chi_{AB} = \left(\frac{\Delta E_{mix}}{RT} \right) V_m \tag{4.8}$$

where V_m is the molar volume of the repeating unit chosen as a reference. V_m of PLA was selected as a reference in this study (57.7 $cm^3 \cdot mol^{-1}$), R is the molar gas constant and T is the temperature in Kelvin. The energy of mixing, ΔE_{mix} can be calculated according to the following Equation.

$$\Delta E_{mix} = \phi_A \left(\frac{E_{coh}}{V} \right)_A + \phi_B \left(\frac{E_{coh}}{V} \right)_B - \phi_{mix} \left(\frac{E_{coh}}{V} \right)_{mix} \tag{4.9}$$

where the terms in parenthesis represent the cohesive energies (E_{coh}/V) of pure polymers (A and B) and the blend (mix), ϕ_A and ϕ_B represent volume fractions of polymers in the blend, $\phi_A + \phi_B = 1$.

A positive value of the χ_{AB} indicates immiscibility for blends of high molecular weight polymers. Generally, the critical value of χ-parameter (χ_c) was used to compare χ_{AB} for predicting the miscibility of polymer blend. χ_c of the polymer blend was calculated by Equation (4.10).

$$\chi_c = \frac{1}{2}\left(\frac{1}{\sqrt{n_A}} - \frac{1}{\sqrt{n_B}}\right)^2 \qquad (4.10)$$

where n_A and n_B represent the degree of polymerization of the pure polymers. If χ_{AB} of the blend is smaller than χ_c, the system is miscible. If χ_{AB} is slightly larger than the χ_c, the blend exhibits partial miscibility. For larger values of χ_{AB}, the components are completely immiscible.

In this work, the degree of polymerization of PLA (n_{PLA}) and PEG (n_{PEG}) are 30 and 50, respectively. The obtained value of χ_c is 0.053. The plot of χ-parameter of PLA/PEG and PLA/PLA-PEG-PLA blends versus weight fraction of PEG is displayed in Figure 4.1.

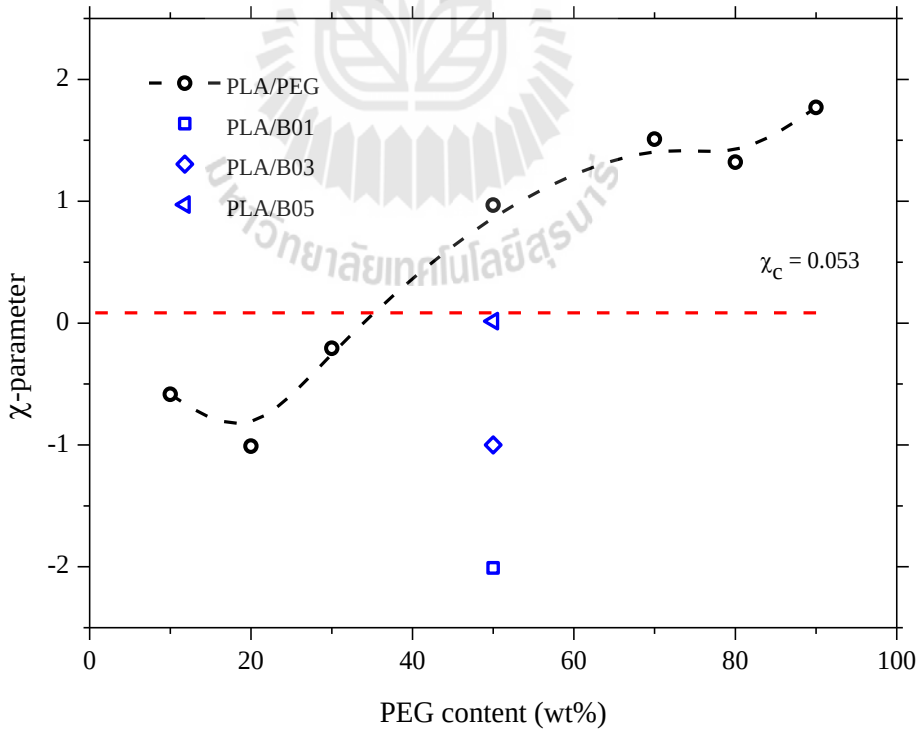

Figure 4.1 The plot of Flory-Huggins interaction parameter at different PEG contents.

The tendency of χ-parameter of the polymer blends calculated by MD simulation was increased from -1.01 to 1.77 with increasing PEG content. In the cases of 90/10, 80/20 and 70/30 wt% of PLA/PEG blend systems, the simulated values of $\chi_{PLA\text{-}PEG}$ are clearly below the χ_c line as shown in Figure 4.2. This indicates that the 90/10, 80/20 and 70/30 wt% of PLA/PEG blends is completely miscible. For 50/50, 30/70, 20/80 and 10/90 wt% PLA/PEG blends, $\chi_{PLA\text{-}PEG}$ values are all above the χ_c line, indicating immiscibility of PLA and PEG blends.

To verify our hypothesis, the miscibility of PLA and PEG can be enhanced by modifying PEG to PLA-PEG-PLA block copolymer. The χ-parameter of PLA/PLA-PEG-PLA was calculated to evaluate the miscibility. It is apparent that the χ-parameter of 50/50 wt% PLA/PLA-PEG-PLA blends is lower than the χ-parameter of PLA/PEG blends at the same PEG content. In addition, these values are also below the χ_c line (Figure 4.2). This result exhibits that the miscibility of polymer blends was enhanced by blending with PLA-PEG-PLA block copolymer.

- **Radial distribution functions**

Radial distribution function *g(r)* is commonly used to characterize the molecular structure which gives the probability of finding a particle in the distance *r* from another particle. It is defined as the following equation.

$$g_{AB}(r) = \frac{1}{\rho_{AB} 4\pi r^2 \delta_r} \frac{\sum_{t=1}^{k} \sum_{j=1}^{N_{AB}} \Delta N_{AB}(r \to r + \delta r)}{N_{AB} k} \qquad (4.11)$$

where N_{AB} is the total number of atoms of A and B in the system, k is the number of time steps, δr is the distance interval, ΔN_{AB} is the number of B (or A) atoms between r

to $r + \delta r$ around an A (or B) atom and ρ_{AB} is the bulk density (Fu *et al*., 2012; Rapaport, 2001). It has been observed that if a binary system is miscible, the intermolecular *g(r)* of A-B pairs between two different polymers is larger than those of AA and BB pairs.

Figure 4.2(a) and 4.2(b) exhibit the *g(r)* curves of intra-molecular carbon atoms of PLA and PEG in the pure and blend systems. In these Figures, some systems are selected to report. For neat PLA system, the highest peak is at 1.5 Å, which simply indicates bond connectivity. The atomic pairs without connectivity have the spatial vicinities at 2.4 Å for the first adjacent pairs and at 4.6 Å for the second adjacent pairs. The peak intensities increase with decreasing PLA composition which is caused primarily by the decrease of PLA bulk density in the denominator of Equation 4.12. For PEG chain, the peaks illustrating bond connectivity, the first adjacent and the second adjacent atomic pairs are located at 1.5, 2.4 and 3.7 Å, respectively. Similar to PLA, the peak values also increase with increasing PLA composition.

Figure 4.3 shows *g(r)* of inter-molecular carbon atoms of PLA or PEG chains in neat and blend systems. The change of *g(r)* tendency for PLA and PEG chains is very similar. The value of *g(r)* for PLA (PEG) decreases with decreasing PLA (PEG) composition, which implies that the adjacent interactions between different PLA (PEG) polymer chains become weaker upon adding another polymer. Decreasing of *g(r)* curves for the inter molecular carbon-carbon pairs is pronounced in PEG chain. This indicates that PEG is well dispersing in PEG matrix.

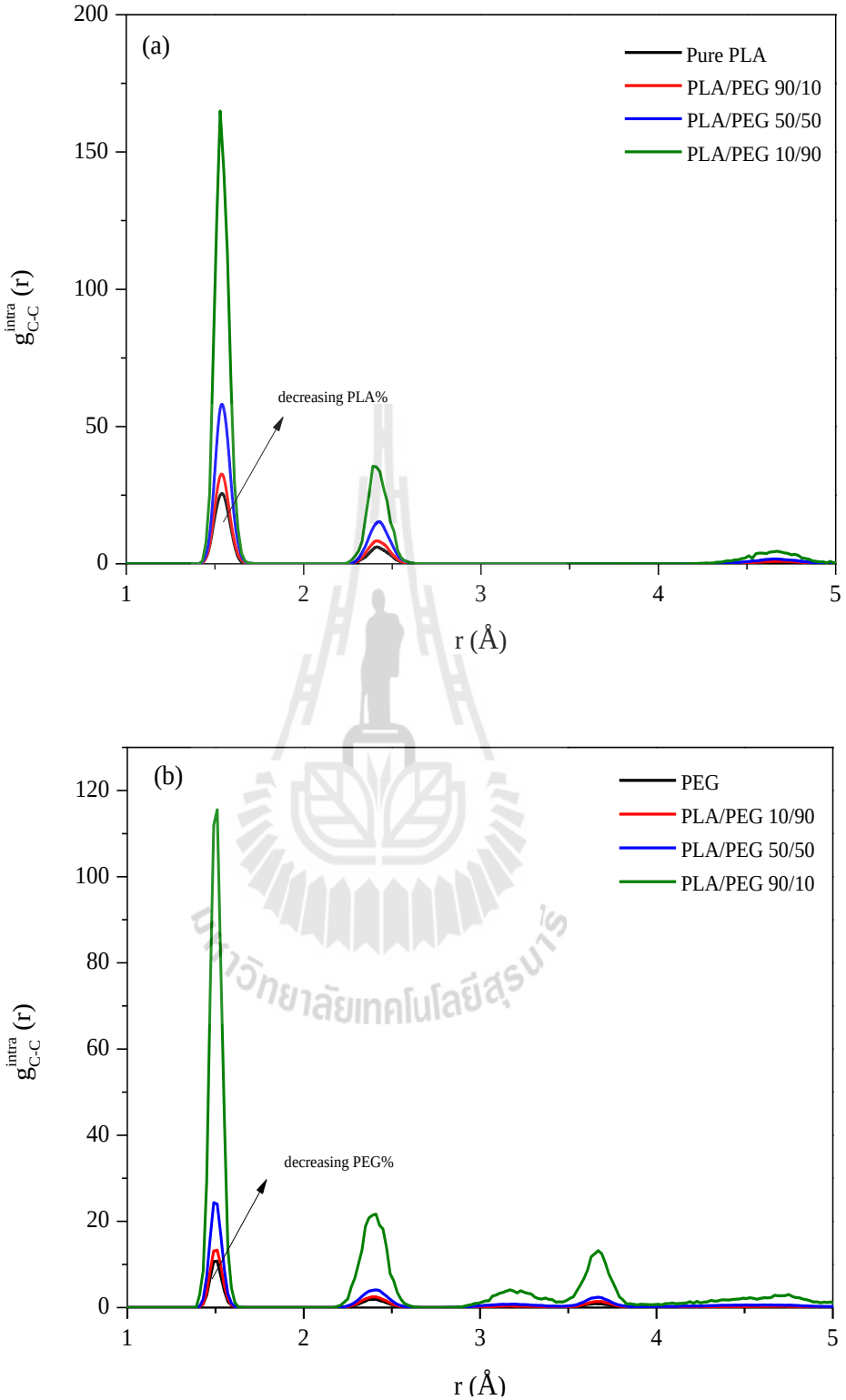

Figure 4.2 Radial distribution functions of the intra-molecular carbon-carbon pairs of (a) PLA and (b) PEG.

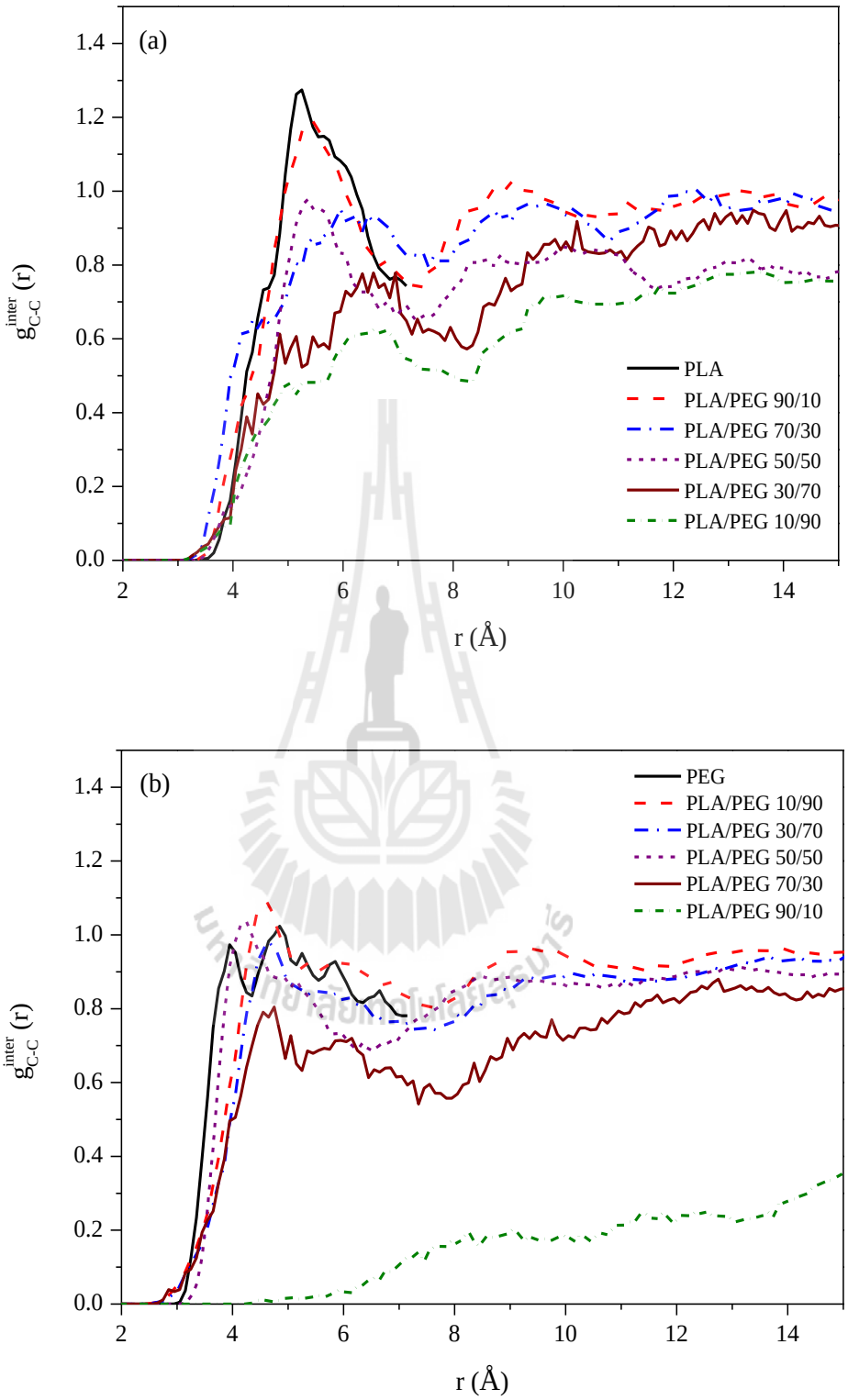

Figure 4.3 Radial distribution functions of the inter-molecular carbon-carbon pairs of (a) PLA and (b) PEG.

In addition, *g(r)* curves of inter-molecular carbon atomic pairs for PLA–PLA, PEG-PEG and PEG–PLA chain in the blends were also calculated to evaluate the miscibility of these polymer blends. Figure 4.4(a) to 4.4(c) show *g(r)* curves for 90/10, 50/50 and 10/90 wt% PLA/PEG blends. The inter-molecular distribution functions have been used to ascertain the degree of miscibility of polymer blends, several studies have proposed that, when heterocontacts between the two components in the blends reach to higher *g(r)* values than the contacts between the same component, miscibility occurs, whereas when this is not the case, the system phase separates (Rapaport, 2001; Fu *et al*., 2012).

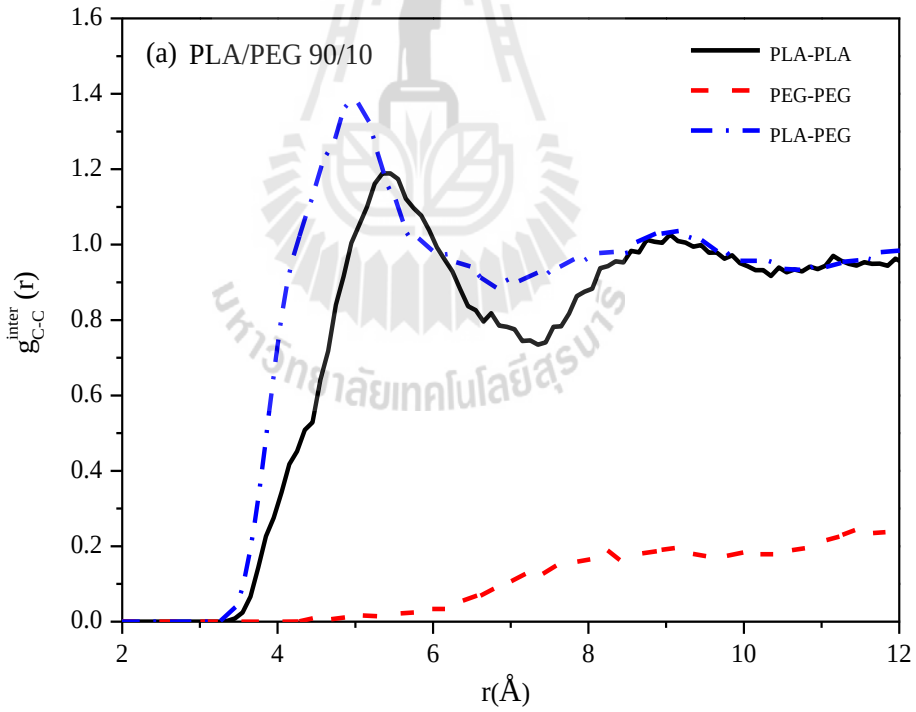

Figure 4.4 Radial distribution functions of the inter-molecular carbon-carbon pairs of PLA/PEG blends at different compositions of (a) 90/10 (b) 50/50 and (c) 10/90 wt%.

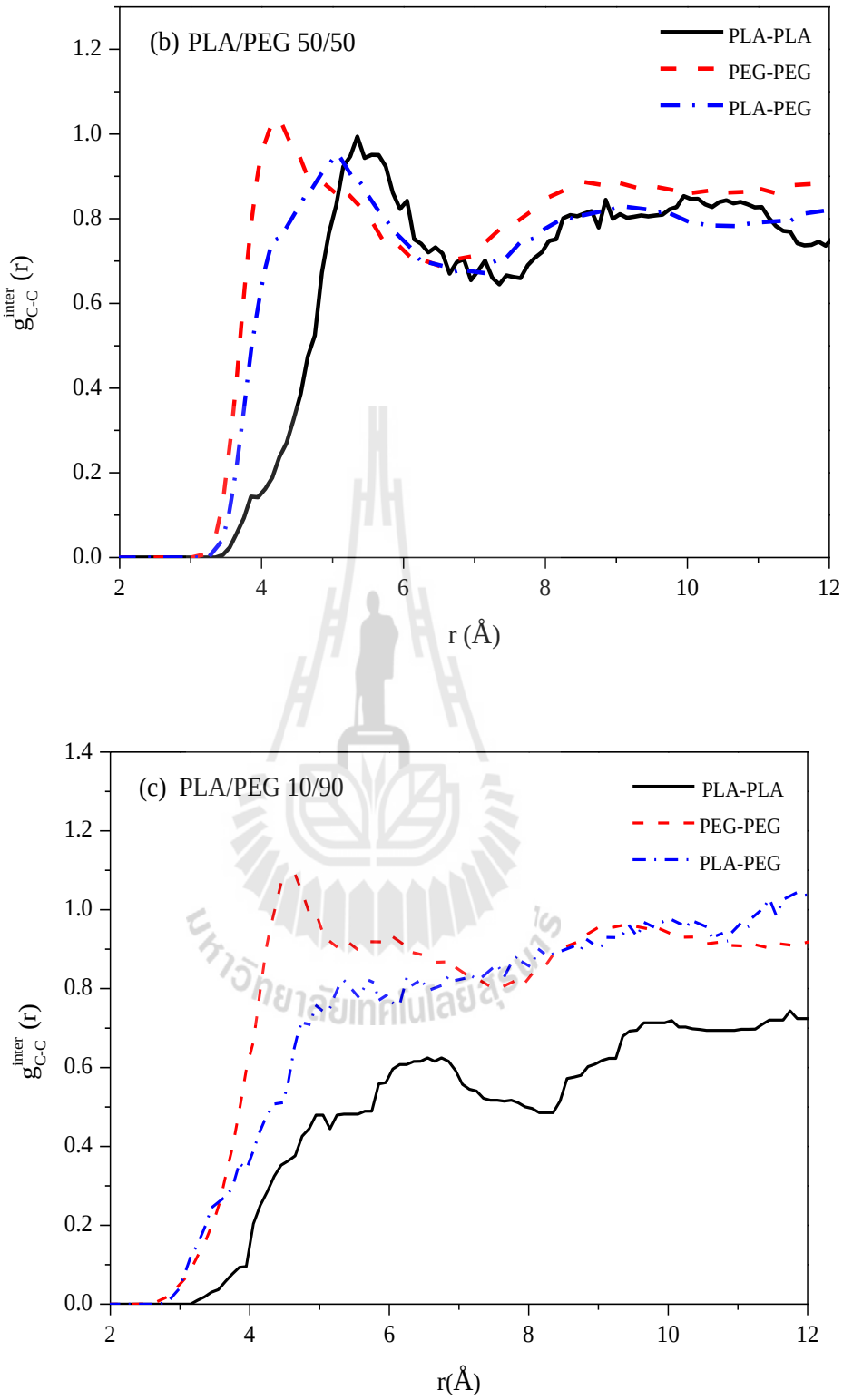

Figure 4.4 (Continued).

For 90/10 wt% PLA/PEG blend (Figure 4.4(a)), *g(r)* values of PLA-PLA and PEG-PEG are clearly lower than the *g(r)* value of PLA-PEG, indicating the PLA/PEG blend at this composition is miscible. This result was also observed in 80/20 and 70/30 wt% PLA/PEG blends (not shown here). In contrast, for other compositions (50/50, 30/70, 20/80 and 10/90 PLA/PEG blends), it is evident that *g(r)* values of PLA-PLA or PEG-PEG are higher than that PLA-PEG, implying that these polymer blends are immiscible. The typical results are shown in Figure 4.3(b) and 4.3(c).

In the cases of 50/50 wt% PLA/PLA-PEG-PLA blends, *g(r)* curves of inter-molecular of the carbon atomic pairs of PLA–PLA, PEG-PEG and PEG–PLA were calculated and shown in Figure 4.5(a) to 4.5(c). As expected, the *g(r)* values of PLA-PLA are higher than the *g(r)* values of PEG-PEG and PLA-PEG in all systems. This finding result indicates that PLA chains prefer to interact with themselves more than the other chains. On other hand, the high *g(r)* value of PLA-PLA can be implied that the interaction between PLA chains of homopolymer and PLA segments in PLA-PEG-PLA was also increased. This phenomenon increases the dispersion of PEG segments in PLA matrix.

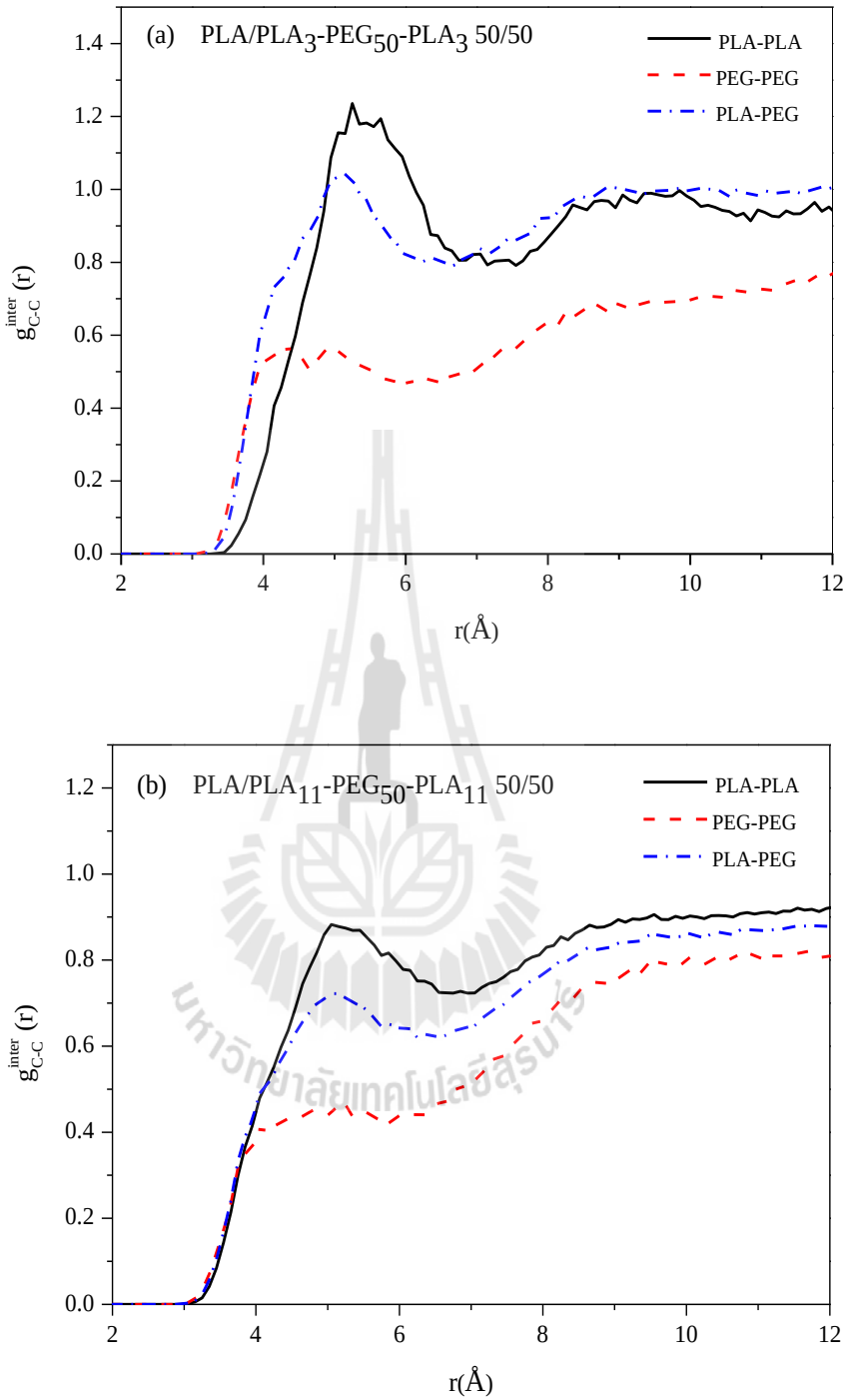

Figure 4.5 Radial distribution functions of the inter-molecular carbon–carbon pairs of 50/50 wt% PLA/PLA-PEGPLA blends. (a) PLA/PLA_3-PEG_{50}-PLA_3, (b) PLA/PLA_{11}-PEG_{50}-PLA_{11} and (c) PLA/PLA_{25}-PEG_{50}-PLA_{25}.

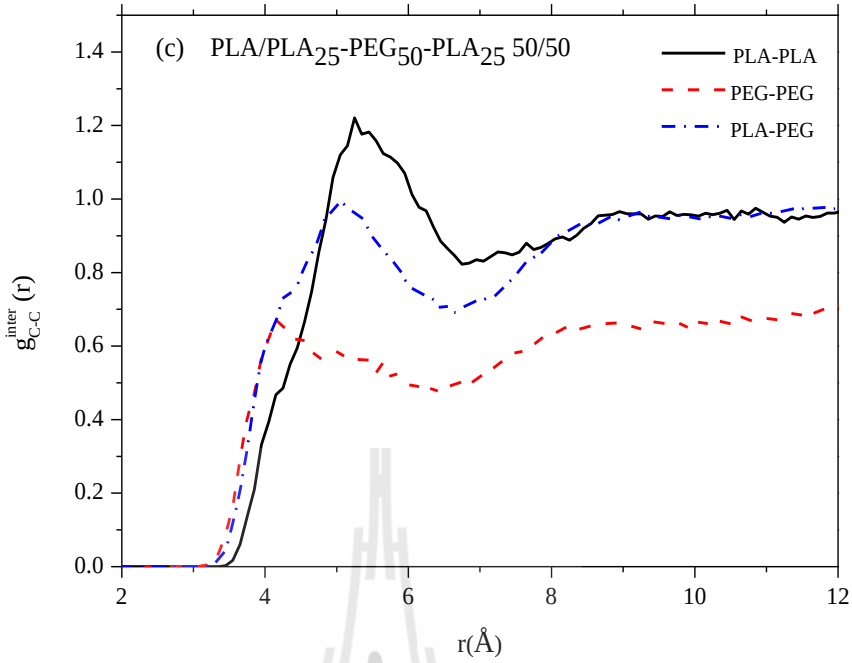

Figure 4.5 (Continued).

4.4.2 DPD simulation

- **PLA/PEG blends**

Phase morphology was generally used to determine the miscibility of binary blends. In this work, DPD simulation was used to predict the phase morphology of PLA/PEG blends with different concentration of PEG. Root mean square (RMS) end-to-end distances, density profiles and diffusivity of PLA and PEG chains were also calculated. All simulations start from a random disordered state where the PLA and PEG polymer chains are in homogeneous phase.

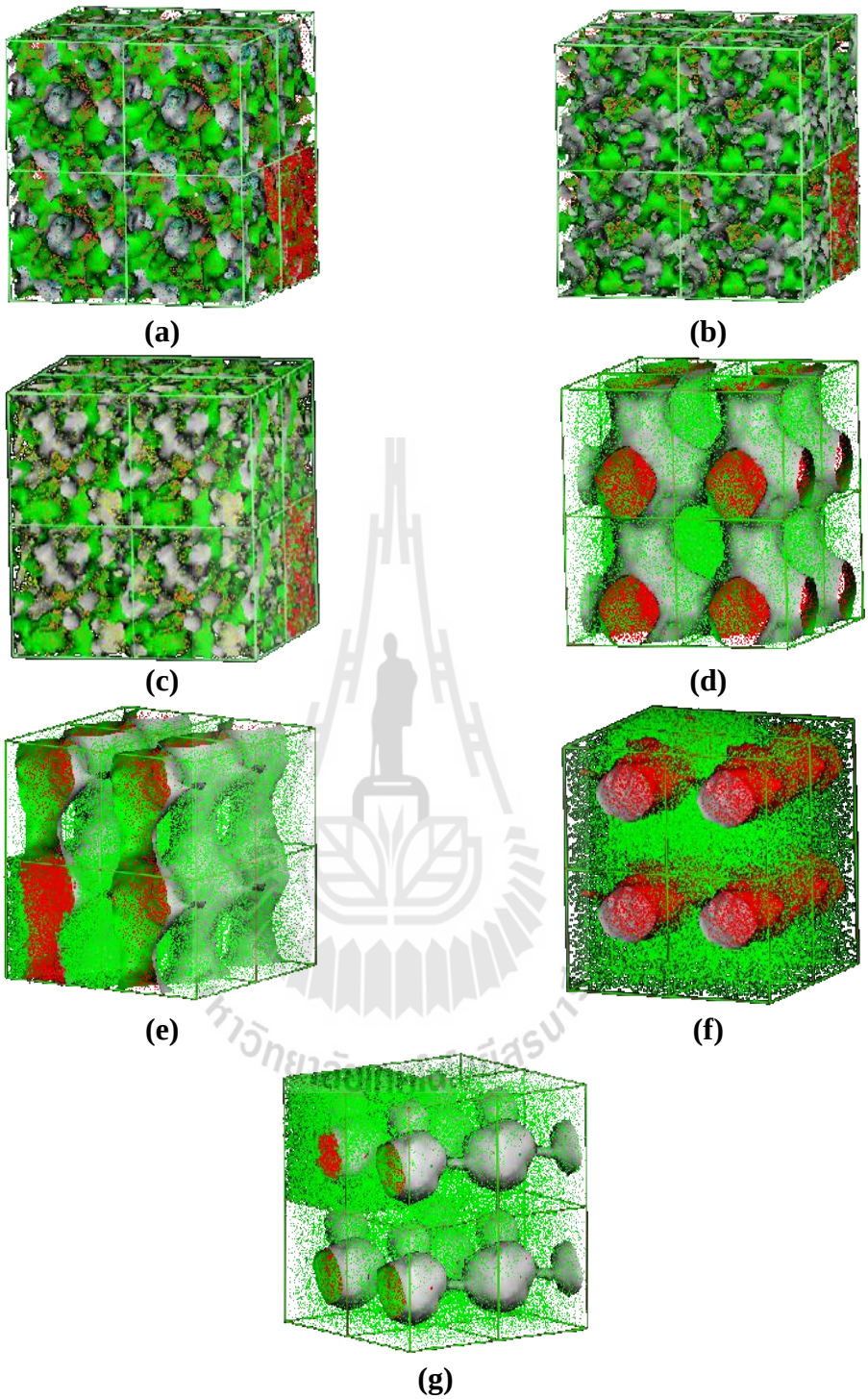

Figure 4.6 Iso-density surfaces of PLA and PEG for PLA/PEG blends at the different composition of; (a) 90/10, (b) 80/20, (c) 70/30, (d) 50/50 (e) 30/70, (f) 20/80 and (g) 10/90. Red and green colors are represented as PLA and PEG, respectively.

Figure 4.6(a) to 4.6(g) show the morphologies of PLA/PEG blend with different compositions. Apparently a totally disorder and homogeneous phase occurs in PLA/PEG 90/10, 80/20 and 70/30 blends, as shown in Figure 4.6(a), (b) and (c). These results are consistent with the density profiles of PLA/PEG blend as shown in Figure 4.7(a), (b) and (c). There are hardly any fluctuations of densities distribution for PLA and PEG in the blends. The predicted morphologies of these blends agree well with the results from MD simulation and our experimental studies.

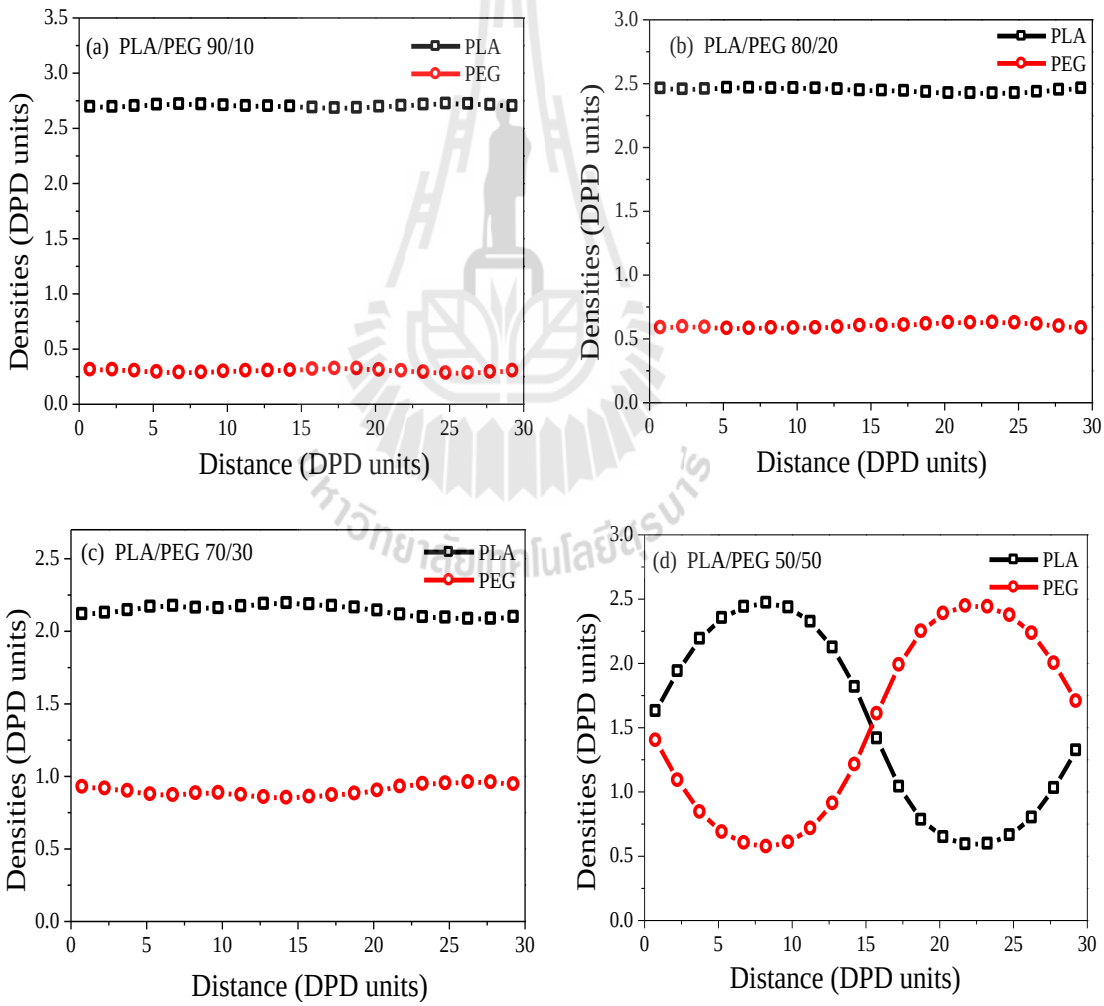

Figure 4.7 Density profiles of the PLA/PEG blend for: (a) 90/10, (b) 80/20, (c) 70/30 (d) 50/50, (e) 30/70, (f) 20/80 and (g) 10/90 wt%.

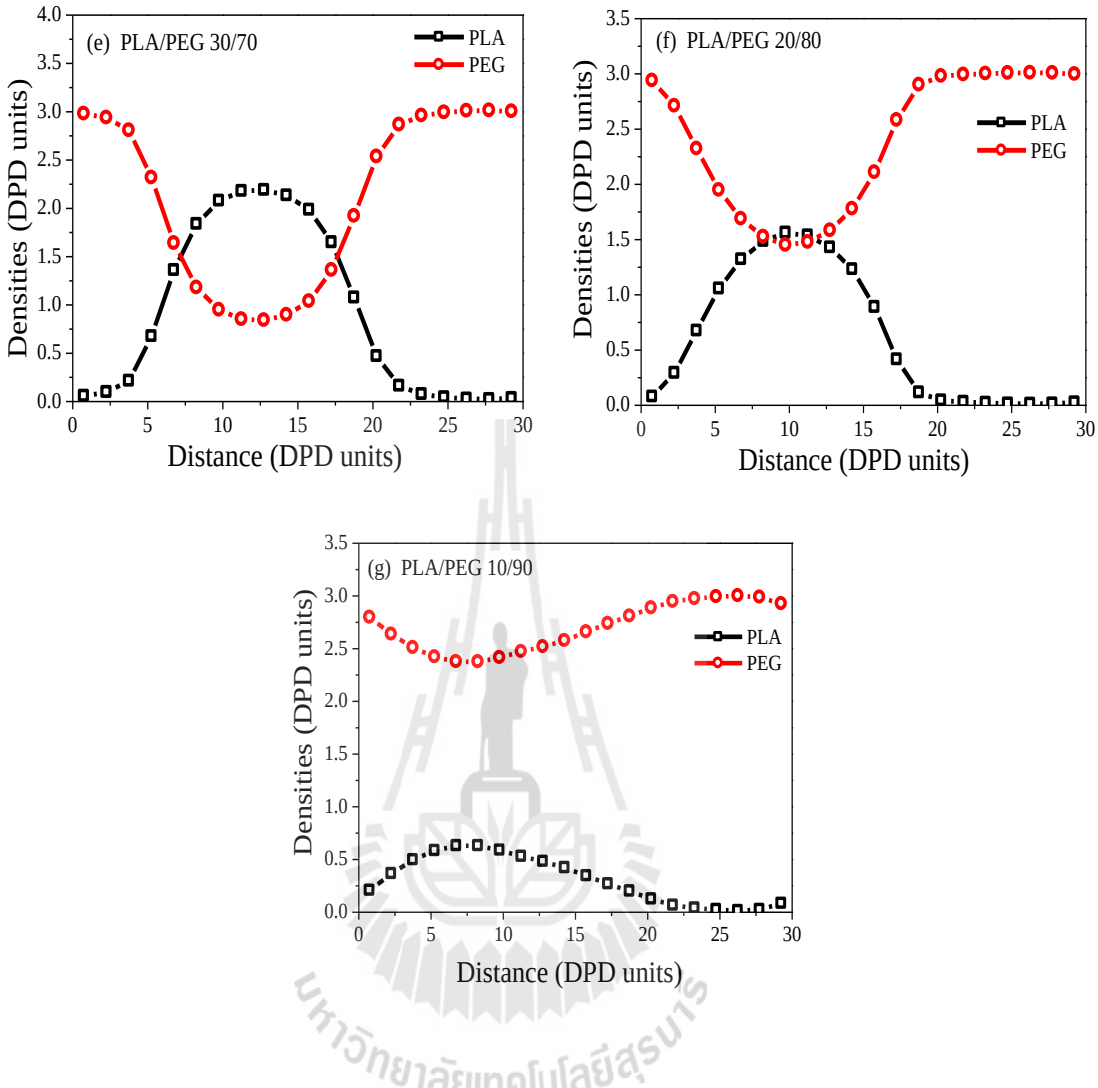

Figure 4.7 (Continued).

As the concentration of PEG increases (>30 wt%), the evolution of phase morphologies of PLA/PEG blends was observed. As seen in the density profile in Figure 4.7(d) to 4.7(g), PLA/PEG blends flavor the formation of two phase morphologies. Figure 4.6(d) exhibit that PLA tends to form ordered phase (Im3m) in the PLA/PEG (50/50) blend. At 70 wt% concentration of PEG, two phases including continuous phase of PEG and stable perforated lamella (PL) structure of PLA occur. In this phase morphology, Gai *et al*. mentioned that the perforations in the PL

structures are always larger, more stable, and foursquare ordered (Gai, Li, Schrauwen, and Hu, 2009). The order structure of cylinder and spherical of PLA in the blends were observed at the 80 and 90 wt% PEG concentration, respectively.

Figure 4.8 represents the changes in diffusivities of PLA and PEG with respect to a change in PEG concentration in PLA/PEG blends. It is clear that the diffusivity of PEG is better than that of PLA because the chain length of PEG is shorter than that of PLA. Hence, PLA is easier to accumulate and separate phase than PEG which are demonstrated in Figure 4.6(a) to 4.6(g). Furthermore, the diffusivities of PLA and PEG tend to increase with increasing of PEG concentration in the PLA/PEG blends (Figure 4.8(a) and (b)). Our experimental observations (Chapter III) showed that the melt zero shear viscosity of the PLA/PEG blends decreased with the increase of PEG content in the blends, which might be attributed to the enhancement of diffusivities for both PLA and PEG.

The root mean square (RMS) end-to-end distance of the polymer chains is an important structural property which is generally used to describe the size or feature of the polymer chains in polymer materials. Figure 4.9 shows the RMS end-to-end distance of PLA molecules in PLA/PEG blends at different PEG contents. It is evident that the RMS end-to-end distances of PLA molecules in the PLA/PEG blends decrease in the following order: PLA/PEG 90/10 ≈ PLA/PEG 80/20 > PLA/PEG 70/30 > PLA/PEG 20/80 > PLA/PEG 50/50 ≈ PLA/PEG 30/70 > PLA/PEG 10/90.

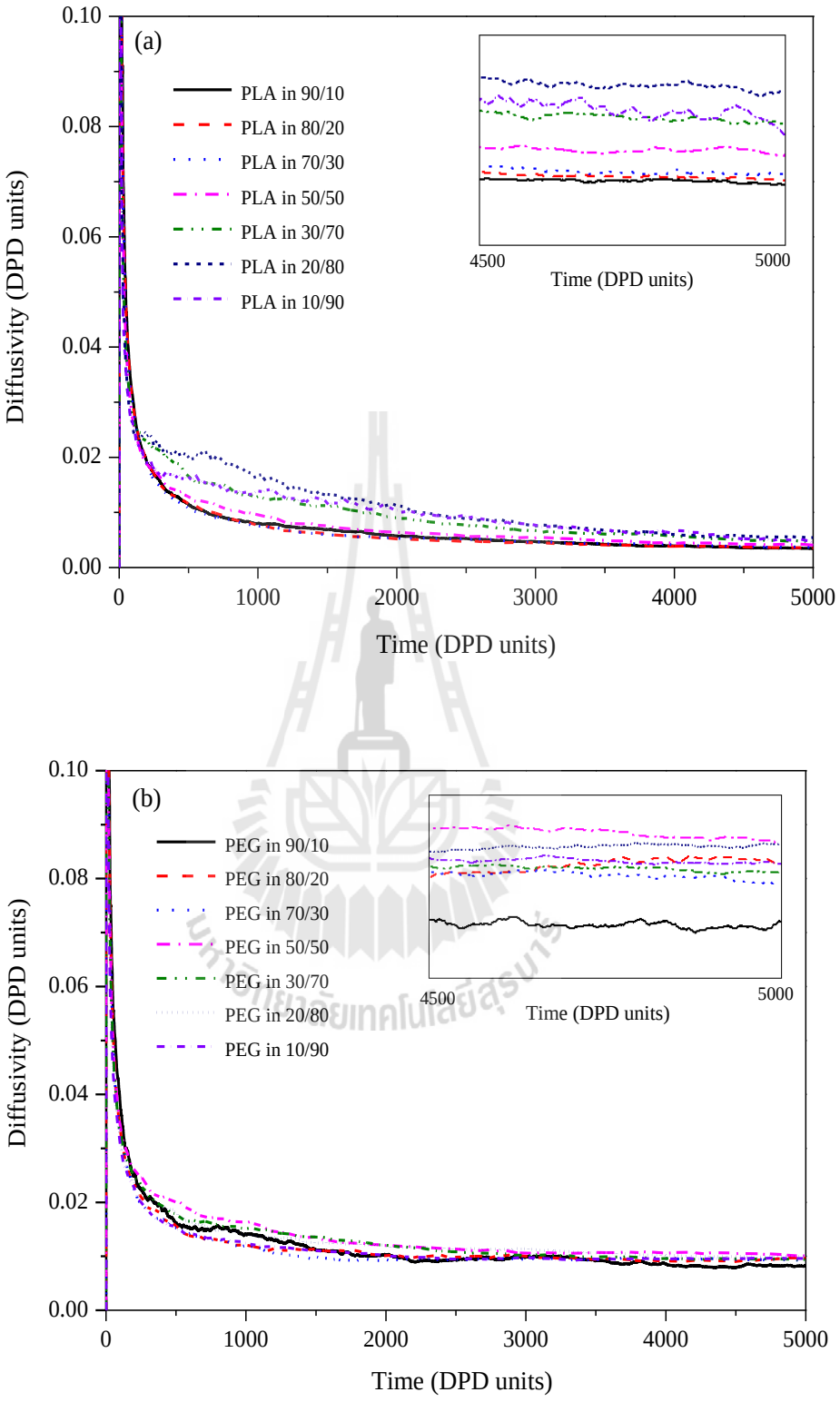

Figure 4.8 Time evolution of diffusivities of (a) PLA and (b) PEG in the PLA/PEG blends with varying the proportion of the PLA/PEG blends from 90/10 to 10/90.

These observations indicate that the diameter of PLA molecules decrease with increasing the concentrations of PEG, mesoscopic morphology of PLA transits in the order as: disorder (Figure 4.6(a), 4.6(b) and 4.6(c)), cylinder (Figure 4.6(f)), Im3m structure (Figure 4.6(d)), perforated lamella structure (Figure 4.6(e)) and spherical structure (Figure 4.6(g)).

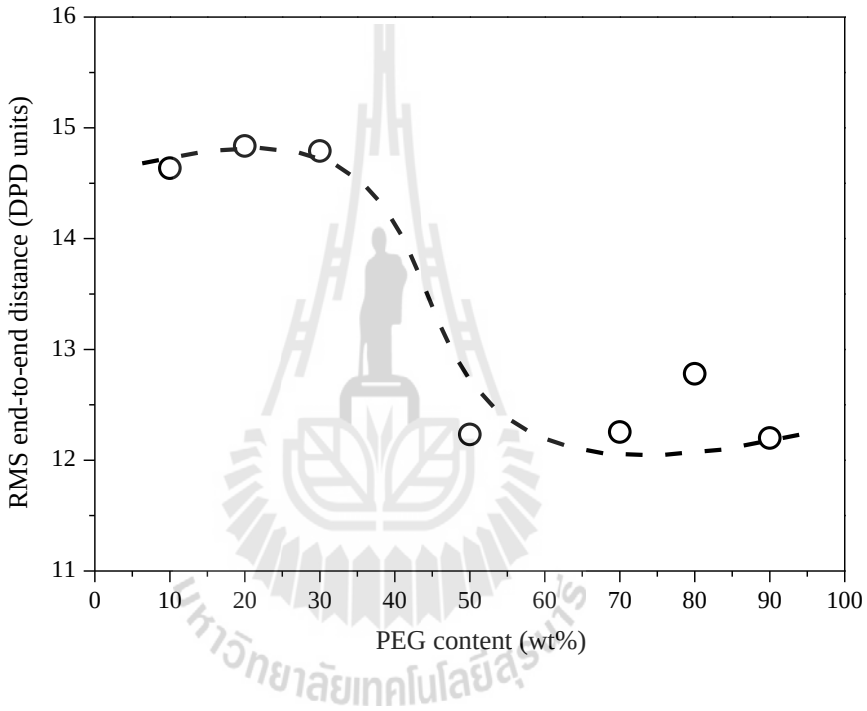

Figure 4.9 Simulated RMS end-to-end distance of PLA with different concentrations of PEG.

- **PLA-PEG-PLA triblock copolymers**

In addition to DPD simulation of PLA/PEG blends, triblock copolymer of PLA-PEG-PLA was also simulated to investigate the morphology. The effect of block composition on the morphology of PLA-PEG-PLA was elucidated at room temperature (298K). For DPD interaction parameters ($a_{PLA\text{-}PEG}$) of triblock

copolymers are the same as in polymer blends (Table 4.4). These values show a slight decrease as the block fraction of PLA (f_{PLA}) increases.

Before the construction of the simulation in details, the influences of box sizes and simulation time steps (t) on the morphologies of block copolymers were checked by varying box sizes and simulation time steps. Figure 4.10 displays the morphologies of PLA_{241}-PEG_{37}-PLA_{241} with different box sizes and simulation time steps.

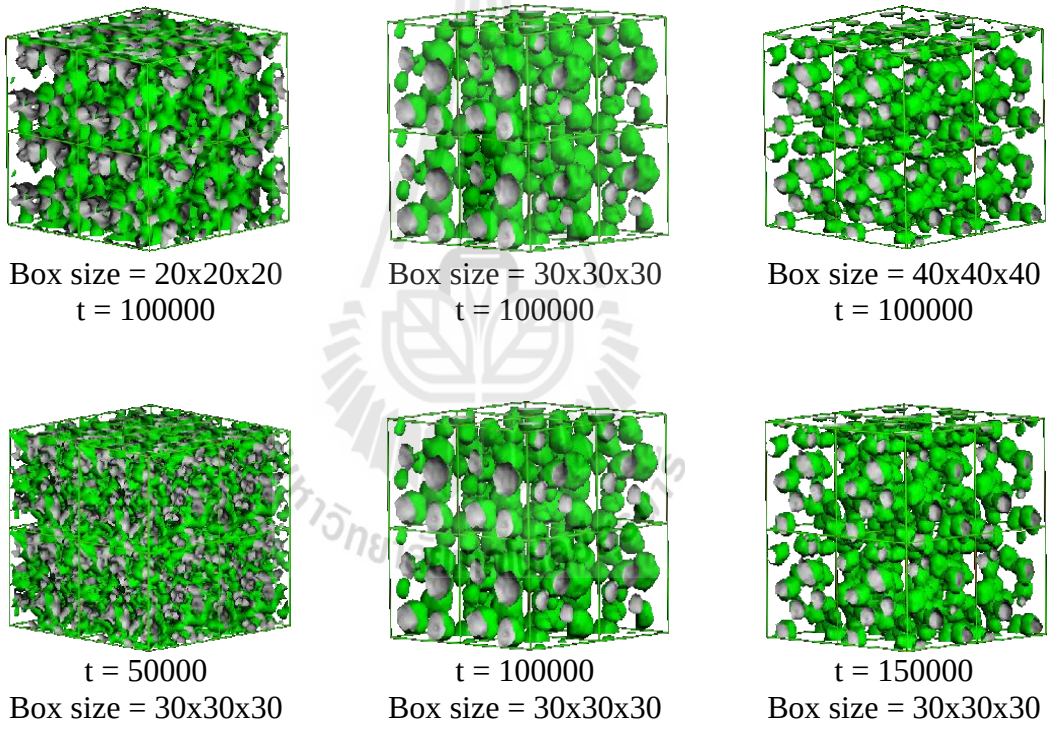

Figure 4.10 The morphologies of PLA_{241}-PEG_{37}-PLA_{241} with different box sizes and simulation time steps.

As seen in Figure 4.10, the morphologies of selected system did not change at the simulation box size of 30x30x30 and t = 100000, respectively. Hence, these parameters are appropriate of this DPD simulation.

Figure 4.11 exhibits the equilibrium morphologies of PLA-PEG-PLA at different (f_{PLA}) values. The red and green colors were represented as PLA and PEG chains, respectively. The morphologies of PLA-PEG-PLA blend with different of f_{PLA} values were summarized in Table 4.5.

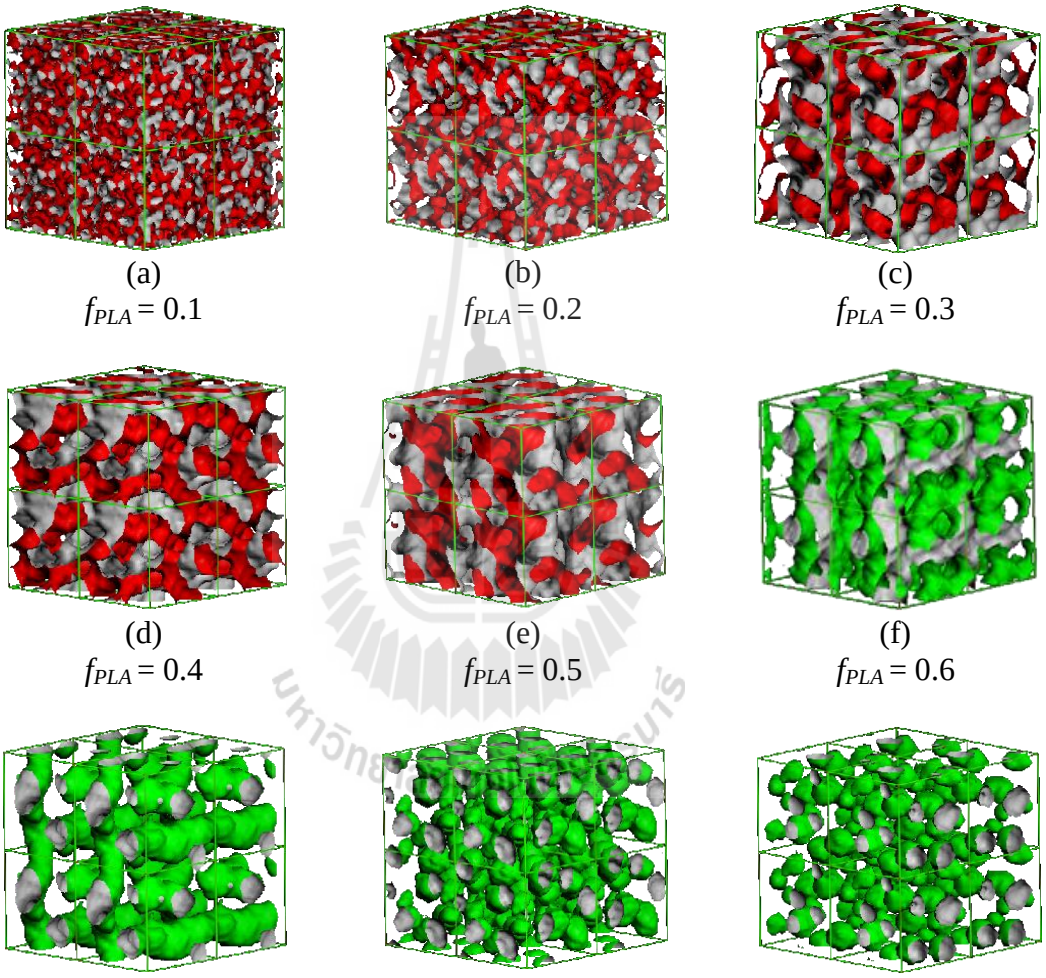

Figure 4.11 Iso-density surfaces of PLA and PEG in PLA-PEG-PLA at different of f_{PLA} values at t = 100000 DPD time steps; (a) 0.1, (b) 0.2, (c) 0.3, (d) 0.4 (e) 0.5, (f) 0.6, (g) 0.7, (h) 0.8 and (i) 0.9.

Table 4.5 Morphologies of PLA-PEG-PLA block copolymers at different PLA block fractions (f_{PLA}).

PLA-PEG-PLA block composition (f_{PLA})	**Phase morphologies**
0.1	Disorder structure
0.2	Disorder structure
0.3	Bicontinuous structure
0.4	Bicontinuous structure
0.5	Bicontinuous structure
0.6	Perforated lamella structure
0.7	Bicontinuous structure
0.8	Spherical structure
0.9	Spherical structure

As seen in Figure 4.11, four characteristic structures were found for different PLA block fractions. The phase structures include disorder, bicontinuous, perforated lamella and spherical structures. Figure 4.11(a) and 4.11(b) show the disordered structure for PLA-PEG-PLA at low PLA block fraction. The PLA block length is too short to aggregate with other PLA blocks and they were also constrained by the big PEG block. Therefore, they are only able to form disorder structure at these compositions. At higher PEG block length ratios (f_{PLA} of 0.3-0.4), the bicontinuous structure of PEG were observed as displayed in Figure 4.11(c) to 4.11(e). When the PEG block lengths are minority, the excluded volumes of the PEG parts string outward, and are not close enough to form a geometric barrier. Consequently, the PLA block in different copolymer chains can aggregate together to form the ordered

structures. For example in f_{PLA} of 0.6, PLA can form the perforated lamella structure (Figure 4.10(f)). At the high PLA block lengths (f_{PLA} of 0.8 and 0.9), the morphologies of the copolymers show the spherical structure of PEG embed in PLA blocks. In these compositions, the formation of order structure looks like the micellization process. Compared to the PLA/PEG blend system at the same composition, the disorder morphologies of polymer blends were observed because PEG chains are easy to diffuse in PLA matrix. While in block copolymer system, PLA and PEG segment are connected by a bond, PEG segments are restricted to diffuse in PLA phase.

Bridge and loop structures of block copolymers are an important characteristic which influence to their physical properties. In the bridge conformation, the two ends of the ABA chain belong to two different A domains, while in the loop type the ends belong to the same A domain. Bridge and loop fraction have been extensive studied both theoretical and experimental approaches (Sharkh and AlSunaidi, 2006; Takano, Kamaya, Takahashi, and Matsushita, 2005). Therefore, the bridge and loop fractions (f_{bridge}) of polymer chains in PLA-PEG-PLA were estimated by analyzing the distribution of the end-to-end distances. The bridge and loop fractions are estimated by fitting the bimodal curve with two Gaussian distributions and determining the area under each distribution curve. This methodology was reported by Sharkh *et al*. (Sharkh and AlSunaidi, 2006). The example of end-to-end distance distribution of PLA_{12}-PEG_{37}-PLA_{12} (f_{PLA} = 0.3) was shown in Figure 4.12. We define the first and second peaks in bimodal curve as the characteristics of loop and bridge conformations, respectively. The bridge and loop fractions of PLA-PEG-PLA block copolymers were summarized in Table 4.6.

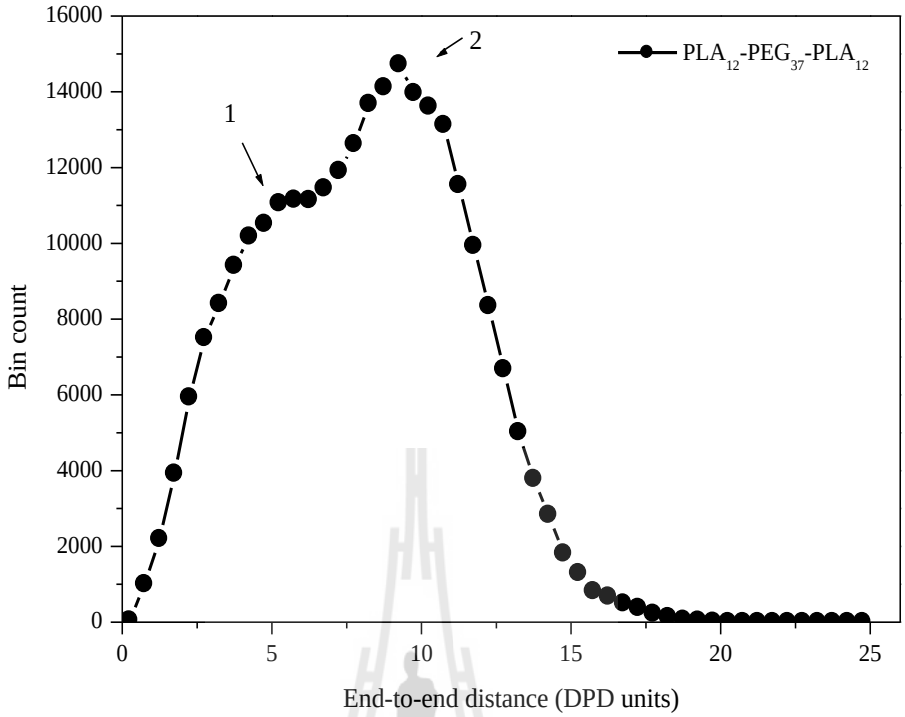

Figure 4.12 End-to-end distance distribution of PLA_{12}-PEG_{37}-PLA_{12} (f_{PLA} = 0.3).

Table 4.6 The bridge and loop fraction values of PLA-PEG-PLA with different PLA block fractions.

PLA-PEG-PLA block composition (f_{PLA})	**Bridge fraction (f_{bridge})**
0.3	0.73
0.4	0.76
0.5	0.73
0.6	0.67
0.7	0.52
0.8	0.54
0.9	0.49

The calculated f_{bridge} values in this study are in the range of 0.49-0.73 depending on morphologies and polymer chain lengths of the block copolymers. It is clear that no bridging structure is in the disorder morphology (f_{PLA} = 0.1 and 0.2). There has been reported that the bridging fraction should be a bit less than 0.8 for the spherical micelles, about 0.6 for the cylindrical micelles and about 0.45 for the lamellar morphology (Sharkh and AlSunaidi, 2006). The calculated f_{bridge} values tend to decrease with increasing of PLA block length. The perforated lamella structure (f_{PLA} = 0.6) shows the calculated f_{bridge} values of 0.67. While the spherical micelles give a bridge fraction of 0.49 and 0.54 for PLA_{107}-PEG_{37}-PLA_{107} and PLA_{241}-PEG_{37}-PLA_{241}, respectively.

- **PLA/PLA-PEG-PLA blends**

The morphologies of PLA/PLA-PEG-PLA blends were predicted using DPD simulation at room temperature. The PEG concentration in the blends are 50 wt%. Therefore, 50 wt% PLA/PEG blend was used to compare with this system. The effect of PLA block lengths of PLA-PEG-PLA on the morphologies of the blends was investigated. The obtained results were analyzed to determine the miscibility of the blends.

The morphologies and iso-density surfaces of PEG for PLA/PEG, PLA/PLA_3-PEG_{37}-PLA_3, PLA/PLA_{12}-PEG_{37}-PLA_{12} and PLA/PLA_{12}-PEG_{37}-PLA_{12} are displayed in Figure 4.13. The red, green and blue colors were represented as the PLA homopolymer, PEG in block copolymer and PLA in block copolymer chains, respectively.

(a) PLA/PEG

(b) PLA/PLA_3-PEG_{37}-PLA_3

(c) PLA/PLA_{12}-PEG_{37}-PLA_{12}

(d) PLA/PLA_{27}-PEG_{37}-PLA_{27}

Figure 4.13 Morphologies (left hand side) and iso-density surfaces of PEG segment (right hand side) of 50/50 (wt/wt) PLA/PEG and PLA/PLA-PEG-PLA blends.

The morphologies of PLA/PLA-PEG-PLA blends and the corresponding density distribution of PLA and PEG particles are shown in Figure 4.13. The left hand side of Figure 4.13 shows the iso-density surfaces of PEG in the PLA/PLA-PEG-PLA blends. Obviously, the size and shape of PEG domain in the blends was changed at the different PLA block lengths as seen in the left hand side of the Figure 4.13. The bicontinuous structures of PEG were observed in PLA/PLA_3-PEG_{37}-PLA_3 and PLA/PLA_{12}-PEG_{37}-PLA_{12} systems. While the fine rod and spherical structures of PEG were formed in PLA/PLA_{27}-PEG_{37}-PLA_{27} systems.

The reduction of PEG domain sizes in the blends can be implied that the PEG aggregated structures tend to break up and would be more disperses in PLA homopolymer. This corresponds to the density profiles of PLA homopolymer (PLA_H), PEG of block copolymer (PEG_B) and PLA of block copolymer (PLA_B) in the blends as displayed in Figure 4.14. It is clear that the PLA segments of block copolymer (blue color) are located in the interface between PLA homopolymer (red color) and PEG block segments of PLA-PEG-PLA (green color). This observation indicates that the PEG segments can be distributed in the PLA phase by contributing to those PLA end blocks of block copolymer.

Figure 4.14(a) to 4.14(c) show the density profiles of PLA_H, PEG_B and PLA_B in PLA/PLA-PEG-PLA blends. Apparently, the density profiles of each species in PLA/PLA-PEG-PLA show the phase separation. However the density profiles of PLA_H, PEG_B and PLA_B in PLA/PLA_{27}-PEG_{37}-PLA_{27} (Figure 4.14(c)) are more constant than other systems. This indicates that PLA_{27}-PEG_{37}-PLA_{27} is more dispersed in the PLA phase than other block copolymers. On other hand, the different values between $\chi_{PLA_B-PEG_B}$ and $\chi_{PLA_H-PEG_B}$ of PLA/PLA_{27}-PEG_{37}-PLA_{27} is lowest

when comparing with other systems, leading PEG to be concentrated more preferably in the phase of PLA homopolymer.

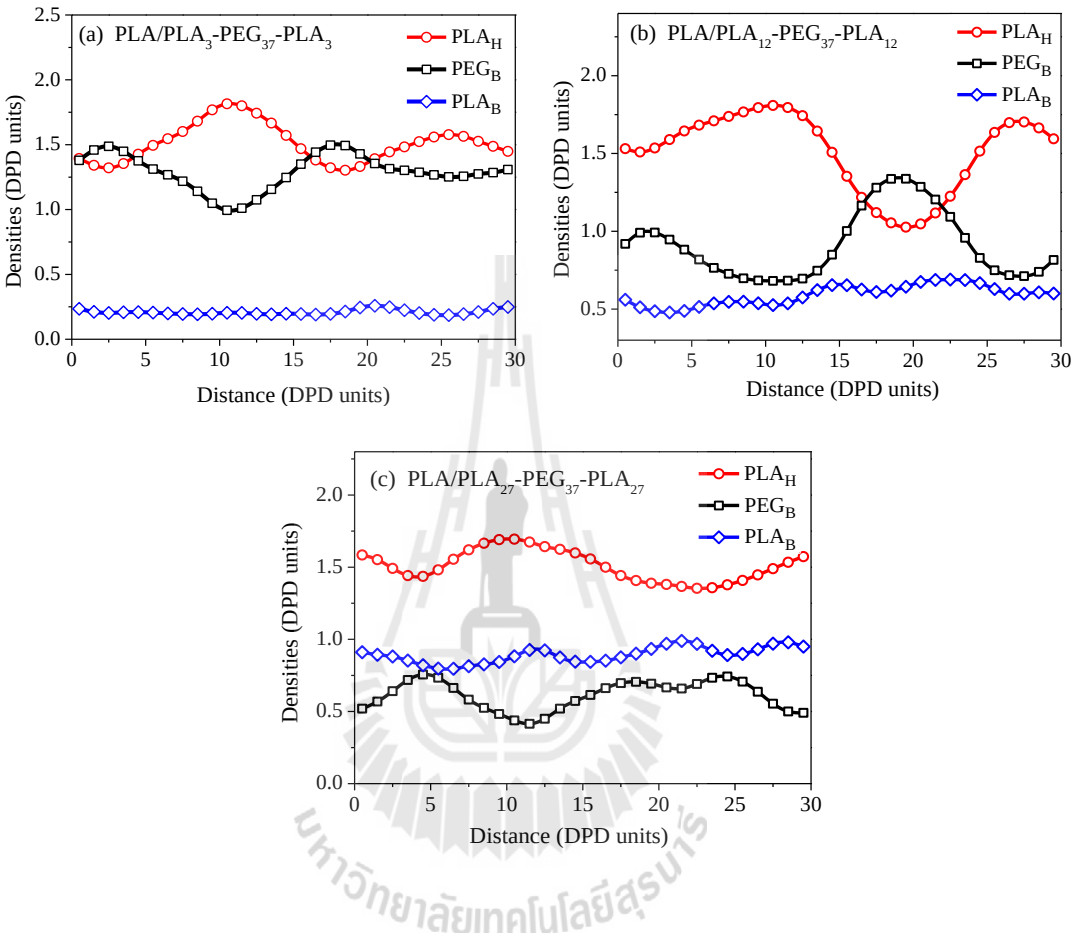

Figure 4.14 Density profiles of (a) PLA/PLA_3-PEG_{37}-PLA_3, (b) PLA/PLA_{12}-PEG_{37}-PLA_{12} and (c) PLA/PLA_{27}-PEG_{37}-PLA_{27} blends.

4.5 Conclusions

MD and DPD simulations were employed to predict the miscibility and morphology of PLA/PEG, PLA-PEG-PLA and PLA/PLA-PEG-PLA systems. Flory-Huggins interaction parameters (χ_{ij}-parameter) for PLA/PEG blends at different PEG concentrations were calculated by MD simulation. PEG concentrations of 10 to 90 wt% were varied to blend with PLA homopolymer. χ_{ij} parameters of PLA and PEG were analyzed to determine the miscibility of PLA/PEG blends. The results show that the PLA and PEG are miscible at low PEG concentrations (10, 20 and 30 wt%). Moreover, we also investigated the miscibility of PLA/PLA-PEG-PLA blends at PEG concentration of 50 wt% in the blends. The PLA block fractions of PLA-PEG-PLA were varied from 0.1 to 0.5. It was found that the χ_{ij}-parameter values of PLA and PEG for all PLA/PLA-PEG-PLA systems are lower than the χ_{ij}-parameter value of 50/50 (wt/wt) PLA/PEG blend. The χ_{ij}-parameters of PLA/PLA-PEG-PLA decrease with increasing of PLA block fractions. The radial distribution functions *g(r)* of the inter-molecular carbon atomic pairs of PLA-PEG, PLA-PLA and PEG-PEG also indicate that 90/10, 80/20 and 70/30 (wt/wt) PLA/PEG is miscible. The morphologies of PLA/PEG, PLA-PEG-PLA and PLA/PLA-PEG-PLA systems were predicted using DPD simulation method. The bead-bead pairs interaction parameters (a_{ij}), which were used as an input parameters in DPD simulation, were calculated from χ_{ij}-parameter. The morphologies of disorder, bicontinuous, perforated lamella and spherical structures of both polymer blends and block copolymers were observed at different components. Bead density profiles and diffusivity of polymer beads were also calculated to determine the miscibility of PLA/PEG blends. The finding results agree well with the results from MD simulations. The morphology of PLA-PEG-PLA block

copolymers was also investigated at different block compositions. The bridge and loop fractions (f_{bridge}) of these block copolymers were calculated by analyzing the distribution of the end-to-end distances curve. The f_{bridge} values were found to be 0.49-0.73 at different morphologies. The f_{bridge} values tend to decrease with increasing of PLA block lengths. The morphologies of PLA/PLA-PEG-PLA blends exhibited the reduction of PEG domain size comparing to the PLA/PEG blend. This implies that the PLA end blocks in block copolymer contribute to an enhancement the miscibility of PLA and PEG in the blends.

4.6 References

Agrawal A, Saran A. D., Rath, S. S. and Khanna A. (2004). Constrained nonlinear optimization for solubility parameters of poly(lactic acid) and poly(glycolic acid)-validation and comparison. **Polymer** 45: 8603-8612.

Arenaza, I. M., Meaurio, E., Coto, B. and Sarasua, J. R. (2010). Molecular dynamics modeling for the analysis and prediction of miscibility in polylactide/ polyvinilphenol blends. **Polymer** 51: 4431-4438.

Chen, S., Nhan Phan-Thien, Fan, X. J. and Khoo, B. C. (2004). Dissipative particle dynamics simulation of polymer drops in a periodic shear flow. **Journal of Non-newtonian Fluid Mechanics** 118: 65-81.

Flory, P. J. (1989). Statistical mechanics of chain molecules. Germany: Hanser.

Fu, Y., Liao, L., Lan Y., Yang, L., Mei, L., Liu, Y. and Hu, S. (2012). Molecular dynamics and mesoscopic dynamics simulations for prediction of miscibility in polypropylene/polyamide-11 blends. **Journal of Molecular Structure** 1012: 113-118.

Gai, J. G., Li, H. L., Schrauwen, C. and Hu, G. H. (2009). Dissipative particle dynamics study on the phase morphologies of the ultrahigh molecular weight polyethylene/polypropylene/poly(ethylene glycol) blends. **Polymer** 50: 336-346.

Glotzer, S. C. and Paul, W. (2002). Molecular and mesoscale simulation methods for polymer materials. **Annual Review of Materials Research** 32: 401-436.

Groot R. D. and Warren P. B. (1997). Dissipative particle dynamics: Bridging the gap between atomistic and mesoscopic simulation. **The Journal of Chemical Physical** 107: 4423-4435.

Hoogerbrugge P. J. and Koelman J. M. V. A. (1992). Simulating microscopic hydrodynamic phenomena with dissipative particle dynamics. **Europhyics Letters** 19: 155.

Hu, Y., Hu, Y. S., Topolkaraev, V., Hiltner, A. and Baer, E. (2003). Crystallization and phase separation in blends of high stereoregular poly(lactide) with poly(ethylene glycol). **Polymer** 44: 5681-5689.

Jawalkar, S. S. and Aminabhavi, T. M. (2006). Molecular modeling simulations and thermodynamic approaches to investigate compatibility/incompatibility of poly(L-lactide) and poly(vinyl alcohol) blends. **Polymer** 47: 8061-8071.

Jia, Z., Tan, J., Han, C., Yang, Y. and Dong, L. (2009). Poly(ethylene glycol-co-propylene glycol) as a macromolecular plasticizing agent for polylactide: Thermomechanical properties and aging. **Journal of Applied and Polymer Science** 114: 1105-1117.

Lemmouchi, Y., Murariu, M., Margarida Dos Santos, A., Amass, A. J., Schacht, E. and Dubois, P. (2009). Plasticization of poly(lactide) with blends of tributyl

citrate and low molecular weight poly(D,L-lactide)-b-poly(ethylene glycol) copolymers. **European Polymer Journal** 45: 2839-2848.

Meirovitch, H. (1983). Computer simulation of self-avoiding walks: Testing the scanning method. **Journal of Chemical Physics** 79: 502.

Mu, D., Huang, X. R., Lu, Z. Y. and Sun, C. C. (2008). Computer simulation study on the compatibility of poly(ethylene oxide)/poly(methyl methacrylate) blends. **Chemical physics** 348: 122-129.

Rapaport, D. C. (2001). **The art of molecular dynamics simulation** (2 nd ed.). New York: Cambridge University Press.

Rathi, S., Chen, X., Coughlin, E. B., Hsu, S. L., Golub, C. S. and Tzivanis, M. J. (2011). Toughening semicrystalline poly(lactic acid) by morphology alteration. **Polymer** 52: 4181-4188.

Ran, X., Jia, Z., Han, C., Yang, Y. and Dong, L. (2010). Thermal and mechanical properties of blends of polylactide and poly(ethylene glycol-co-propylene glycol): influence of annealing. **Journal of Applied Polymer Science** 116: 2050-2057.

Sharkh, B. A. and AlSunaidi, A. (2006). Morphology and conformation analysis of self-assembled triblock copolymer melts. **Macromolecular Theory Simulation** 25: 507-515.

Sheth, M., Kumar, R. A., Dave, V., Gross, R. A. and McCarthy, S. P. (1997). Biodegradable polymer blends of poly(lactic acid) and poly(ethylene glycol) **Journal of Applied and Polymer Science** 66: 1495-1505.

Spyriouni, T. and Vergelat,i C. (2001). Molecular modeling study of binary blend compatibility of polyamide 6 and poly(vinyl acetate) with different degrees of

Hydrolysis: An atomistic and mesoscopic approach. **Macromolecules** 34: 5306-5316.

Sun, H. (1998). COMPASS: An Ab initio forcefield optimized for condensed-phase application-overview with details on alkane and benzene Compounds, **The Journal of Physical Chemistry B** 102: 7338-7364.

Takano, A., Kamaya, I., Takahashi, Y. and Matsushita, Y. (2005). Effect of loop/ bridge conformation ratio on elastic properties of the sphere-forming ABA triblock copolymers: preparation of samples and determination of loop/bridge ratio. **Macromolecules** 38: 9718-9723.

Theodorou D. N. and Suter U. W. (1986). Atomistic modeling of mechanical properties of polymeric glasses. **Macromolecules** 19: 139-154.

Tükan, H. and Mattice, W. L. (1999). Detection of the onset of demixing in simulations of polypropylene melts in which the chains differ only in stereochemical composition. **Journal of Chemical Physics** 111: 4327-4333.

Yang, H., Sheng, L. Z., Qian, H. J., Yang, Y. B., Zhang, X. B. and Sun, C. C. (2004). Molecular dynamics simulation studies of binary blend miscibility of poly(3-hydroxybutyrate) and poly(ethylene oxide). **Polymer** 45: 453-457.

CHAPTER VI

STRUCTURE AND DYNAMICS OF BIDISPERSE POLYETHYLENE NANOCOMPOSITES

6.1 Abstract

The structure and dynamics of bidisperse polyethylene (PE) nanocomposite mixtures of 50:50 (by mole) of long and short chains of $C_{160}H_{322}/C_{80}H_{162}$ and $C_{160}H_{322}/C_{40}H_{82}$ filled with spherical nanoparticles were investigated by a coarse-grained, on lattice Monte Carlo method using rotational isomeric state theory for short-range and Lennard-Jones for long-range energetic interactions. Simulations were performed to evaluate the effect of wall-to-wall distance between fillers (*D*), polymer-filler interaction (*w*) and polydispersity (number of short chains in the mixture) on the behavior of the long PE chains. The results indicate that long chain conformation statistics remain Gaussian regardless of the effects of confinement, interaction strength and polydispersity. The various long PE subchain structures (bridges, dangling ends, trains, and loops) are influenced strongly by confinement whereas monomer-filler interaction and polydispersity did not have any impact. In addition, the average number of subchain segments per filler in bidisperse PE nanocomposites decreased about 50% compared to the nanocomposite system with monodisperse PE chains. The presence of short PE chains in the polymer matrix leads to a reduction of the repeat unit density of long PE chains at the interface suggesting

that the interface is preferentially populated by short chains. Chain dynamics were monitored by computing the Rouse relaxation modes and the mean square displacement of the center of mass. The dynamics were slowed by both the confinement (D) and monomer-particle energetic interaction (w) effects. Under the greatest confinement studied (D=1.26R_g), the mobility of the long chains in bidisperse nanocomposites was slower than those in the monodisperse nanocomposite systems.

6.2 Introduction

Polymer materials reinforced with nanoparticles have been the subject of interest in both scientific and industrial communities due to their extraordinary and improved performance. The improved properties (Koo, 2006; Guth, 1945; Zhang and Archer, 2002, Coleman, Khan, Blau, and Gun′ko, 2006), although very different in nature according to the application of interest and polymers used, are generally termed as the reinforcement effect (Guth, 1945). Though an understanding of the reinforcement mechanism behind these improvements is still developing, it is well accepted that the well dispersion of nanoparticles in polymer matrix and the filler spacing between neighboring particles, when it is comparable to the unperturbed chain dimensions, are both factors that play important roles in the property enhancement (Zhang and Archer, 2002, Anderson and Zukoski, 2010).

Several theoretical and experimental studies (Zhang and Archer, 2002; Dionne, Ozisik, and Picu, 2005) have proposed that the reinforcement is obtained once the neighboring fillers were connected by adsorbed polymer chains forming a “secondary” network, which is also called a polymer-mediated transient network. This

network can be formed when the wall-to-wall distance (D) between fillers is of the order of several times the radius of gyration (R_g) of the polymer chain. The polymer-filler structure is formed as sequences (subsections) of the chain adsorb onto the filler particles (Vacatello, 2003). The various types of subchain segments in transient network model are illustrated in Figure 6.1. This model was successfully used to qualitatively explain the viscoelastic properties of polymer nanocomposites (Dionne, Ozisik, and Picu, 2005; Zeng, Yu, and Lu, 2008).

Molecular simulations provide an excellent opportunity to directly study the effect of nanoparticles on structure and dynamics of polymer chains, since detailed information on the properties near a nanoparticle surface is difficult to obtain experimentally. The melt structure of polymer chains in the vicinity of the flat and curve solid surfaces have been studied by both molecular dynamics (MD) and Monte Carlo (MC) methods. The results suggest that polymer chains near flat walls do not distort even when they are confined into films as thin as R_g but they are preferentially aligned in the direction parallel to the surface (Jang and Mattice, 2000; Zeng, Yu, and Lu, 2008). In contrast to polymer chains in the presence of curve nanoparticles, polymer chains near flat surfaces were found to be either stretched or compressed depending on the ratio of the chain dimension and the average wall-to-wall distance (Kloczkowski, Sharaf, and Mark, 1994). However, recent MC (Picu and Ozmusul, 2003; Vacattello, 2001) and MD (Starr, Schrøder, and Glotzer, 2002) simulations of polymer melts in the presence of nanosized spherical fillers imply that the chain dimensions are always smaller compared to the bulk at high and moderate filler concentrations.

The change in dynamic properties of polymer chains near the interfaces of nanocomposites is also an interesting study. Several computational studies in this area shed light into the issue of the change in the glass transition temperature (T_g) in nanoparticle filled polymers, as well as the effect of surface interactions on melt diffusion and viscosity (Desai, Keblinski, and Kumar, 2005).

Most computational studies of the structure and dynamics of polymer nanocomposites have been dedicated to monodisperse polymer matrices. However, in reality, polymers are polydisperse. It is well known that the polydispersity of the polymer matrix plays a critical role in defining the properties of polymer nanocomposites but a comprehensive understanding of the effect of polydispersity on polymer chain structure and dynamics in polymer nanocomposites is lacking. Therefore, the study of polydispersity via molecular computations is both appealing and timely.

In the current study, the structure and dynamics of bidisperse polyethylene (PE) melts composed of two different chain lengths (long and short) filled with a spherical nanoparticle was studied using coarse-grained, on lattice Monte Carlo simulations. The structure and dynamics of long PE chains were investigated as a function of polydispersity, confinement (as defined by the wall-to-wall distance between nanofillers, *D*), and polymer-filler interaction strength (as defined by the Lennard-Jones potential well depth prefactor, *w*). The key questions that the current study aims to address are as follows: (i) What is the nature of the transient polymer network in the presence of short PE chains? (2) How does the polymer-filler interface structure and dynamics change in bidisperse matrices?

6.3 Simulation setup

Simulations were performed on a high coordination lattice called second nearest neighbor diamond (2nnd or SNND) lattice (Dionne, Ozisik, and Picu, 2005; Dionne, Ozisik, and Picu, 2008) employing Metropolis Monte Carlo algorithm (Landau and Binder, 2000). This simulation method was previously employed by our groups on various types of polymers and geometries (bulk, thin film, polymer droplet) to investigate chain conformation, dynamics, crystallization, etc. with success (Dionne, Ozisik, and Picu, 2005; Jang and Mattice, 2000; Xu and Mattice, 2001; Jang, Ozisik, and Mattice, 2000; Vao-Soongnern, Ozisik, and Mattice, 2001). A concise summary is provided here to highlight the basic principles of this method. The high coordination lattice has a lattice constant of 0.25 nm and 60° angles between any unit vectors along the axes. This geometry corresponds to close packing of uniform spheres, and therefore, has 12 nearest neighbors, much greater than the tetrahedral (diamond) lattice onto which polymers with all carbon backbones would fit naturally. To map polymer chains onto the SNND lattice, every two repeat units of polyethylene (PE) are coarse-grained as a single bead on the lattice. With C-C bond length of 0.154 nm and ~109° bond angle, polyethylene chains fit perfectly onto the SNND lattice. The coarse-graining of the polymer chains is reversible; therefore, after simulation is performed on the SNND lattice (or at any stage during the simulation), coarse-grained chains can be mapped back to fully atomistic chains for analysis.

In the current study, simulations were performed for linear polyethylene (PE) chains of $C_{160}H_{322}$, $C_{80}H_{162}$ and $C_{40}H_{82}$. Three different types of systems were studied: neat $C_{160}H_{322}$ (monodisperse system), 50:50 mixtures of $C_{160}H_{322}$:$C_{80}H_{162}$, and

$C_{160}H_{322}$:$C_{40}H_{82}$ (by mole). Because coarse-graining technique used represents a PE repeat unit as a single spherical bead on the simulation lattice, these systems were represented as PE80, PE80/40 and PE80/20, respectively, throughout the remainder of the document. An approximately spherical nanoparticle of varying size (diameter, D_p) was placed at the center of the simulation box. Periodic boundary conditions were employed along all three axes thereby enabling the study of confinement by controlling the distance (D) between the filler (in the parent box) and its images via the box size and filler size. Particle size (D_p) and wall-to-wall distance (D) were both kept comparable to the average radius of gyration (R_g) of the PE80 (long) chains. Wall-to-wall distance was defined as the smallest distance between two points located on the surface of two fillers. Wall-to-wall distances of 1.26xR_g, 1.91xR_g and 2.50xR_g were investigated in the current study.

The simulation method employed in this study used single bead moves that were local and were accepted through the Metropolis Monte Carlo algorithm, which was shown to effectively sample the conformational space. The filler was not moved during the simulations.

The interaction energy used in this model contains a short-range interaction based on the rotational isomeric state (RIS) model and a long-range interaction based on the 6-12 Lennard-Jones (LJ) potential. Energetic interactions, $u(r)$, between polymer-polymer and polymer-filler beads were defined using the same LJ potential. The monomer-filler affinity is controlled by the prefactor (w), as shown in Equation 6.1. The w values of 0.1, 1.0 and 2.0 were used corresponding to repulsive, neutral and attractive interactions, respectively. In Equation 6.1, ϵ is the minimum potential

energy, σ is the location of the minimum energy, and *r* is the distance between bead centers.

$$u(r) = \begin{cases} 4w\varepsilon \left[\left(\frac{\sigma}{r} \right)^{12} - \left(\frac{\sigma}{r} \right)^{6} \right] & for \quad r \geq 0.25nm \\ hard & for \quad r < 0.25nm \end{cases} \tag{6.1}$$

All simulations were performed at 473 K. The space occupied by the polymer was filled to a density of ~0.76 g/cm^3, which is the melt density of PE at 473 K. After the initial structure was created, an equilibration run was performed for at least 10 million Monte Carlo steps (MCS). Each MCS is defined as an attempt to move each bead (except the filler beads) in the system once. Once the system reached equilibrium, production run of 20 million MCS were performed. Each system was replicated three times with different starting configurations to decrease statistical error. The details of the various simulations performed are provided in Table 6.1.

Table 6.1 Details of the various polyethylene nanocomposite simulations performed.

System	l_x x l_y x l_z (Å)	n	I	N	N_p	D_p/R_g	D/R_g	ρ (g/cm^3)	w
A1	19x18x18	80	1	14	-	-	-	0.767	-
A2	18x18x18	80	1	12	1	1.38	1.26	0.776	1.0
A3	18x18x18	80	1	13	1	0.73	1.91	0.764	1.0
A4	22x22x22	80	1	24	1	0.73	2.50	0.767	1.0
A5	18x18x18	80	1	13	1	0.73	1.91	0.764	2.0
A6	18x18x18	80	1	13	1	0.73	1.91	0.764	0.1
A7	18x18x18	80/40	1.124	7/13	1	1.38	1.26	0.776	1.0
A8	18x18x18	80/40	1.124	7/13	1	0.73	1.91	0.776	1.0
A9	18x18x18	80/20	1.562	7/26	1	1.38	1.26	0.777	1.0
A10	18x18x18	80/20	1.562	7/26	1	0.73	1.91	0.777	1.0
A11	22x22x22	80/20	1.563	12/48	1	0.73	2.50	0.767	1.0
A12	18x18x18	80/20	1.562	7/26	1	0.73	1.91	0.777	2.0
A13	18x18x18	80/20	1.562	7/26	1	0.73	1.91	0.777	0.1

l_i: Simulation box size along axis i; n: Number of repeat units (also the number of coarse-grained beads per chain); I: Polydispersity index; N: Number of PE chains; N_p: Number of spherical nanoparticles; D_p: Particle diameter; R_g: Average radius of gyration of the PE80 chains; D: Shortest distance between two nanoparticles; ρ: Density of the polymer matrix; w: monomer-particle interaction energy prefactor.

6.4 Results and discussion

The static (conformational) and dynamic properties of long polyethylene (PE) chains in monodisperse and bidisperse melts containing spherical nanoparticles were investigated via coarse-grained, on lattice, Metropolis Monte Carlo simulations. Neat PE melts were used as control and all other simulations were compared to the neat PE simulations when appropriate. The conformational analysis considers both entire chains and subchain segments such as bridges, loops, trains and dangling ends that could form on the filler as illustrated in Figure 6.1. Dynamic properties were investigated by examining both Rouse relaxation times and mean square displacements (MSDs) of the chain center of mass (g_3) as a function of time (MCS).

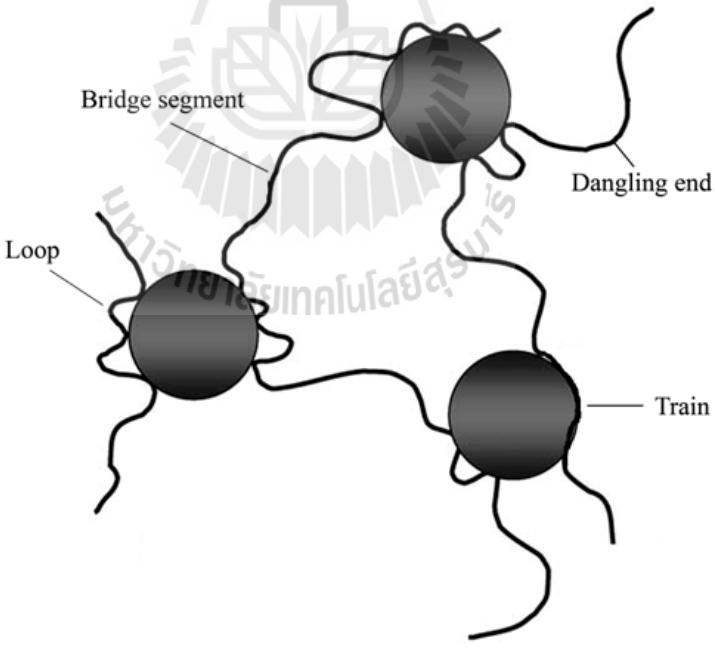

Figure 6.1 Schematic representation of the various types of subchain segments investigated.

6.4.1 Conformational analysis

- **Overall chain conformation**

We first focus our attention on the effect of the nanoparticle on the conformation of PE chains in the melt. Figure 6.2 shows the probability distribution function of the end-to-end vector (**R**) of PE80 chains in various systems for different values of *D* and *w* parameters. All curves are identical for all conditions indicating that PE80 chains retain the same Gaussian statistics even when they are confined between solid spherical nanoparticles.

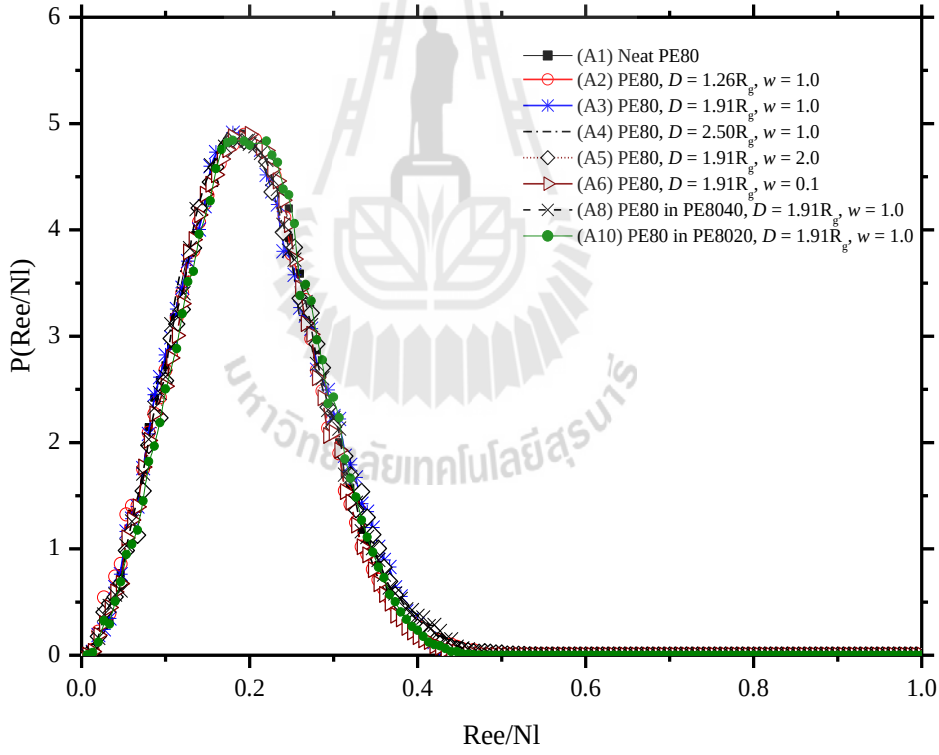

Figure 6.2 Probability distribution function of the end-to-end vector of PE80 chains in neat PE80 melt, and monodisperse and bidisperse PE mixtures in the presence of nanofillers.

- **Monomer density profile**

The bead density of the PE80 chains as a function of radial distance from the nanoparticle surface in both monodisperse and bidisperse systems with different *D* and *w* are illustrated in Figure 6.3. As can be seen in Figure 6.3, all systems considered have a well-defined layered structure. The first layer is generally observed at ~0.25 nm from the nanofiller surface and is generally the densest layer. The exception to this behavior was observed in systems with repulsive polymer-filler interaction (*w*=0.1). As the interaction parameter value increased and the system became more attractive, the density of the first layer increased substantially as shown in Figure 6.3(a). The density of the first layer did not show a strong dependence on confinement as measured by parameter *D* as shown in Figure 6.3(b). On the other hand, the spacing between layers increased with increasing *D* values. Figure 6.3(c) shows the effect of bidispersity on the density profile of PE80 chains. It is important to note that although bidisperse systems contain shorter PE chains, the density profile was plotted for PE80 chains only and as a result, the density profiles change drastically. The density profiles of the PE80 chains in A8 and A10 systems, which have the same number of PE80 chains but have differing short chain molecular weights, are almost the same. When the density profiles are normalized by the number of PE80 chains present in each system (See Figure 6.3(d)), the PE80 chain density profiles look exactly the same. This result shows that even when the system is diluted with shorter chains, the density profile of the long chains as a function of distance from the filler surface does not change.

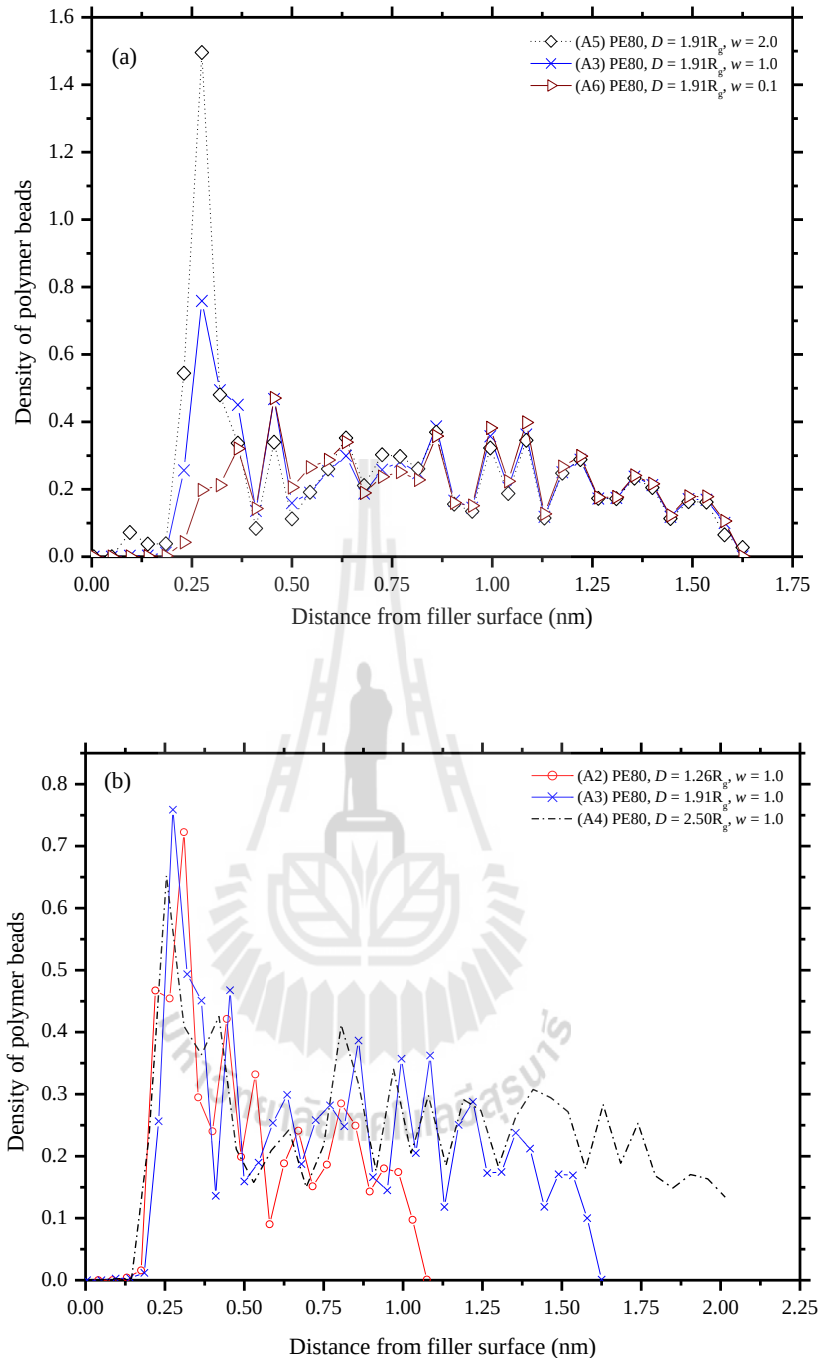

Figure 6.3 Monomer density profiles of PE80 chains as a function of radial distance from the filler surface as a function of (a) polymer-filler interaction parameter (*w*), (b) confinement (*D*), and (c, d) polydispersity. In (d) the density profiles from (c) are normalized by the number of PE80 chains in each system.

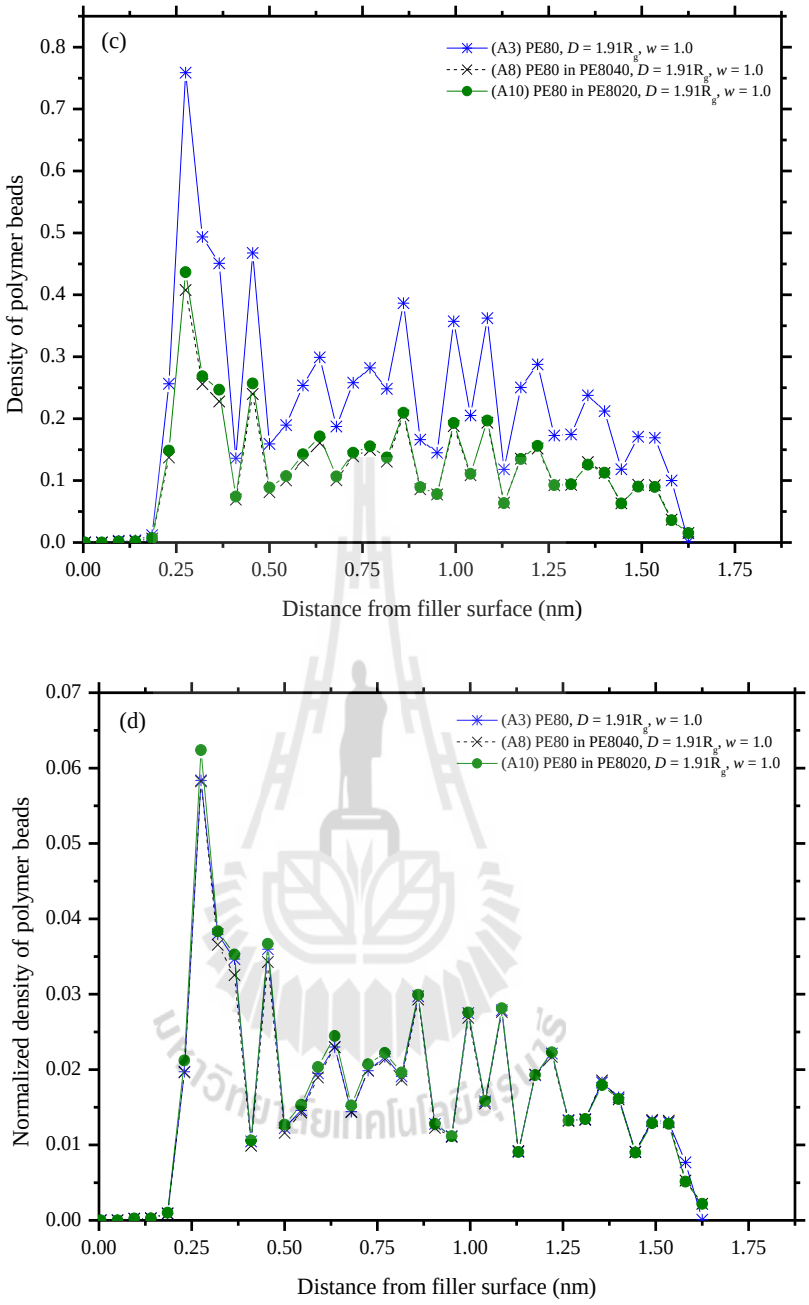

Figure 6.3 (Continued).

- **Subchain segment statistics**

An interesting aspect that deserves consideration is how *D*, *w* and bidispersity of polymer matrix affect the various types of subchain segments because subchain segments play a critical role in the transient network model. Table 6.2 presents the average number of bridges, dangling ends, loops and train segments; the average fraction of chains forming at least one bridge segment; and the average fraction of free chains that are not involved in any subchain segments. To study the effect of confinement (*D*) on the average number of subchain segments per filler A2, A3 and A4 systems were considered. It was found that the average number of bridges decreases rapidly with decreasing confinement (increasing distance between fillers, *D*). Dionne *et al*. (Dionne, Ozisik, and Picu, 2008) reported that no bridges were formed between nanofillers when $D>3R_g$. This result is consistent with the observed behavior of the dangling ends: increasing filler-filler distance leads to increased number of dangling ends. On the other hand, the average number of loops and trains remain constant when $D\geq1.91R_g$ suggesting that the effect of confinement on these types of subchain segments ends at some critical length scale. This observation is logical given that both trains and loops involve only one filler; therefore, they are local structures and they feel the effect of confinement when it is quite strong.

The effect of monomer-filler interactions (*w*) can be observed by comparing A3, A5, and A6 systems. It can be seen that this parameter has essentially no effect on the average number of subchain segments.

Table 6.2 Summary of the statistic chain structure of PE80.

Systems	Average number of subchain segments per filler				Av. fraction of chains forming at least one bridge	Av. fraction of free chains
	Bridge	Dangling	Loop	Train		
A1	-	-	-	-	-	-
A2	18.7	16.1	15.8	33.9	0.87	0.00*
A3	4.3	19.4	7.6	17.3	0.30	0.14
A4	1.8	24.3	7.1	17.3	0.05	0.41
A5	4.3	19.1	9.2	18.2	0.33	0.16
A6	4.3	19.1	8.4	18.9	0.31	0.12
A7	11.1	9.01	10.5	20.4	0.88	0.00*
A8	2.1	10.3	4.2	9.0	0.27	0.13
A9	11.7	9.1	10.6	21.3	0.89	0.00*
A10	2.3	10.5	4.6	9.8	0.30	0.12
A11	0.6	12.5	4.5	9.1	0.05	0.40
A12	2.2	11.2	5.5	10.5	0.29	0.09
A13	2.4	9.9	3.9	9.6	0.31	0.15

*No free chains were found in these systems.

The above observations were made comparing systems that contained only PE80 chains. However, same tendencies were found to be correct for systems containing bidisperse PE chains. The main difference in the bidisperse systems is that the average number of all subchain segments decreased compared to the monodisperse PE80 systems. However, when the PE80 subchain segment averages were normalized by the number of PE80 chains in each system studied, the bidisperse systems showed lower average number of bridges, dangling ends and trains but similar number of loops. This finding suggests that the effect of adding short

chains to the system is not simply a dilution effect but rather the short chains are preventing long chains from forming subchain segments particularly bridges, which are important in the formation of the transient network.

- **Subchain segment distributions**

The subchain segment structure of the PE80 chains are represented by the probability distribution functions of the number of monomers in the segment (*n*) normalized by the total number of monomer units (*N*). The probability distributions, *P(n/N)*, of the number of monomers per bridge, dangling end, loop, and train segments were normalized by the number of monomers in the chain, *N*, and are shown in Figure 6.4(a), 6.4(b), 6.4(c), and 6.4(d), respectively.

To investigate the effect of confinement A2, A3, and A4 systems were compared. The number of monomers in bridge and dangling end distributions of PE80 chains were found to be strongly dependent on confinement. With increasing confinement, the bridge distribution becomes narrower indicating that bridge segments were shorter; and therefore, contained less monomers. The dangling end distribution (Figure 6.4(b)) changes from a nearly constant probability to a highly skewed distribution. This observation indicates that dangling ends of any length was almost equally possible when filler-to-filler distance was greater than ~1.3R_g. However, with the onset of confinement below ~1.3R_g, only dangling ends with small number of monomers were allowed. This finding is expected because at high confinement (<1.3R_g), long dangling ends would end up forming bridges. As can be seen in Figure 6.4(c) and 6.4(d), the data show little variation in the distribution of loop and train segments with confinement and polymer-filler interaction. Both loop

and train segments are structures local to the filler; therefore they are not influenced by confinement, which is happening at much longer length scales (Ozmusul, Picu, Steinstein, and Kumar, 2005). The polymer-filler interaction parameter showed a strong influence on the loop and train segments compared to confinement because this parameter controls the structure at the interfacial region, local to the filler structure. The bidispersity effect was investigated via A3, A8 and A10 systems. The results showed that the segment distribution profiles of PE80 chains are almost identical in each of these systems.

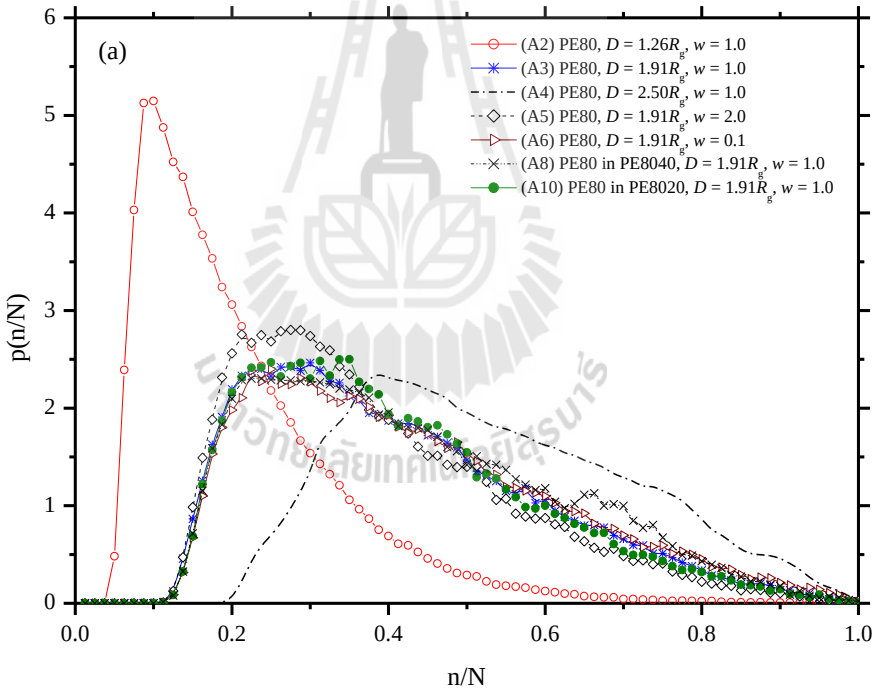

Figure 6.4 Probability density distribution function of the normalized number of bonds of PE80 chains in (a) bridges, (b) dangling ends, (c) loops, and (d) trains for monodisperse and bidisperse PE nanocomposite systems.

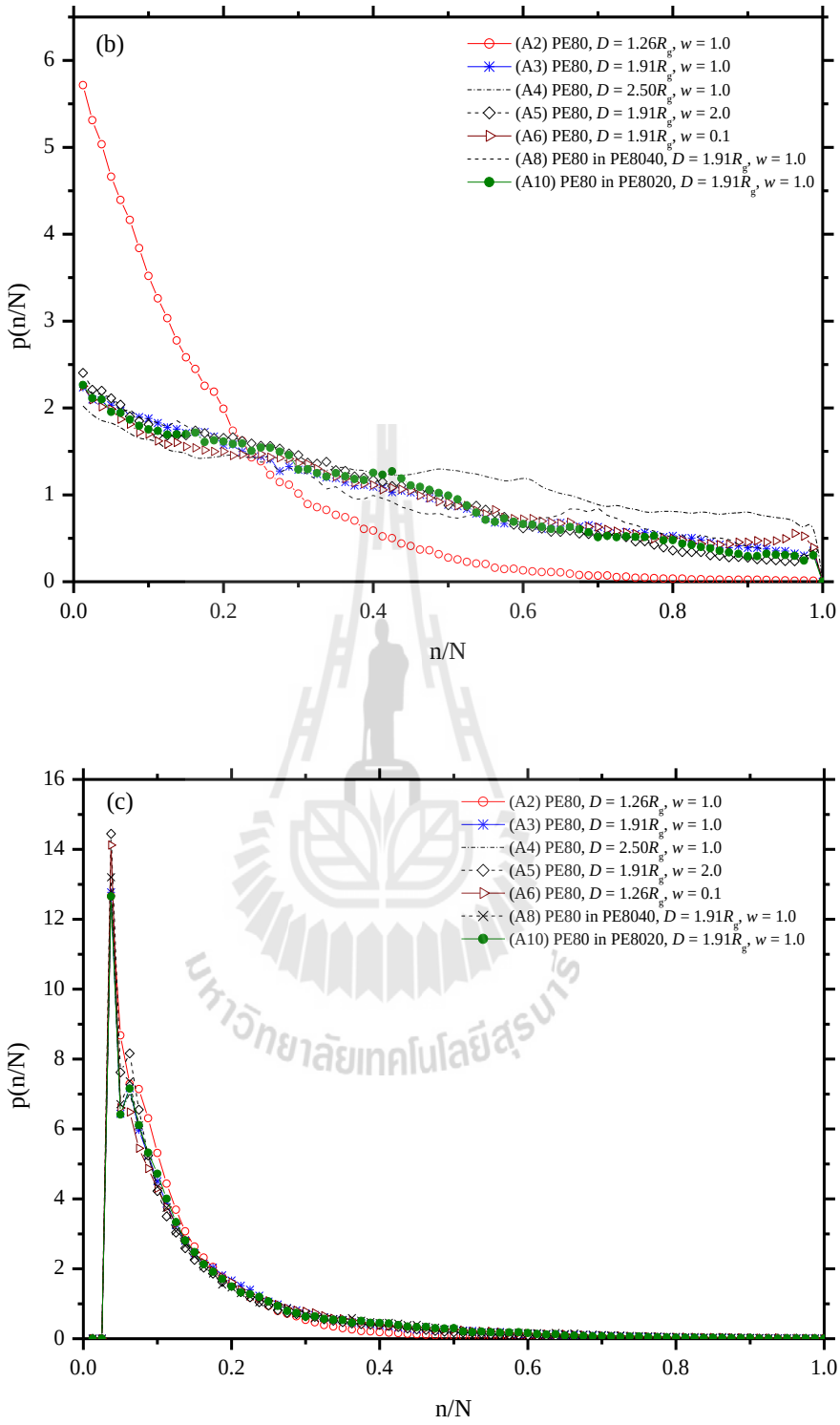

Figure 6.4 (Continued).

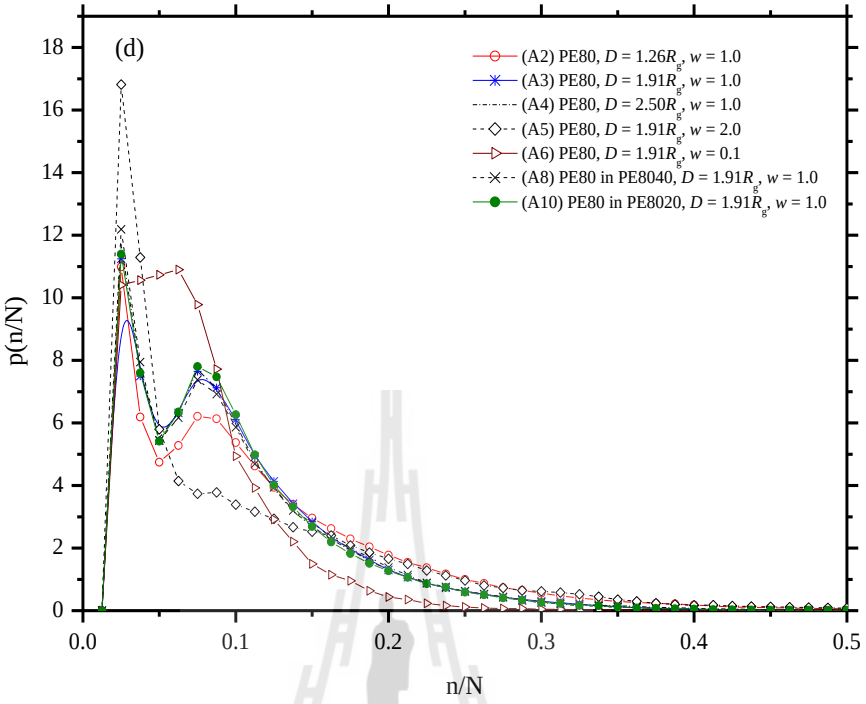

Figure 6.4 (Continued).

6.4.2 Dynamic properties

Rouse mode analysis and mean square displacement (MSD) of the center of mass (g_3(t)) of PE80 chains were employed to investigate the influence of confinement (D), monomer-filler interactions (w), and bidispersity on PE80 chain dynamics in the presence of spherical nanofiller.

The characteristic relaxation times were determined in the usual way by computing the autocorrelation function (ACF) of the normal modes. Figure 6.5 shows ACF of the first Rouse mode (p=1) for various systems. The effect of confinement in A2, A3, and A4 systems are illustrated in Figure 6.5(a). The relaxation time of the neat PE80 system (A1) was used as a reference. As can be seen in Figure

6.5(a), the relaxation of PE80 chains for $D \geq 1.91R_g$ are quite similar to those in the neat PE80 system. At higher confinement, (D=1.26R_g), the relaxation of the PE80 chains are retarded compared to the PE80 chains in the neat PE80 system. The effect of polymer-filler interaction parameter (w) is shown in Figure 6.5(b) in which the filler-to-filler distance (D) was held constant (A3, A5 and A6 systems). As expected, increasing polymer-filler adhesion leads to an additional slow down of the chain dynamics, however, the effect is little less than that observed at the highest confinement. The effect of bidispersity is shown at two different confinements in Figure 6.5(c): A3, A8, and A10 systems with D=1.91R_g. There is an interesting behavior in these bidisperse systems. It was found that the relaxation time of PE80 in both PE8040 (A7) and PE8020 (A9) nanocomposites systems in confined systems (D=1.26R_g) with w=1.0 is slower than those of monodisperse PE80 nanocomposites (A2) at the same confinement (D) and monomer-filler interaction (w). However, when confinement is decreased (D>1.91R_g), the relaxation time of PE80 in bidisperse PE8040 nanocomposites (see A8 system) is close to that of the neat PE80 system. This observation can be explained by the fact that PE80 chains in A7 (with high confinement) are trapped or entangled with the loop segments of adsorbed PE40 chains, which causes the PE80 chains to be constrained and reduces PE80 chains' mobility and hence the relaxation time of PE80 chains is increased. The degree of trapped/entangled chains is depended on the average number of loop segments of PE40 per filler. In the current study, it was found that the average number of loops formed by PE40 chains in A7 (D=1.26R_g) is larger than that in A8 system

(D=1.91R_g). This explanation is consistent with the previous study by Steinstein and Zhu (Steinstein and Zhu, 2002).

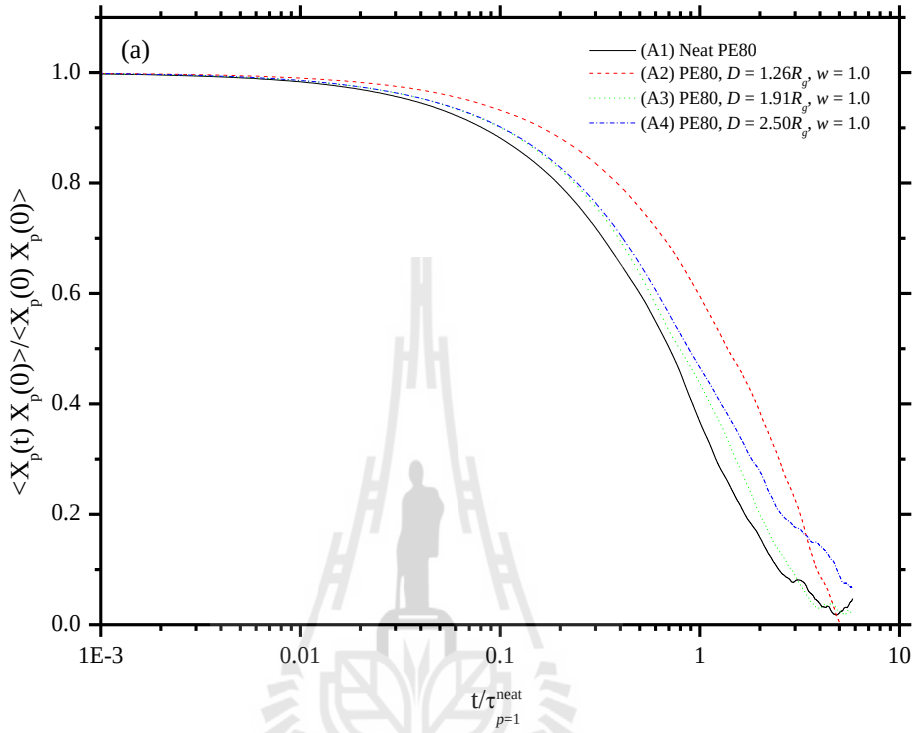

Figure 6.5 Normal mode autocorrelation function of the first Rouse mode (p=1) as a function of (a) confinement, (b) polymer-filler interaction, and (c) bidispersity. The time scales are normalized by the Rouse time of the whole chain in the neat system.

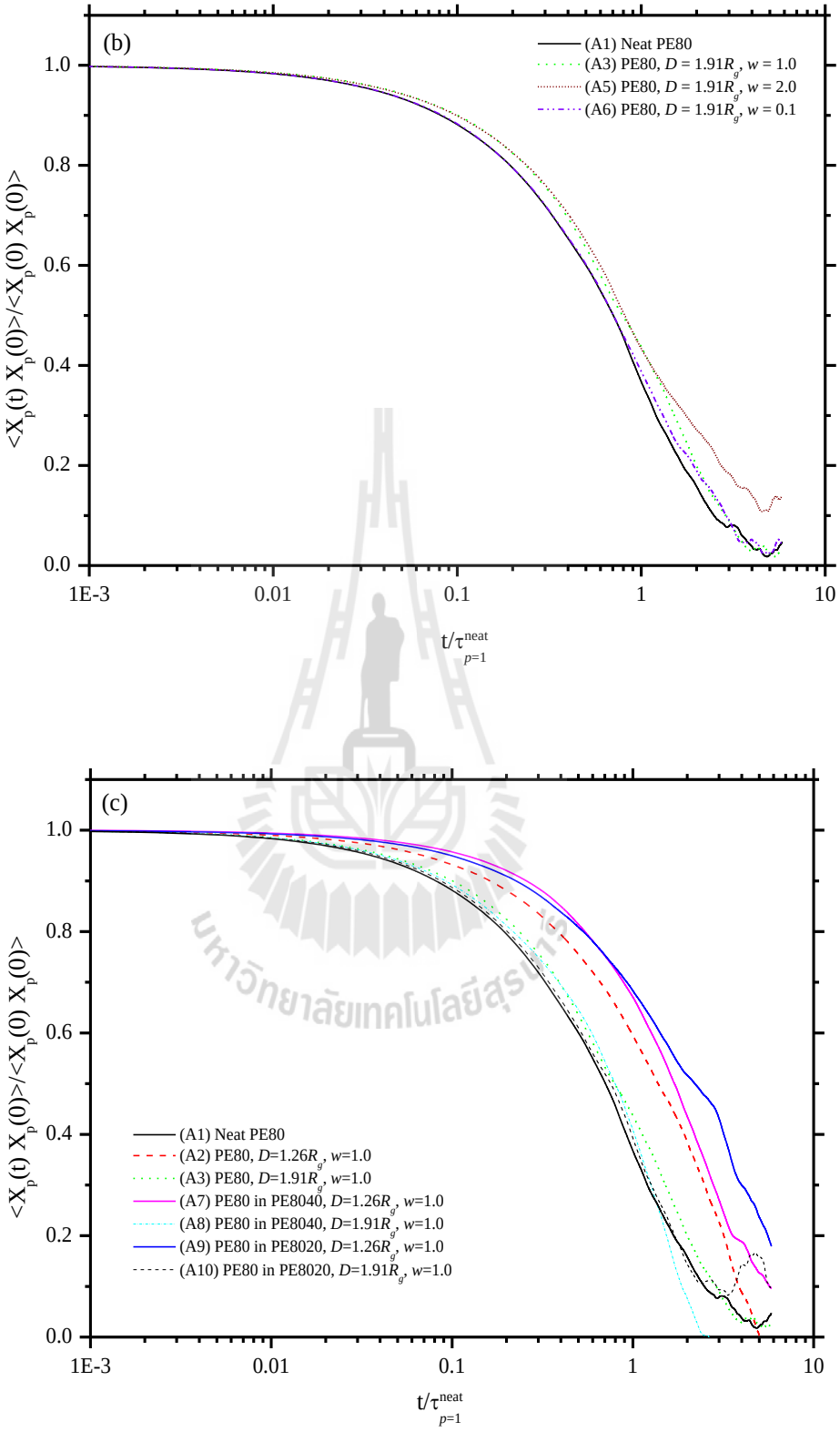

Figure 6.5 (Continued).

The diffusion of PE80 chains was further analyzed by evaluating the center of mass displacement, $g_3(t)$, and the results are shown in Figure 6.6, where the time axis is normalized by the Rouse time obtained from the neat PE80 system (A1).

The $g_3(t)$ results for translational motion are consistent with the data obtained from the Rouse analysis for rotational motion. The slowing down of PE80 chains was observed only at the most confined system with D=1.26R_g. The effect of polymer-filler interaction was quite small, the $g_3(t)$ curves of various systems were almost indistinguishable from each other. Once again, the effect of confinement was found to be stronger than the effect of polymer-filler interaction.

The dynamics of the PE80 chains in bidisperse nanocomposites are presented in Figure 6.6(c), compared to the monodisperse nanocomposite system. It was found that in the case of low confinement (D=1.91R_g), the g_3(t) curves completely overlapped. However, under high confinement (D=1.91R_g), the mobility of PE80 in bidisperse nanocomposites is slower than that in the monodisperse nanocomposite. The effect is worse when the molecular weight of the short chains is greater. This suggests that the dynamics of the whole PE80 chains are influenced strongly by both confinement and polydispersity. The polydispersity effect is more complicated and one needs to involve the molecular weight of the short chains. As the molecular weight of the short chains increase, they are able to form more and longer local structures at the filler interface that slows down the dynamics of the long chains.

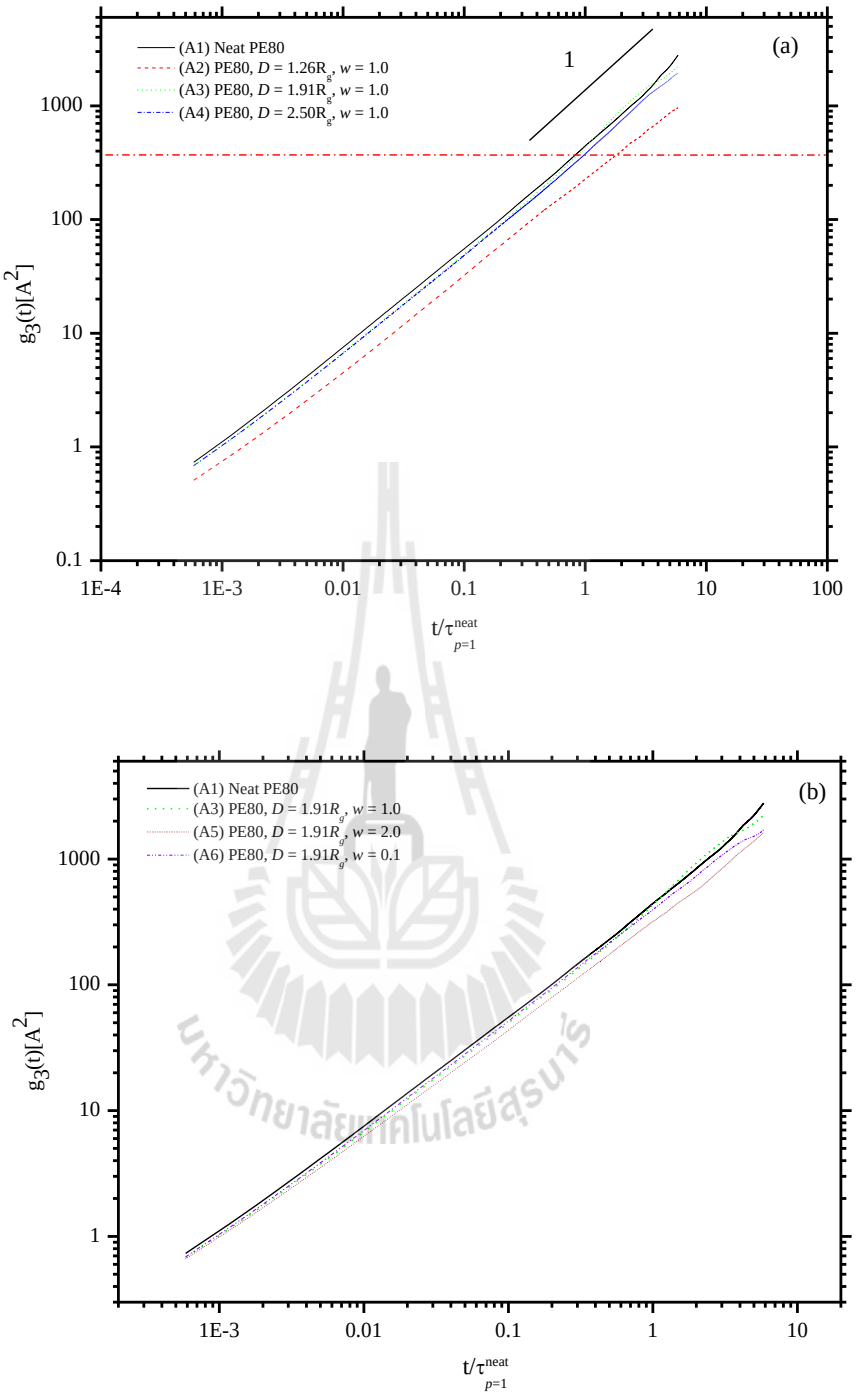

Figure 6.6 Mean squared displacement of the chain center of mass (g_3) of PE80 chains vs. normalized simulation time as a function of (a) confinement, (b) monomer-filler interaction, and (c) polydispersity. The value of $<Rg^2>$ is shown as a horizontal dashed line in (a) to show that the chains diffused greater distances than R_g.

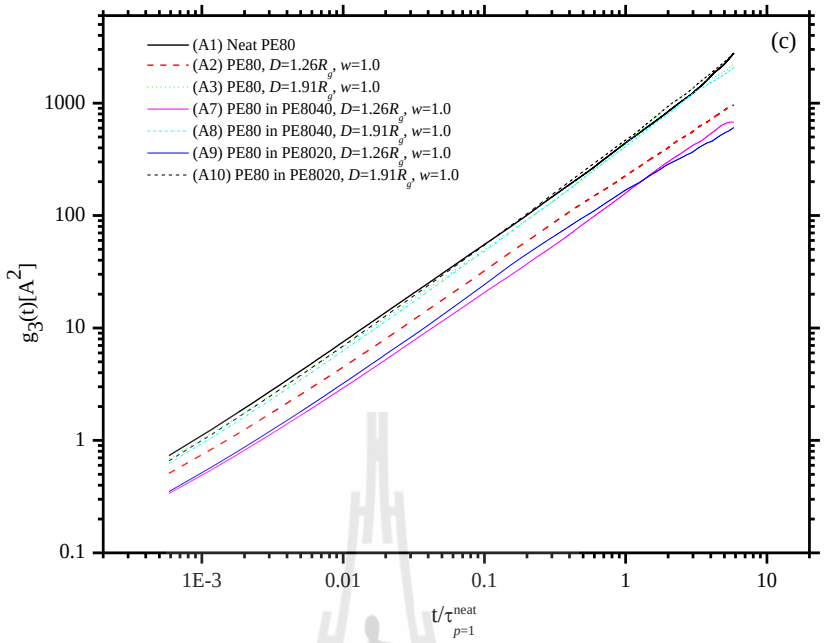

Figure 6.6 (Continued).

6.5 Conclusions

The structure and dynamics of monodisperse and bidisperse polyethylene melts filled with a spherical nanoparticle were investigated by means of a coarse-grained, on-lattice, Monte Carlo method. Bidisperse polyethylene matrix was represented as the mixture of long and short chains. The simulations were performed to evaluate the effect of confinement due to nanofillers, monomer-filler interaction and polydispersity on the behavior of the long polyethylene chains.

In all cases, the long polyethylene chains essentially retained their conformational behavior in the presence of nanofiller, consistent with the notion that it is hard to distort chains in the melt. Polymer-filler structure can be considered as sequences of the chains that are attached to the nanofiller. The subchain segment

structures (bridges, dangling ends, loops and trains) were represented by probability distribution functions of the number of monomers in each segment. The distribution of monomers in bridge and dangling end segments drastically changed with increasing confinement. Only small variations in the distribution of local structures (loop and train segments) were observed with confinement. The effect of monomer-filler interaction and polydispersity of polymer matrix were mostly found to be too weak to affect subchain segment structure and their probability distributions.

The statistic chain structure of polyethylene nanocomposites was investigated by examining the average number of subchain segments per filler. The average number of subchain segments per filler in bidisperse polyethylene nanocomposites decreased about 50%, compared to the monodisperse polyethylene nanocomposite. This result was explained by the observed decrease in bead density of long polyethylene chains at the interface.

Dynamic properties were investigated by examining both the Rouse modes and the mean square displacement (MSD) of the chain center of mass ($g_3(t)$) as a function of (Monte Carlo simulation) time. The normal modes of Rouse relaxation time, $\tau_{p=1}$, of polyethylene chains increased rather suddenly with increasing confinement (below D~1.91Rg). In addition, $\tau_{p=1}$ also increased for systems with attractive monomer-particle interaction energy compared to the neutral and repulsive interactions.

There was interesting relaxation time behavior in the bidisperse nanocomposite systems. The relaxation times of long polyethylene chains in bidisperse nanocomposites were greater than that in the monodisperse polyethylene

nanocomposite under the same conditions (confinement and polymer-filler interaction energy). However, this behavior was only observed under high confinement (D=1.26R_g). These results were consistent with the observed transitional motion of the center of mass displacement.

6.6 References

Anderson, B. J. and Zukoski, C. F. (2010), Rheology and microstructure of polymer nanocomposite melts: Variation of polymer segment-surface interaction. **Langmuir** 26: 8709-8720.

Coleman, J. N., Khan, U. Blau, W. J. and Gun′ko, Y. K. (2006). Small but strong: A review of the mechanical properties of carbon nanotube-polymer composites. **Carbon** 44: 1624-1652.

Desai, T., Keblinski, P. and Kumar, S. (2005). Molecular dynamics simulation of polymer transport in nanocomposites. **The Journal of Chemical Physics** 122: 134910.

Dionne, P. J., Ozisik, R. and Picu, C. R. (2005). Structure and dynamics of polyethylene nanocomposites. **Macromolecules** 38: 9351-9358.

Dionne, P. J. Ozisik, R. and Picu, C. R. (2008). **In Polyolefin Composites**, Eds.: Nwabunma, D. and Kyu, T.; John Wiley & Sons, Inc.: Canada, Chapter 16: 449-484.

Guth, E. (1945). Theory of reinforcement. **Journal of Applied Physics** 16: 20-25.

Jang, J. H. and Mattice, W. L. (2000). A Monte Carlo simulation for the effect of compression on an amorphous polyethylene melts in very thin confined geometry. **Macromolecules** 33(4): 1467-1472.

Jang, J. H., Ozisik, R. and Mattice, W. L. (2000). A Monte Carlo simulation on the effects of chains end modification on freely standing thin films of amorphous polyethylene melts. **Macromolecules** 33(20): 7663-7671.

Kloczkowski, A., Sharaf, M. A. and Mark, J. E. (1994). Computer simulations on filled elastomeric materials. **Chemical Engineering Science** 49: 2889-2897.

Koo, J. H. (2006). **Polymer Nanocomposites**. In Nanoscience and Technology; Manasreh, O., Ed.; McGraw-Hill: New York.

Landau, D. P. and Binder, K. (2000). A guide to Monte Carlo simulation in statistical physics, 2nd ed. Cambridge university press: New York.

Ozmusul, M. S., Picu, C. R., Steinstein, S. S. and Kumar, S. K. (2005). Lattice Monte Carlo simulations of chain conformations in polymer nanocomposites. **Macromolecules** 38: 4495-4500.

Picu, R. C. and Ozmusul, M. S. (2003). Structure of linear polymeric chains confined between impenetrable spherical walls. **The Journal of Chemical Physics** 118: 11239.

Starr, F. W., Schrøder, T. B. and Glotzer, S. C. (2002). Molecular dynamics simulation of a polymer melts with a nanoscopic particle. **Macromolecules** 35: 4481-4492.

Steinstein, S. S. and Zhu, A. (2002). Reinforcement mechanism of nanofilled polymer melt as elucidated by non linear viscoelastic behavior. **Macromolecules** 35: 7262-7273.

Vacattello, M. (2001). Monte Carlo simulations of polymer melts filled with solid nanoparticles. **Macromolecules** 34: 1946-1952.

Vacatello, M. (2003), Predicting the molecular arrangements in polymer-based nanocomposites. **Molecular Theory and Simulations** 12: 86-91.

Vao-Soongnern, V., Ozisik, R. and Mattice, W. L. (2001). Monte Carlo simulation of the structures and dynamics of amorphous polyethylene nanoparticles. **Macromolecular Theory and Simulations** 10: 553-563.

Xu, G. and Mattice, W. L. (2001). Study on structure formation of short polyethylene chains via dynamics Monte Carlo simulation. **Computational and Theoretical Polymer Science** 11: 405-413.

Zeng, Q. H., Yu, A. B. and Lu, G. Q. (2008). Multiscale modeling and simulation of polymer nanocomposites. **Progress in Polymer Science** 33: 191-269.

Zhang, Q. and Archer, L. (2002). Polyethylene oxide/silica nanocomposites: Structure and rheology. **Langmuir** 18: 10435-10442.

CHAPTER VII

CONCLUSION

According to the disadvantage properties of neat poly(lactic acid) (PLA) *i.e.*, brittleness and low elongation at break, therefore frequently not good enough to fulfill all applications and limited its uses. Several attempts have been performed to overcome these drawbacks. Blending of PLA with polyethylene glycol (PEG) has been recognized as an effective method to toughen of PLA. Unfortunately, PLA/PEG blend is phase separation with time at room temperature. To reduce the phase separation of the blends, triblock copolymer of PLA and PEG (PLA-PEG-PLA) was proposed as the plasticizer for PLA in this work.

The series of PLA-PEG-PLA triblock copolymers with different LA/EG ratios were prepared by ring opening polymerization. Two kinds of stereochemical lactide (LA) monomer, L-LA and D, L-LA were used to prepare PLLA-PEG-PLLA and PDLLA-PEG-PDLLA block copolymers, respectively. PEG with $\bar{M}_w$ of 8,000 and 10,000 $g \cdot mol^{-1}$ was used as initiator polymerization. Thermal and rheological properties of PLA, PEG, PLA-PEG-PLA, PLA/PEG, and PLA/PLA-PEG-PLA were investigated. DSC thermograms, XRD spectra and POM images revealed the microphase separation of PLLA-PEG-PLLA block copolymers at ϕ_{PLLA} of 0.37 and 0.47, observing two distinct melting peaks for the PLLA and PEG. The crystallization process of PLLA segments in the block copolymer occurs in two-dimensional

aggregates. From DSC results, blending with PEG and PDLLA-PEG-PDLLA accelerated the crystallization of PLLA. When a PLLA/PEG 70/30 (wt/wt) blend was slowly cooled from the melt, phase separation of PLLA and PEG was observed due to the crystallization of PEG. However, this phenomenon was not observed in PLLA/PDLLA-PEG-PDLLA blend. These indicate that PDLLA-PEG-PDLLA is more miscible in PLLA than PEG. The finding results showed that the slope of G′ curves for PLLA/PEG 75/25 and 70/30 (wt/wt) was less than 2 while this deviation was found only at 70/30 (wt/wt) for PLLA/PDLLA-PEG-PDLLA. This indicates that the PDLLA block in PDLLA-PEG-PDLLA copolymer contribute the PEG miscible in PLLA.

The miscibility and morphology of PLA and PEG based on block copolymers and blends were also investigated using MD and DPD simulations. The χ_{ij}-parameters of PLA/PEG blends (MD simulation) exhibit that the PLA and PEG is miscible at the low PEG concentrations (10-30 wt%) but it is immiscible at the PEG concentrations of 50-90 wt%. These results were confirmed by the radial distribution functions *g(r)* curves of the inter-molecular carbon atomic pairs of PLA-PEG, PLA-PLA and PEG-PEG of the blends. The disorder morphologies of PLA/PEG blends were observed at the PEG concentration of 10-30 wt%. In the cases of PLA-PEG-PLA block copolymers, the mesoscale simulations predicted the phase structures with defined morphologies of disorder, bicontinuous, perforated lamellas and spheres were detected at different compositions. These phase morphologies correspond to the bridge/loop fractions values of 0.49-0.73.

For PE/PP blends, the influence of the tacticity of PP chains including, *a*PP, *i*PP and *s*PP, on miscibility of 50 (wt/wt) PE/PP blend was investigated using a

coarse-grained model based on Monte Carlo simulation. The chain dimensions, characteristic ratio (C_n) and self-diffusion coefficient (D) of PE chains in the blends are sensitive to stereochemistry of PP. Comparing with pure PE, the decreasing of chain dimensions of PE in the blends was observed in PE/*i*PP and PE/*s*PP systems. This implies that the PE and PP chains tend to be demixing. Interchain pair correlation functions, *g(r)*, are used to assess the miscibility of the mixtures. Partial miscibility of PE/*a*PP and PE/*i*PP blends were observed while the phase separation was found in PE/*s*PP blend.

The structure and dynamics of bidisperse polyethylene (PE) nanocomposite mixtures of 50:50 (by mole) of long and short chains of $C_{160}H_{322}/C_{80}H_{162}$ and $C_{160}H_{322}/C_{40}H_{82}$ filled with spherical nanoparticles were investigated by a coarse-grained, on lattice Monte Carlo method using rotational isomeric state theory for short-range and Lennard-Jones for long-range energetic interactions. The simulations were performed to evaluate the effect of confinement due to nanofillers, monomer-filler interaction and polydispersity on the behavior of the long polyethylene chains. The various long PE subchain structures (bridges, dangling ends, trains, and loops) are influenced strongly by confinement whereas monomer-filler interaction and polydispersity did not have any impact. In addition, the average number of subchain segments per filler in bidisperse PE nanocomposites decreased about 50% compared to the nanocomposite system with monodisperse PE chains. The presence of short PE chains in the polymer matrix leads to a reduction of the repeat unit density of long PE chains at the interface suggesting that the interface is preferentially populated by short chains. Chain dynamics were monitored by computing the Rouse relaxation modes and the mean square displacement of the center of mass. The dynamics were slowed

by both the confinement (D) and monomer-particle energetic interaction (w) effects. Under the greatest confinement studied (D=1.26R_g), the mobility of the long chains in bidisperse nanocomposites was slower than those in the monodisperse nanocomposite systems.

APPENDICES

APPENDIX A

THE POTENTIAL ENERGY EXPRESSION USED TO REPRESENT THE ENERGY SURFACE IN COMPASS FORCE-FIELD

$$E_{pot} = \underbrace{\sum_{b}\left[K_2(b-b_0)^2 + K_3(b-b_0)^3 + K_4(b-b_0)^4\right]}_{(1)}$$

$$\underbrace{+\sum_{\theta}\left[H_2(\theta-\theta_0)^2 + H_3(\theta-\theta_0)^3 + H_4(\theta-\theta_0)^4\right]}_{(2)}$$

$$\underbrace{+\sum_{\phi}\left[V_1\left[1-\cos(\phi-\phi_1^0)\right]+V_2\left[1-\cos(2\phi-\phi_2^0\right]+V_3\left[1-\cos(3\phi-\phi_3^0)\right]\right]}_{(3)}$$

$$\underbrace{+\sum_{\chi}K_\chi\chi^2}_{(4)} \quad \underbrace{+\sum_{b}\sum_{b}F_{bb'}(b-b_0)(b'-b_0')}_{(5)} \quad \underbrace{+\sum_{\theta}\sum_{\theta'}F_{\theta\theta'}(\theta-\theta_0)(\theta'-\theta_0')}_{(6)}$$

$$\underbrace{+\sum_{b}\sum_{\theta}F_{b\theta}(b-b_0)(\theta-\theta_0)}_{(7)} \quad \underbrace{+\sum_{b}\sum_{\phi}(b-b_0)\left[V_1\cos\phi+V_2\cos2\phi+V_3\cos3\phi)\right]}_{(8)}$$

$$\underbrace{+\sum_{b'}\sum_{\phi}(b'-b_0')\left[V_1\cos\phi+V_2\cos2\phi+V_3\cos3\phi\right]}_{(9)}$$

$$\underbrace{+\sum_{\theta}\sum_{\phi}(\theta-\theta_0)\left[V_1\cos\phi+V_2\cos2\phi+V_3\cos3\phi\right]}_{(10)}$$

$$\underbrace{+\sum_{\phi}\sum_{\theta}\sum_{\theta'}K_{\phi\theta\theta'}\cos\phi(\theta-\theta_0)(\theta'-\theta_0')}_{(11)} \quad \underbrace{+\sum_{i>j}\frac{q_iq_j}{\in r_{ij}}}_{(12)} \quad \underbrace{+\sum_{i>j}\left[\frac{A_{ij}}{r_{ij}^9}-\frac{B_{ij}}{r_{ij}^6}\right]}_{(13)}$$

Term (1): Bond stretching energy

Term (2): Angle bending energy

Term (3): Torsion energy

Term (4): Out-of-plane coordinates energy

Term (5-11): Cross term energy

Term (12): Coulombic interaction energy

Term (13) van der Waals interactions energy

APPENDIX B

^{1}H-NMR SPECTRA OF STUDIED POLYMER

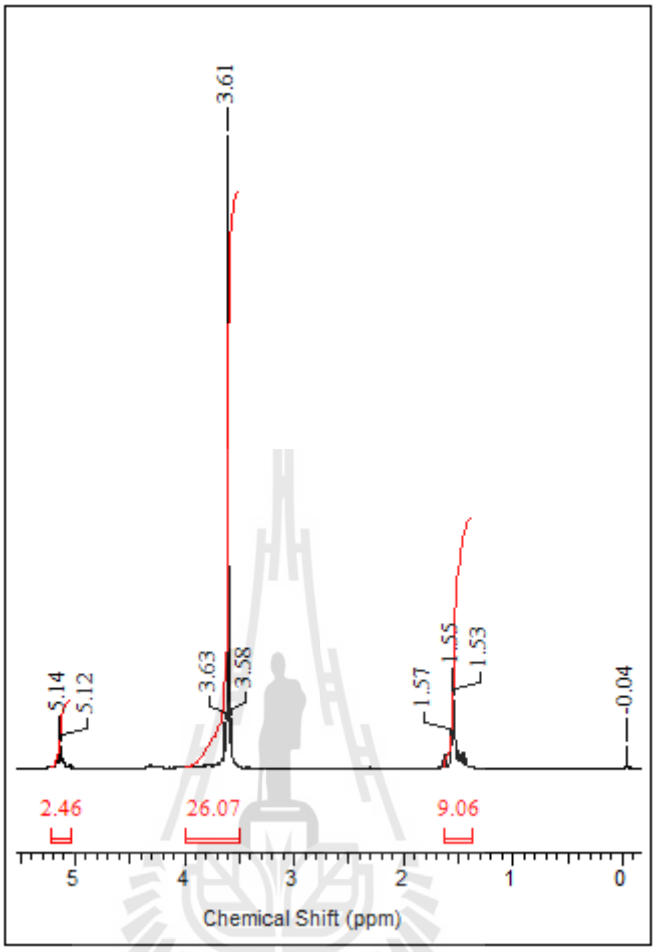

^{1}H-NMR of DLA_{36}-EG_{187}-DLA_{36}

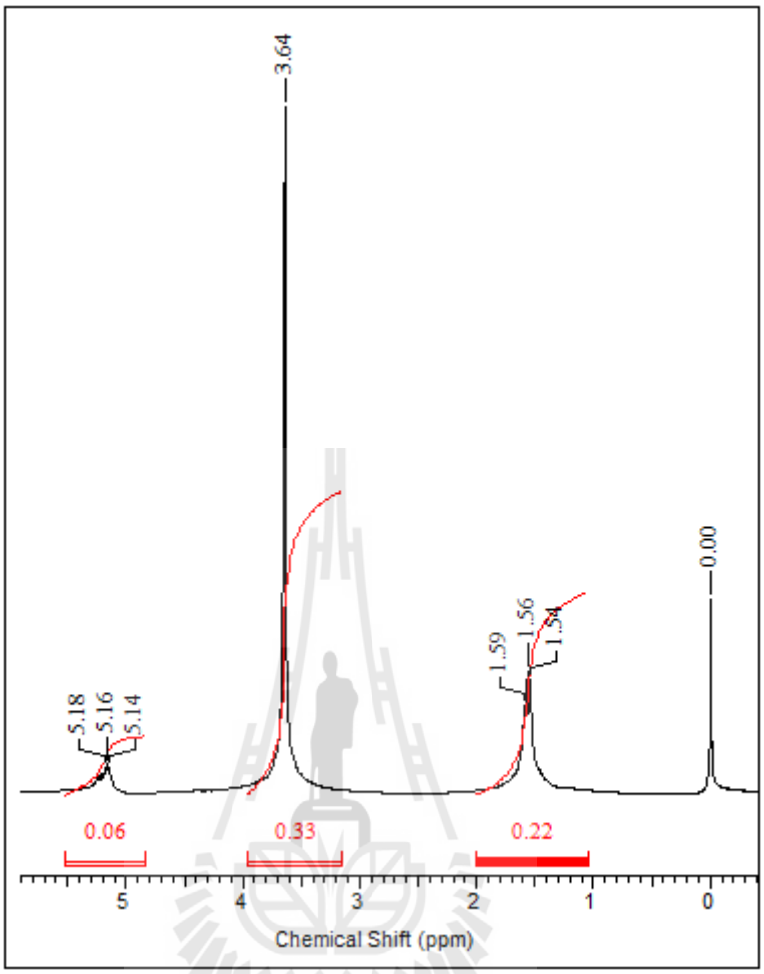

^{1}H-NMR of DLA_{72}-EG_{187}-DLA_{72}

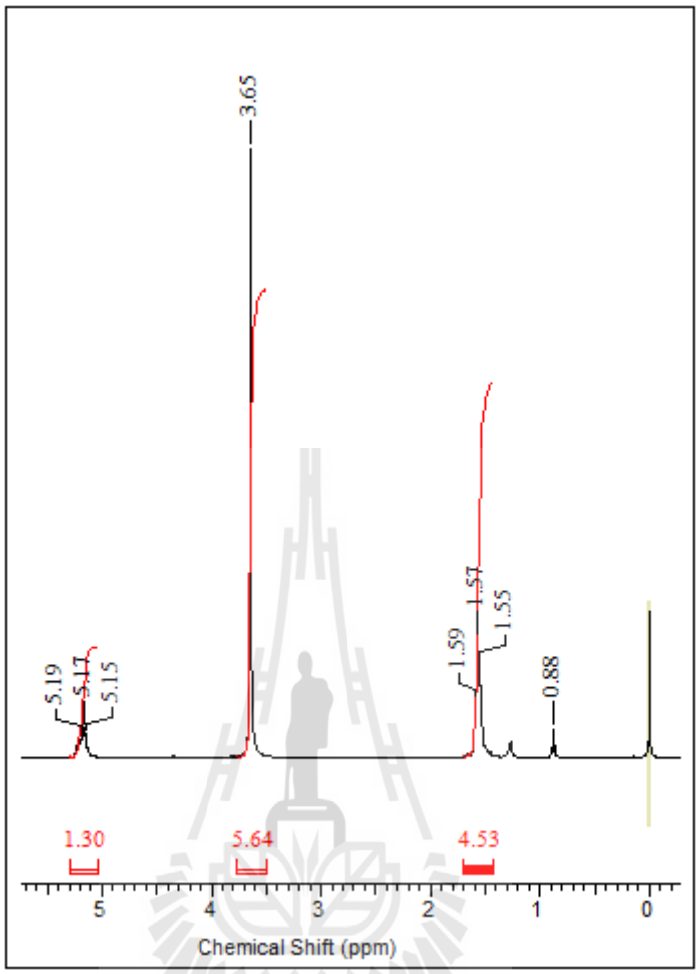

^{1}H-NMR of DLA_{87}-EG_{187}-DLA_{87}

CURRICULUM VITAE

Name : Adisak Takhulee

Date of birth : 8 May 1977

Address : 401 Moo 3 Chum Phae, Chum Phae, Khon Kaen, Thailand.

E-mail : adtakhulee@hotmail.com

Education :

1986 - 1991 Elementary education,
Banhae elementary school, Khon Kaen, Thailand.

1991 - 1996 Secondary school education,
Chum Phae Suksa high school, Khon Kaen, Thailand.

1997 - 2001 Bachelor of Science (Chemistry), Faculty of Science, Khon Kaen University, Thailand.

2001 - 2004 Master of Science (Physical chemistry), Faculty of Science, Khon Kaen University, Thailand.

2006 - Present Ph.D. student (Chemistry), Institute of Science, Suranaree University of technology, Thailand.

Experience : 2004 - Present Lecturer position in Department of Chemistry, Faculty of Science, Udon Thani Rajabhat University, 64 Tahan Road, Muang district, Udon Thani, 41000, Thailand.

2011 - 2012 Visiting researcher for 1 year in Laboratory of molecular rheology, Department of Advanced Device Materials, Institute for Materials Chemistry and Engineering, Kyushu University, Japan under the supervision of Professor Dr. Yoshiaki Takahashi.